



DEPARTMENT OF CIVIL ENGINEERING

PhD Course in

***Risk and Sustainability in Civil Engineering,
Architecture, Environmental Engineering Systems***

XXXV CYCLE

Simplified Methods for the Evaluation of Seismic Performances of steel MRFs and CBFs

Paolo Todisco

Tutor

Prof. Rosario Montuori

Co-tutor

Prof. Elide Nastri

PhD Coordinator

Prof. Fernando Fraternali

TABLE OF CONTENTS

Summary

1	INTRODUCTION	7
1.1	Background	7
1.2	Motivations of the Work	8
1.3	Investigated Structural Types	9
1.4	Organization of the work.....	13
2	DESIGN APPROACHES	15
2.1	Introduction	15
2.2	Collapse Mechanisms for MRFs and CBFs	16
2.3	Theory of Plastic Mechanism Control: Generalities	19
2.4	Global Moment Resisting Frames Design.....	22
2.4.1	First-Order Collapse Multipliers and Slopes of the Mechanism Equilibrium Curve for MRFs	24
2.4.2	TPMC Design steps for MRFs	26
2.5	Global Concentrically Braced Frames design	29
2.5.1	First-Order Collapse Multipliers and Slopes of the Mechanism Equilibrium Curve for MRFs	32
2.5.2	TPMC Design steps for simple CBFs	34

2.5.3	Definition of the Axial Force in Compressed Members According to Georgescus's Model	37
2.6	Upper Partial and Shear Band Collapse Mechanisms	40
2.6.1	First-Order Collapse Multipliers and Slopes of the Mechanism Equilibrium Curve for MRFs	41
2.6.2	First-Order Collapse Multipliers and Slopes of the Mechanism Equilibrium Curve for CBFs	42
3	SIMPLIFIED PERFORMANCE-BASED APPROACH FOR THE EVALUATION OF SEISMIC CAPACITY	45
3.1	Introduction	45
3.2	Trilinear Approximation of the Non-Dimensional Pushover Curve for MRFs	46
3.3	Performance-Based Capacity Definition Approach for MRFs.....	49
3.3.1	Equations for the Definition of the Performance Points (MRFs)	51
3.4	Trilinear Approximation of the Non-Dimensional Pushover Curve for CBFs	54
3.5	Performance-Based Capacity Definition Approach for CBFs.....	57
3.5.1	Equations for the Definition of the Performance Points (CBFs)	58
4	CALIBRATION AND VALIDATION OF THE METHOD THROUGH REGRESSION ANALYSIS	61
4.1	Introduction	61
4.2	Calibration Through Pushover Analysis.....	65
4.2.1	Mechanical Modelling of Members for MRFs.....	65
4.2.2	Mechanical Modelling of Members for CBFs.....	66
4.3	Evaluation of Maximum Multiplier of Horizontal Forces according to Merchant-Rankine Formula for MRFs.....	68
4.3.1	Assessment of the precision of the method through δC (MRFs)	73
4.4	Evaluation of Maximum Multiplier of Horizontal Forces according to Merchant-Rankine Formula for CBFs.....	75
4.4.1	Assessment of the precision of the method through δC (CBFs).	80

4.5	Evaluation of the Plastic Hinge Rotation Demand $\theta_{p.mec}$ and $\theta_{p.amax}$ for MRFs	83
5	PERFORMANCE-BASED ASSESSMENT PROCEDURES	97
5.1	Introduction	97
5.2	Definition of the Equivalent SDOF System Transformation, SDOF Dynamic Parameters and Capacity Curve in ADRS Plane	98
5.2.1	Evaluation of the stiffness k^* of the equivalent SDOF system for MRFs and CBFs	99
5.3	Assessment Procedure in Terms of Spectral Displacements into ADRS Plane According to Italian and European Codes	100
5.4	Graphic Assessment Procedure through ADRS Plane	102
5.5	Assessment Procedure in Terms of Spectral Acceleration through the ADRS Plane	104
5.6	Assessment Procedure in Terms of Spectral Acceleration According to Nassar & Krawinkler.....	105
5.6.1	Assessment procedure for MRFs.....	106
5.6.2	Assessment procedure for CBFs	108
6	EXAMPLES OF APPLICATION OF THE PERFORMANCE-BASED ASSESSMENT APPROACH.....	111
6.1	Introduction	111
6.2	MRFs Numeric Examples	111
6.2.1	Global Moment Resisting Frames	113
6.2.2	Special Moment Resisting Frames	117
6.2.3	Ordinary Moment Resisting Frames	121
6.3	CBFs Numeric Examples	125
6.3.1	Global Concentrically Braced Frames.....	127
6.3.2	Special Concentrically Braced Frames.....	130
6.3.3	Ordinary Concentrically Braced Frames	133
7	VALIDATION OF THE METHODOLOGY THROUGH INCREMENTAL DYNAMIC ANALYSIS (IDA).....	137

7.1	Introduction	137
7.2	Incremental Dynamic Analyses (IDA)	138
7.2.1	Evaluation of the reference earthquakes	138
7.3	Modelling in OpenSees	140
7.3.1	Model construction syntax.....	140
7.3.2	Fiber Elements and Uniaxial Material.....	141
7.3.3	“Steel 02” Giuffré-Menegotto-Pinto uniaxial material.....	143
7.4	Fiber Elements, Sections and Uniaxial Material in OpenSees for MRFs	145
7.5	Non-linear Cyclic behaviour of Bracing Members.....	148
7.5.1	Studies on the fundamental parameters affecting the cyclic behaviour of axially loaded members.....	148
7.5.2	An analytical model for the characterization of the cyclic behavior of the axially loaded members.....	151
7.6	Characterization of the Cyclic Behaviour of Diagonal Members in OpenSees	162
7.7	Fiber Elements, Sections and Uniaxial Material in OpenSees for CBFs	166
7.7.1	Calibration of the cyclic behaviour.....	167
7.8	Case Study 1 for MRFs	171
7.8.1	Application of the Trilinear Simplified Model.....	173
7.8.2	IDA Results and Comparison with the Simplified Method (MRF)	177
7.9	Case Study 2 for MRFs	180
7.9.1	Application of the Trilinear Simplified Model.....	182
7.9.2	IDA Results and Comparison with the Simplified Method (MRF 2)	187
7.10	Case Study for CBFs	188
7.10.1	Application of the simplified method – X direction.....	191
7.10.1	Application of the simplified method – X direction.....	195

7.10.2	IDA Results and Comparison with the Simplified Method (CBF)	198
8	CONCLUSIONS.....	207

CHAPTER 1

1 INTRODUCTION

1.1 Background

The seismic events that have affected our peninsula and the world over the last decade have highlighted the importance of a correct design of structures in seismic zone and the seismic inadequacy of a large part of the built heritage [1]-[3]. In particular, the social and media impact of the catastrophic consequences of these events, linked to the extreme vulnerability of the buildings, has accompanied and pushed the implementation of modern rules on the design and verification of structures in seismic areas that, however, are still lacking in content in terms of assessing the seismic performance of existing buildings [4]. In addition, many countries do not have a large-scale mapping of the seismic vulnerability of the built heritage, according to performance criteria based on the "capacity-demand" comparison.

In particular, they do not provide specific rules for different structural typologies. Moreover, the code-compliant rules are mainly set up on reinforced concrete structures resulting inadequate for the evaluation of steel structures [5].

These procedures also do not lend themselves to seismic classification and code liability being strongly influenced by the software used to develop them and for the modeling of the members which is characterized by numerous variables that are difficult to standardize.

Consequently, a completely analytical simplified model that allows to control these complexities in a univocal way is introduced for steel Moment Resisting Frames (MRFs) [6]-[8] and Centrically Braced Frames (CBFs) [9]-[12].

The Performance levels, intended as a combination of structural and non-structural performance, define levels of damage considered acceptable in relation to the severity of the seismic event. In its classical formulation, performance-based design theory identifies five fundamental performance levels [13],[14]:

- **“Fully Operational”**: no interruption of activities and negligible damage;
- **“Operational”**: no interruption of activities and marginal damage to non-structural components;
- **“Reparability”**: occurrence of damage such as to cause the interruption of activities but of such magnitude as to be repairable in any case;
- **“Life safety”**: the occurrence of extensive damage, repairable, with interruption of activities but without danger to human life;
- **“Near Collapse”**: significant damage such as endangering the stability of the structure and human life.

The work described here aims to define a simplified and unique method, applicable on a large scale or in the immediacy of a seismic event, for the evaluation of the seismic performance of steel buildings, depending on the performance levels provided by performance-based design.

1.2 Motivations of the Work

Emphasis is placed on two adjectives referring to the word "method" which are decisive in the explanatory statement behind the research work:

- **Simplified**: a large-scale classification of the building or an evaluation to be carried out in the immediate post-earthquake period requires the use of a methodology providing quick results. In the first case for the huge building basin to be analyzed, and in the second case for the need to receive "answers" in the shortest possible time.
- **Unique**: the classification of the built heritage on a large scale and the analysis of results obtained in the immediate post-earthquake period require a criterion for the evaluation of seismic performance not susceptible to contour variables such as not allowing a direct comparison between the outputs obtained.

The proposed solution is a fully analytical (therefore unique) methodology that allows to represent the capacity curve of a structure through a trilinear approximation.

This methodology solves the problems of multiple voices (polydromy) of the result that arises with the use of structural analysis software. The result, in these cases, is the result of different input data, modeling, and assumptions of the specific user that can lead to completely different results even for the same structure. Uniqueness is the prerogative of analytical methods, which determine unambiguously and uniquely a result if wisely used.

A great advantage, moreover, lies in the possibility of automating the calculation through input files containing the information (geometric, mechanical, etc.) concerning the structures to be analyzed, obtaining in the output the corresponding capacity values in terms of spectral acceleration or spectral displacements. In this way, quickly and unambiguously, it will be possible to recreate maps of seismic vulnerability on a large scale once all the structural types and construction materials have been implemented.

The validation of the proposed methodology has been performed through a calibration procedure on a total of 840 designed structures, and then through Incremental Dynamic Analysis (IDA) applied to simulated designs and real structures available in the literature [15]-[17].

1.3 Investigated Structural Types

The methodology has been calibrated on steel buildings, considering the most widespread structural typologies in accordance with the built-up heritage. The horizontal actions in steel structures can be faced by different types of seismic-resistant structures, as reported in Eurocode 8 [18]-[21]:

- **Moment resisting frames;**
- **Concentrically braced frames;**
- Eccentrically braced frames.

The moment resisting frames are characterized by a limited lateral stiffness and high ductility linked to the possibility of forming a large number of plastic hinges. The dissipative zones consist of the end sections of the beams for which the dissipation of seismic energy is demanded to the flexural behavior of these elements, and therefore to the moment-rotation cycles. In order to ensure an

adequate level of overall ductility, it is necessary to prevent the formation of local mechanisms, such as the “soft storey” ones (Figure 1.3.1b) which, by involving few dissipative elements, quickly lead to the exploitation of local ductility resources, and are therefore accompanied by low energy dissipation. In this context, the hierarchy criterion provided by the current codes (Eurocode 8, NTC 2018) [18],[20], aims to promote the formation of plastic hinges at the ends of the beams ensuring adequate over resistance of the columns. This criterion, however, fails to ensure the development of a highly dissipative mechanism (global collapse mechanism reported in Figure 1.3.1a). This objective can be achieved through the application of more sophisticated design procedures.

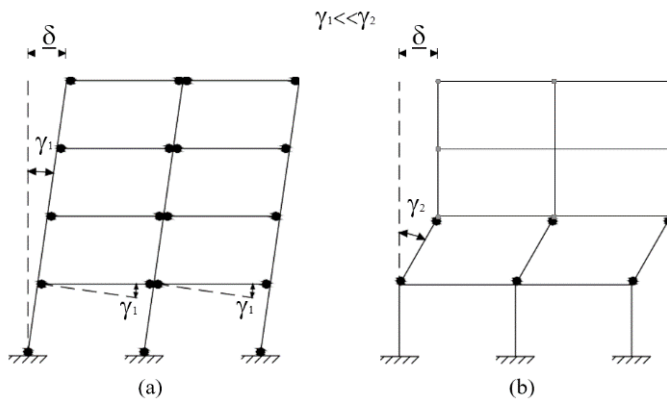


Figure 1.3.1 Collapse mechanisms for moment resisting frames: difference in terms of ductility demand.

In addition, the performance design implemented by the current seismic codes is based on the satisfaction of two main objectives: damage limit state (DLS), i.e. containment of structural damage (interstorey drift) during seismic events with a return period comparable with the working life of the structure, and life-safety limit (LS), which consists in preventing structural collapse, even at the cost of significant damage to the structure (provided that inelastic deformations are compatible with local ductility resources), on the occasion of seismic events with a return period greater than the working life of the structure. A necessary condition to satisfy the DLS is that the structure is equipped with sufficient lateral stiffness; on the contrary, adequate local and global ductility resources are required to meet the LS requirements. The frames have a high dissipative capacity, making it easy to meet the SLV checks; on the other hand, they are equipped with a contained lateral stiffness so that deformability checks

are generally the most difficult requirement to meet and that, as a result, governs the design.

Concentric braces counteract the lateral actions that affect the structure by means of the axial resistance of the diagonal members; therefore, they are characterized by a high lateral stiffness that allows to easily meet the checks in terms of interstorey drift. Dissipative elements are basically diagonals. However, the cyclic behaviour of the axial members is asymmetric and nonlinear, as well as rapidly degrading, due to the instability in compression. For this reason, the single diagonal solution (Figure 1.3.2a) is not covered by current codes, but it is necessary to equip these structures in such a way as to have, for each direction of seismic action, at least one stretched diagonal. This solution is equivalent to that of the “X” braced frames). In both cases, in fact, the incoming seismic energy is dissipated mainly by the stretched diagonals.

Inverted “V” and “V” braces (Figure 1.3.2b and c) are characterized, like the previous ones, by the presence of diagonals in both directions that ensure the presence of at least one stretched member for each direction of seismic action. However, due to the imbalance between the actions in the stretched and compressed diagonals (given the post-critical behavior), a concentrated action is generated on the beam that results in strong vertical displacements. In order to improve the cyclic behavior, it is necessary the use of a continuous beam. In any case, the post-critical behavior of the system is characterized by rapid deterioration due to the inability of the buckled diagonal to recover the initial configuration. The scheme is therefore characterized by a lower dissipative capacity than the X-pattern or single-diagonal coupled pattern; the current codes, in fact, provide structural factors of 2 and 2.5 in low and high ductility class for these systems, respectively, while for X-schemes the structure factor must be assumed equal to 4 in both situations.

Finally, K-braces (Figure 1.3.2e) are characterized by problems related to the instability of the columns due to the lateral displacements inevitably induced, at the mid-sections, by the actions transferred from the diagonals. For this reason, the current seismic codes classify this type among the non-dissipative structures, for which the project must be carried out ensuring that the members remain in the elastic field (structure factor equal to 1).

Ultimately, concentric braces, while easily meeting damage limitation checks, on the other hand, due to the non-linear and rapidly degrading behaviour of diagonals, and therefore the limited dissipative capacity under cyclic loads,

do not lend themselves to meeting the requirements at the limit state of life protection at destructive events.

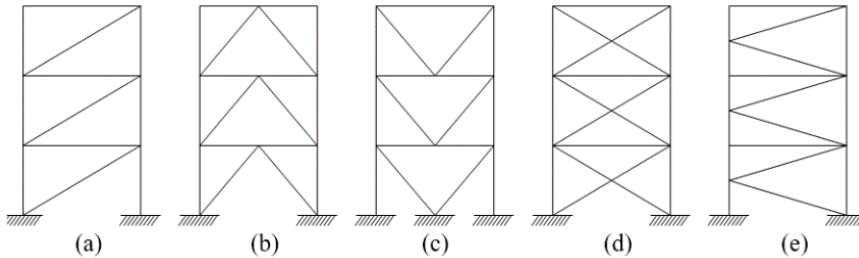


Figure 1.3.2 Concentrically braced frames types: a) single diagonal braced frame; b) inverse "V" braced frame; c) "V" braced frame, d) "X" braced frame; e) "K" braced frame

A good compromise between resistance and ductility is achieved, on the other hand, in eccentric braces. In this type of brace frame, the diagonals are arranged eccentrically with respect to the nodes of the structure, and divide the beams into several parts, depending on the geometric scheme adopted (Figure 1.3.3). The smaller portions in which the beams are divided are called links; these elements dissipate energy by plasticizing by shear or bending. The cyclic behavior of the links is mainly influenced by their length but overall, the hysteresis cycles are wide and stable. This ensures a considerable dissipation capacity of the incoming energy and gives this type of bracing a high ductility that makes it easy to meet the checks at the Near Collapse limit state. On the other hand, the presence of the diagonals in an eccentric position gives a lateral stiffness such as to satisfy the checking for lateral deformation. Finally, these types provide, from an architectural point of view, greater freedom in the positioning of openings than concentric braces.

The research work aims to define a simplified methodology for the assessment of the seismic vulnerability of the existing built heritage. As a result, the focus was on MRFs and CBFs typologies, more widespread in the building scene.

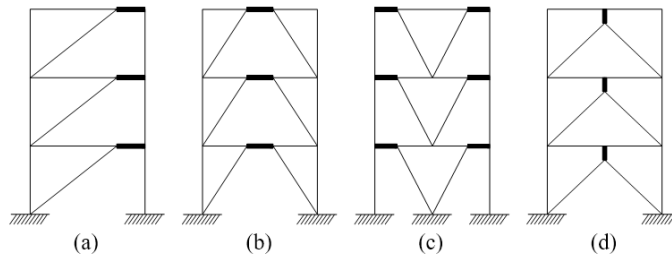


Figure 1.3.3 Eccentrically braced frames types: a) "D" scheme; b) "split-K" scheme; c) "V" scheme; d) "Y" scheme.

1.4 Organization of the work

The dissertation is comprised of seven chapters, and a conclusive section:

CHAPTER 1 provides the background and motivation, objective and scope, and organization of the work.

CHAPTER 2 provides an overall view of the design approaches adopted for the database of buildings used for the calibration of the method. In particular, the Theory of Plastic Mechanism Control is addressed in detail.

CHAPTER 3 provides in the first part the description of the proposed simplified method for MRFs and CBFs. In the following the equations of the branches for the characterization of the non-dimensional pushover curve are addressed.

CHAPTER 4 is based on the calibration procedure adopted to assure a wide applicability of the method. In particular, summary graphs on the accuracy of the method are shown in the final part.

CHAPTER 5 introduces two assessment procedures based on the ADRS spectrum and a formulation proposed by Nassar & Krawinkler.

CHAPTER 6 provides examples of application of the performance-based assessment approach. In particular, three examples for each structural type are reported.

CHAPTER 7 provides the application of the simplified method on simulated designs and the validation through Incremental Dynamic Analysis (IDA). In the final part, summary graphs on the accuracy of the method are shown.

CONCLUSIONS present the summary of the work with some suggestions for future research.

CHAPTER 2

2 DESIGN APPROACHES

2.1 Introduction

Defining a simplified analytical methodology requires a large database of structures to calibrate and validate the procedure. The database was recreated through simulated design of Moment Resisting Frames (MRFs) [6] and Concentrically Braced Frames (CBFs) [9] according to three approaches deriving from the most modern design philosophies, which aim to develop a global collapse mechanism, up to the older ones, which did not include special requirements to be met in response to seismic actions.

Below are the 3 design approaches considered for each structural typology and related synthetic nomenclature that will be used to identify them.

For structures of type Moment Resisting Frames (MRFs):

- Global Moment Resisting Frames (GMRFs)
- Special Moment Resisting Frames (SMRFs)
- Ordinary Moment Resisting Frames (OMRFs)

For structures of type Concentrically Braced Frames (CBFs):

- Global Concentrically Braced Frames (GCBFs)
- Special Concentrically Braced Frames (SCBFs)
- Ordinary Concentrically Braced Frames (OCBFs)

The adjective "Global" refers to structures designed with advanced methodologies capable of ensuring the development of global collapse mechanisms. In particular, reference is made to the "Theory of Plastic

Mechanism Control" which is based on rigid plastic analysis extended to the second-order effects and which allows to achieve the result through a closed-form solution.

The adjective "Special", on the other hand, refers to structures designed by applying the criteria provided by the existing European codes, in particular Eurocode 8, which should avoid the development of single storey mechanisms.

Finally, the adjective "Ordinary" refers to structures designed before modern anti-seismic regulations, and which consequently do not provide for compliance with particular requirements aimed at dissipating incoming seismic energy. Such structures, when faced with a seismic event, generally show "soft storey" collapse mechanisms (design for only horizontal loads).

2.2 Collapse Mechanisms for MRFs and CBFs

The term "collapse mechanism" has been mentioned several times because there is a strong relationship between the type of collapse mechanism developed by the structure, the local ductility, the global ductility, and consequently the seismic performance exhibited under horizontal action.

The (Global) ductility expresses the ability of a structure to exhibit deformations in the plastic field before reaching the structural collapse condition, *i.e.* $\mu = \delta_u / \delta_y$, where δ_u represents the top sway displacement exhibited at the collapse while δ_y top sway displacement corresponding to the elastic limit. The capacity to exhibit inelastic deformations is representative of the structure's ability to dissipate incoming seismic energy, and thus survive the earthquake. It is a function not only of the ductility of the material and the elements (*local ductility*), which are a necessary but not sufficient condition to ensure adequate ductility of the structure (*Global ductility*); structures with elements with high local ductility but distributed in a way that is not consistent with the demand distribution, in fact, can exhibit non dissipative collapse mechanisms, a symptom of low overall ductility of the structure.

In this regard, it is of fundamental importance to highlight that the collapse mechanisms typical of MRF [6] and CBF [10] type structures subject to horizontal forces can be distinguished into three fundamental types (Figure 2.2.1) provided that some specific hypotheses for the structural typology considered are respected, which will be deepened in the following. The three main typologies are completed by the global collapse mechanism, which is a particular case of type 2 collapse mechanism [22],[23].

The explanation of the various collapse mechanisms will take place with reference to the "mechanism i_m indices". They are plan indicators that allow to identify the collapse mechanism and define its extension in association with the mechanism typology.

Type 1 collapse mechanisms are partial mechanisms called "Lower partial" because they involve the first i_m storeys. In this case, the higher is the mechanism index, the more are plans involved into the collapse mechanism. Type 2 collapse mechanisms are partial mechanisms called "Upper partial" since they involve storeys from i_m to n_s , being n_s the total number of storeys. In this case, the lower is the mechanism index, the more are storeys involved in the collapse mechanism. Type 3 collapse mechanisms, on the other hand, are local collapse mechanisms, also called "soft storey", which involve only the columns of the storey i_m to dissipate the incoming energy. For each of the types of collapse mechanisms identified, n_s mechanisms are possible ($i_m = 1, 2, \dots, n_s$). Then there is the global collapse mechanism (type 2 mechanism with i_m equal to 1) which is optimal from the point of view of structural ductility and the ability to dissipate the incoming seismic energy being characterized by the involvement in the plastic field of all the dissipative elements of the structure.

Differently, the single storey or "soft storey" mechanisms lead to collapse through the formation few plastic hinges, i.e. to the head and foot of the columns of the same storey. These hinges are also placed in members, the columns, characterized by having low local ductility supplies due to the influence of axial force.

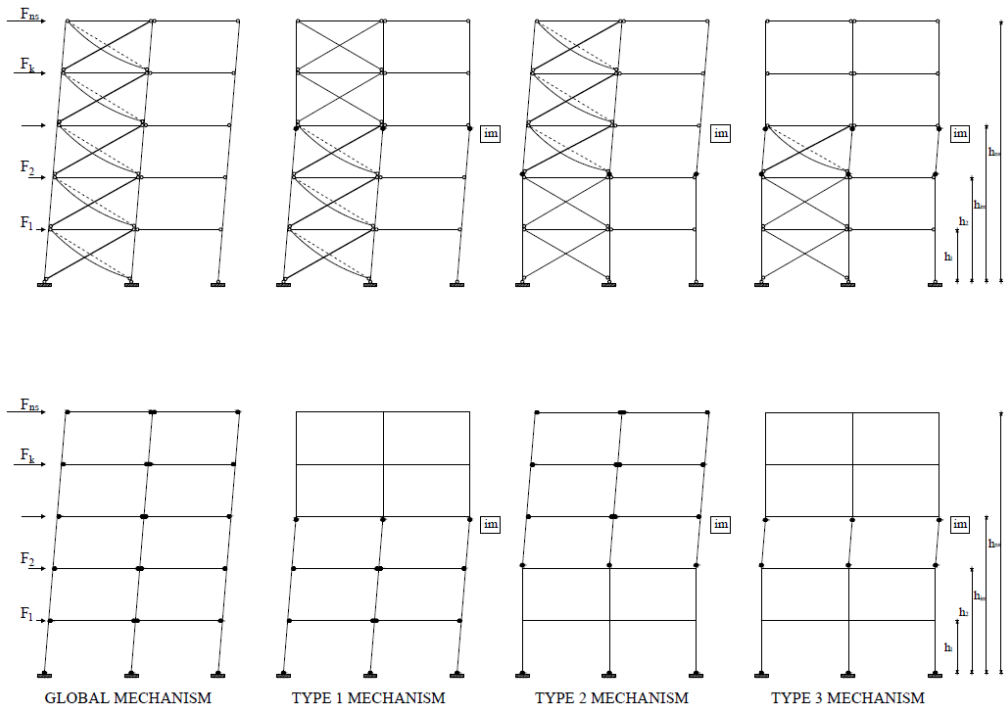


Figure 2.2.1 Collapse mechanism types for CBFs and MRFs

It is possible to confirm what has been said through rigid-plastic analysis, that is, in the hypothesis of simultaneous formation of all plastic hinges, it can be noted that the plastic rotation required at the hinges for a fixed value of the plastic displacement δ_p at the top of the structure, is given by:

$$\theta_p = \frac{\delta}{H_0} \quad (2.2.1)$$

Where H_0 is the sum of the interstorey heights of the storeys involved into the collapse mechanism; Therefore:

- type 1 mechanisms: $H_0 = h_{im}$
- type 2 mechanisms: $H_0 = h_{ns} - h_{im-1}$
- type 3 mechanisms: $H_0 = h_{im} - h_{im-1}$
- global mechanism: $H_0 = h_{ns}$

The maximum value of H_0 is achieved in the case of a global collapse mechanism, in which H_0 coincides with the height of the entire building and minimum value in the case of soft storey mechanisms where H_0 coincides with the interstorey height of the only storey involved into the collapse mechanism. Therefore, it is evident that, when a lateral displacement limit value is set, the global collapse mechanism leads to the minimum demand for plastic rotation, i.e, translated in terms of ductility, to the minimum local ductility demand. Finally, it is important to note that the type of collapse mechanism also influences structural sensitivity to second-order effects in the plastic field. This sensitivity is maximum in the case of soft storey mechanisms and minimum for global mechanisms. Of course, partial collapse mechanisms lead to intermediate inelastic performance between those of the global mechanism and those of the soft storey mechanisms.

2.3 Theory of Plastic Mechanism Control: Generalities

The Theory of the Plastic Mechanism Control [22],[23] is based on the extension, to the mechanism equilibrium curve, of the of the kinetic theorem of the plastic collapse which is one of the fundamental theorems of the limit analysis. The kinematic theorem states that the collapse multiplier is the minimum among all the kinetically admissible multipliers. Thanks to TPMC, rigid-plastic analysis is for the first time recognised as a useful tool for seismic design of structures.

In particular, TPMC allows the theoretical solution to the problem of designing a structure failing in global mode, i.e. assuring the plasticization of all the dissipative zones before the collapse mechanism develops. The sections of the dissipative members are assumed to be known quantities, because they are preliminarily designed to withstand vertical loads according to the non-seismic load combination, or to withstand the design value of the seismic horizontal forces, according to the considered structural typology, while the unknowns of the design problem are the column sections needed to assure the desired collapse mechanism, i.e. the global mechanism.

According to the theory of limit analysis, the assumption of a rigid-plastic behaviour of the structure until the complete development of a collapse mechanism is made. It means that the attention is focused on the condition the structure exhibits in the collapse state by neglecting each intermediate condition.

However, the simple application of the kinematic theorem of plastic collapse is not sufficient to assure the desired collapse mechanism, because high horizontal displacements occur before the complete development of the kinematic mechanism. These displacements give rise to significant second-order effects which cannot be neglected in the seismic design of structures. Therefore, the basic principle of TPMC is essentially constituted by the extension of the kinematic theorem of plastic collapse to the concept of mechanism equilibrium curve. Within the framework of a kinematic approach, for any given collapse mechanism, the mechanism equilibrium curve can be easily derived by equating the external work to the internal work due to the plastic hinges involved in the collapse mechanism, provided that the external second-order external work due to vertical loads is also evaluated.

In this way the mechanism equilibrium curve is a straight line having the following form:

$$\alpha = \alpha_0 - \gamma_s \delta \quad (2.3.1)$$

where α_0 is the collapse multiplier of horizontal forces according to first-order rigid-plastic analysis and γ_s is the (non-dimensional) slope of the mechanism equilibrium curve.

In the framework of the limit analysis, the collapse multiplier is intended as the scalar value the actions have to be increased by to reach the structure collapse, namely the development of the collapse mechanism. In common practice, reference is made to the first-order analysis given on the undeformed configuration. However, as steel frames are more prone to exhibit overall buckling phenomena due to their intrinsic slenderness, the sensitivity to second-order effects cannot be neglected. For this reason, the kinematic theorem of plastic collapse is extended to second-order effects on the deformed shape by the concept of collapse mechanism equilibrium curve, thus introducing the second-order collapse multiplier. The sensitivity to second-order effects is directly related to the slope of the mechanism equilibrium curve γ_s .

According to the extension to the mechanism equilibrium curve of the kinetic theorem of the plastic collapse, it can be stated that:

given the sections of the columns, of the dissipative members, and the static force distribution, the mechanism that will be more prone to develop is the one corresponding to the curve characterized by the lower values of α , in the range of displacements compatible with the local ductility resources.

From a checking point of view, the procedure will result in the determination of the first order collapse multipliers α_0 and the slopes γ_s of the collapse mechanism equilibrium curve for each possible triggering collapse mechanism of a pre-designed structure. The triggering mechanism will be the one corresponding to the curve characterized by the lower values of α , in the range of displacements compatible with the local ductility supplies.

From a design point of view, the objective is to obtain a global collapse mechanism. Consequently, to avoid all the undesired collapse mechanisms, the design condition must be the following:

the mechanism equilibrium curve corresponding to the global mechanism must be located below those corresponding to all the undesired mechanisms in a range of displacements δ compatible with the local ductility supplies.

This design procedure has been applied to different structural typologies. In the thesis work the application on Moment Resisting Frames (MRFs) and Concentrically Braced Frames (CBFs) will be reported.

2.4 Global Moment Resisting Frames Design

The TPMC applied to MRFs [22] allows the theoretical solution of the problem of designing a structure failing in global mode, i.e. assuring that plastic hinges develop only at beam ends while all the columns remain in elastic range with the only exception of base sections at first storey columns. The beam sections are assumed to be known quantities, because they are preliminarily designed to withstand vertical loads according to the non-seismic load combination, or to withstand the design value of the seismic horizontal forces while the unknowns of the design problem are the column sections needed to assure the desired collapse mechanism, i.e. the global mechanism.

In the following, for the sake of simplicity, reference is made to the case of uniform vertical loads acting on the beams satisfying the limitation:

$$q_{jk} \leq \frac{4M_{b,jk}}{l_j^2} \quad (2.4.1)$$

where q_{jk} is the uniform vertical load applied to the beam of j -th bay and k -th storey, $M_{b,jk}$ is the corresponding beam plastic moment and l_j is the j -th bay span. Such limitation assures that beam plastic hinges develop at the beam ends. In case of vertical loads exceeding the above limit the second plastic hinge in the beam develops in an intermediate section, so that the external work due to the uniform vertical loads has also to be considered.

In the case of global mechanism, the external work is given due to a virtual rotation $d\theta$ of columns plastic hinges is given by

$$W_e = \alpha_0^{(g)} \left(\sum_{k=1}^{n_s} F_k h_k \right) d\theta + \frac{\delta \sum_{k=1}^{n_s} V_k h_k}{h_{n_s} \sum_{k=1}^{n_s} F_k h_k} d\theta \quad (2.4.2)$$

where α is the multiplier of horizontal forces, F_k and h_k are, respectively, the seismic force applied at k -th storey and the k -th storey height with respect to the foundation level, h_{n_s} is the value of h_k at the top storey, δ is the top sway displacement and V_k is the total vertical load acting at k -th storey.

Equation (2.4.2) has been derived considering work due to the vector of vertical and horizontal virtual displacements, defined according to Figure 2.4.1.

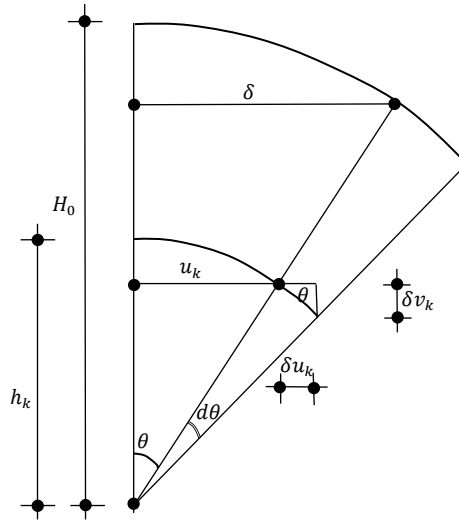


Figure 2.4.1 Second order vertical displacements

From the analysis of the figure, in case of small displacements, it is possible to define the k-th component of the vector of virtual horizontal displacements as:

$$du_k = h_k \cos\theta d\theta \approx h_k d\theta \quad (2.4.3)$$

Where h_k is the height of the considered storey level and $d\theta$ is the virtual rotation.

The vector of virtual vertical displacements has the same shape of the one of horizontal displacements and can be expressed as:

$$dv_k = \frac{\delta}{h_{ns}} h_k d\theta \quad (2.4.4)$$

Consequently, equation (2.4.3) will allow determining the first order external work, due to the horizontal forces (first term of Eq.(2.4.2)), while equation (2.4.4) the second order external work, due to the vertical loads (second term of Eq.(2.4.2)).

2.4.1 First-Order Collapse Multipliers and Slopes of the Mechanism Equilibrium Curve for MRFs

The internal work due to a virtual rotation $d\theta$ of column plastic hinges can be easily computed considering the work due to the dissipative zones activated by the triggering collapse mechanism.

- **Global collapse mechanism**

In the case of global collapse mechanism, it can be computed as:

$$W_i = \left(\sum_{i=1}^{n_c} M_{ci.1} + 2 \sum_{k=1}^{n_s} \sum_{j=1}^{n_b} M_{b.jk} \right) d\theta \quad (2.4.5)$$

where $M_{ci.1}$ is the plastic moment of i -th column of the first storey reduced due to the contemporary action of the axial force; n_c , n_b and n_s are the number of columns, bays and storeys, respectively.

The mechanism equilibrium curve for the global collapse mechanism can be derived by equating the internal work to the external one (Eq.(2.4.5), Eq.(2.4.2)) and can be written as:

$$\alpha^{(g)} = \frac{\sum_{k=1}^{n_c} M_{c.i1} + 2 \sum_{k=1}^{n_s} \sum_{j=1}^{n_b} M_{b.jk}}{\sum_{k=1}^{n_s} F_k h_k} - \frac{1}{h_{n_s}} \frac{\sum_{k=1}^{n_s} V_k h_k}{\sum_{k=1}^{n_s} F_k h_k} \delta \quad (2.4.6)$$

where the kinematically admissible multiplier of horizontal forces according to first-order rigid plastic analysis $\alpha_0^{(g)}$ is given by:

$$\alpha_0^{(g)} = \frac{\sum_{k=1}^{n_c} M_{c.i1} + 2 \sum_{k=1}^{n_s} \sum_{j=1}^{n_b} M_{b.jk}}{\sum_{k=1}^{n_s} F_k h_k} \quad (2.4.7)$$

And the slope of the mechanism equilibrium curve $\gamma^{(g)}$ by:

$$\gamma^{(g)} = \frac{1}{h_{n_s}} \frac{\sum_{k=1}^{n_s} V_k h_k}{\sum_{k=1}^{n_s} F_k h_k} \quad (2.4.8)$$

The procedure for the definition of the mechanism equilibrium curves for all the considered collapse mechanisms exploits the same assumptions reported in the global case. The only difference lies in the specific collapse configuration which, for each mechanism, will lead to a different definition of the collapse multiplier α_0 and the slope γ .

For the sake of simplicity, the collapse multipliers α_0 and the slopes γ for each mechanism typology considered, are reported in a schematic way.

- **Type 1 collapse mechanisms**

With reference to i_m th mechanism of type 1, the first order collapse multiplier of seismic horizontal forces $\alpha_{0.i_m}^{(1)}$ is given by:

$$\alpha_{0.i_m}^{(1)} = \frac{\sum_{i=1}^{n_c} M_{c.i.i_m} + 2 \sum_{k=1}^{i_m-1} \sum_{j=1}^{n_b} M_{b.jk} + \sum_{i=1}^{n_c} M_{c.i.i_m}}{\sum_{k=1}^{i_m} F_k h_k + h_{i_m} \sum_{k=i_m+1}^{n_s} F_k} \quad (2.4.9)$$

while $\gamma_{i_m}^{(1)}$ is the slope of the Type 1 mechanism equilibrium curve, and can be reported as:

$$\gamma_{i_m}^{(1)} = \frac{1}{h_{i_m}} \frac{\sum_{k=1}^{i_m} V_k h_k + h_{i_m} \sum_{k=i_m+1}^{n_s} V_k}{\sum_{k=1}^{i_m} F_k h_k + h_{i_m} \sum_{k=i_m+1}^{n_s} F_k} \quad (2.4.10)$$

- **Type 2 collapse mechanisms**

With reference to i_m th mechanism of type 2, the first order collapse multiplier of seismic horizontal forces $\alpha_{0.i_m}^{(2)}$ is given by:

$$\alpha_{0.i_m}^{(2)} = \frac{\sum_{i=1}^{n_c} M_{c.i.i_m} + 2 \sum_{k=i_m}^{n_s} \sum_{j=1}^{n_b} M_{b.jk}}{\sum_{k=i_m}^{n_s} F_k (h_k - h_{i_m-1})} \quad (2.4.11)$$

while $\gamma_{i_m}^{(2)}$ is the slope of the Type 2 mechanism equilibrium curve, and can be reported as:

$$\gamma_{i_m}^{(2)} = \frac{1}{h_{n_s} - h_{i_m-1}} \frac{\sum_{k=i_m}^{n_s} V_k (h_k - h_{i_m-1})}{\sum_{k=i_m}^{n_s} F_k (h_k - h_{i_m-1})} \quad (2.4.12)$$

- **Type 3 collapse mechanisms**

With reference to i_m -th mechanism of type 3 (“Soft Storey” mechanisms), the first order collapse multiplier of seismic horizontal forces $\alpha_{0.i_m}^{(3)}$ is given by:

$$\alpha_{0.i_m}^{(3)} = \frac{2 \sum_{i=1}^{n_c} M_{c.i.i_m}}{(h_{i_m} - h_{i_m-1}) \sum_{k=i_m}^{n_s} F_k} \quad (2.4.13)$$

while $\gamma_{im}^{(3)}$ is the slope of the Type 1 mechanism equilibrium curve, and can be reported as:

$$\gamma_{im}^{(3)} = \frac{1}{h_{i_m} - h_{i_m-1}} \frac{\sum_{k=i_m}^{n_s} V_k}{\sum_{k=i_m}^{n_s} F_k} \quad (2.4.14)$$

The design conditions to be fulfilled in order to avoid all the undesired collapse mechanisms require that the mechanism equilibrium curve corresponding to the global mechanism has to be located below those corresponding to all the undesired mechanisms within a top sway displacement range, δ_u , compatible with the ductility supply of structural members.

The considerations just made lead to define the design conditions that must be verified for each mechanism index and for every typology:

$$\alpha_0^{(g)} - \gamma^{(g)} \delta_u \leq \alpha_{0.i_m}^{(t)} - \gamma_{i_m}^{(t)} \delta_u \quad \text{for } t=1, \dots, 3 \quad i_m=1, \dots, n_s \quad (2.4.15)$$

Equation (2.4.15) constitutes the statement of the theory of plastic mechanism control and it is valid independently of the structural typology.

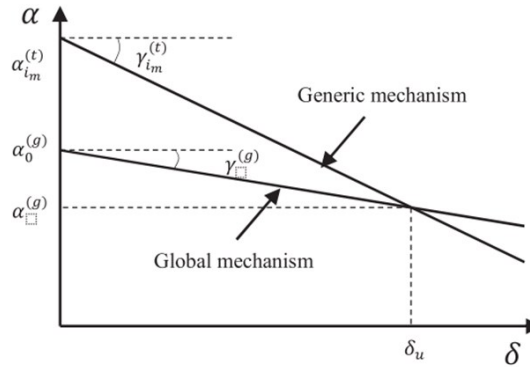


Figure 2.4.2 Design condition

2.4.2 TPMC Design steps for MRFs

The TPMC presents a solution in closed form thanks to some considerations about the collapse mechanisms. The mechanism of type 1 and type 3 for $i_m=1$ are coincident, as are the mechanism of type 2 and global.

In particular, the solution is obtained according to the following steps:

- a) Selection of a design top sway displacement δ_u compatible with the ductility supplies of structural members. To this scope, in the following, the plastic rotation capacity is assumed equal to 0.04 rad so that $\delta_u = 0.04 h_{ns}$ where h_{ns} is the height of the structure.
- b) Computation of the slopes of mechanism equilibrium curves $\gamma_{im}^{(t)}$ by means of Equations (2.4.10), (2.4.12) and (2.4.14). The slope of the global mechanism equilibrium curve $\gamma^{(g)}$ is provided by Equation (2.4.8) and it's the minimum among the $\gamma_{im}^{(t)}$ values computed before.
- c) Design of first storey columns sections. This is probably the most important design step. Referring to the case where the frame is orthogonal to the secondary beams of the deck, the vertical loads lead the design of the beams. Consequently, the preliminary design of the beams can be carried out by estimating the maximum bending moment that occurs in the combination of non-seismic loads. According to these premises, In such a case (high gravity loads), the required sum of plastic moment of columns, reduced due to the contemporary action of the axial force, $\sum_{i=1}^{n_c} M_{c.i.1}$, for $i_m = 1$, i.e. at the first storey, to avoid the development of undesired collapse mechanisms, is computed by means of the following relation:

$$\sum_{i=1}^{n_c} M_{c.i.1} \geq \frac{2 \sum_{k=1}^{n_s} \sum_{j=1}^{n_b} M_{b.jk} + (\gamma_1^{(3)} - \gamma^{(g)}) \delta_u \sum_{k=1}^{n_s} F_k h_k}{2 \frac{\sum_{k=1}^{n_s} F_k h_k}{h_1 \sum_{k=1}^{n_s} F_k} - 1} \quad (2.4.16)$$

The second case occurs when the moment resisting frame is parallel to the secondary beams of the decks. In such a case, being the tributary area for the gravity loads small, the simple design of beams for vertical loads only would lead to beam sections too small which could be not sufficient

In this second case, it is desirable to have the distribution of the beam flexural strength along the building height that follows the distribution of the design storey shears, i.e. $M_{b.jk} = \beta_k M_{b.jn_s}$ where β_k is the ratio between the design seismic shear at k-th storey and the design seismic shear at the top storey.

- d) The sum of the required plastic moments of columns at first storey is distributed among the columns proportionally to the axial load

acting at the collapse state, so that, the design internal actions ($M_{c.i1}, N_{c.i1}$ for $i = 1, 2, \dots, n_c$) are derived and the column sections at first storey can be designed. As column sections are selected from standard shapes, the value obtained of $\sum_{i=1}^{n_c} M_{c.i.1}$, namely $\sum_{i=1}^{n_c} M_{c.i.1}^*$ is generally greater than the required minimum value provided by Eq. (2.4.16).

- e) Computation of the required sum of plastic moment of columns, reduced due to the contemporary action of the axial force, $\sum_{i=1}^{n_c} M_{c.i.i_m}^{(t)}$, for $i_m > 1$ and $t = 1, 2, 3$ by means of the following relations:

$$\sum_{i=1}^{n_c} M_{c.i.i_m}^{(1)} \geq \left(\alpha^{(g)} + \gamma_{i_m}^{(1)} \delta_u \right) \left(\sum_{k=1}^{i_m} F_k h_k + h_{i_m} \sum_{k=i_m+1}^{n_s} F_k \right) - \sum_{i=1}^{n_c} M_{c.i.1}^* - 2 \sum_{k=1}^{i_m-1} \sum_{j=1}^{n_b} M_{b.jk} \quad (2.4.17)$$

needed to avoid type 1 mechanisms;

$$\sum_{i=1}^{n_c} M_{c.i.i_m}^{(2)} \geq \left(\alpha^{(g)} + \gamma_{i_m}^{(2)} \delta_u \right) \sum_{k=i_m}^{n_s} F_k (h_k - h_{i_m-1}) - 2 \sum_{k=i_m}^{n_s} \sum_{j=1}^{n_b} M_{b.jk} \quad (2.4.18)$$

needed to avoid type 2 mechanisms;

$$\sum_{i=1}^{n_c} M_{c.i.i_m}^{(3)} \geq \left(\alpha^{(g)} + \gamma_{i_m}^{(3)} \delta_u \right) \frac{(h_{i_m} - h_{i_m-1})}{2} \sum_{k=i_m}^{n_s} F_k \quad (2.4.19)$$

needed to avoid type-3 mechanisms.

Equations (2.4.16)-(2.4.19) have been directly derived from Eq. (2.4.15) for $i_m > 1$ and $t = 1$, $t = 2$ and $t = 3$, respectively.

- f) Computation of the required sum of the reduced plastic moments of columns for each storey as the maximum value among those coming from the above design conditions:

$$\sum_{i=1}^{n_c} M_{c.i.i_m} = \max \left\{ \sum_{i=1}^{n_c} M_{c.i.i_m}^{(1)}, \sum_{i=1}^{n_c} M_{c.i.i_m}^{(2)}, \sum_{i=1}^{n_c} M_{c.i.i_m}^{(3)} \right\} \quad (2.4.20)$$

- g) The sums of the required plastic moments of the columns on each floor, reduced for the simultaneous action of the axial force, are distributed among all the columns of the storey proportionally to the axial force acting in collapse condition. The knowledge of the plastic moments $M_{c.i.i_m}$, coupled with the axial forces in collapse conditions $N_{c.i.i_m}$, allows to design the columns by selecting them using standard shapes.
- h) If necessary, a technological condition is imposed by requiring, starting from the base, that the column sections cannot increase along the building height. If this condition requires the change of column sections at first storey then the procedure needs to be repeated from point e). In fact, in this case, a new value of $\sum_{i=1}^{n_c} M_{c.i.1}^*$ is obtained and, as a consequence, the value of the sum of the required plastic moments of columns at each storey changes.

2.5 Global Concentrically Braced Frames design

In the case of CBF systems (reference is made to simple “X-shaped” CBFs) [9],[11],[12], the global mechanism is characterised by the yielding of all the tensile diagonals while the compressed ones are buckled. The control of the failure mode requires the analysis of $3n_s$ mechanisms (being n_s the number of storeys). The beam sections are designed to withstand vertical loads while the diagonal sections are designed for a given percentage of the design horizontal forces. Therefore, diagonal sections are considered as input data of the design problem.

Consequently, the only unknowns of the design procedure are the column sections.

According to TPMC, column sections are designed by imposing that the mechanism equilibrium curve corresponding to the global mechanism has to be located below those corresponding to all the undesired partial or soft-storey

mechanisms within a top sway displacement range compatible with the plastic deformation capacity of members.

Regarding the calculation of first-order kinematically admissible multiplier of horizontal forces, it is preliminarily convenient to define the internal work $W_{d,jk}$ due to dissipative zones (diagonal braces) of j -th bay of k -th storey, occurring for a unit virtual rotation of plastic hinges of columns:

$$W_{d,jk} = N_{t,jk} \cdot e_{t,jk} + N_{c,jk}(\delta) \cdot e_{c,jk} \quad (2.5.1)$$

where $e_{t,jk} = e_{c,jk} = (h_k - h_{k-1}) \cdot \cos \beta_{jk}$ represent, respectively, the elongation of tensile diagonal and the shortening of the buckled compressed diagonal of j -th bay of k -th storey, occurring for a unit virtual rotation of plastic hinges of columns; h_k is the storey height of k -th storey with respect to the foundation; β_{jk} is the inclination of the diagonal of k -th storey and j -th bay with respect to the horizontal direction; L_j is the bay span. In addition, $N_{t,jk}$ is the yielding axial force of the tensile diagonal of j -th bay of k -th storey, and $N_{c,jk}$, for the same bay and the same storey, is the axial force in the compressed diagonal accounting for the post-buckling behaviour according to Georgescu's model (Figure 2.5.1).

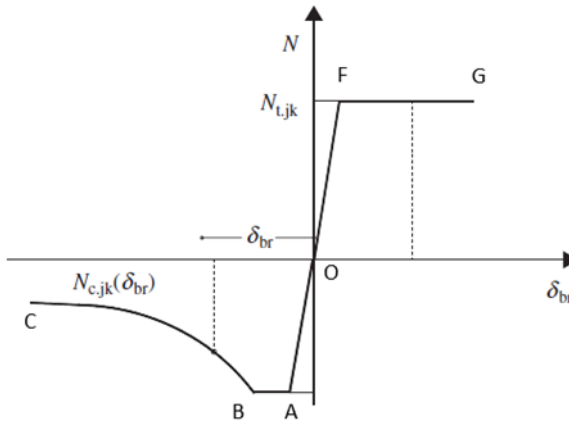


Figure 2.5.1 Evaluation of compression and tension axial force depending on diagonal axial deformation.

The compressive acting axial force is dependent on the shortening δ_{br} of the diagonal braces which is related to the ultimate top sway displacement δ_u . Depending on the collapse mechanism, δ_{br} can be computed according to the following relationships:

$$\delta_{br} = \frac{\delta_u}{H_0} \cdot h_i \cdot \cos \beta \quad (2.5.2)$$

where h_i is the interstorey height, β is the inclination of the generic diagonal referred to the horizontal direction and H_0 is the sum of inter-storey heights of storeys involved in the collapse mechanism. More precisely, $H_0 = h_{im}$, $H_0 = h_{ns} - h_{im-1}$ and $H_0 = h_{im} - h_{im-1}$ for im-th mechanism of type-1, type-2 and type-3, respectively.

The ultimate top sway displacement δ_u is defined as a function of the interstorey drift limit:

$$\varphi_{max} = \max_{i=1}^n \varphi_i = \max_{i=1}^n \frac{\delta_{br.lim}}{h_i \cdot \cos \beta_i} \quad (2.5.3)$$

$$\delta_u = \varphi_{max} \cdot H_0 \quad (2.5.4)$$

where $\delta_{br.lim}$ is the limit value of elongation for the diagonal members (Figure 2.5.2.a)

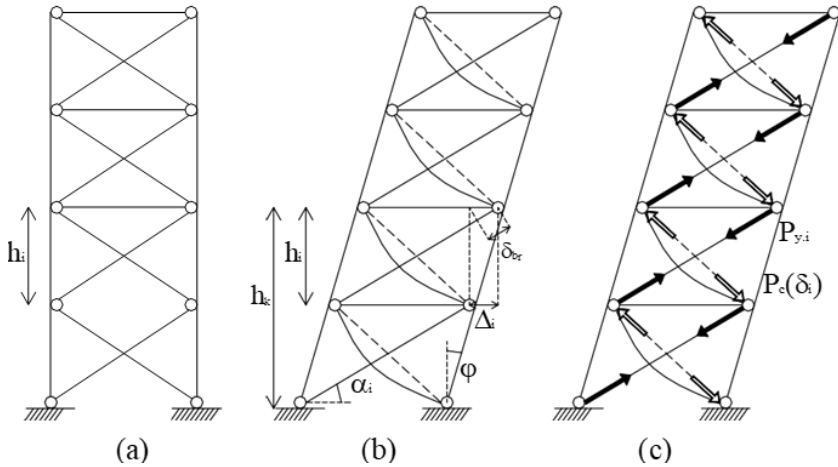


Figure 2.5.2 a) Undeformed configuration; b) collapse configuration; c) axial forces transmitted at the collapse by dissipative elements.

For design purposes, obviously, $H_0 = h_{ns}$ in the case of global collapse mechanism.

Concerning the axial force $N_{c,jk}$ that needs to be evaluated to compute the plastic moment of columns $M_{c,jk}$ reduced by the effect of the axial load, reference

has to be made to the distribution of internal actions occurring at collapse. This evaluation can be easily carried out starting from the knowledge of the forces which the diagonal members transmit to the columns in collapse condition (Figure 2.5.2.c)

As regards the external work, it can be computed starting from the same considerations made for Moment Resisting Frames. In fact, the external work depends on the collapse configuration of the structure and, for assumption, MRFs and CBFs are characterized by the same possible triggering collapse mechanisms (Figure 2.2.1).

2.5.1 First-Order Collapse Multipliers and Slopes of the Mechanism Equilibrium Curve for MRFs

By means of the virtual work principle, the first-order kinematically admissible multiplier of horizontal forces and the slopes of the mechanism equilibrium curve can be easily evaluated for all the possible collapse mechanisms. The following relationships are obtained:

- **Global collapse mechanism**

The kinematically admissible multiplier of horizontal forces according to first-order rigid plastic analysis $\alpha_0^{(g)}$ is given by:

$$\alpha_0^{(g)} = \frac{\sum_{k=1}^{n_s} \sum_{j=1}^{n_b} W_{d,jk}}{\sum_{k=1}^{n_s} F_k h_k} \quad (2.5.5)$$

And the slope of the mechanism equilibrium curve $\gamma^{(g)}$ by:

$$\gamma^{(g)} = \frac{1}{h_{n_s}} \frac{\sum_{k=1}^{n_s} V_k h_k}{\sum_{k=1}^{n_s} F_k h_k} \quad (2.5.6)$$

- **Type 1 collapse mechanisms**

With reference to i_m th mechanism of type 1, the first order collapse multiplier of seismic horizontal forces $\alpha_{0,i_m}^{(1)}$ is given by:

$$\alpha_{0,i_m}^{(1)} = \frac{\sum_{k=1}^{i_m-1} \sum_{j=1}^{n_b} W_{d,jk} + \sum_{i=1}^{n_c} M_{c,ii_m}}{\sum_{k=1}^{i_m} F_k h_k + h_{i_m} \sum_{k=i_m+1}^{n_s} F_k}; \quad i_m = 1, 2, \dots, n_s-1 \quad (2.5.7)$$

For $i_m = n_s$, $\alpha_{0,n_s}^{(1)} = \alpha_0^{(g)}$

while $\gamma_{im}^{(1)}$ is the slope of the Type 1 mechanism equilibrium curve, and can be reported as:

$$\gamma_{im}^{(1)} = \frac{1}{h_{i_m}} \frac{\sum_{k=1}^{i_m} V_k h_k + h_{i_m} \sum_{k=i_m+1}^{n_s} V_k}{\sum_{k=1}^{i_m} F_k h_k + h_{i_m} \sum_{k=i_m+1}^{n_s} F_k} \quad (2.5.8)$$

- **Type 2 collapse mechanisms**

With reference to i_m th mechanism of type 2, the first order collapse multiplier of seismic horizontal forces $\alpha_{0.i_m}^{(2)}$ is given by:

$$\alpha_{0.i_m}^{(2)} = \frac{\sum_{k=i_m}^{n_s} \sum_{j=1}^{n_b} W_{d.jk} + \sum_{i=1}^{n_c} M_{c.ii_m}}{\sum_{k=i_m}^{n_s} F_k \cdot (h_k - h_{i_m-1})}; \quad i_m = 2, 3, \dots, n_s \quad (2.5.9)$$

$$\text{for } i_m = 1, \alpha_{0.1}^{(2)} = \alpha_0^{(g)}$$

while $\gamma_{im}^{(2)}$ is the slope of the Type 1 mechanism equilibrium curve, and can be reported as:

$$\gamma_{im}^{(2)} = \frac{1}{h_{n_s} - h_{i_m-1}} \frac{\sum_{k=i_m}^{n_s} V_k (h_k - h_{i_m-1})}{\sum_{k=i_m}^{n_s} F_k (h_k - h_{i_m-1})} \quad (2.5.10)$$

- **Type 3 collapse mechanisms**

With reference to i_m th mechanism of type 3 (“Soft Storey” mechanisms), the first order collapse multiplier of seismic horizontal forces $\alpha_{0.i_m}^{(3)}$ is given by:

$$\alpha_{0.i_m}^{(3)} = \frac{2 \cdot \sum_{i=1}^{n_c} M_{c.ii_m} + \sum_{j=1}^{n_b} W_{d.ji_m}}{(h_{i_m} - h_{i_m-1}) \cdot \sum_{k=i_m}^{n_s} F_k}; \quad 2 < i_m < n_s \quad (2.5.11)$$

$$\alpha_{0.n_s}^{(3)} = \frac{\sum_{i=1}^{n_c} M_{c.in_s} + \sum_{j=1}^{n_b} W_{d.jn_s}}{(h_{n_s} - h_{n_s-1}) \cdot F_{n_s}}; \quad i_m = n_s \quad (2.5.12)$$

$$\alpha_{0.1}^{(3)} = \frac{\sum_{i=1}^{n_c} M_{c.i1} + \sum_{j=1}^{n_b} W_{d.j1}}{h_1 \cdot \sum_{k=1}^{n_s} F_k}; \quad i_m = 1 \quad (2.5.13)$$

while $\gamma_{im}^{(3)}$ is the slope of the Type 1 mechanism equilibrium curve, and can be reported as:

$$\gamma_{i_m}^{(3)} = \frac{1}{h_{i_m} - h_{i_m-1}} \frac{\sum_{k=i_m}^{n_s} V_k}{\sum_{k=i_m}^{n_s} F_k} \quad (2.5.14)$$

where n_c , n_b and n_s are, respectively, the number of columns, bays and storeys; $M_{c,ik}$ is the plastic moment of i th column of k -th storey, reduced due to the contemporaneous action of the axial force; $M_{b,jk}$ is the plastic moment of the beam of j -th bay of k -th storey; q_{jk} is the vertical uniform load acting on the beam of j -th bay of k -th storey and, finally, F_k is the design horizontal force applied at k -th storey and V_k is the total vertical load acting at k -th store. With respect to the axial force $N_{c,jk}$ that needs to be evaluated to compute the plastic moment $M_{c,jk}$ reduced to account for M–N interaction, reference has to be made to the distribution of internal actions occurring at collapse (Figure 2.5.2.c)

2.5.2 TPMC Design steps for simple CBFs

In order to assure the development of the desired global mechanism, according to TPMC, column sections have to be designed by imposing that the mechanism equilibrium curve corresponding to the global mechanism is located below those corresponding to all the other undesired partial mechanisms up to a selected design ultimate top sway displacement δ_u compatible with the plastic deformation capacity of members.

The design condition for GCBFs can be expressed as:

$$\alpha_0^{(g)} - \gamma^{(g)} \delta_u \leq \alpha_{i_m}^{(t)} - \gamma_{i_m}^{(t)} \delta_u \quad (2.5.15)$$

with $i_m = 1, 2, 3, \dots, n_s$ and $t = 1, 2, 3$.

The design procedure can be summarised into the following steps:

(a) Design of beam and diagonal sections to withstand vertical loads and seismic horizontal forces, respectively.

(b) Selection of the design top sway displacement δ_u depending on the ductility supply of dissipative zones. In the specific case, the limitations defined by Eurocode 8 for tensile and compressed diagonals have been used. As a function of the extensional limit, a drift limitation has been derived. Consequently, the ultimate displacement has been computed as $\delta_u = \varphi_{lim} h_{ns}$ is assumed, where h_{ns} is the overall height of the structure and φ_{lim} is the drift limitation.

(c) Computation of the axial load acting at collapse state in the columns. This step can be easily carried out considering that, when the global mechanism is completely developed, the column axial forces can be obtained, at each storey, from the sum of the shear forces transmitted by the beam ends and the vertical component of axial forces occurring in diagonal braces. Obviously, beams and diagonal braces at and above the analysed storey need to be considered.

(d) Design of first storey column sections by computing the required sum of plastic moment of columns, reduced due to the contemporaneous action of the axial load, by means of the following relation:

$$\sum_{i=1}^{n_c} M_{c,i1} \geq \frac{\sum_{k=1}^{n_s} \sum_{j=1}^{n_b} W_{d,jk} + \sum_{k=1}^{n_s} F_k h_k (\gamma_1^{(3)} - \gamma^{(g)}) \delta_u - \frac{\sum_{k=1}^{n_s} F_k h_k}{F_k h_k + h_1 \sum_{k=1}^{n_s} F_k} \sum_{j=1}^{n_b} W_{d,j1}}{\frac{\sum_{k=1}^{n_s} F_k h_k}{F_k h_k + h_1 \sum_{k=1}^{n_s} F_k}} \quad (2.5.16)$$

Equation (2.5.16) is derived from design conditions (2.5.15) for $i_m = 1$ and $t = 1$ or $t = 3$ (because for $i_m = 1$, type 1 mechanism and type 3 mechanism are coincident). In addition, it is important to underline that, for $i_m = 1$, type 2 mechanism is coincident with the global mechanism, so that Equation (2.5.15) becomes an identity. This observation is of paramount importance from a practical point of view because it allows to design the first-storey columns directly by means of Equation (2.5.16) and to avoid any iterative procedure providing a closed-form solution easy to be applied by hand calculations.

As soon as the sum of plastic moments of first storey columns has been computed according to Equation (2.5.16), the plastic moment of i -th column is derived by assuming that the above sum is distributed among the different columns proportionally to the corresponding axial force $N_{c,il}$ obtained according to step (c). Therefore, the column section can be selected from standard shapes by imposing that the point representative of internal actions ($M_{c,il}$; $N_{c,il}$) is located inside or, at least, on the boundary line of the design M–N plastic domain.

(e) Because of the selection of column sections from standard shapes, some column overstrength can occur. Therefore, the bending moment $M^*_{c,il}$ corresponding to $N_{c,il}$ on the boundary line of the design M–N plastic domain is $M^*_{c,il} \geq M_{c,il}$, and the equations depending on $M_{c,il}$ need to be computed applying $M^*_{c,il}$ instead of $M_{c,il}$.

(f) Computation of the required sum of plastic moments of columns, reduced due to the contemporaneous action of the axial load, for $i_m > 1$, by means of the following relations needed to avoid type-1, type-2 and type-3 mechanisms, respectively:

for mechanism of type 1

$$\sum_{i=1}^{n_c} M_{c,ii_m}^{(1)} \geq \left(\alpha^{(g)} + \gamma_{i_m}^{(1)} \delta_u \right) \left(\sum_{k=1}^{i_m} F_k h_k + h_{i_m} \sum_{k=i_m+1}^{n_s} F_k \right) - \sum_{k=1}^{i_m} \sum_{j=1}^{n_b} W_{d,jk} \quad (2.5.17)$$

for mechanism of type 2

$$\sum_{i=1}^{n_c} M_{c,ii_m}^{(2)} \geq \left(\alpha^{(g)} + \gamma_{i_m}^{(2)} \delta_u \right) \sum_{k=i_m}^{n_s} F_k (h_k + h_{i_m-1}) - \sum_{k=i_m}^{n_s} \sum_{j=1}^{n_b} W_{d,jk} \quad (2.5.18)$$

for mechanism of type 3

$$\sum_{i=1}^{n_c} M_{c,ii_m}^{(3)} \geq \frac{1}{2} \left[\left(\alpha^{(g)} + \gamma_{i_m}^{(3)} \delta_u \right) (h_{i_m} - h_{i_m-1}) \sum_{k=i_m}^{n_s} F_k - \sum_{j=1}^{n_b} W_{d,ji_m} \right] \quad (2.5.19)$$

Equations (2.5.17)(2.5.19) have been directly derived from Equation (2.5.16) for $i_m > 1$.

(g) Computation of the required sum of the reduced plastic moments of columns for each storey as the maximum value among those coming from the above design conditions:

$$\sum_{i=1}^{n_c} M_{c,ii_m} = \max \left\{ \sum_{i=1}^{n_c} M_{c,ii_m}^{(1)}, \sum_{i=1}^{n_c} M_{c,ii_m}^{(2)}, \sum_{i=1}^{n_c} M_{c,ii_m}^{(3)} \right\} \quad (2.5.20)$$

(h) For each column, the required plastic moment $M_{c.iim}$, reduced due to the contemporaneous action of the axial load $N_{c.iim}$, is computed and the column section is designed with the same procedure pointed out in step (d) with reference to the first storey.

(i) If needed, a technological condition is imposed requiring that, starting from the base, the column sections cannot increase along the building height. If this condition leads to the revision of column sections at first storey, then the value of $M_{c.i1}^*$ has to be updated and the design procedure needs to be repeated from step (f).

Before introducing the design procedure for Global Concentrically Braced Frames, it is necessary to define how the axial force in compressed members, in collapse condition, are defined.

2.5.3 Definition of the Axial Force in Compressed Members According to Georgescu's Model

The behaviour of the axially loaded member is described through three parameters: the axial stress P , the axial deformation δ , and the transverse deflection f .

Georgescu's model [24],[25] refers to a cycle that is divided into zones corresponding to several characteristic behaviours, the definition of which is closely related to the physical interpretation of the inelastic cyclic behaviour.

In the specific case, Georgescu's model has been adapted to a monotonic behaviour considering only the tension/elongation and the compression/shortening phases, as depicted in Figure 2.5.1. Consequently, only the OA, AB, and BC branches will be used to describe the behaviour in compression.

Branch **OA** of elastic shortening in compression: because of axial compression, a progressive shortening that ends in point A with the achievement of the unstable condition occurs. It corresponds to the value of the resistant load in compression P_{cr} .

Branch **AB**: once the unstable condition is reached, the member begins to buckle laterally. As a consequence, a variable second order bending moment occurs along the beam equal to $P \cdot f(z)$, where $f(z)$ represents the deformation of the axis line. The lateral displacement increases under constant load up to point

B, at which, because of the second-order, a plastic hinge is formed in the centre section.

Branch **BC**: represents the equilibrium curve of the mechanism into which the member has been transformed. Because of the formation of the plastic hinge, the bending moment in the middle section remains constant; therefore, the axial and transversal deformation increase must be accompanied by a load reduction. The plastic hinge continues to rotate until it reaches point C at which the load is reversed. The section is characterized by a non-linear trend due to the interaction of normal stress-bending moment.

The equations describing the model depend on the initial imperfection f_0 , defined according to Georgescu's model and Eurocode 3:

$$f_0 = \frac{W}{A} \alpha (\bar{\lambda}^2 - 0.04) \quad \text{with } \alpha = 0.21, \bar{\lambda} = \frac{\lambda}{\lambda_y} \quad (2.5.21)$$

where W is the plastic section modulus, A is the section area, α is a coefficient depending on the buckling curve, defined by Eurocode 3, λ is the geometric slenderness defined as the ratio between the effective buckling length L_0 and the radius of gyration ρ . $\lambda_y = \pi(E/f_y)^{1/2}$ is the slenderness corresponding to the yielding condition, E is the elastic modulus and f_y is the resistance of the steel in tension.

The equations representing the branches of the model are reported in the following:

OA branch:

$$P = \frac{EA}{L} \delta_{OA} = K_d \delta_{OA} \quad \text{with } P \leq P_{crit}; \quad \delta_A = \frac{P_{crit}}{K_d} \quad (2.5.22)$$

Where P_{crit} is the critical axial load defined according to Eurocode 3.

AB branch:

$$f_{tB} = \frac{M_{pl}}{P_{crit}} \left(1 - \frac{P_{crit}}{P_y} \right) \quad (2.5.23)$$

$$\delta_B = -\frac{P_{crit}L}{EA} + \frac{\pi^2}{4L} (f_{tB}^2 - f_0^2) \quad (2.5.24)$$

Where M_{pl} is the plastic resisting moment of the section and P_y is the axial resistance in tension.

BC branch:

$$f_t = \frac{M_{pl}}{P} \left(1 - \frac{P}{P_y} \right) \text{ with } P \text{ generic } < P_{crit} \quad (2.5.25)$$

$$f_0 = \delta_{BC} = -\frac{PL}{EA} + \frac{\pi^2}{4L} (f_t^2 - f_0^2) \quad (2.5.26)$$

The link describing the monotonic behaviour of compressed diagonals is completed by defining the elastic and the plastic branch in tension, respectively branch OF and FG, as reported in Figure 2.5.1.

OF branch:

$$P = \frac{EA}{L} \delta_{OF} = K_d \delta_{OF} \quad \text{with } P \leq P_y; \quad \delta_F = \frac{P_y}{K_d} \quad (2.5.27)$$

FG branch:

$$P = P_y \quad \forall \delta_{FG} \quad (2.5.28)$$

Once defined the stresses in the dissipative elements (in compression and tension) in the collapse configuration, the axial force acting on columns, influencing the plastic resisting moment $M_{c,ik}$, is evaluated in the seismic conditions considering the stresses transmitted by the diagonals at collapse, according to the second principle of capacity design. Therefore, concerning the scheme shown in Figure 2.5.2c, we have for columns [9]:

$$N_{c,k} = \sum P_{y,k} \cdot \sin \alpha_j + \sum P_{c,k}(\delta_{u,j}) \cdot \sin \beta_j; \quad k < n_s \quad (2.5.29)$$

$$N_{c,k} = P_{y,k} \cdot \sin \beta_j; \quad \text{with } k = n_s \quad (2.5.30)$$

where $P_{c,k}(\delta_{u,j})$ is the axial force in compression corresponding to the interstorey displacement of the j-th diagonal at k-th storey in collapse condition. The axial force in diagonals is assumed in absolute value.

The design stresses of beams and columns are finally obtained by the addition of the normal stresses estimated through Eqs.(2.5.29) and (2.5.30) and the stresses resulting from the action of the non-seismic loads of the seismic load combination ($Gk+\psi Qk$).

2.6 Upper Partial and Shear Band Collapse Mechanisms

Another more complete way to describe all possible collapse mechanisms for MRFs and CBFs structures involves the introduction of "Shear band" mechanisms.

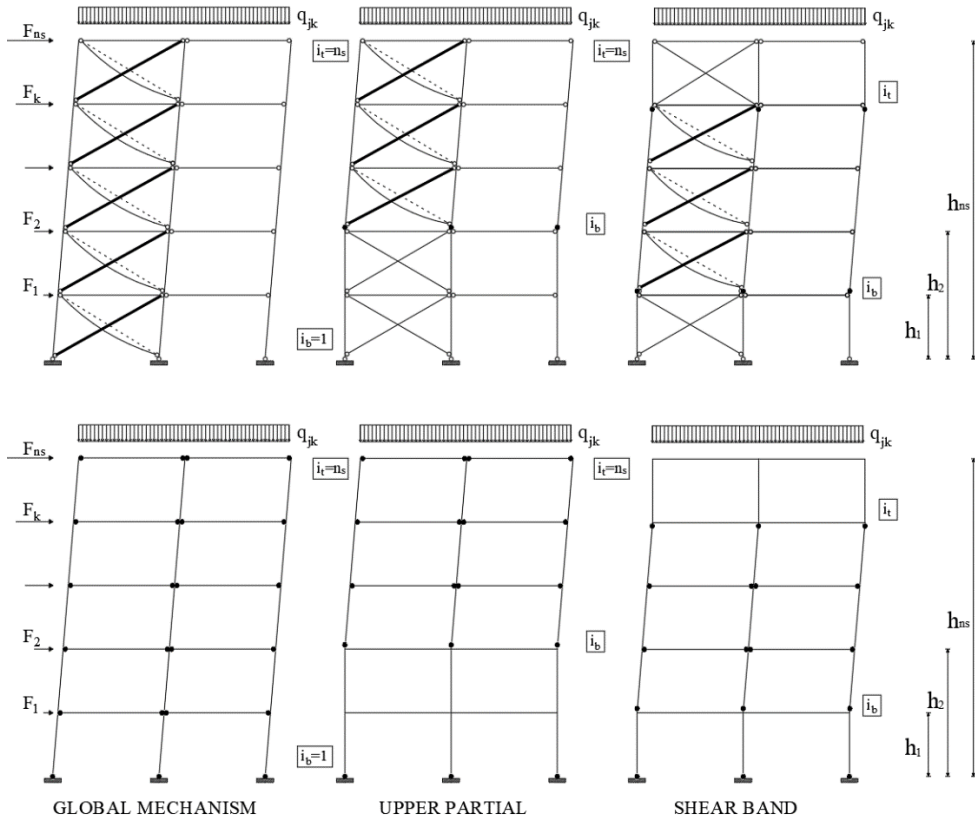


Figure 2.6.1 "Upper partial" and "Shear band" mechanisms for MRFs and CBFs.

These partial collapse mechanisms are characterized by also affecting intermediate bands of storeys and require the introduction of two storey indices to be defined.

In order to enclose all possible types of collapse mechanism, two patterns of yielding corresponding to two mechanism typologies, named "upper partial" and "shear band" have been defined. These mechanisms are depicted in Figure

2.6.1 for given mechanism indexes i_b and i_t , additionally in the same figure, it is also pointed out that the global mechanism is a particular case of the upper partial mechanisms occurring when $i_b = 1$ and $i_t = n_s$.

Type-1 mechanisms are specific cases of shear band mechanisms occurring for $i_b = 1$; Type-2 mechanisms are herein referred as upper partial mechanisms characterized by $i_t = n_s$; finally, Type-3 mechanisms are particular cases of shear band mechanisms occurring for $i_b = i_t$, i.e. soft storey mechanisms).

Given the number of storeys, n_s , it is possible to demonstrate that the total number of possible mechanisms, with the exclusion of the global one, is given by:

$$N_{tot} = \frac{n_s(n_s + 1)}{2} + n_s - 1 \quad (2.6.1)$$

2.6.1 First-Order Collapse Multipliers and Slopes of the Mechanism Equilibrium Curve for MRFs

By means of the virtual work principle, the first-order kinematically admissible multiplier of horizontal forces and the slopes of the mechanism equilibrium curve can be easily evaluated for all the possible collapse mechanisms. The following relationships are obtained.

- **Upper partial collapse mechanisms**

With reference to upper partial mechanisms, ($i_t = n_s$), the first order kinematically admissible multiplier of horizontal forces is given by:

$$\alpha_{0.i_b i_t}^{(up)} = \frac{\sum_{i=1}^{n_c} M_{c.i.i_b} + 2 \sum_{k=i_b}^{n_s} \sum_{j=1}^{n_b} M_{b.jk}}{\sum_{k=i_b}^{n_s} F_k (h_k - h_{b-1})} \quad (2.6.2)$$

while $\gamma_{i_b i_t}^{(up)}$ is the slope of the Upper partial mechanism equilibrium curve, and can be reported as:

$$\gamma_{i_b i_t}^{(up)} = \frac{1}{h_{n_s} - h_{b-1}} \frac{\sum_{k=i_b}^{n_s} V_k (h_k - h_{i_b-1})}{\sum_{k=i_b}^{n_s} F_k (h_k - h_{i_b-1})} \quad (2.6.3)$$

- **Shear band collapse mechanisms**

Similarly, with reference to shear band mechanisms, the first order kinematically admissible multiplier of horizontal forces is given by:

$$\alpha_{0.i_b i_t}^{(sb)} = \frac{\sum_{i=1}^{n_c} M_{c.i.i_b} + 2 \sum_{k=i_b}^{i_t-1} \sum_{j=1}^{n_b} M_{b.jk} + \sum_{i=1}^{n_c} M_{c.i.i_t}}{\sum_{k=i_b}^{i_t-1} F_k (h_k - h_{i_b-1}) + (h_{i_t} - h_{i_b-1}) \sum_{k=i_t}^{n_s} F_k} \quad (2.6.4)$$

while $\gamma_{i_b i_t}^{(up)}$ is the slope of the Upper partial mechanism equilibrium curve, and can be reported as:

$$\gamma_{i_b i_t}^{(sb)} = \frac{1}{(h_{i_t} - h_{i_b-1})} \frac{\sum_{k=1}^{i_t-1} V_k (h_k - h_{i_b-1}) + (h_{i_t} - h_{i_b-1}) \sum_{k=i_t}^{n_s} V_k}{\sum_{k=i_b}^{i_t-1} F_k (h_k - h_{i_b-1}) + (h_{i_t} - h_{i_b-1}) \sum_{k=i_t}^{n_s} F_k} \quad (2.6.5)$$

2.6.2 First-Order Collapse Multipliers and Slopes of the Mechanism Equilibrium Curve for CBFs

By means of the virtual work principle, the first-order kinematically admissible multiplier of horizontal forces and the slopes of the mechanism equilibrium curve can be easily evaluated for all the possible collapse mechanisms. The following relationships are obtained.

- **Upper partial collapse mechanisms**

With reference to upper partial mechanisms, ($i_t = n_s$), the first order kinematically admissible multiplier of horizontal forces is given by:

$$\alpha_{0.i_b i_t}^{(up)} = \frac{\sum_{i=1}^{n_c} M_{c.i.i_b} + \sum_{k=i_b}^{n_s} \sum_{j=1}^{n_b} W_{d,jk}}{\sum_{k=i_b}^{n_s} F_k (h_k - h_{i_b-1})} \quad (2.6.6)$$

while $\gamma_{i_b i_t}^{(up)}$ is the slope of the Upper partial mechanism equilibrium curve, and can be reported as:

$$\gamma_{i_b i_t}^{(up)} = \frac{1}{h_{n_s} - h_{i_b-1}} \frac{\sum_{k=i_b}^{n_s} V_k (h_k - h_{i_b-1})}{\sum_{k=i_b}^{n_s} F_k (h_k - h_{i_b-1})} \quad (2.6.7)$$

- **Shear band collapse mechanisms**

Similarly, with reference to shear band mechanisms, the first order kinematically admissible multiplier of horizontal forces is given by:

$$\alpha_{0.i_b i_t}^{(sb)} = \frac{\sum_{i=1}^{n_c} M_{c.i.i_b} + \sum_{k=i_b}^{i_t-1} \sum_{j=1}^{n_b} W_{d,jk} + \sum_{i=1}^{n_c} M_{c.i.i_t}}{\sum_{k=i_b}^{i_t-1} F_k (h_k - h_{i_b-1}) + (h_{i_t} - h_{i_b-1}) \sum_{k=i_t}^{n_s} F_k} \quad (2.6.8)$$

while $\gamma_{i_b i_t}^{(up)}$ is the slope of the Upper partial mechanism equilibrium curve, and can be reported as:

$$\gamma_{i_b i_t}^{(sb)} = \frac{1}{(h_{i_t} - h_{i_b-1})} \frac{\sum_{k=1}^{i_t-1} V_k (h_k - h_{i_b-1}) + (h_{i_t} - h_{i_b-1}) \sum_{k=i_t}^{n_s} V_k}{\sum_{k=i_b}^{i_t-1} F_k (h_k - h_{i_b-1}) + (h_{i_t} - h_{i_b-1}) \sum_{k=i_t}^{n_s} F_k} \quad (2.6.9)$$

It is important to note that in the case of simple CBFs, the terms $M_{c.i.i_b}$ for $i_b = 1$ and $M_{c.i.i_t}$ for $i_t = 1$, are equal to 0 (Real hinge on top and at the base).

CHAPTER 3

3 SIMPLIFIED PERFORMANCE-BASED APPROACH FOR THE EVALUATION OF SEISMIC CAPACITY

3.1 Introduction

One of the most common strategies adopted to assess the capacity of a structure is the pushover analysis. Many times, these procedures are not under the control of the professional engineer who is usually not aware of what the software is precisely making and computing.

The simplified method herein proposed can be used in the immediate aftermath of an earthquake because it does not require any non-linear analyses, but only the use of common analyses such as the elastic structural analysis and the rigid-plastic analysis. In fact, the user can easily build a capacity curve constituted by three branches, whose target points can be computed by simple equations proposed in the following [6]-[10].

The methodology associates four characteristic points of the frame behavioural curve, to specific limit states, provided by codes.

The procedure also involves the evaluation of the triggered collapse mechanism therefore it is important to investigate the types of collapse mechanism possible for the structural type considered.

The methodology has been designed for general use. For both CBFs and MRFs it is based on the use of elastic analysis combined with rigid plastic analysis. The difference lies in the definition of some characteristic points. In particular, CBFs [9] are characterized by presenting a second elastic branch with reduced stiffness for the buckling of the compressed diagonals while MRFs [6]

have an horizontal branch due to the plastic redistribution capacity typical of the structural type.

However, some assumptions for the modelling of the structure should be made for the modelling of dissipative zones. For example, MRFs are modelled considering rigid perfectly-plastic hinges where the resistance threshold accounts for the ultimate condition of dissipative zones through the use of an overstrength coefficient. In addition, from a benefits safety point of view, the plastic hinges are put at the end of the beams not accounting for the real dimension of the panel zone. In the case of CBFs, the plastic behavior is defined through a simplified trilinear monotonic Georgescu's model.

3.2 Trilinear Approximation of the Non-Dimensional Pushover Curve for MRFs

The simplified trilinear model needs only the elastic structural analysis and the rigid-plastic analysis not requiring any static or dynamic non-linear analyses. Therefore, the user can quickly obtain the non-dimensional pushover curve through the intersection of three linear branches [6].

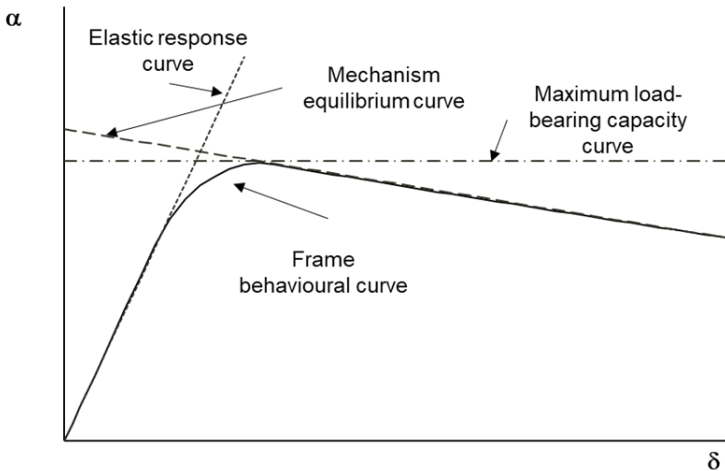


Figure 3.2.1 Trilinear approximation of the non-dimensional pushover curve for MRFs.

The first branch is affected by the elastic behavior of the structure. The knee depends on the plastic capacity distribution, appearing sharper as more as the plastic hinges develop simultaneously. The softening branch is sensitive to the second-order effects.

In the case of MRFs, it is simple observing that the behavioural curve can be easily approximated by a trilinear curve where the first branch can be represented by the elastic response curve, the horizontal one is provided by the maximum load bearing capacity, while the softening branch is given by the collapse mechanism equilibrium curve of the structure.

Being known the sections of columns and beams of the structure and the design loads, both the first order collapse multiplier α_0 and the slopes γ_s can be computed for each type of possible collapse mechanism. The triggering mechanism is the one characterized by the collapse mechanism equilibrium curve located below the others into a given displacement range compatible with the dissipative supplies.

The evaluation of α_0 and γ_s has been reported in chapter 2.4.1 for MRFs

A summary is reported in Table 3.2.1:

Table 3.2.1 Collapse multipliers and slopes summary for MRFs

Type	α_0
(g)	$\alpha_0^{(g)} = \frac{\sum_{k=1}^{n_c} M_{c.i1} + 2 \sum_{k=1}^{n_s} \sum_{j=1}^{n_b} M_{b.jk}}{\sum_{k=1}^{n_s} F_k h_k}$
(1)	$\alpha_{0.i_m}^{(1)} = \frac{\sum_{i=1}^{n_c} M_{c.i.1} + 2 \sum_{k=1}^{i_m-1} \sum_{j=1}^{n_b} M_{b.jk} + \sum_{i=1}^{n_c} M_{c.i.i_m}}{\sum_{k=1}^{i_m} F_k h_k + h_{i_m} \sum_{k=i_m+1}^{n_s} F_k}$
(2)	$\alpha_{0.i_m}^{(2)} = \frac{\sum_{i=1}^{n_c} M_{c.i.i_m} + 2 \sum_{k=i_m}^{n_s} \sum_{j=1}^{n_b} M_{b.jk}}{\sum_{k=i_m}^{n_s} F_k (h_k - h_{i_m-1})}$
(3)	$\alpha_{0.i_m}^{(3)} = \frac{2 \sum_{i=1}^{n_c} M_{c.i.i_m}}{(h_{i_m} - h_{i_m-1}) \sum_{k=i_m}^{n_s} F_k}$
Type	γ_s
(g)	$\gamma^{(g)} = \frac{1 \sum_{k=1}^{n_s} V_k h_k}{h_{n_s} \sum_{k=1}^{n_s} F_k h_k}$
(1)	$\gamma_{i_m}^{(1)} = \frac{1 \sum_{k=1}^{i_m} V_k h_k + h_{i_m} \sum_{k=i_m+1}^{n_s} V_k}{h_{i_m} \sum_{k=1}^{i_m} F_k h_k + h_{i_m} \sum_{k=i_m+1}^{n_s} F_k}$

(2)	$\gamma_{i_m}^{(2)} = \frac{1}{h_{n_s} - h_{i_m-1}} \frac{\sum_{k=i_m}^{n_s} V_k (h_k - h_{i_m-1})}{\sum_{k=i_m}^{n_s} F_k (h_k - h_{i_m-1})}$
(3)	$\gamma_{i_m}^{(3)} = \frac{1}{h_{i_m} - h_{i_m-1}} \frac{\sum_{k=i_m}^{n_s} V_k}{\sum_{k=i_m}^{n_s} F_k}$
δ_u	$0.04 \cdot H_0$

Another way to define the collapse multipliers and the slopes involves Shear band collapse mechanisms.

The evaluation of α_0 and γ_s has been reported in chapter 2.6.1 for MRFs.

A summary is reported in Table 3.2.2:

Table 3.2.2 Collapse multipliers and slopes summary for MRFs (Shear band)

Type	α_0
(up)	$\alpha_{0.i_b i_t}^{(up)} = \frac{\sum_{i=1}^{n_c} M_{c.i.i_b} + 2 \sum_{k=i_b}^{n_s} \sum_{j=1}^{n_b} M_{b.jk}}{\sum_{k=i_b}^{n_s} F_k (h_k - h_{b-1})}$
(sb)	$\alpha_{0.i_b i_t}^{(sb)} = \frac{\sum_{i=1}^{n_c} M_{c.i.i_b} + 2 \sum_{k=i_b}^{i_t-1} \sum_{j=1}^{n_b} M_{b.jk} + \sum_{i=1}^{n_c} M_{c.i.i_t}}{\sum_{k=i_b}^{i_t-1} F_k (h_k - h_{i_b-1}) + (h_{i_t} - h_{i_b-1}) \sum_{k=i_t}^{n_s} F_k}$
Type	γ_s
(up)	$\gamma_{i_b i_t}^{(up)} = \frac{1}{h_{n_s} - h_{b-1}} \frac{\sum_{k=i_b}^{n_s} V_k (h_k - h_{i_b-1})}{\sum_{k=i_b}^{n_s} F_k (h_k - h_{i_b-1})}$
(sb)	$\gamma_{i_b i_t}^{(sb)} = \frac{1}{(h_{i_t} - h_{i_b-1})} \frac{\sum_{k=1}^{i_t-1} V_k (h_k - h_{i_b-1}) + (h_{i_t} - h_{i_b-1}) \sum_{k=i_t}^{n_s} V_k}{\sum_{k=i_b}^{i_t-1} F_k (h_k - h_{i_b-1}) + (h_{i_t} - h_{i_b-1}) \sum_{k=i_t}^{n_s} F_k}$
δ_u	$0.04 \cdot H_0$

Since the collapse mechanism equilibrium curve is obtained by a second order rigid-plastic analysis, the displacement δ appearing in the relationship $\alpha = \alpha_0 - \gamma_s \delta$ represents only the plastic part of the total displacement, with a fully developed mechanism. However, it is advisable to account also for the elastic part of the displacements, rearranging Eq. (2.3.1) in the following form:

$$\alpha = \alpha_0 - \gamma_s (\delta - \delta_y) \quad (3.2.1)$$

where $(\delta - \delta_y)$ is the plastic displacement range and δ_y is the displacement corresponding to the formation of the first plastic hinge. Consequently, the intersection with the ordinate axis is $\alpha = \alpha_0 + \gamma_s \delta_y$. This correction is significant especially if the frames exhibit soft-storey mechanisms. In these cases, the displacements that the structure suffers in the elastic field, constitute a large percentage of the total displacements and are more relevant than those in the plastic field. Moreover, it is important to introduce α_{max} as the collapse multiplier corresponding to the achievement of the maximum load-bearing capacity of the structure.

The equations of the three identified branches in the α - δ plane (horizontal force multiplier - top sway displacement) are reported below:

Elastic response curve

$$\alpha^{(I)} = \frac{1}{\delta_1} \delta \quad (3.2.2)$$

where δ_1 is the elastic top sway displacement, corresponding to the design value of the seismic forces.

Maximum load-bearing capacity curve

$$\alpha^{(II)} = \alpha_{max} \quad (3.2.3)$$

Where α_{max} is the multiplier corresponding to the maximum load-bearing capacity of the structure. The maximum multiplier will be evaluated starting from the Merchant-Rankine formula subjected to a calibration procedure, reported in Chapter 4.

Mechanism equilibrium curve

$$\alpha^{(III)} = \alpha_0 - \gamma_s (\delta - \delta_y) \quad (3.2.4)$$

Where δ_y , the displacement corresponding to the formation of the first plastic hinge, is obtained through an iterative incremental elastic analysis.

3.3 Performance-Based Capacity Definition Approach for MRFs

In this section, the definition of the performance points used to define the capacity of the structure is provided. Starting from the trilinear approximation model, a performance-based methodology is proposed. It associates four

characteristic points of the frame behavioral curve (points A, B, C, D of Figure 3.3.1), to specific limit states, provided by codes [6], [18]-[20]. These limit states have the meaning of identifying the achievement of a performance target such as the formation of the first plastic hinge or the attainment of the ultimate plastic rotation of the most involved member.

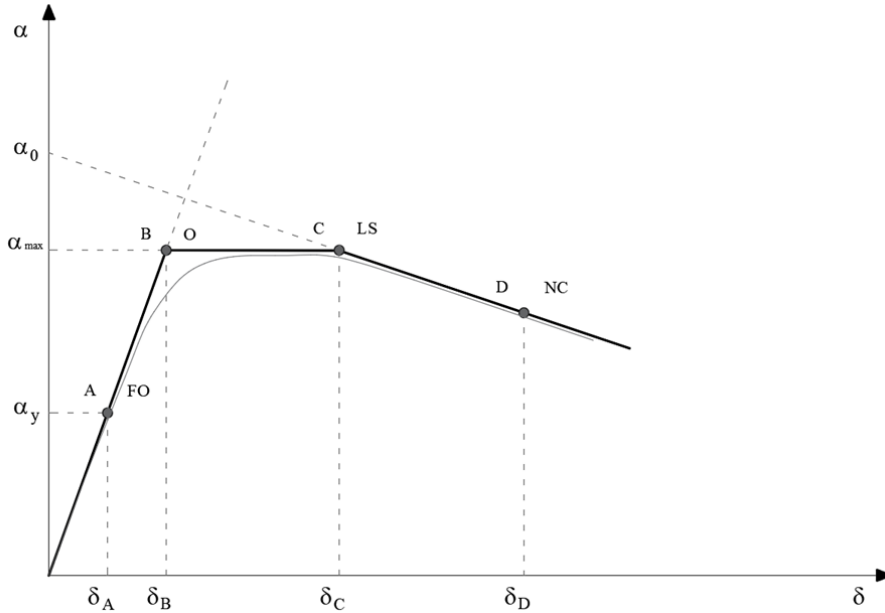


Figure 3.3.1 Performance points of the trilinear model for MFRs.

- *Point A*

Point A corresponds to the minimum value between the multiplier of the horizontal forces, due to the formation of the first plastic hinge and the one corresponding to the maximum storey displacement admitted under serviceability conditions. This point is associated with the "Fully Operational" limit state, fully operational structure.

- *Point B*

Point B corresponds to the development of the maximum bearing capacity of the structure and to the first significant deviation of the structure from linear elastic behaviour (towards non-linear plastic). The Overcapacity due to plastic redistribution is exploited with limited demands for plastic rotation $\vartheta_{p,B}$ (or

$\vartheta_{p,\alpha_{max}}$) to which the top sway displacement δ_B corresponds. The "Operational" limit state is associated with this point.

- *Point C*

Under the action of rare seismic events, the frame draws on high resources of ductility. Point C, in trilinear modelling, corresponds to the complete development of the collapse mechanism. The corresponding top sway displacement δ_C and plastic rotation $\vartheta_{p,C}$ (or $\vartheta_{p,mecc}$) are associated with the "Life Safety" limit state.

- *Point D*

In the case of very rare seismic events, the dynamic equilibrium is still possible thanks to the inertia forces, but considerable local ductility is required. The limit point D is identified, which is characterised by the fact that, at least in one member, the reserves of local ductility are exceeded. It is associated with the "Near Collapse" limit state.

3.3.1 Equations for the Definition of the Performance Points (MRFs)

As mentioned above, **point A (Fully Operational)** corresponds to the minimum value between the horizontal force multiplier, corresponding to the formation of the first plastic hinge and the one corresponding to the maximum storey displacement admitted in serviceability conditions. The point belongs to the elastic branch of the curve and the top sway displacement δ_A (o δ_y) is determined, known the slope of the elastic branch $1/\delta_1$ (for $\alpha=1$) and the multiplier corresponding to point A, obtained iteratively through elastic analysis.

The top sway displacement δ_A (o δ_y) can be calculated as follows:

$$\delta_A = \delta_y = \alpha_y \delta_1 = \alpha_A \delta_1 \quad (3.3.1)$$

Point B (Operational), characterised by the attainment of the maximum bearing capacity of the structure, derives from the intersection of the horizontal branch $\alpha = \alpha_{max}$ with the elastic branch $\alpha = \frac{1}{\delta_1} \delta$. To locate point B, the maximum collapse multiplier ($\alpha_{max} = \alpha_B$) has to be analytically computed, by means of the Merchant-Rankine formula, calibrated by means of the regression analysis (CHAPTER 4).

Therefore, it can be stated that:

$$\alpha_{max} = \alpha_B = \frac{1}{\delta_1} \delta_B \quad (3.3.2)$$

where the unknown, represented by the top sway displacement δ_B , can be derived as follows:

$$\delta_B = \alpha_{max} \delta_1 \quad (3.3.3)$$

Point C (Life Safety), characterized by the complete development of the collapse mechanism, derives from the intersection of the horizontal branch of equation $\alpha = \alpha_{max}$ with the descending branch, representative of the collapse mechanism equilibrium curve (Eq.(3.2.4)).

The displacement δ_C can be derived as follows:

$$\delta_C = \delta_{mecc} = \frac{\alpha_0 - \alpha_{max}}{\gamma_s} + \delta_y \quad (3.3.4)$$

Point D (Near Collapse), in which the equilibrium is guaranteed by the forces of inertia and considerable local ductility supplies are required, can be detected along the descending branch of the trilinear non-dimensional pushover curve.

The top sway displacement $\delta_D = \delta_u$, is expressed as a function of the residual plastic rotation capacity occurring at point C ($\vartheta_{p,u} - \vartheta_{p,mecc}$) and can be calculated as follows:

$$\delta_D = \delta_C + (\vartheta_{p,u} - \vartheta_{p,mecc}) H_0 \quad (3.3.5)$$

where $\vartheta_{p,u}$ is the plastic hinge rotation capacity assumed equal to 8.0 ϑ_y according to EC8-part 3 provisions [19], $\vartheta_{p,mecc}$ is the plastic hinge rotation demand corresponding to the formation of the collapse mechanism and H_0 is the total height of the storeys involved into the collapse mechanism.

For the definition of the demand in terms of plastic rotation corresponding to the development of the collapse mechanism $\vartheta_{p,mecc}$, an analytic formulation has been derived and calibrated. The details are reported in Chapter 4

As regards the plastic hinge rotation capacity $\vartheta_{p,u}$, it has been defined according to Eurocode 8 – part 3 as a multiple of the chord rotation at yielding ϑ_y (Table 3.3.1).

Table 3.3.1 Plastic rotation capacity at the end of beams or columns with dimensionless axial load v not greater than 0.30.

Class	Limit State		
	DL	SD	NC
1	1.0 ϑ_y	6.0 ϑ_y	8.0 ϑ_y
2	0.25 ϑ_y	2.0 ϑ_y	3.0 ϑ_y

The evaluation of chord rotation ϑ_y is not reported in Eurocode. It has been defined as a property of the member, assumed to be an isolated element. The static model used for beams and for columns involved in “soft storey” collapse mechanisms is a beam on two supports, stressed by bending moments of opposite sign at the ends (simulating a seismic action) and zero vertical loads.

For the determination of the chord rotation at yielding ϑ_y , the beam will be brought in collapse conditions with the ends that will have drawn to the maximum resources of flexural resistance.

Consequently, for beams it can be written:

$$\frac{\gamma_{ov} M_{p,b} l_b}{3EI_b} - \frac{\gamma_{ov} M_{p,b} l_b}{6EI_b} = \vartheta_y \quad (3.3.6)$$

$$\vartheta_y = \frac{\gamma_{ov} M_{p,b} l_b}{6EI_b} \quad (3.3.7)$$

where $M_{p,b}$ is the plastic resisting moment of the beam, l_b is the length of the beam, I_b is the moment of inertia of the beam, E is the elastic modulus and γ_{ov} is the overstrength coefficient.

Referring to columns, equation (3.3.7) can be written as:

$$\vartheta_y = \frac{\gamma_{ov} M_{p,c} l_c}{6EI_c} \quad (3.3.8)$$

where $M_{p,c}$ is the plastic resisting moment of the column, l_c is the length of the beam, I_c is the moment of inertia of the column.

For columns involved in partial or global mechanisms, considering only one end reaching the maximum flexural resistance, Equation (3.3.8) can be written as:

$$\vartheta_y = \frac{\gamma_{ov} M_{p.c} l_c}{4EI_c} \quad (3.3.9)$$

3.4 Trilinear Approximation of the Non-Dimensional Pushover Curve for CBFs

In the case of simple CBFs [9], the plastic redistribution of capacity is limited; consequently, the length of the horizontal branch can be considered negligible according to the performed analyses.

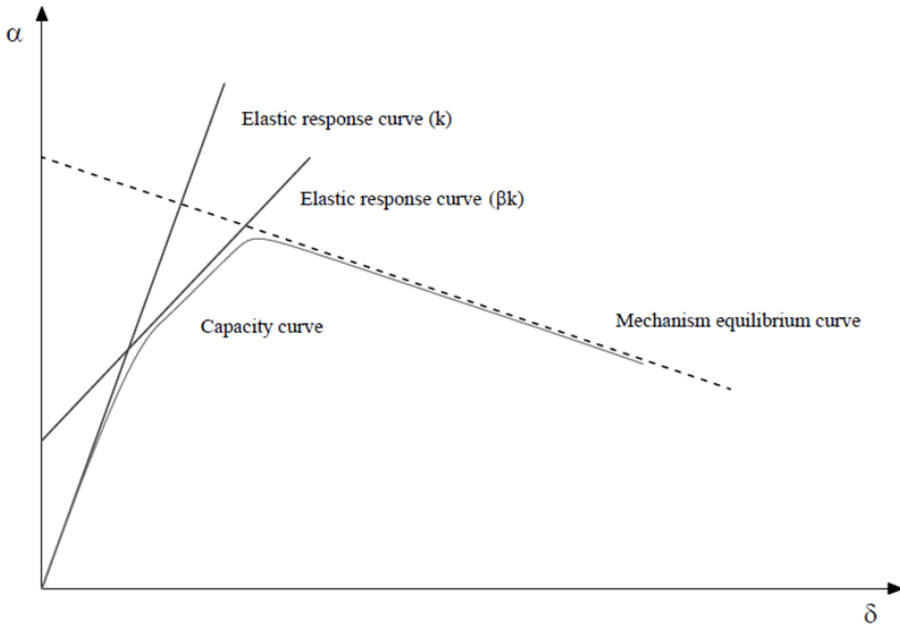


Figure 3.4.1 Trilinear approximation of the non-dimensional pushover curve for CBFs.

The simplified method herein proposed for CBFs is based on a trilinear approximation of the non-dimensional pushover curve obtained as the envelope of three branches:

1. an elastic branch obtained by elastic analysis
2. a branch with a lower slope due to the buckling of diagonal members
3. a softening branch obtained by rigid plastic second-order analysis

The user can easily build a pushover or a non-dimensional pushover curve constituted by three branches (Figure 3.4.1), whose target points, also in this case, are easily identified by simple mathematical relations.

Being known the sections of columns and diagonals of the structure and the design loads, both the first order collapse multiplier α_0 and the slopes γ_s can be computed for each type of possible collapse mechanism. The triggering mechanism is the one characterized by the collapse mechanism equilibrium curve located below the others into a given displacement range compatible with the dissipative supplies.

The evaluation of α_0 and γ_s has been reported in chapter 2.5.1 for CBFs. A summary is reported in Table 3.4.1:

Table 3.4.1 Collapse multipliers and slopes summary for CBFs

Type	α_0
(g)	$\alpha_0^{(g)} = \frac{\sum_{k=1}^{n_s} \sum_{j=1}^{n_b} W_{d.jk}}{\sum_{k=1}^{n_s} F_k h_k}$
(1)	$\alpha_{0.i_m}^{(1)} = \frac{\sum_{k=1}^{i_m-1} \sum_{j=1}^{n_b} W_{d.jk} + \sum_{i=1}^{n_c} M_{c.i i_m}}{\sum_{k=1}^{i_m} F_k h_k + h_{i_m} \sum_{k=i_m+1}^{n_s} F_k}; \quad i_m = 1, 2, \dots, n_{s-1}$
(2)	$\alpha_{0.i_m}^{(2)} = \frac{\sum_{k=i_m}^{n_s} \sum_{j=1}^{n_b} W_{d.jk} + \sum_{i=1}^{n_c} M_{c.i i_m}}{\sum_{k=i_m}^{n_s} F_k \cdot (h_k - h_{i_m-1})}; \quad i_m = 2, 3, \dots, n_s$ $\alpha_{0.n_s}^{(1)} = \alpha_0^{(g)}; \quad i_m = n_s$
(3)	$\alpha_{0.i_m}^{(3)} = \frac{2 \cdot \sum_{i=1}^{n_c} M_{c.i i_m} + \sum_{j=1}^{n_b} W_{d.j i_m}}{(h_{i_m} - h_{i_m-1}) \cdot \sum_{k=i_m}^{n_s} F_k}; \quad 2 \leq i_m < n_s$ $\alpha_{0.n_s}^{(3)} = \frac{\sum_{i=1}^{n_c} M_{c.i n_s} + \sum_{j=1}^{n_b} W_{d.j n_s}}{(h_{n_s} - h_{n_s-1}) \cdot F_{n_s}}; \quad i_m = n_s$ $\alpha_{0.1}^{(3)} = \frac{\sum_{i=1}^{n_c} M_{c.i 1} + \sum_{j=1}^{n_b} W_{d.j 1}}{h_1 \cdot \sum_{k=1}^{n_s} F_k}; \quad i_m = 1$
Type	γ_s
(g)	$\gamma^{(g)} = \frac{1 \sum_{k=1}^{n_s} V_k h_k}{h_{n_s} \sum_{k=1}^{n_s} F_k h_k}$

(1)	$\gamma_{im}^{(1)} = \frac{1}{h_{im}} \frac{\sum_{k=1}^{i_m} V_k h_k + h_{im} \sum_{k=i_m+1}^{n_s} V_k}{\sum_{k=1}^{i_m} F_k h_k + h_{im} \sum_{k=i_m+1}^{n_s} F_k}$
(2)	$\gamma_{im}^{(2)} = \frac{1}{h_{n_s} - h_{i_m-1}} \frac{\sum_{k=i_m}^{n_s} V_k (h_k - h_{i_m-1})}{\sum_{k=i_m}^{n_s} F_k (h_k - h_{i_m-1})}$
(3)	$\gamma_{im}^{(3)} = \frac{1}{h_{im} - h_{i_m-1}} \frac{\sum_{k=i_m}^{n_s} V_k}{\sum_{k=i_m}^{n_s} F_k}$
δ_u	$\varphi_{max} = \max_{i=1}^n \varphi_i = \max_{i=1}^n \frac{\delta_{br.lim}}{h_i \cdot \cos \beta_i}$ $\delta_u = \varphi_{max} \cdot H_0$ <p>The axial force in the compressed diagonal accounting for the post-buckling behaviour is defined according to Georgescu's model.</p>

Another way to define the collapse multipliers and the slopes involves Shear band collapse mechanisms.

The evaluation of α_0 and γ_s has been reported in chapter 2.6.2 for CBFs

A summary is reported in Table 3.4.2:

Table 3.4.2 Collapse multipliers and slopes summary for CBFs (Shear band)

Type	α_0
(up)	$\alpha_{0.ib^i_t}^{(up)} = \frac{\sum_{i=1}^{n_c} M_{c.i.ib} + \sum_{k=i_b}^{n_s} \sum_{j=1}^{n_b} W_{d.jk}}{\sum_{k=i_b}^{n_s} F_k (h_k - h_{b-1})}$
(sb)	$\alpha_{0.ib^i_t}^{(sb)} = \frac{\sum_{i=1}^{n_c} M_{c.i.ib} + \sum_{k=i_b}^{i_t-1} \sum_{j=1}^{n_b} W_{d.jk} + \sum_{i=1}^{n_c} M_{c.i.i_t}}{\sum_{k=i_b}^{i_t-1} F_k (h_k - h_{i_b-1}) + (h_{i_t} - h_{i_b-1}) \sum_{k=i_t}^{n_s} F_k}$
Type	γ_s
(up)	$\gamma_{ib^i_t}^{(up)} = \frac{1}{h_{n_s} - h_{b-1}} \frac{\sum_{k=i_b}^{n_s} V_k (h_k - h_{i_b-1})}{\sum_{k=i_b}^{n_s} F_k (h_k - h_{i_b-1})}$
(sb)	$\gamma_{ib^i_t}^{(sb)} = \frac{1}{(h_{i_t} - h_{i_b-1})} \frac{\sum_{k=1}^{i_t-1} V_k (h_k - h_{i_b-1}) + (h_{i_t} - h_{i_b-1}) \sum_{k=i_t}^{n_s} V_k}{\sum_{k=i_b}^{i_t-1} F_k (h_k - h_{i_b-1}) + (h_{i_t} - h_{i_b-1}) \sum_{k=i_t}^{n_s} F_k}$
δ_u	$\varphi_{max} = \max_{i=1}^n \varphi_i = \max_{i=1}^n \frac{\delta_{br.lim}}{h_i \cdot \cos \beta_i}$

	$\delta_u = \varphi_{max} \cdot H_0$ <p>The axial force in the compressed diagonal accounting for the post-buckling behaviour is defined according to Georgescu's model.</p>
--	------------------------------------------------------------------------------------------------------------------------------------------------------------------------------

3.5 Performance-Based Capacity Definition Approach for CBFs

In this section, the definition of the performance points used to define the capacity of the structure is provided. In particular, four characteristic points of the non-dimensional pushover curve (points A, B, C, D of Figure 3.5.1) are associated with specific performance objectives related to the limit states provided by codes [9], [18]-[20].

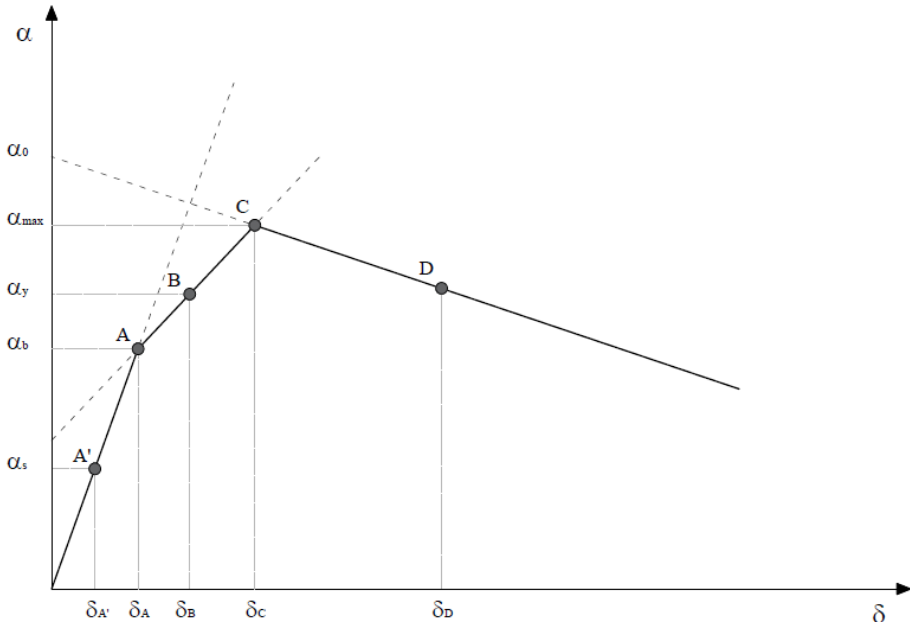


Figure 3.5.1 Performance points of the trilinear model for CBFs.

These performance objectives are set up as target achievements, as the yielding of the first diagonal in tension or the attainment of the collapse mechanism. In the case of CBFs, before defining the equations of the three branches it is necessary to introduce the performance points since the second branch, for example, is a function of the multiplier corresponding to point A.

- *Point A*

Point A corresponds to the minimum value between the multiplier of the horizontal forces, due to the buckling of the first compressed diagonal and the one corresponding to the maximum storey displacement admitted under serviceability conditions. In this case, a second point A' is introduced. This point is associated with the "Fully Operational" limit state, fully operational structure.

- *Point B*

Point B corresponds to the yielding of the first stretched diagonal and is associated with the "Operational" limit state; it can be identified above the second elastic branch, characterized by reduced stiffness due to the buckling of the compressive diagonals.

- *Point C*

Point C in the trilinear model corresponds to the complete development of the collapse mechanism and is associated with the "Life Safety" limit state. In the case of CBFs, this point corresponds also to the development of the maximum bearing capacity of the structure because of the limited plastic redistribution capacity.

- *Point D*

Point D is reached in the case of very rare seismic events, the dynamic equilibrium is still possible thanks to the inertia forces, but considerable local ductility is required. The limit point D is identified, which is characterised by the fact that, at least in one member, the reserves of local ductility are exceeded. It is associated with the "Near Collapse" limit state.

3.5.1 Equations for the Definition of the Performance Points (CBFs)

As mentioned above, **point A (Fully Operational)** corresponds to the minimum value between the horizontal force multiplier, due to the buckling of the first compressed diagonal and the one corresponding to the maximum storey displacement admitted under serviceability conditions. The point belongs to the first elastic branch of the curve and the top sway displacement δ_A (or $\delta_{b,s}$) is determined. Known the displacement and the slope of the elastic branch $K = 1/\delta_1$ (for $\alpha=1$), the multiplier corresponding to point A, will be calculated as follows:

$$\alpha_{b,s} = \alpha_A = \frac{1}{\delta_1} \delta_A \quad (3.5.1)$$

where δ_l is the top sway displacement corresponding to the design forces.

Point B (Operational), corresponding to the yielding of the first stretched diagonal belongs to the second elastic branch. The representative line of the second elastic branch can be expressed as follows:

$$\alpha_{e,2} = \alpha_A + K'(\delta - \delta_A) \quad (3.5.2)$$

where K' is the slope of the second elastic branch accounting for the buckling of the compressed diagonals and that is derived through a reduction factor applied to the slope of the first elastic branch:

$$K' = \beta K \quad (3.5.3)$$

where β is the reduction factor defined as a function of the mechanism height H_0 and the tensile-compressive percentage difference:

$$\beta = 1 - \left(\frac{P_{y,1} - P_{crit.1}}{P_{y,1}} \right) 0.5 \cdot \frac{H_0}{H} \quad (3.5.4)$$

H_0 is the mechanism height derived by the rigid-plastic analysis and H is the total height of the structure and $\left(\frac{P_y - P_{crit}}{P_y} \right)$ represents the percentage difference between the axial resistance in tension and compression of the diagonal members of the first storey. It can be observed that in the limit case $P_{crit.1} = 0$ the β coefficient is equal to 0.5 (halved stiffness), while for the case $P_{crit.1} = P_{y,1}$, the β coefficient is equal to 1 (no reduction in stiffness).

Therefore, to calculate the displacement δ_B it can be stated that:

$$\alpha_y = \alpha_A + K'(\delta_B - \delta_A) \quad (3.5.5)$$

where the unknown is represented by the top sway displacement δ_B , which can be derived as follows:

$$\delta_B = \frac{\alpha_y - \alpha_A}{K'} + \delta_A \quad (3.5.6)$$

Point C (Life Safety), characterized by the complete development of the collapse mechanism and the attainment of the maximum bearing capacity of the structure, derives from the intersection of the second elastic branch with the mechanism equilibrium curve. The displacement δ_C can be derived as follows:

$$\delta_C = \frac{\alpha_0 - \alpha_A + K' \delta_A}{K' + \gamma_s} \quad (3.5.7)$$

Point D (Near Collapse), in which the equilibrium is guaranteed by the forces of inertia and requiring considerable resources of local ductility, can be detected along the descending branch of the trilinear approximation of the α - δ curve. This corresponds to the displacement $\delta_D = \delta_u$, calculated as follows:

$$\delta_D = \varphi_{lim} \cdot H_0 \quad (3.5.8)$$

$$\delta_D = \left(\frac{\delta_{d,cp}}{h_i \cdot \cos \theta} \right) \cdot H_0 \quad (3.5.9)$$

where θ is the angle between the first yielded diagonal and the horizontal direction, φ_{lim} is the capacity in terms of interstorey drift, and $\delta_{d,cp}$ is the capacity in terms of shortening (if buckling of connection plates occurs) or elongation of the diagonal according to Eurocode 8 limitations (Table 3.5.1) [19].

For braces in compression, the inelastic deformation capacity should be expressed in terms of the axial deformation of the brace, as a multiple of the axial deformation of the brace at buckling load, Δ_C .

For braces in tension, the inelastic deformation capacity should be expressed in terms of the axial deformation of the brace, as a multiple of the axial deformation of the brace at yielding load, Δ_T .

Table 3.5.1 Axial deformation capacity for braces in compression according to Eurocode 8 - part 3[19].

Class of cross-section	Limit State		
	DL	SD	NC
1	0.25 Δ_C	4.0 Δ_C	6.0 Δ_C
2	0.25 Δ_C	1.0 Δ_C	2.0 Δ_C

Table 3.5.2 Axial deformation capacity for braces in tension according to Eurocode 8 - part 3[19].

Limit State		
DL	SD	NC
0.25 Δ_T	7.0 Δ_T	9.0 Δ_T

CHAPTER 4

4 CALIBRATION AND VALIDATION OF THE METHOD THROUGH REGRESSION ANALYSIS

4.1 Introduction

Within the framework of an approach for evaluating performance levels, which does not require any nonlinear analysis, it is important to assure a wide application and the calibration of the analytic relationships that have been proposed. A wide parametric analysis has been carried out on 420 steel Simple “X-Shaped” Concentrically Braced frames and 420 steel Moment Resisting Frames, concerning three categories of structures [6],[9].

The parametric analysis has regarded 140 geometrical schemes of low-rise buildings. The parameters are:

- Number of bays: between 2 and 6
- Number of storeys: between 2 and 8
- Design approaches for MRFs: GMRFs, SMRFs, OMRFs
- Design approaches for CBFs: GCBFs, SCBFs, OCBFs
- Bay span: 3,00 m, 4.50 m, 6.00 m, 7.50m

All the combinations were analysed considering dead loads G_k equal to 3.5kN/m^2 , live loads Q_k equal to 3 kN/m^2 , and interstorey height equal to 3.5m. Each frame has been designed considering the design levels previously specified so that $140 \times 3 = 420$ frames have been investigated in the parametric analysis. The study cases here investigated are referred to buildings whose general plan configurations are depicted in Figure 4.1.1 for MRFs and Figure 4.1.2 for CBFs, whose beams are designed for gravity loads.

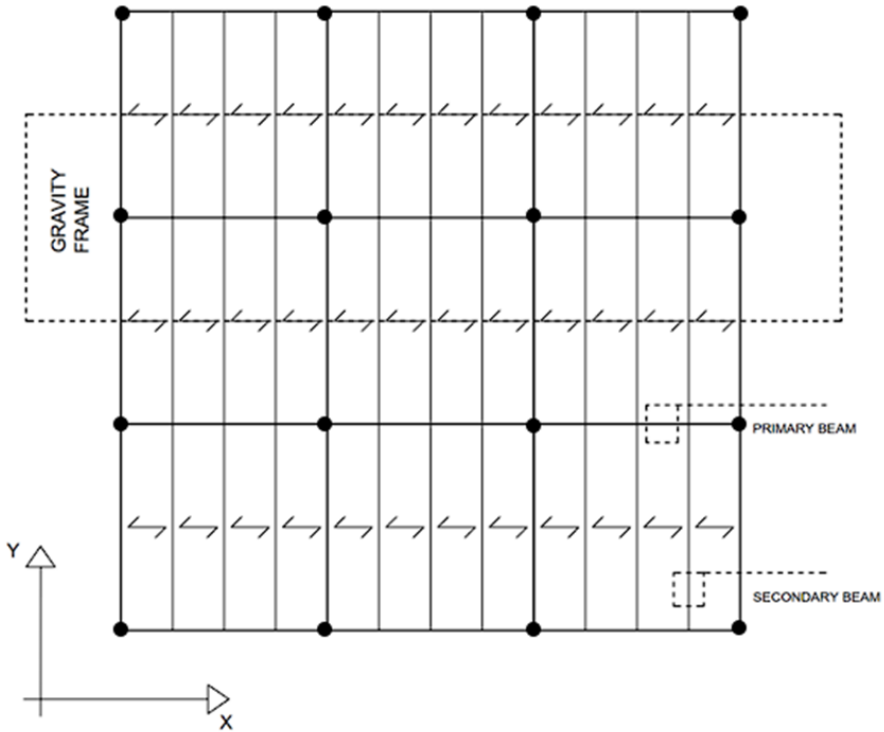


Figure 4.1.1 General plan configuration for MRFs

Both for MRFs and CBFs Each floor is equipped with a double frame of beams, one main and one secondary.

The secondary beams are spaced at $i_{sb} = 1.50$ m so the number of secondary beams (n_{sb}) varies as the length of the spans varies.

The secondary beams are schematized as doubly supported beams subjected to a uniformly distributed load. The load is obtained considering the portion of the deck on which the influence of the secondary beam drops, and which has a width equal to the distance between the secondary beams themselves.

The main beams are schematized as doubly supported beams subject to several concentrated forces equal to the number of secondary beams dropping on the main beam considered. This number varies as the length of the spans varies. The concentrated forces are the reactions (R_{sb}) of the secondary beams supported on the main beams.

In the preliminary design, the loads are to be compared at ULS combination according to Eurocode.

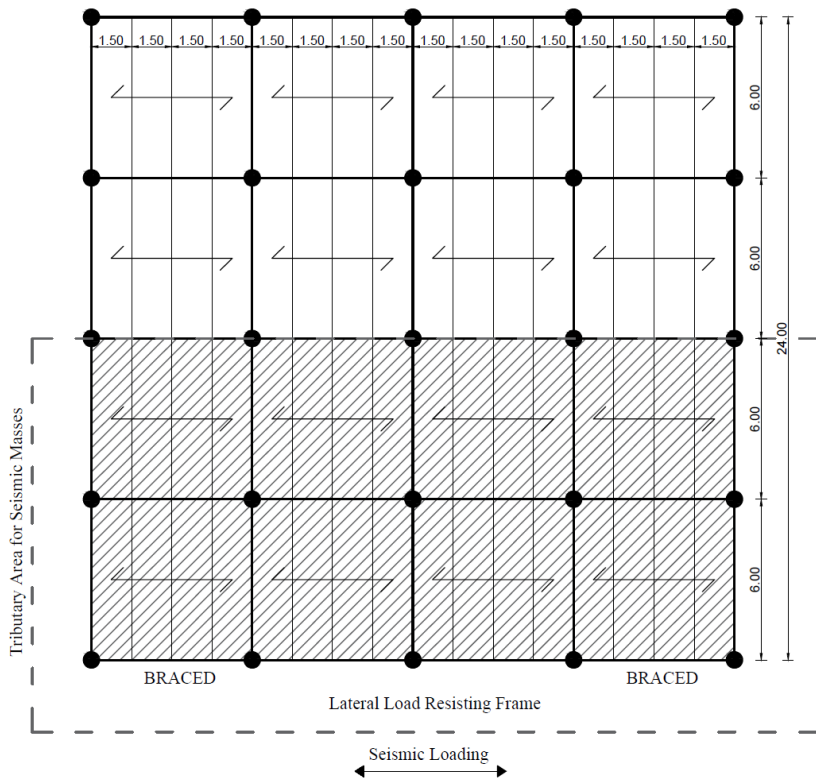


Figure 4.1.2 General plan configuration for CBFs

The 140 geometric patterns are shown in the table, which also provides details on the variable parameters considered and on the design approaches for MRFs and CBFs.

Table 4.1.1 Geometric patterns, variable parameters and design approaches for MRFs and CBFs.

Scheme name	N. of storeys	N. of spans	Span length [m]	Q_k [kN/m^2]	Design Approach MRFs	Design Approach CBFs
2S2B	2	2	3, 4.5, 6, 7.5	3.00	GMRF, SMRF, OMRF	GCBF, SCBF, OCBF
2S3B	2	3	3, 4.5, 6, 7.5	3.00	GMRF, SMRF, OMRF	GCBF, SCBF, OCBF

2S4B	2	4	3, 4.5, 6, 7.5	3.00	GMRF, SMRF OMRF	GCBF, SCBF, OCBF
2S5B	2	5	3, 4.5, 6, 7.5	3.00	GMRF, SMRF OMRF	GCBF, SCBF, OCBF
2S6B	2	6	3, 4.5, 6, 7.5	3.00	GMRF, SMRF OMRF	GCBF, SCBF, OCBF
3S2B	3	2	3, 4.5, 6, 7.5	3.00	GMRF, SMRF OMRF	GCBF, SCBF, OCBF
3S3B	3	3	3, 4.5, 6, 7.5	3.00	GMRF, SMRF OMRF	GCBF, SCBF, OCBF
3S4B	3	4	3, 4.5, 6, 7.5	3.00	GMRF, SMRF OMRF	GCBF, SCBF, OCBF
3S5B	3	5	3, 4.5, 6, 7.5	3.00	GMRF, SMRF OMRF	GCBF, SCBF, OCBF
3S6B	3	6	3, 4.5, 6, 7.5	3.00	GMRF, SMRF OMRF	GCBF, SCBF, OCBF
4S2B	4	2	3, 4.5, 6, 7.5	3.00	GMRF, SMRF OMRF	GCBF, SCBF, OCBF
4S3B	4	3	3, 4.5, 6, 7.5	3.00	GMRF, SMRF OMRF	GCBF, SCBF, OCBF
4S4B	4	4	3, 4.5, 6, 7.5	3.00	GMRF, SMRF OMRF	GCBF, SCBF, OCBF
4S5B	4	5	3, 4.5, 6, 7.5	3.00	GMRF, SMRF OMRF	GCBF, SCBF, OCBF
4S6B	4	6	3, 4.5, 6, 7.5	3.00	GMRF, SMRF OMRF	GCBF, SCBF, OCBF
5S2B	5	2	3, 4.5, 6, 7.5	3.00	GMRF, SMRF OMRF	GCBF, SCBF, OCBF
5S3B	5	3	3, 4.5, 6, 7.5	3.00	GMRF, SMRF OMRF	GCBF, SCBF, OCBF
5S4B	5	4	3, 4.5, 6, 7.5	3.00	GMRF, SMRF OMRF	GCBF, SCBF, OCBF
5S5B	5	5	3, 4.5, 6, 7.5	3.00	GMRF, SMRF, OMRF	GCBF, SCBF, OCBF
5S6B	5	6	3, 4.5, 6, 7.5	3.00	GMRF, SMRF, OMRF	GCBF, SCBF, OCBF
6S2B	6	2	3, 4.5, 6, 7.5	3.00	GMRF, SMRF, OMRF	GCBF, SCBF, OCBF
6S3B	6	3	3, 4.5, 6, 7.5	3.00	GMRF, SMRF, OMRF	GCBF, SCBF, OCBF
6S4B	6	4	3, 4.5, 6, 7.5	3.00	GMRF, SMRF, OMRF	GCBF, SCBF, OCBF
6S5B	6	5	3, 4.5, 6, 7.5	3.00	GMRF, SMRF, OMRF	GCBF, SCBF, OCBF

6S6B	6	6	3, 4.5, 6, 7.5	3.00	GMRF, SMRF, OMRF	GCBF, SCBF, OCBF
7S2B	6	2	3, 4.5, 6, 7.5	3.00	GMRF, SMRF, OMRF	GCBF, SCBF, OCBF
7S3B	6	3	3, 4.5, 6, 7.5	3.00	GMRF, SMRF, OMRF	GCBF, SCBF, OCBF
7S4B	6	4	3, 4.5, 6, 7.5	3.00	GMRF, SMRF, OMRF	GCBF, SCBF, OCBF
7S5B	6	5	3, 4.5, 6, 7.5	3.00	GMRF, SMRF, OMRF	GCBF, SCBF, OCBF
7S6B	6	6	3, 4.5, 6, 7.5	3.00	GMRF, SMRF, OMRF	GCBF, SCBF, OCBF
8S2B	8	2	3, 4.5, 6, 7.5	3.00	GMRF, SMRF, OMRF	GCBF, SCBF, OCBF
8S3B	8	3	3, 4.5, 6, 7.5	3.00	GMRF, SMRF, OMRF	GCBF, SCBF, OCBF
8S4B	8	4	3, 4.5, 6, 7.5	3.00	GMRF, SMRF, OMRF	GCBF, SCBF, OCBF
8S5B	8	5	3, 4.5, 6, 7.5	3.00	GMRF, SMRF, OMRF	GCBF, SCBF, OCBF
8S6B	8	6	3, 4.5, 6, 7.5	3.00	GMRF, SMRF, OMRF	GCBF, SCBF, OCBF

4.2 Calibration Through Pushover Analysis

To evaluate the overall seismic performances of the structures, non-linear static analyses (pushover) have been carried out for each designed structure by SAP 2000 computer program. The primary aim of this analysis is to collect results to impose as a target value for the calibration procedure of the proposed analytical relationship, through regression analysis.

The secondary aim is the assessment of the collapse mechanism typology, to compare with the one evaluated by the second-order rigid-plastic analysis.

4.2.1 Mechanical Modelling of Members for MRFs

Pushovers have been carried out by means of SAP2000 computer program [30] with a load pattern distribution compliant with the first vibration mode [6].

Beams and columns have been modelled by means of beam-column elements whose non-linearities have been concentrated in plastic hinges (“P-hinge” elements) located at their ends. A simple M3 moment P-hinge has been selected for beams (Table 4.2.1). Plastic hinges accounting for the interaction between axial force and bending moment have been defined for columns (Table

4.2.2). Both the maximum resistance of columns and beams has been computed considering the random material variability and hardening (1.10×1.25).

Table 4.2.1 Moment/rotation model for beams.

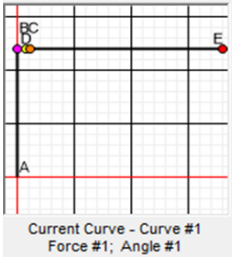
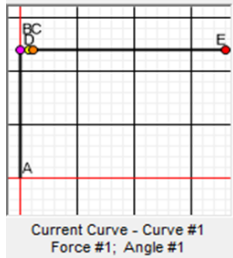
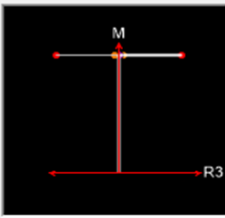
Point	Moment/Yield Moment	Rotation/SF	Moment SF= M_{pl}	Rotation SF =1
A	0	0		
B	1	0		
C	1	0.04		
D	1	0.06		
E	1	1		

Table 4.2.2 Moment/rotation model for columns.

Point	Moment/Yield Moment	Rotation/SF	$P=P_y$	$M3=M_{pl}$
A	0	0		
B	1	0		
C	1	0.04		
D	1	0.06		
E	1	1		

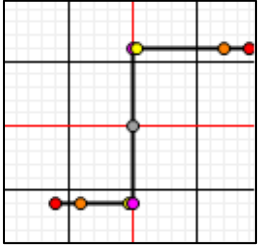
The pushover analysis has been led under displacement control considering both geometrical and mechanical non-linearities. The pushover curve is provided with reference to a structural model based on the use of simple rigid-perfectly plastic hinges.

4.2.2 Mechanical Modelling of Members for CBFs

In the case of CBFs, Columns have been modelled by means of beam-column elements, whose non-linearities have been concentrated in plastic hinges (“p-hinge” elements) located at their ends [9]. In particular, plastic hinges accounting for the interaction between axial force and bending moment have been defined for columns (Table 4.2.2).

An axial P hinge element accounting for buckling has been located at the middle length of the column (Table 4.2.3).

Table 4.2.3 Force/Displacement parameters for axial P hinge - columns.

Point	Force/SF	Displacement/SF	Force SF	Disp SF
E-	-1	-6	P_y - positive	Δ_t - positive
D-	-1	-4	P_{crit} - negative	Δ_c - negative
C-	-1	-0.25		
B-	-1	0		
A	0	0		
B	1	0		
C	1	0.25		
D	1	7		
E	1	9		

As regards diagonal members, an axial P hinge element with an asymmetric link has been located at the midspan (Table 4.2.4). The compression branch accounting for buckling has been modelled using the simplified Georgescu multi-linear model by introducing target points defined according to Eurocode 8 limitations in terms of elongation (Table 4.2.5) and shortening (Table 3.5.1).

Table 4.2.4 Force/Displacement parameters for axial P hinge - braces.

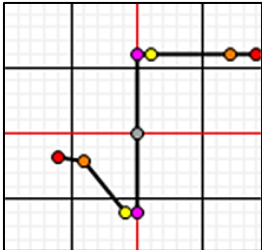
Point	Force/SF	Displacement/SF	Force SF	Disp SF
E-	$-P(\delta_{NC})/P_{crit}$	-6	P_y - positive	Δ_t - positive
D-	$-P(\delta_{SD})/P_{crit}$	-4	P_{crit} - negative	Δ_c - negative
C-	-1	$\delta_{br.B}/\Delta_c$		
B-	-1	0		
A	0	0		
B	1	0		
C	1	1		
D	1	7		
E	1	9		

Table 4.2.5 Axial deformation capacity for braces in tension according to Eurocode 8 - part 3

Limit State		
DL	SD	NC
$0.25 \Delta_T$	$7.0 \Delta_T$	$9.0 \Delta_T$

For braces in compression, the inelastic deformation capacity should be expressed in terms of the axial deformation of the brace, as a multiple of the axial deformation of the brace at buckling load, Δ_c . For braces in compression, the inelastic deformation capacities at the three limit states may be taken in accordance with Table 3.5.1. For braces in tension, the elongation limit is expressed as a multiple of the Plastic axial deformation Δ_T .

4.3 Evaluation of Maximum Multiplier of Horizontal Forces according to Merchant-Rankine Formula for MRFs

The trilinear approximation of the curve can be obtained by defining the mechanism equilibrium curve (Eq.(3.2.4)), the maximum load-bearing capacity curve (Eq.(3.2.3)), and the elastic branch (Eq.(3.2.2)). The determination of the maximum multiplier α_{max} , corresponding to the maximum bearing capacity, needs the use of the Merchant-Rankine formula. This formula expresses α_{max} , as a combination of the collapse multiplier obtained by the rigid-plastic analysis α_0 and the critical collapse multiplier for vertical loads α_{cr} [13]:

$$\frac{1}{\alpha_{max}} = \frac{1}{\alpha_0} + \frac{1}{\alpha_{cr}} \quad (4.3.1)$$

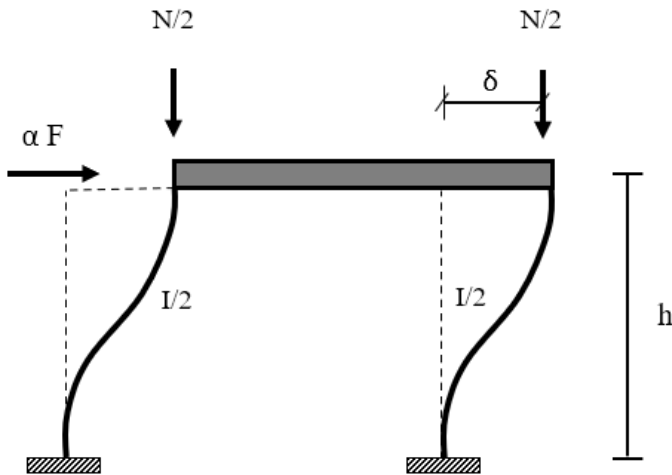


Figure 4.3.1 Kinematics of single-storey MRF subject to seismic force.

A single storey Grinter MRF, subjected to vertical and horizontal actions has been defined (Figure 4.3.1). The critical collapse multiplier for vertical loads α_{cr} can be defined as:

$$\alpha_{cr} = \frac{N_{cr}}{N} = \frac{\pi^2 EI_c}{Nh^2} \quad (4.3.2)$$

Where N_{cr} is the critical buckling load for the columns, I_c is the inertia of the columns, N is the sum of the vertical loads acting on the structure and h is the height of the structure (see Figure 4.3.1).

Accounting for second-order effects, the initial stiffness k_1 and the slope γ can be defined as follows:

$$k_1 = \frac{12EI_c}{h^3} \quad (4.3.3)$$

$$\gamma = \frac{N}{K_1 h} \quad (4.3.4)$$

The critical multiplier α_{cr} can be written as:

$$\alpha_{cr} = \frac{\pi^2 EI_c}{K_1 \gamma h^3} = \frac{\pi^2 EI_c}{\gamma h^3} \cdot \frac{h^3}{12EI_c} \cong \frac{1}{\gamma} \quad (4.3.5)$$

Consequently, it is possible to rearrange Eq.(4.3.5) in the following form:

$$\alpha_{max} = \frac{\alpha_0}{1 + \alpha_0 \gamma_s \delta_1} \quad (4.3.6)$$

To improve the level of accuracy in the estimation of α_{max} , and calibrate the formulation on many structural configurations, the following relation is proposed:

$$\alpha_{max} = \frac{\alpha_0}{1 + \Psi \alpha_0 \gamma_s \delta_1} \quad (4.3.7)$$

where:

$$\Psi = a + b\xi \quad (4.3.8)$$

$$\xi = \frac{\sum \frac{EI_b}{L_b}}{\sum \frac{EI_c}{L_c}} \quad (4.3.9)$$

and I_b and L_b are respectively the moment of inertia and the length of the beam; I_c e L_c are the moment of inertia and the height of the column; E is the elastic modulus; a and b are coefficients obtained from regression analysis. The parameter ξ is a stability coefficient and it is calculated with reference to the members of the first storey.

Regression analyses were conducted, evaluating the a and b with the aim of making the values obtained analytically (pushover analyses), as close as possible to those obtained through the non-linear structural analysis considering OMRFs, SMRFs and GMRFs. The determination of the coefficient has been performed through the least squares method [6].

The coefficient Ψ can be computed according to the following relationship, considering a regression analysis accounting for all the design approaches:

$$\Psi = 0.28488 - 0.14042 \xi \quad (4.3.10)$$

More precisely, the coefficients a and b can be distinguished according to the design approach of the building analyzed.

For Ordinary Moment Resisting Frames (OMRFs), i.e. structures designed without special provisions aimed at controlling the collapse mechanism:

$$\Psi = 0.331455 - 0.2239 \xi \quad (4.3.11)$$

For Special Moment Resisting Frames (SMRFs), i.e. structures designed according to hierarchy criteria (EC8, NTC 08, NTC18):

$$\Psi = 0.313266 - 0.081307 \xi \quad (4.3.12)$$

For Global Moment Resisting Frames (GMRFs), i.e. structures designed to exhibit global collapse mechanisms:

$$\Psi = 0.358 - 1.331 \xi \quad (4.3.13)$$

Below are the results of the regression analysis through graphs in which on the x-axis there are the maximum multiplier α_{max} values, obtained analytically, while on the y-axis there are the values obtained through the pushover analyses (Figure 4.3.2-Figure 4.3.5).

The precision of the results obtained is testified by the trendline showing a slope close to the bisector, the regression points leaning against the trendline, and the determination coefficient R^2 close to the unit.

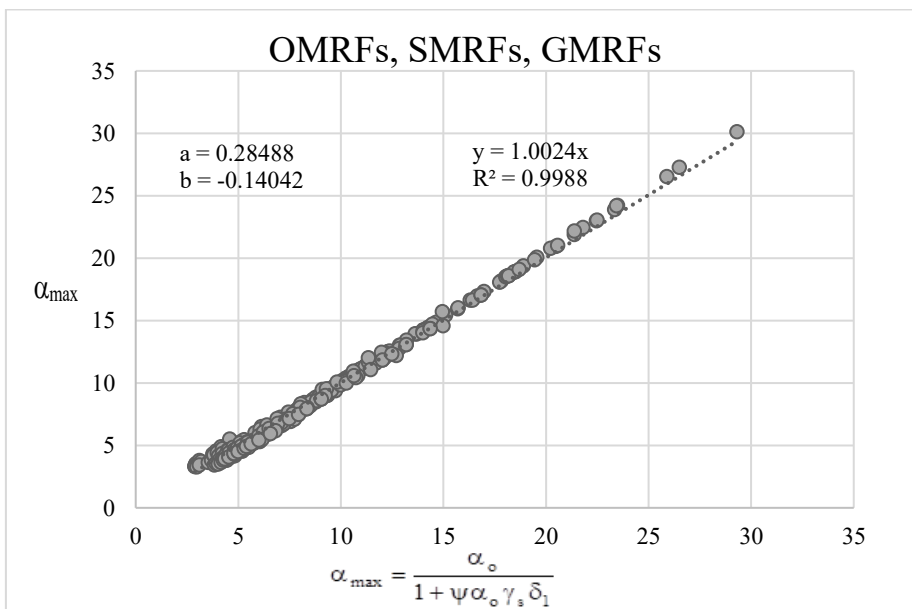


Figure 4.3.2 Regression analysis for GMRFs, SMRFs, OMRFs.

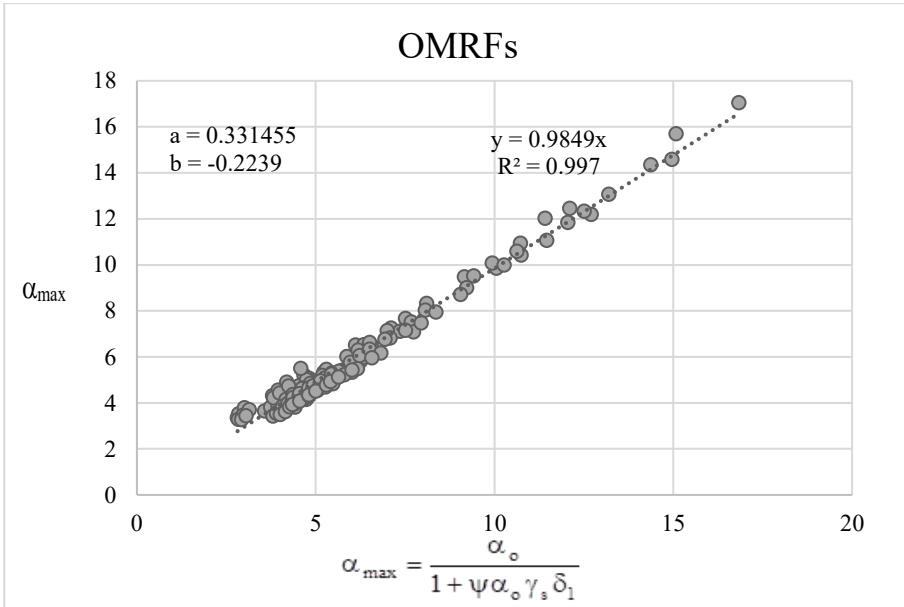


Figure 4.3.3 Regression analysis for OMRFs.

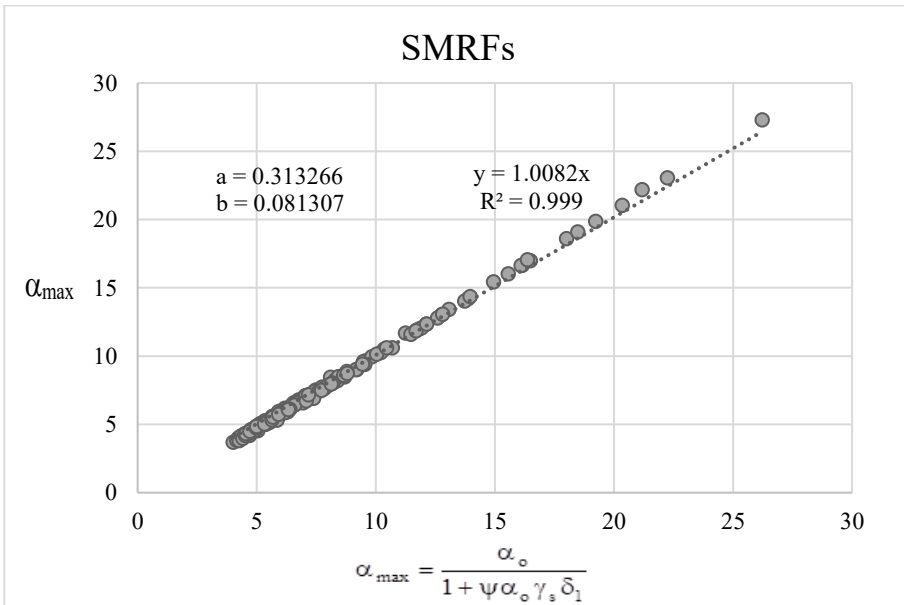


Figure 4.3.4 Regression analysis for SMRFs.

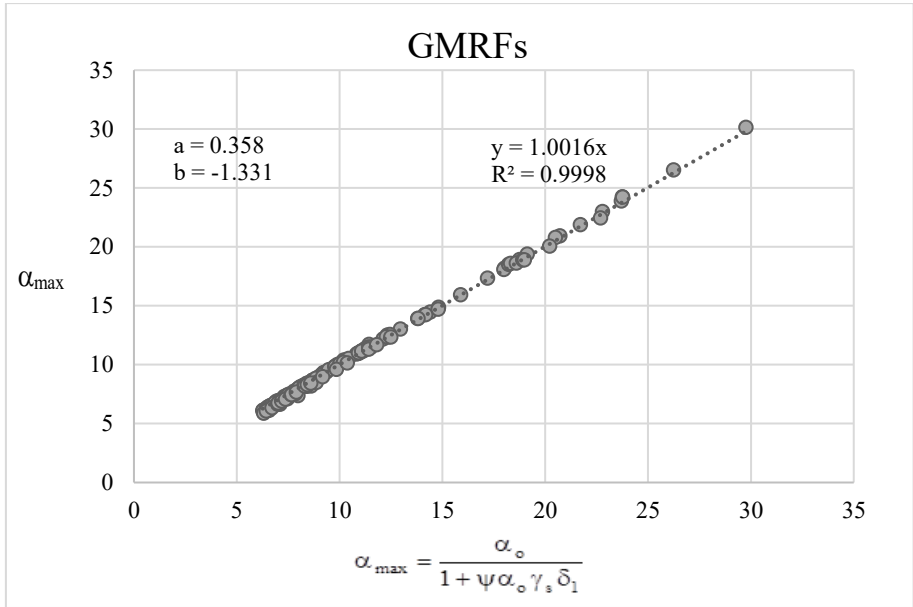


Figure 4.3.5 Regression analysis for GMRFs.

The accuracy of the results obtained is of considerable importance. The accuracy in determining the maximum multiplier and the high adaptability to the different parameters shown by the Merchant-Rankine formula is the first strong signal of the actual accuracy with which the pushover curve can be approximated through the proposed methodology.

4.3.1 Assessment of the precision of the method through δ_C (MRFs)

To assess the precision of the proposed trilinear model, in the case of MRFs, reference is made to point C, corresponding to the full development of the collapse mechanism. Referring to Eq. (3.3.4), it can be noted that to analytically evaluate the displacement δ_C it is necessary to evaluate first the collapse multiplier α_0 , the slope of the mechanism equilibrium curve γ_s , the maximum multiplier α_{\max} , and the top sway displacement at yielding δ_A . Consequently, a high correspondence between the δ_C values analytically evaluated and those evaluated by structural analysis, would guarantee great precision in defining the capacity of the structure until collapse, through the simplified method.

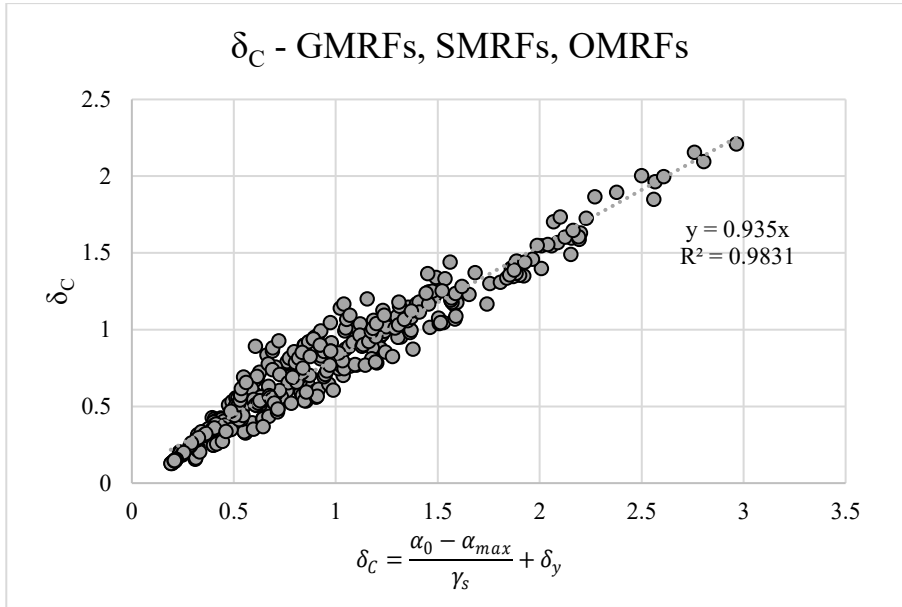


Figure 4.3.6 Precision in the simplified evaluation of δ_C (MRFs).

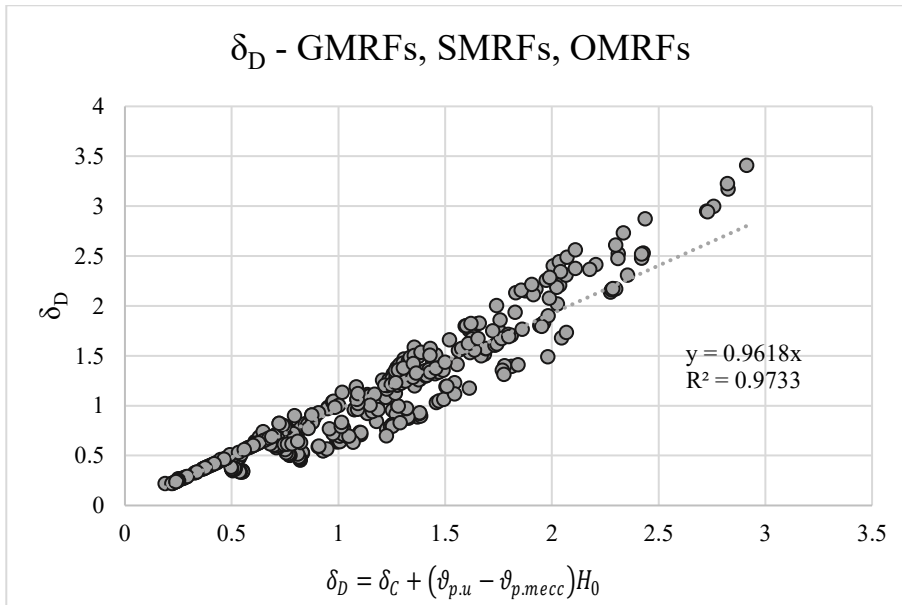


Figure 4.3.7 Precision in the simplified evaluation of δ_D (MRFs).

In Figure 4.3.6 is reported a graph in which on the x-axis there are the δ_C values, obtained analytically, while on the y-axis there are the values obtained through the pushover analyses. The precision of the results obtained is testified by the trendline with a slope close to the bisector, the regression points leaning against the trendline, and the determination coefficient R^2 close to the unit. In Figure 4.3.7 is reported a graph in which on the x-axis there are the δ_D values, obtained analytically, while on the y-axis there are the values obtained through the pushover analyses. The precision of the results obtained is very high as for the top sway displacement δ_C

4.4 Evaluation of Maximum Multiplier of Horizontal Forces according to Merchant-Rankine Formula for CBFs

The evaluation of the maximum multiplier of horizontal forces is useful to check the precision of the model and is also suitable to correct the value of the first order collapse multiplier α_0 in the cases in which the elastic deformability of the structure, relevant for structures with pinned bases, makes the rigid-plastic analysis being imprecise.

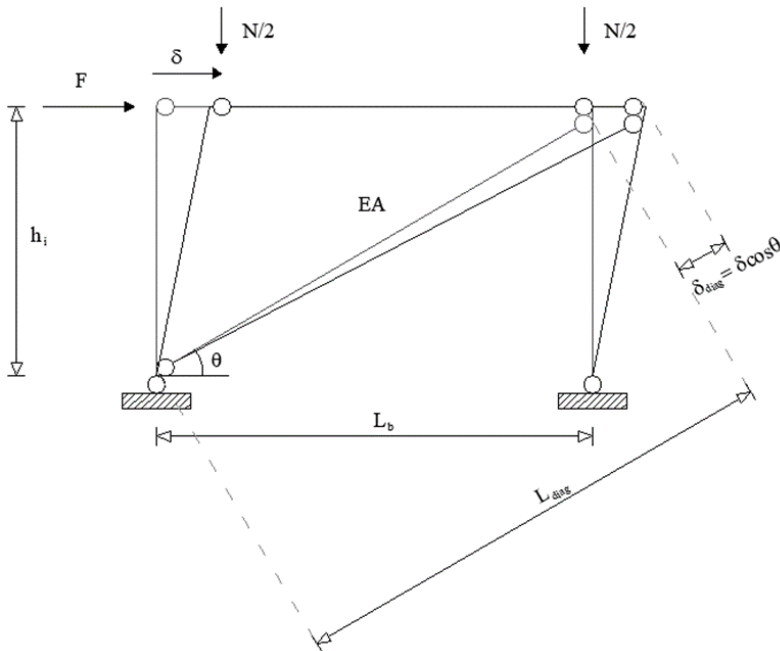


Figure 4.4.1 Kinematics of single-storey CBF subject to seismic force.

Since for simple CBFs the plastic redistribution capacity is limited, the point corresponding to the first yielding is very close to the one corresponding to the maximum bearing capacity in α - δ plane. Consequently, a way to define a corrected estimation of the first-order collapse multiplier is to sum the elastic part of the total displacement δ_y along the mechanism equilibrium curve to the maximum multiplier α_{max} [9].

The determination of the maximum multiplier α_{max} , corresponding to the maximum bearing capacity is defined using the Merchant-Rankine formula as a combination of the collapse multiplier obtained by the rigid-plastic analysis α_0 and the critical collapse multiplier for vertical loads α_{cr} as reported in Eq.(4.3.1)[9].

Considering a single storey simple CBF and accounting for second-order effects, as depicted in Figure 4.4.1, The initial stiffness k_l and the slope γ can be defined as follows:

$$k_{1,d} = \frac{EA_{diag}}{L_{diag}} \cos^2 \theta \quad (4.4.1)$$

$$\gamma = \frac{N}{K_{1,d}h} \quad (4.4.2)$$

where A_{diag} is the area of diagonals, L_{diag} is the length of the diagonal, θ is the angle between the diagonal and horizontal direction.

Consequently, the critical multiplier α_{cr} can be written as:

$$\alpha_{cr} = \frac{\pi^2 EI_c}{K_1 \gamma h^3} = \frac{1}{D\gamma} \quad (4.4.3)$$

where

$$D = \frac{K_1 h^3}{\pi^2 EI_c} \quad (4.4.4)$$

Analysing the D coefficient, it is evident that it depends on the ratio between the lateral stiffness given by the diagonal k_l and the one given by the column, less than a factor and considering that:

$$\frac{1}{\alpha_{cr}} \approx D\gamma = D\gamma_s \delta_1 \quad (4.4.5)$$

It is possible to rearrange Eq. (4.3.1) in the following form:

$$\alpha_{max} = \frac{\alpha_0}{1 + \alpha_0 D \gamma_s \delta_1} \quad (4.4.6)$$

To improve the level of accuracy in the estimation of α_{max} , and calibrate the formulation on many structural configurations, the following relation is proposed:

$$\alpha_{max} = \frac{\alpha_0}{1 + \Psi_{CBF} \alpha_0 \gamma_s \delta_1} \quad (4.4.7)$$

where:

$$\Psi_{CBF} = a + b \xi_{CBF} \quad (4.4.8)$$

$$\xi_{CBF} = \frac{\sum n_{bc} \frac{EA_{diag}}{L_{diag}} \cdot \frac{1}{1 + (L_b/h)^2}}{\sum n_c \frac{EI_c}{h^3}} \quad (4.4.9)$$

L_b is the bay span, a and b are coefficients obtained from regression analysis. The parameter ξ_{CBF} is evaluated by considering the members of the first storey.

Regression analyses have been conducted, evaluating a and b , to make the values obtained analytically, as close as possible to those obtained through the non-linear structural analysis considering SCBFs and GCBFs. OCBFs are structures whose diagonal braces strength has been evaluated according to the seismic design loading. Therefore, column sections are dimensioned to withstand the unloading actions coming from the diagonals without any specific hierarchy criterion design provision. It is worth observing that columns fail for buckling before the development of any possible dissipative mechanism. All the 140 OCBFs have been analyzed as well as the other frames but the obtained result in terms of pushover curve is in perfect agreement with the expected behaviour of the structure, namely a brittle overall failure.

For this reason, the simplified method provides only the first 2 branches, and the OCBFs are set aside by the calibration of the Merchant-Rankine formula [9].

The coefficient Ψ_{CBF} can be computed according to the following relationship, considering both the design approaches:

$$\Psi_{CBF} = 1.00421 + 0.10265 \xi_{CBF} \quad (4.4.10)$$

The coefficient Ψ_{CBF} has been determined also for the single approaches. For Global Concentrically Braced frames

$$\Psi_{CBF} = 1.410677 + 0.294433 \xi_{CBF} \quad (4.4.11)$$

while for Special Concentrically Braced frames

$$\Psi_{CBF} = 0.18799 + 0.11338 \xi_{CBF} \quad (4.4.12)$$

The results of the regression analysis are reported in Figure 4.4.2-Figure 4.4.4.

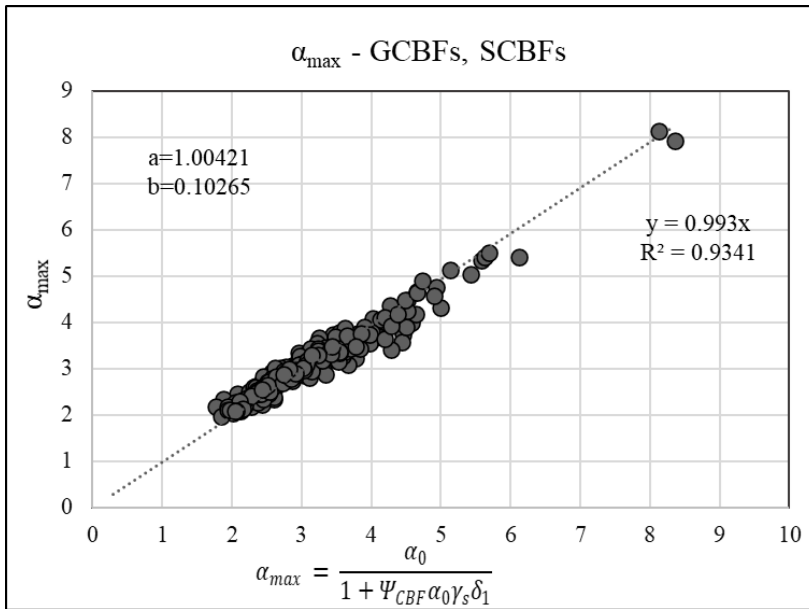


Figure 4.4.2 Regression analysis for GCBFs, SCBFs.

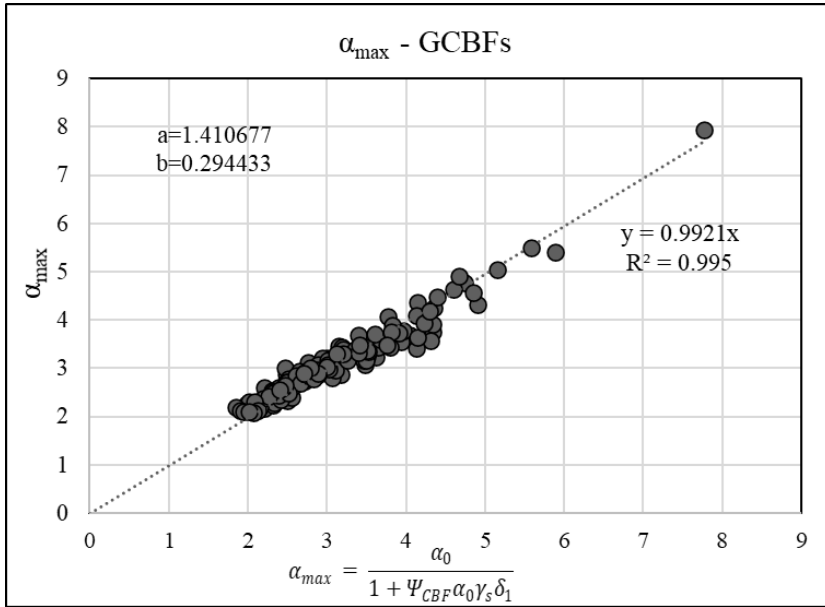


Figure 4.4.3 Regression analysis for GCBFs.

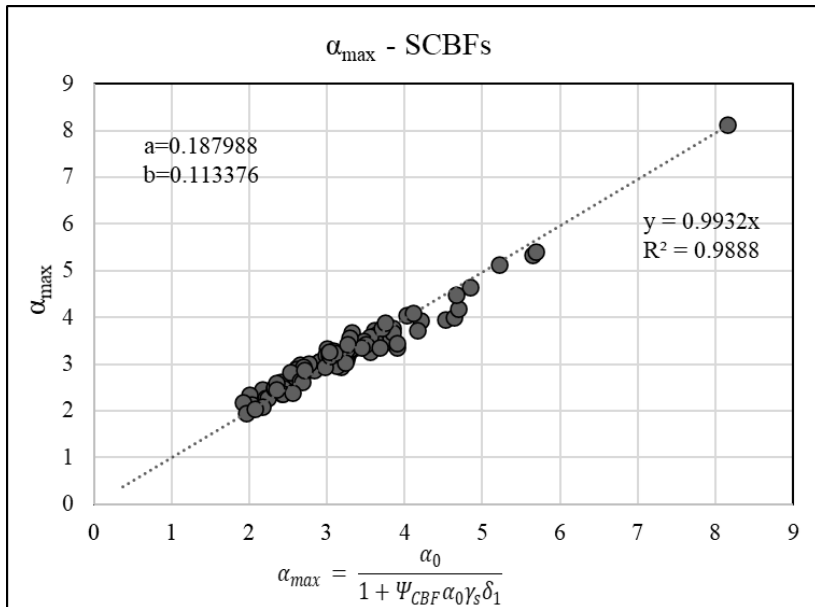


Figure 4.4.4 Regression analysis for SCBFs.

Given the accuracy in estimating the maximum collapse multiplier, it is possible to calculate, if $\alpha_0 > \alpha_{max}$ a correct multiplier $\bar{\alpha}_0$ in the following way:

$$\bar{\alpha}_0 = \alpha_{max} + \gamma_s \delta_y \quad (4.4.13)$$

The obtained multiplier can be used for the evaluation of the multiplier and the displacement corresponding to point C.

4.4.1 Assessment of the precision of the method through δ_C (CBFs)

To assess the precision of the proposed trilinear model, in the case of CBFs, reference is made to point C, corresponding to the achievement of maximum bearing capacity and the formation of the collapse mechanism [9]. Referring to Eq. (3.5.7), it can be noted that to analytically evaluate the displacement δ_C it is necessary to evaluate first the collapse multiplier α_0 , the slope of the mechanism equilibrium curve γ_s , the stiffness of the second elastic branch K' , the multiplier associated with the first buckling of a diagonal α_A and the corresponding top sway displacement δ_A .

Consequently, the accuracy of the analysis can be testified by the precision obtained in the analytical evaluation of the individual components of the formula. The first buckling multiplier α_A and the corresponding top sway displacement δ_A can be determined by iterative elastic analysis with increasing horizontal loads. Finally, it remains evaluating the accuracy of the slope of the second elastic branch whose stiffness is K' . Based on the considerations made, a high correspondence between the analytical evaluation and that resulting from the pushover analysis of point C would confirm the accuracy in estimating the stiffness of the second elastic branch, and the precision of the entire model. The validation is reported in Figure 4.4.5 where the values of δ_C obtained by pushover analysis and the values obtained analytically are reported in the x and y axes, respectively. The graph in Figure 4.4.5 shows the high level of precision achieved, evidenced by the coefficient of determination close to the unit and by the presence of points leaning against the trend line which is very close to the bisector.

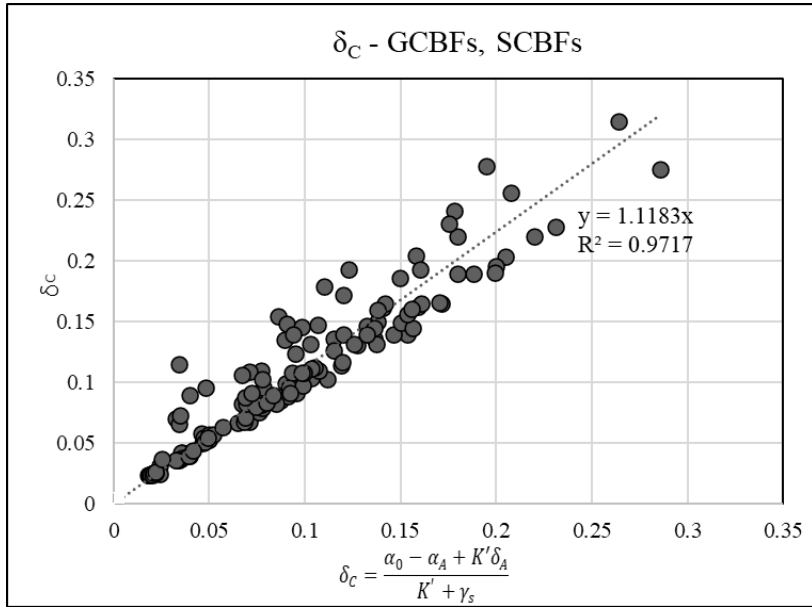


Figure 4.4.5 Precision in the evaluation of δ_C (CBFs).

A further study was carried out by defining variation ranges of the slope reduction β and the value of α_A expressed as a reduced multiplier compared to α_{max} . The results of the structural analysis showed variability of β between 0.6 e 0.7, also confirmed by the application of the analytical relationship, while for the reduced multiplier a range was found between $0.5\alpha_{max}$ e $0.6\alpha_{max}$. Because of the small variation range, a linear regression was carried out to define the exact coefficients that could minimize the deviations between δ_C defined through pushover analysis and analytically (Figure 4.4.6). Downstream of the regression analysis, a simplified, alternative, formula is proposed for the evaluation of δ_C , characterized by similarly high precision (Eq.(4.4.14)).

$$\delta_C = \frac{\alpha_0 - 0.55\alpha_{max} + 0.7K\delta_A}{0.7K + \gamma_S} \quad (4.4.14)$$

In Figure 4.4.7 the values of δ_D obtained by pushover analysis and the values obtained analytically are reported in the x and y axes, respectively. The graph in Figure 4.4.5 shows the high level of precision achieved.

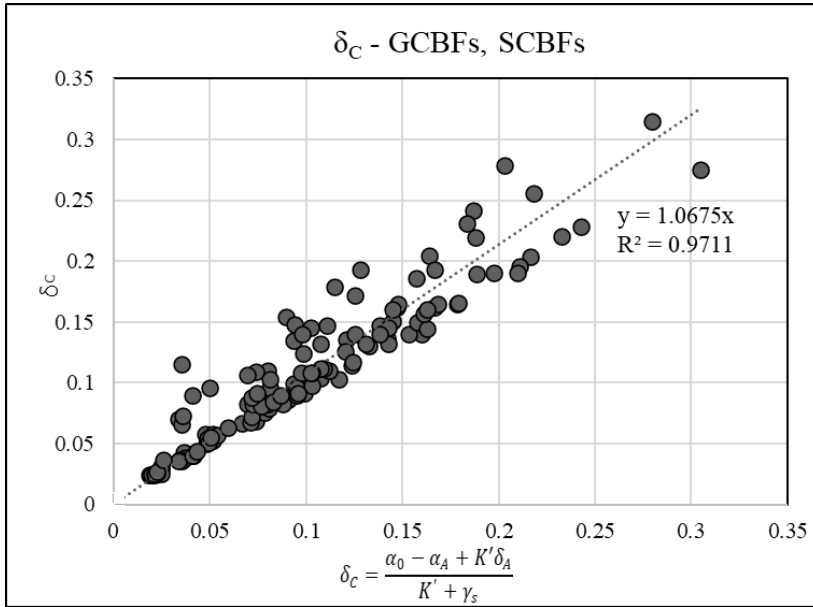


Figure 4.4.6 Precision in the simplified evaluation of δ_c (CBFs).

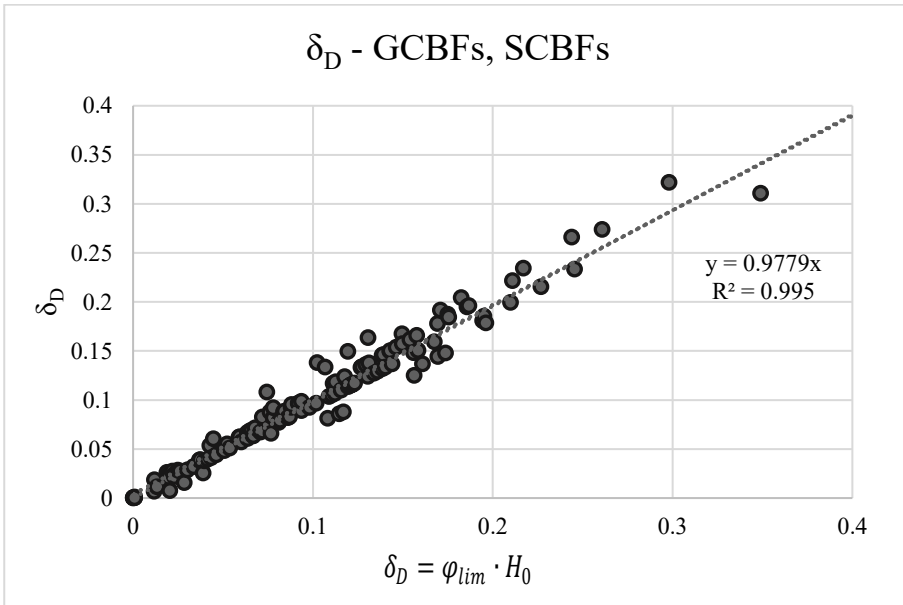


Figure 4.4.7 Precision in the simplified evaluation of δ_D (CBFs).

4.5 Evaluation of the Plastic Hinge Rotation Demand $\theta_{p.mec}$ and $\theta_{p.amax}$ for MRFs

The most important behavioural parameters characterizing the inelastic performance of a structure are the following [13],[14]:

- the global ductility $\mu = \frac{\delta_u}{\delta_y}$
- the plastic redistribution parameter $\frac{\alpha_u}{\alpha_y}$
- the slope of the softening branch γ (i.e. stability coefficient)
- the rotational capacity of the critical plastic hinge R
- the typology of collapse mechanism

Referring to global ductility, it is affected by the plastic redistribution capacity that leads, on one hand, to an increase of the load-carrying capacity and on the other hand, to a more severe plastic engagement of plastic hinges, due to their premature formation. In addition, the frame sensitivity to second-order effects influences the slope of the softening branch of the behavioural curve α - δ and, consequently, it affects the value of the available global ductility.

Therefore, the parameters affecting the value of the available global ductility can be summarized as follows:

- the plastic redistribution parameter $\frac{\alpha_u}{\alpha_y}$
- the member rotation capacity R
- the stability coefficient γ

The most simple model that can be used to explain the role that play the above parameters for the available global ductility, is represented by a Grinter's (shear type) single storey portal in which, to represent the plastic redistribution capacity characterizing real frames, it is assumed that the plastic moments are different at the top and at the base of the columns. In Figure 4.5.1 is represented the model from which the subsequent relations will be obtained [6],[13].

As mentioned in Chapter 3.3.1(Eq.(3.3.5)), to define point D of the performance-based model, it is necessary to know, in addition to the rotational capacity of the members, also the demand in terms of plastic rotations

corresponding to the development of the collapse mechanism $\vartheta_{p.mecc}$. An analytical formulation is proposed, based on the model reported in Figure 4.5.1. In addition, a similar relationship for the definition of the plastic rotation demand corresponding to the attainment of the maximum load-bearing capacity $\vartheta_{p.\alpha_{max}}$ is reported, with the aim of evaluating if the departure from elastic to plastic behaviour occurred at point B.

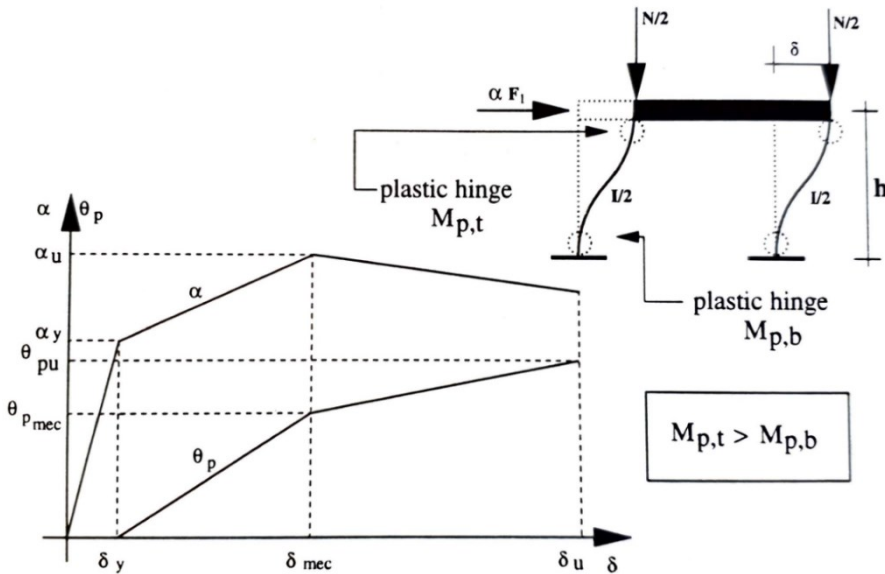


Figure 4.5.1 Grinter's single storey portal model.

Starting from the simplified model, two lateral stiffness values have been defined. A first value K_1 is valid until the elastic threshold is reached, and K_2 post-yielding stiffness, valid until the formation of the collapse mechanism occurs.

Considering second-order effects in the equilibrium of horizontal forces it is obtained the following relation:

$$F + \frac{N\delta}{h} = K_1\delta \quad (4.5.1)$$

The frame is subjected to the vertical load N , and to the horizontal force F . At the elastic threshold, considering the second-order effects, the equilibrium in the horizontal direction provides (first yielding condition):

$$\alpha_y F_1 + \frac{N \delta_y}{h} = K_1 \delta_y \quad (4.5.2)$$

At the activation of the collapse mechanism, the plastic top-sway displacement δ_{pl} is given by:

$$\delta_{pl} = \delta_{mec} - \delta_y \quad (4.5.3)$$

where δ_{mec} is the top-sway displacement corresponding to the formation of the plastic mechanism.

As a result of the first yielding, there is also a reduction in the lateral stiffness of the frame, so that in the plastic field the lateral stiffness will be $K_2 < K_1$ (Figure 4.5.2).

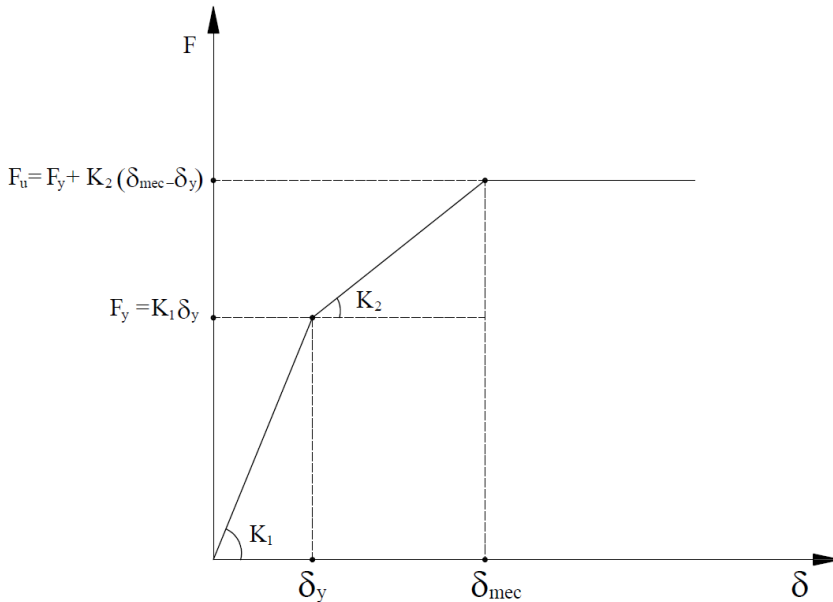


Figure 4.5.2 Lateral stiffness model adopted for the analysed structural scheme.

In collapse condition, the horizontal direction equilibrium changes and becomes:

$$\alpha_u F_1 + \frac{N \delta_{mec}}{h} = K_1 \delta_y + K_2 (\delta_{mec} - \delta_y) \quad (4.5.4)$$

δ_y can be obtained from the Equation (4.5.2) as:

$$\delta_y = \frac{1}{K_1} \left(\alpha_y F_1 + \frac{N \delta_y}{h} \right) \quad (4.5.5)$$

That replaced in the Equation (4.5.4) gives:

$$\alpha_u F_1 + \frac{N \delta_{mec}}{h} = K_1 \frac{1}{K_1} \left(\alpha_y F_1 + \frac{N \delta_y}{h} \right) + K_2 (\delta_{mec} - \delta_y) \quad (4.5.6)$$

Rearranging Equation (4.5.6) appropriately, returns:

$$(\delta_{mec} - \delta_y) = \frac{1}{K_2} \left[(\alpha_u - \alpha_y) F_1 + \frac{N}{h} (\delta_{mec} - \delta_y) \right] \quad (4.5.7)$$

Returning to the first yielding condition Eq.(4.5.2), it is possible to obtain F_1 as follows:

$$F_1 = \frac{K_1}{\alpha_y} \delta_y \left(1 - \frac{N}{K_1 h} \right) \quad (4.5.8)$$

Provided that:

$$\gamma = \frac{N}{K_1 h} \quad (4.5.9)$$

Equation (4.5.8) becomes:

$$F_1 = \frac{K_1}{\alpha_y} \delta_y (1 - \gamma) \quad (4.5.10)$$

Substituting Equation (4.5.10) in Equation (4.5.7), it is obtained:

$$(\delta_{mec} - \delta_y) = \frac{1}{K_2} \left[(\alpha_u - \alpha_y) \frac{K_1}{\alpha_y} \delta_y (1 - \gamma) + \frac{N}{h} (\delta_{mec} - \delta_y) \right] \quad (4.5.11)$$

Factoring out $(\delta_{mec} - \delta_y)$ and multiplying and dividing by K_1 :

$$(\delta_{mec} - \delta_y) \left(1 - \frac{K_1 N}{K_2 K_1 h} \right) = \frac{K_1}{K_2} \left[\frac{(\alpha_u - \alpha_y)}{\alpha_y} \delta_y (1 - \gamma) \right] \quad (4.5.12)$$

from which, recalling the Equations (4.5.9) and (4.5.3), it is obtained:

$$\frac{\delta_{Pl}}{\delta_y} = \frac{K_1}{K_2} \left(\frac{\alpha_u}{\alpha_y} - 1 \right) \frac{(1 - \gamma)}{\left(1 - \frac{K_1}{K_2} \gamma \right)} \quad (4.5.13)$$

The plastic rotations at the base of the structure θ_{Pl} are directly related to displacement δ_{Pl} through the height h considering a rigid collapse mechanism. As a result, Equation (4.5.13) can be written as:

$$\theta_{Pl} = c \frac{K_1}{K_2} \left(\frac{\alpha_u}{\alpha_y} - 1 \right) \frac{\delta_y}{h} \frac{(1 - \gamma)}{\left(1 - \frac{K_1}{K_2} \gamma \right)} \quad (4.5.14)$$

where c is a corrective coefficient linked to the structural typology and to the conversion from displacements to rotations.

Having to adapt Equation (4.5.14) to multi-storey structures, it is better to express h as H_0/n_s where H_0 is the mechanism height of the examined structure and n_s is the number of storeys of the structure.

$$\frac{\theta_{Pl} H_0}{\delta_y n_s} = c \frac{K_1}{K_2} \left(\frac{\alpha_u}{\alpha_y} - 1 \right) \frac{(1 - \gamma)}{\left(1 - \frac{K_1}{K_2} \gamma \right)} \quad (4.5.15)$$

Similarly, the relationship for the evaluation of the plastic rotation demand for the development of the collapse mechanism is proposed as follows:

$$\frac{\theta_{p.mec} H_0}{n_s \delta_y} = \frac{\Psi_1}{\Psi_2} \Psi_3 \left(\frac{\alpha_{max}}{\alpha_y} - 1 \right)^{\Psi_4} \frac{1 - \Psi_5 \gamma_s}{1 - \Psi_6 \gamma_s} \quad (4.5.16)$$

$$\frac{\theta_{p.mec} H_0}{n_s \delta_y} = \frac{\Psi'_1}{\Psi'_2} \Psi'_3 \left(\frac{\alpha_{max}}{\alpha_y} - 1 \right)^{\Psi'_4} \frac{1 - \Psi'_5 \gamma_s}{1 - \Psi'_6 \gamma_s} \quad (4.5.17)$$

for the first yielded element and the critical column, respectively.

Similarly, the relationship to evaluate the plastic rotations corresponding to the achievement of the maximum bearing capacity is given in the form:

$$\frac{\theta_{p.\alpha_{max}} H_0}{n_s \delta_y} = \frac{\Psi_7}{\Psi_8} \Psi_9 \left(\frac{\alpha_{max}}{\alpha_y} - 1 \right)^{\Psi_{10}} \frac{1 - \Psi_{11} \gamma_s}{1 - \Psi_{12} \gamma_s} \quad (4.5.18)$$

where H_0 is the total height of storeys involved into the collapse mechanism, n_s is the number of storeys, α_y is the multiplier of the horizontal forces corresponding to the formation of the first plastic hinge, δ_y is the

displacement corresponding to the formation of the first plastic hinge and is equal to $\delta_1 \alpha_y$ with δ_1 displacement under the design seismic forces.

The Ψ_i coefficients are determined by regression analyses with the least square method and are given by:

$$\Psi_1 = a_1 + b_1 n_b \quad \Psi'_1 = a'_1 + b'_1 n_b \quad (4.5.19)$$

$$\Psi_2 = a_2 + b_2 n_s \quad \Psi'_2 = a'_2 + b'_2 n_s \quad (4.5.20)$$

$$\Psi_i = a_i + b_i \xi \quad \Psi'_i = a'_i + b'_i \xi \quad (4.5.21)$$

$$i = 3, \dots, 6$$

$$\Psi_7 = a_7 + b_7 n_b \quad (4.5.22)$$

$$\Psi_8 = a_8 + b_8 n_s \quad (4.5.23)$$

$$\Psi_k = a_k + b_k \xi \quad k = 9, \dots, 12 \quad (4.5.24)$$

where n_b is the number of bays, n_s is the number of storeys and $\xi = \frac{\sum \frac{EI_b}{L_b}}{\sum \frac{EI_c}{L_c}}$.

These relationships link the plastic rotations corresponding to the maximum multiplier $\vartheta_{p,\alpha_{max}}$ and the formation of the collapse mechanism $\vartheta_{p,mec}$, to the main parameters characterizing the structural behaviour (α_y , multiplier of horizontal forces corresponding to the formation of the first plastic hinge, α_{max} maximum multiplier and γ_s , slope of the collapse mechanism equilibrium curve). They are calibrated by means of a wide parametric analysis, thanks to the data obtained from the Pushover analyses carried out.

Given that, in many cases, the first yielded element and the critical element exceeding the local ductility capacity do not coincide.

Consequently, the evaluation of plastic rotations at the formation of the collapse mechanism requires the selection of the most prone collapsing element. Therefore, two linear regressions are considered (Eqs. (4.5.16) and (4.5.17)). The most unfavourable condition provided by the two regressions must be applied with the scope of not overestimating the actual dissipative capacity.

It is important referring to both the plastic rotation of the first yielded element and the plastic rotation of the critical column, which will be identified according to the typology of collapse mechanism, defined by rigid plastic analysis. In fact, by performing a single linear regression containing the critical

element only for local ductility, it would not be possible to know through the analytical methodology, if the critical element is a column or a beam, thus causing possible non-real member-rotation associations. The proposed formulations are valid also in the case of other rotation capacity model adopted, in other words, the methodology proposed does not fall if the way for the evaluation of the plastic rotation changes.

In order to evaluate the critical member, it is also important to remember the variability of the rotational capacity according to the profile considered, for this, it is important to introduce the coefficient of rotational exploitation, given by the ratio between plastic rotation demand of the member and its rotational capacity θ_d/θ_u . The critical element will be the one characterized by the maximum coefficient of rotational exploitation between the cases “first plastic hinge” and “critical column”. The values of the parameters a_i and b_i , have been determined to make the values obtained analytically, as close as possible to those obtained through the structural analysis program, for OMRFs, SMRFs and GMRFs and are reported in Table 1. The coefficients with apex are referred to the critical column case.

Table 4.5.1 Values of the parameters a_i and b_i

	GMRFs	SMRFs	OMRFs
a₁	2.7747755	2.982417	19.542818
b₁	0.0207354	-0.14356	-1.372652
a₂	1.817070	1.370201	-144.9099
b₂	-0.07731	0.652663	123.8454
a₃	0.0844528	0.964755	-0.028950
b₃	1.616165	1.802312	0.1820582
a₄	-0.112433	0.737624	-1.840828
b₄	1.4966937	-0.51209	3.0361764
a₅	1.0606602	0.976295	97.159963
b₅	0.6787599	1.027818	25.416893
a₆	1.0528759	0.975839	1.8666626
b₆	0.7200734	1.030732	-0.429104
a₇	1.0416842	1.307034	0.5193375
b₇	-0.010106	-0.04927	-0.026298
a₈	1.4746805	-0.51629	-8.989332
b₈	1.9600399	2.089958	8.1703708
a₉	2.4191909	1.177776	0.9718614
b₉	-3.197633	0.564625	-0.101879
a₁₀	1.15158	0.62573	0.1638561
b₁₀	-2.771682	0.665697	0.2129056
a₁₁	0.7467686	1.002079	3.7814613

b₁₁	1.7354908	0.980063	2.3614914
a₁₂	0.7464403	1.007887	1.482424
b₁₂	1.7354092	0.95805	0.275188
a'₁	1.1674452	3.415537	19.508374
b'₁	0.0575325	-0.07355	-0.637701
a'₂	6.0112325	0.251316	-89.8716
b'₂	0.3665074	1.394603	73.87363
a'₃	1.0944684	3.860496	-0.044146
b'₃	-1.169347	-0.09045	0.3181349
a'₄	-2.322765	1.415893	-2.345411
b'₄	7.462743	-1.18406	3.917804
a'₅	0.993180	0.968454	-17.06279
b'₅	0.95649	1.11087	95.899727
a'₆	1.0150939	0.976968	1.5715063
b'₆	0.7912074	1.069351	-0.053770

As evidence, from the results of the pushover analyses developed on the frames subject to parametric analysis and from some theoretical assessments concerning how the structures collapse, it can be noted that the frames designed according to TPMC and therefore characterized by global collapse mechanism, will dissipate energy mainly by means of plastic hinges formed on the beams, which in many cases, but not all, will be the critical collapse element due to lack of resources of local ductility. The coincidence between the first plasticized element and the critical element (beam) is often verified. In the case of the frames designed for only horizontal loads, characterized mainly by soft storey mechanisms, the beams are excluded from the energy dissipation process and for this reason, the plasticized beam elements will be discarded and will be considered the first plasticized column to evaluate plastic rotations when the maximum carrying capacity is reached and when the collapse mechanism is formed. In this case, the coincidence between the first plasticized element and the critical element (column) for local ductility is often verified. The EC8 designed frames will behave in intermediate terms and it will not be possible for them to define a coincidence between the first plasticized element and the critical element.

Given the non-coincidence in many cases between the first plasticised element and the critical element exceeding the local ductility capacity, the evaluation of plastic rotations at the formation of the collapse mechanism will require a double linear regression and consider in any case the most unfavourable condition, in order to ensure universality of application to the

method. We will refer to plastic rotation of the first plasticised element (known by elastic analysis) at the formation of the collapse mechanism and the plastic rotation of the critical column, which will be identified according to the typology of collapse mechanism, defined by rigid plastic analysis.

The results of linear regression carried out on GMRFs, SMRFs, OMRFs are reported in Figure 4.5.3-Figure 4.5.11.

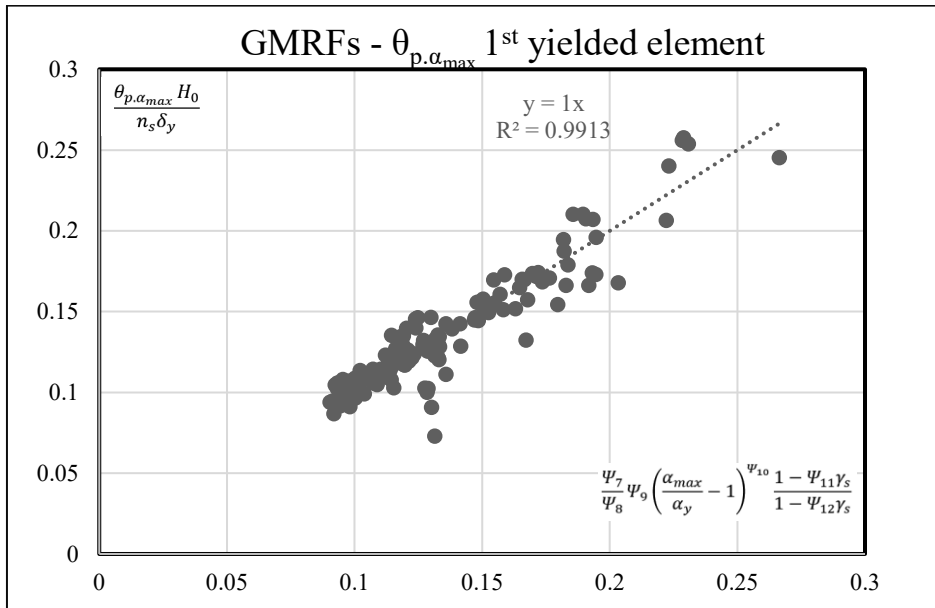


Figure 4.5.3 GMRFs – $\theta_{p,\alpha_{max}}$ 1st yielded element.

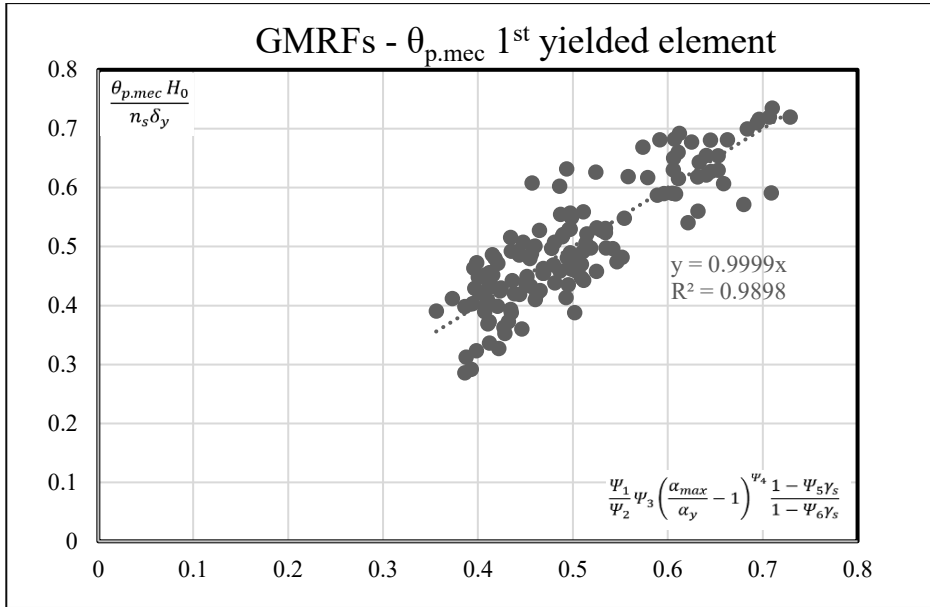


Figure 4.5.4 GMRFs – $\theta_{p.mec}$ 1st yielded element.

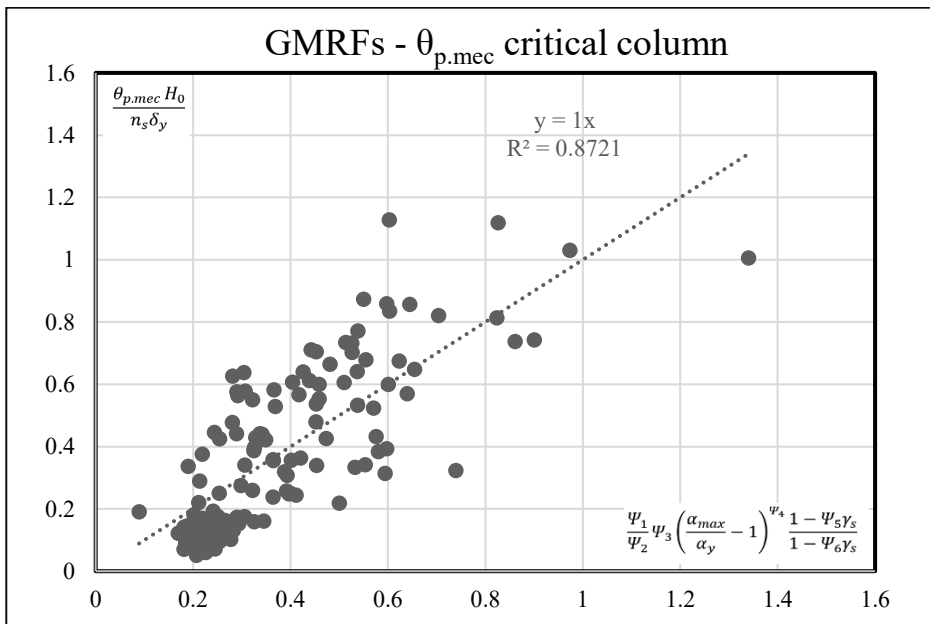


Figure 4.5.5 GMRFs – $\theta_{p.mec}$ critical column.

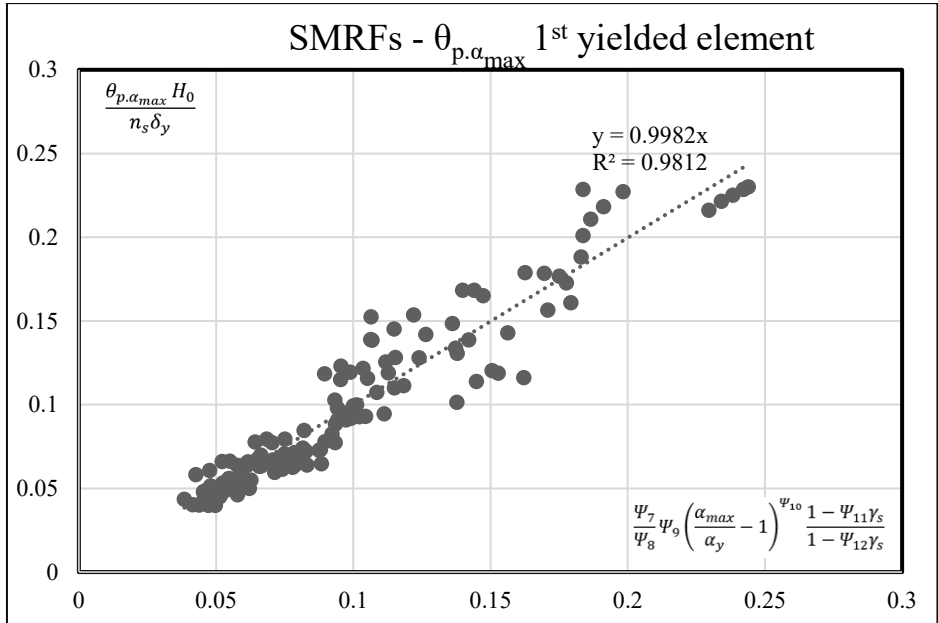


Figure 4.5.6 SMRFs - $\theta_{p,\alpha_{max}}$ 1st yielded element.

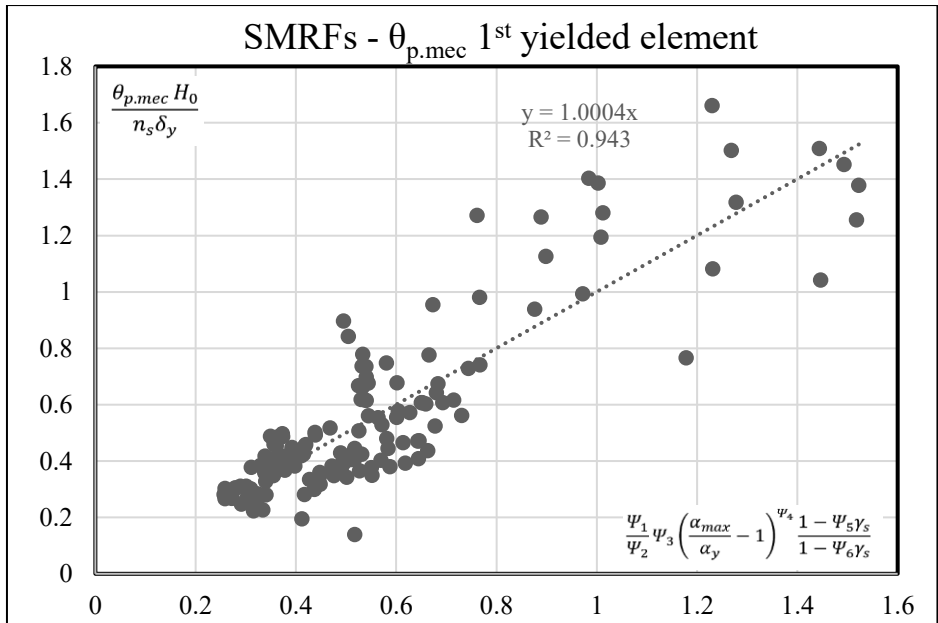


Figure 4.5.7 SMRFs - $\theta_{p,mec}$ 1st yielded element.

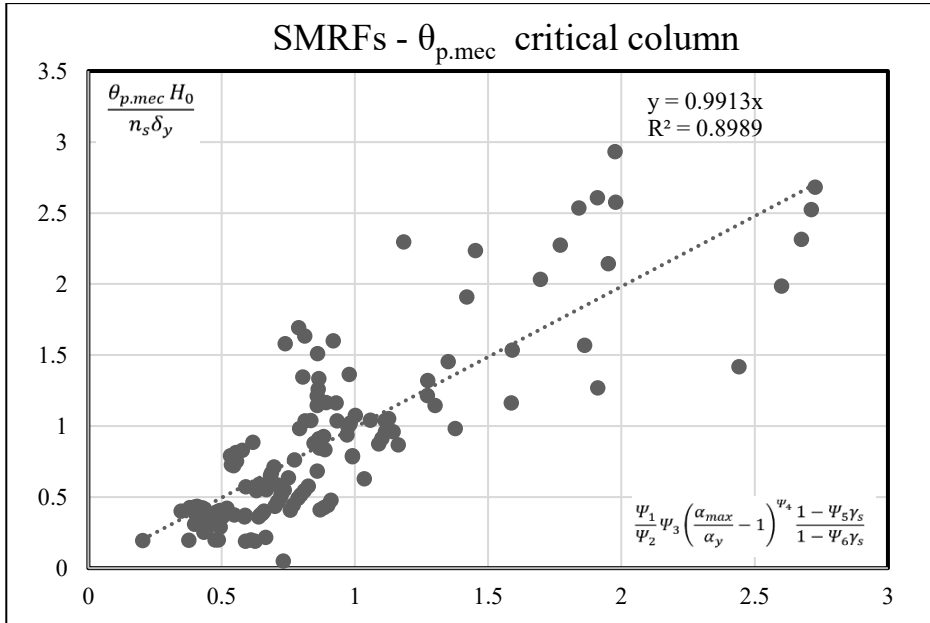


Figure 4.5.8 SMRFs – $\theta_{p,mec}$ critical column.

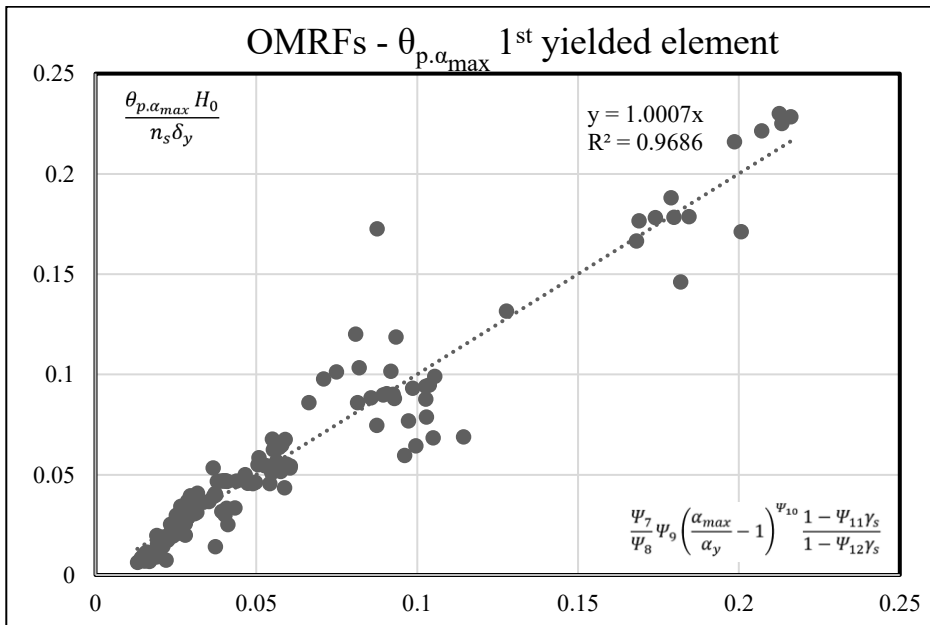


Figure 4.5.9 OMRFs – $\theta_{p,\alpha_{max}}$ 1st yielded element.

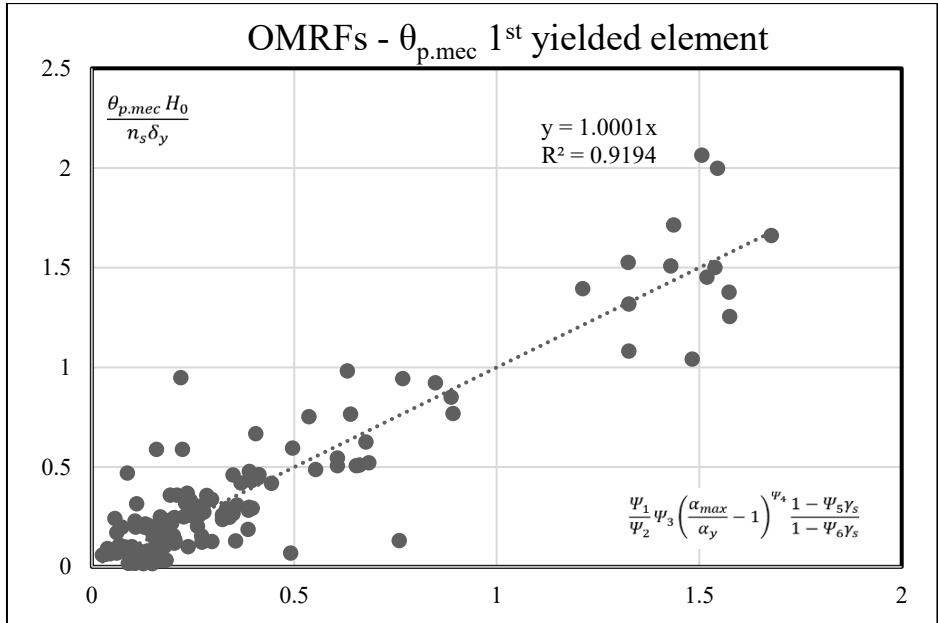


Figure 4.5.10 OMRFs – $\theta_{p.mec}$ 1st yielded element.

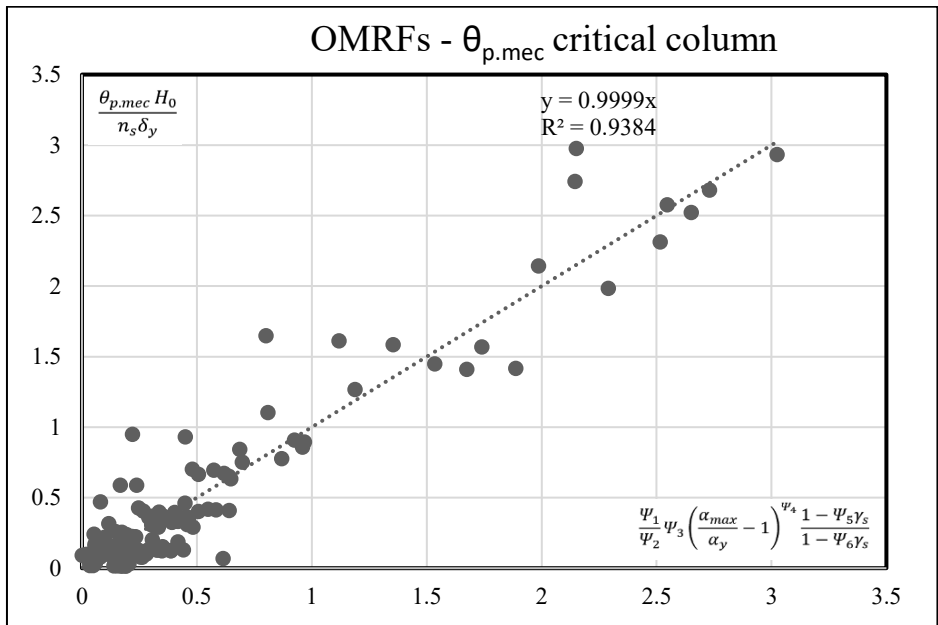


Figure 4.5.11 OMRFs – $\theta_{p.mec}$ critical column.

CHAPTER 5

5 PERFORMANCE-BASED ASSESSMENT PROCEDURES

5.1 Introduction

According to the NTC 18 application circular, Chapter 7, "Design for Seismic Actions" [20] and Eurocode 8 [18],[19], one of the verification methods for constructions is nonlinear static analysis. This method of analysis can be used for constructions whose behaviour under the component of the earthquake considered, is governed by a main mode of vibration, characterized by significant mass participation.

The nonlinear static analysis determines the capacity curve of the structure, expressed by the relation $F_b - d_c$, in which F_b is the seismic shear at the base and d_c is the displacement of a control point, which for buildings is represented by the top sway displacement of the center of mass.

The assessment procedures herein reported have the scope of checking in terms of comparison capacity-demand the performance exhibited by the existing MRFs and CBFs buildings. To this scope, two alternative to code approaches in terms of spectral acceleration, and a graphic ADRS procedure, are reported [6],[9]. The application of the simplified methods has the advantage of allowing an analytical definition of the capacity curve and it is also possible to identify the direct correspondence between the characteristic points of the trilinear model (A, B, C, D) and the code limit states. Moreover, second-order effects are accounted for, allowing to consider the actual energy dissipated.

The first approach exploits the so-called ADRS spectrum and the checking discriminates between low and high periods, the second has a more general validity because it is valid for all the periods range [26]-[29]. The second

approach, in fact, exploits the Nassar & Krawinkler definition of the structure factor q_0 that avoids the distinction between high and low periods of vibration.

5.2 Definition of the Equivalent SDOF System Transformation, SDOF Dynamic Parameters and Capacity Curve in ADRS Plane

The codes and the proposed assessment procedures exploit the definition of an equivalent Single Degree of Freedom (SDOF) replacing the Multiple Degree of Freedom (MDOF) actual system.

Below the schematic steps necessary for the definition of the equivalent system, the capacity curve in the ADRS plan, and the dynamic parameters of the equivalent SDOF system are reported.

- **MDOF – SDOF transformation**

An equivalent structural SDOF system replaces the MDOF actual system introducing the coefficient of participation of the first vibration mode Γ .

$$\Gamma = \frac{\sum_{k=1}^n m_k \phi_k}{\sum_{k=1}^n m_k \phi_k^2} \quad (5.2.1)$$

where m_k is the mass associated to the k-th storey and ϕ_k is the k-th component of the modal vector of the main vibrating mode of the structure.

In order to create a simplified methodology for performance assessment, without carrying out any dynamic analysis of the building to determine the natural vibrating modes, it has been hypothesized a distribution of the displacements of the building, linearly increasing with the height from the foundation plane, according to the distribution of seismic forces.

Consequently, the components of the modal vector ϕ_k can be derived as follows:

$$\phi_k = \frac{F_k}{F_n}; \text{ with } \phi_n = 1 \quad (5.2.2)$$

- **Representation of the capacity curve in the ADRS plan**

The capacity curve must be represented in $F_b - d_c$ plane by multiplying, point by point, the non-dimensional pushover curve with the design base shear.

Therefore, the $F_b - d_c$ curve must be scaled through the modal participation factor and represented in a $F^* - d^*$ plane, in which the shear force F^* and the displacement d^* of the equivalent system are linked to the corresponding quantities of the real system F_b and d_c through the relations $F^* = F_b/\Gamma$, $d^* = d_c/\Gamma$.

To represent the capacity curve in the ADRS plane, where spectral accelerations S_a are represented as a function of spectral displacements S_{De} , the following transformations will be performed for the capacity spectrum:

$$S_a = \frac{F^*}{m^*} \quad (5.2.3)$$

$$S_{De} = d^* \quad (5.2.4)$$

- **Dynamic parameters of the equivalent SDOF system**

To define the "demand", it is necessary to evaluate the period of vibration T^* and the mass m^* of the equivalent SDOF system, through the following relations:

$$T^* = \frac{2\pi}{\omega_0^*} = 2\pi \sqrt{\frac{m^*}{k^*}} \quad (5.2.5)$$

$$m^* = \sum_{k=1}^n m_k \phi_k \quad (5.2.6)$$

$$\text{with } \omega_0^* = \sqrt{\frac{k^*}{m^*}}$$

5.2.1 Evaluation of the stiffness k^* of the equivalent SDOF system for MRFs and CBFs

The stiffness k^* of the equivalent SDOF system, as a result of the representation of the capacity curve in the $F^* - d^*$, it will be equal to k evaluated in plane $F_b - d_c$.

In particular, for MRFs, the stiffness k is the one characterizing the first branch of the trilinear model. It can be obtained as:

$$k_{MRF,1} = \frac{F_{b,A}}{\delta_A} \quad (5.2.7)$$

For CBFs the definition of k can be carried out according to several approaches:

The first approach involves the slope of the first elastic branch in the plane $F_b - d_c$ and can be obtained as:

$$k_{CBF,1} = \frac{F_{b,A}}{\delta_A} \quad (5.2.8)$$

The second approach refers to a secant stiffness that takes into account the slopes of the first and second elastic branches. In this way the stiffness k can be derived as:

$$k_{CBF,2} = \frac{F_{b,C}}{\delta_C} \quad (5.2.9)$$

The first approach is designed for structures that do not reach the plastic threshold due to a lack of local ductility resources.

All the verification procedures shown can be applied indiscriminately and for MRFs and CBFs, paying attention to the definition of the stiffness of the equivalent system k^* .

5.3 Assessment Procedure in Terms of Spectral Displacements into ADRS Plane According to Italian and European Codes

For the quantification of the "demand", the code distinguishes two cases: The first one occurs when the period of the equivalent SDOF system is bigger than the characteristic period T_C . In this case, for equality of displacements, the elastic demand is equal to the plastic one (Figure 5.3.1).

The second one occurs when the period of the equivalent SDOF system is smaller than the characteristic period T_C , and in this case, according to the principle of energy equality, the elastic demand is less than the plastic demand (Figure 5.3.2).

Schematically:

- If $T^* > T_C$, the demand in terms of displacements for the inelastic system is assumed to be the same as that of an elastic system of the same period and will result in:

$$d_{max}^* = d_{e,max}^* = S_{De}(T^*) \quad (5.3.1)$$

where

$$S_{De}(T) = S_a(T) \left(\frac{T}{2\pi} \right)^2 \quad (5.3.2)$$

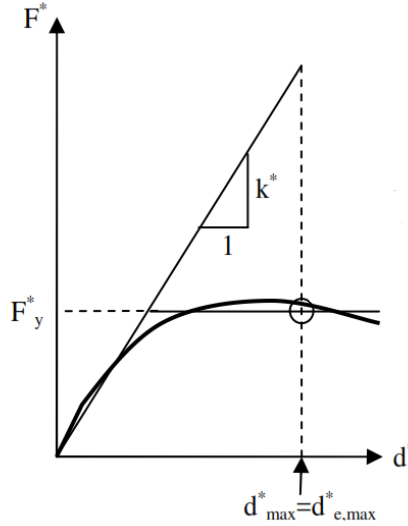


Figure 5.3.1 Displacement demand for $T^* > T_C$

- If $T^* < T_C$, the demand in terms of displacements for the inelastic system is greater than that of an elastic system of equal period and is obtained from it by means of the relation:

$$d_{max}^* = \frac{d_{e,max}^*}{q^*} \left[1 + (q^* - 1) \frac{T_C}{T^*} \right] \geq d_{e,max}^* \quad (5.3.3)$$

Where $q^* = S_e(T^*)m^*/F_y^*$ represents the ratio between the elastic response force and the yielding force of the equivalent system.

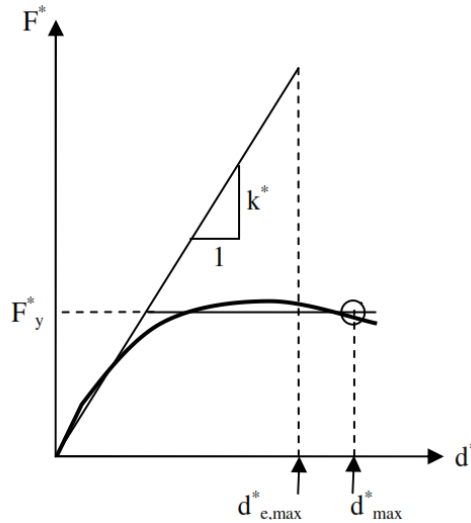


Figure 5.3.2 Displacement demand for $T^* < T_c$

If it results $q^* \leq 1$, consequently $d_{max}^* = d_{e,max}^*$

For the various limit states considered, for the capacity-demand assessment, it will be sufficient to verify the following inequality:

$$d_{max}^* \leq d_{LS}^* \quad (5.3.4)$$

Where d_{LS}^* is the capacity in terms of spectral displacement of the equivalent SDOF system, for the specific Limit State.

5.4 Graphic Assessment Procedure through ADRS Plane

As described, it can be displayed graphically and more intuitively by means of the representation of the capacity and demand spectra on the ADRS plan, for each limit state considered.

The demand spectrum is represented into the ADRS plane, where spectral accelerations S_a are represented as a function of spectral displacements S_{De} , by means of the relation:

$$d_{max}^* \leq d_{LS}^* \quad (5.4.1)$$

In this representation, the periods do not appear explicitly, but are represented by the star of straight lines with centre in the origin of the axes, being the slope of the generic line passing by the origin, equal to $\frac{S_a}{S_{De}} = \left(\frac{2\pi}{T}\right)^2$.

Consequently:

- If $T^* > T_C$, the demand in terms of displacements for the inelastic system is assumed equal to that of an elastic system of the same period for this is obtained by extending the elastic tract (the slope of which is a function of T^*) until the intersection with ADRS spectrum. The projection of the intersection point on the x-axis will represent the demand in terms of displacements $d_{max}^* = d_{e,max}^*$.

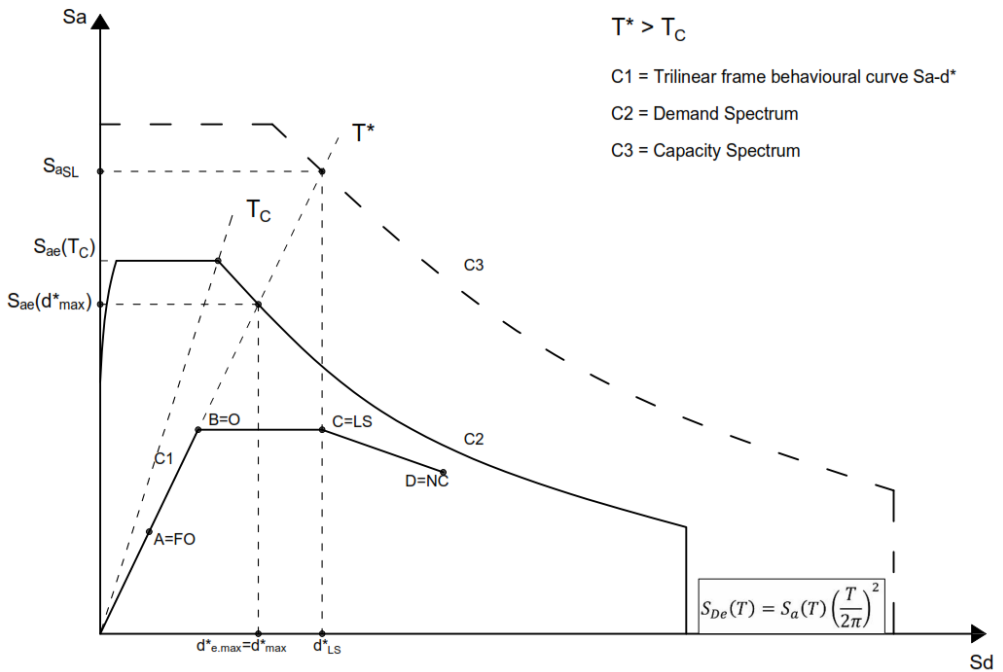


Figure 5.4.1 Graphic assessment procedure for $T^* > T_C$

- If $T^* < T_C$ the demand in terms of displacements for the inelastic system is greater than that of an elastic system of the same period and for this reason the displacement $d_{e,max}^*$ obtained graphically as shown in the previous case, will be increased according to the

criterion of energy equality. $d_{e,max}^*$ will be used to calculate d_{max}^* by means of the equation (5.3.3).

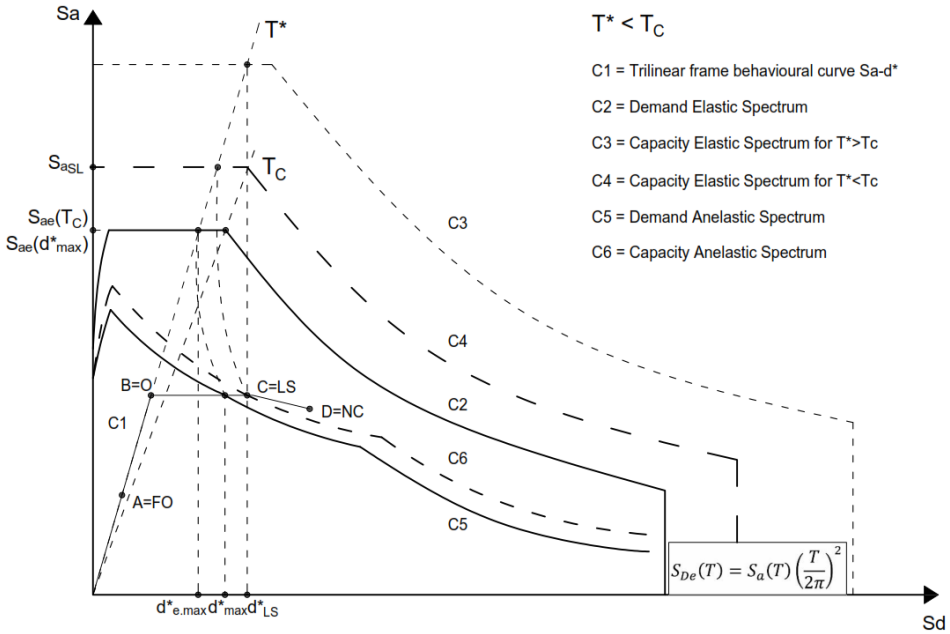


Figure 5.4.2 Graphic assessment procedure for $T^* < T_C$

In conclusion, analysing Figure 5.4.1 and Figure 5.4.2 it can be noted that the scale factor between the dashed line (capacity) and the continuous one (demand), represents the safety factor of the structure.

5.5 Assessment Procedure in Terms of Spectral Acceleration through the ADRS Plane

The capacity-demand assessment procedure can be expressed in terms of spectral accelerations, through the ADRS plane. For each limit state considered, the spectrum $S_a - S_{De}$ will be defined by means of the equation $S_{De}(T) = S_a(T)(T/2\pi)^2$ (demand curve). As regards the capacity, on the other hand, it will be necessary to define in ADRS plane the characteristic points of the behavioural curve of the structure. Of these points, each of which is representative of a limit state, it will be necessary to know the abscissa, that is the displacement $d_{LS}^* = d_{LS}/\Gamma$ where Γ is the modal participation factor

Referring to capacity, it will be necessary to distinguish between cases $T^* > T_C$ e $T^* < T_C$. If $T^* > T_C$ the capacity in terms of spectral acceleration, relative to the limit state considered, can be obtained through the following relation:

$$S_{aSL} = d_{SL}^* \omega_0^{*2} \quad (5.5.1)$$

Graphically, the meaning is to represent the spectrum whose point of intersection with the line characterized by the elastic period $T = T^*$ has abscissa equal to d_{LS}^* (Figure 5.4.1).

If $T^* < T_C$ and $q > 1$, according to the criteria of equality of energy, there is a different procedure to evaluate the capacity in terms of spectral acceleration S_{aLS} that leads to the concept of anelastic spectrum (Figure 5.4.2):

$$F_{LS}^* = \frac{m^* S_a(T^*)}{q_{LS}} \quad (5.5.2)$$

$$q_{LS} = 1 + (\mu_{LS} - 1) \frac{T^*}{T_C} \quad (5.5.3)$$

$$S_{aLS} = q_{LS} \frac{F_{LS}^*}{m^*} \quad (5.5.4)$$

If $T^* < T_C$ and $q \leq 1$, results:

$$F_{LS}^* = m^* S_a(T^*) \quad (5.5.5)$$

$$S_{aLS} = \frac{F_{LS}^*}{m^*} \quad (5.5.6)$$

For the checking procedure, the inequality $S_{aSL} \geq S_a(T^*)$ has to be satisfied, where S_{aSL} is the capacity in terms of spectral acceleration, linked to the limit state considered and $S_a(T^*)$ is the spectral acceleration provided by the code, for the specific limit state.

5.6 Assessment Procedure in Terms of Spectral Acceleration According to Nassar & Krawinkler

In the framework of capacity-demand checking an alternative to the existing ADRS spectrum verification is proposed [6],[9],[28]. An equivalent structural SDOF system replaces the MDOF actual system introducing the coefficient of participation of the first vibration mode Γ . The capacity curve must be reported in $F_b - d_c$ plane by multiplying the multiplier α with the design base shear.

Therefore, the capacity curve must be scaled through the modal participation factor and represented in a $F^* - d^*$ plane, in which the shear force F^* and the displacement d^* of the equivalent system are linked to the corresponding quantities of the real system F_b and d_c through the relations $F^* = F_b/\Gamma$, $d^* = d_c/\Gamma$.

The demand can be estimated through the period T^* and the mass m^* of the equivalent SDOF system. In the following, the verification procedure, for each characteristic point of the trilinear capacity curve, is reported for MRFs and CBFs.

5.6.1 Assessment procedure for MRFs

In the following the verification procedure for each characteristic point of the capacity curve approximated with the trilinear model is reported.

- Point A (Fully operational)

Representation of point A in plane $F_b - d_c$ by means of the transformations $F_{b,A} = F_{b,FO} = \alpha_A \sum_k F_k$ and $d_{c,A} = d_{c,FO} = \delta_A$.

Representation of the equivalent SDOF system in plane $F^* - d^*$ by means of the transformations $F_A^* = F_{FO}^* = F_{b,A}/\Gamma$ and $d_A^* = d_{FO}^* = d_{c,A}/\Gamma$.

The capacity in terms of spectral acceleration for point A is given as follows:

$$F_{FO}^* = m^* S_{aFO}(T^*) \quad (5.6.1)$$

$$S_{aFO}(T^*) = \frac{F_{FO}^*}{m^*} \quad (5.6.2)$$

- Point B (Operational)

Representation of point B in plane $F_b - d_c$ by means of the transformations $F_{b,B} = F_{b,O} = \alpha_{max} \sum_k F_k$ and $d_{c,B} = d_{c,O} = \delta_B$.

Representation of the equivalent SDOF system in plane $F^* - d^*$ by means of the transformations $F_B^* = F_O^* = F_{b,B}/\Gamma$ and $d_B^* = d_O^* = d_{c,B}/\Gamma$.

The capacity in terms of spectral acceleration will be evaluated as follows:

$$F_O^* = m^* S_{aO}(T^*) \quad (5.6.3)$$

$$S_{aO}(T^*) = \frac{F_O^*}{m^*} \quad (5.6.4)$$

- Point C (Life Safety)

Representation of point C in plane $F_b - d_c$ by means of the transformations $F_{b,C} = F_{b,LS} = \alpha_{max} \sum_k F_k$ and $d_{c,C} = d_{c,LS} = \delta_C$.

Representation of the equivalent SDOF system in plane $F^* - d^*$ by means of the transformations $F_C^* = F_{LS}^* = F_{b,C}/\Gamma$ and $d_C^* = d_{LS}^* = d_{c,C}/\Gamma$.

The capacity in terms of spectral acceleration will be evaluated as follows:

$$F_{LS}^* = \frac{m^* S_{aLS}(T^*)}{q_{LS}} \quad (5.6.5)$$

$$S_{aLS}(T^*) = \frac{F_{LS}^*}{m^*} q_{LS} \quad (5.6.6)$$

$$q_{LS} = q_0(\mu, T, \gamma=0) = [c(\mu_{LS} - 1) + 1]^{1/c} \quad (5.6.7)$$

where $c = \frac{T^*}{1+T^*} + \frac{0.42}{T^*}$ and $\mu_{LS} = \frac{d_{LS}^*}{d_0^*}$ according to Nassar & Krawinkler formulation.

In the case of point C (and point D), the structure draws on its own plastic resources to dissipate incoming seismic energy.

In the assessment of capacity in terms of spectral acceleration, the q structure factor comes into play, expressed according to the formulation of Nassar and Krawinkler, and consequently the ductility μ_{LS} that will affect the structure factor itself.

- Point D (Near Collapse)

Representation of point D in plane $F_b - d_c$ by means of the transformations $F_{b,D} = F_{b,NC} = \alpha_0 \sum_k F_k$ and $d_{c,D} = d_{c,NC} = \delta_D$. It's important to note that the shear force $F_{b,NC}$ is calculated referring to the collapse multiplier α_0 , to evaluate, subsequently, the q factor as a function of the slope of the collapse mechanism equilibrium curve.

Representation of the equivalent SDOF system in plane $F^* - d^*$ by means of the transformations $F_D^* = F_{NC}^* = F_{b,D}/\Gamma$ e $d_D^* = d_{NC}^* = d_{c,D}/\Gamma$.

The capacity in terms of spectral acceleration will be evaluated as follows:

$$F_{NC}^* = \frac{m^* S_{aNC}(T^*)}{q_{NC}} \quad (5.6.8)$$

$$S_{aNC}(T^*) = \frac{F_{NC}^*}{m^*} q_{NC} \quad (5.6.9)$$

$$q_{NC} = \frac{q_0}{\varphi} \quad (5.6.10)$$

The structure factor q_0 , expressed in accordance with the formulation of Nassar and Krawinkler, is obtained for $\gamma=0$ and consequently doesn't take in account the second-order effects. To take these into account, the coefficient φ which appears to be a function of the ductility μ and the slope of the equilibrium curve γ (expressing the sensitivity of the structure to second-order effects), has been introduced. Therefore:

$$q_0(\mu, T, \gamma=0) = [c(\mu_{NC} - 1) + 1]^{1/c} \quad (5.6.11)$$

$$\text{where } c = \frac{T^*}{1+T^*} + \frac{0.42}{T^*} \text{ and } \mu_{NC} = \frac{d_{NC}^*}{d_0^*}$$

$$\varphi = \frac{1 + 0.62(\mu_{NC} - 1)^{1.45}\gamma}{(1 - \gamma)} \quad (5.6.12)$$

$$q_{NC} = \frac{q_0}{\varphi} = \frac{[c(\mu_{NC} - 1) + 1]^{1/c}}{1 + 0.62(\mu_{NC} - 1)^{1.45}\gamma / (1 - \gamma)} \quad (5.6.13)$$

To verify all the limit state considered, the following inequality must be satisfied:

$$S_{aLS}(T^*)_{capacity} \geq S_{aLS}(T^*)_{demand}$$

5.6.2 Assessment procedure for CBFs

In the following, the verification procedure, for each characteristic point of the trilinear capacity curve, is reported.

- **Point A (Fully operational)**

Representation of point A in plane $F_b - d_c$ using the transformations $F_{b,A} = F_{b,FO} = \alpha_A \sum_k F_k$ and $d_{c,A} = d_{c,FO} = \delta_A$.

Representation of the equivalent SDOF system in plane $F^* - d^*$ through the transformations $F_A^* = F_{FO}^* = F_{b,A}/\Gamma$ and $d_A^* = d_{FO}^* = d_{c,A}/\Gamma$.

The capacity in terms of spectral acceleration for point A is given as follows:

$$F_{FO}^* = m^* S_{aFO}(T^*) \quad (5.6.14)$$

$$S_{aFO}(T^*) = \frac{F_{FO}^*}{m^*} \quad (5.6.15)$$

- **Point B (Operational)**

Representation of the point B in plane $F_b - d_c$ through the transformations $F_{b.B} = F_{b.O} = \alpha_B \sum_k F_k$ and $d_{c.B} = d_{c.O} = \delta_B$.

Representation of the equivalent SDOF system in plane $F^* - d^*$ through the transformations $F_B^* = F_O^* = F_{b.B}/\Gamma$ and $d_B^* = d_O^* = d_{c.B}/\Gamma$.

The capacity in terms of spectral acceleration will be evaluated as follows:

$$F_O^* = m^* S_{aO}(T^*) \quad (5.6.16)$$

$$S_{aO}(T^*) = \frac{F_O^*}{m^*} \quad (5.6.17)$$

- **Point C (Life Safe)**

Representation of point C in plane $F_b - d_c$ through the transformations $F_{b.C} = F_{b.LS} = \alpha_{max} \sum_k F_k$ and $d_{c.C} = d_{c.LS} = \delta_C$.

Representation of the equivalent SDOF system in plane $F^* - d^*$ through the transformations $F_C^* = F_{LS}^* = F_{b.C}/\Gamma$ and $d_C^* = d_{LS}^* = d_{c.C}/\Gamma$.

The capacity in terms of spectral acceleration will be evaluated as follows:

$$F_{LS}^* = m^* S_{aLS}(T^*) \quad (5.6.18)$$

$$S_{aLS}(T^*) = \frac{F_{LS}^*}{m^*} \quad (5.6.19)$$

In the case of point D, the structure draws on its plastic resources to dissipate incoming seismic energy.

In the assessment of capacity in terms of spectral acceleration, the q structure factor has an important role. It is expressed according to the formulation of Nassar and Krawinkler as a function of the ductility μ_{LS} that will affect the structure factor itself.

- **Point D (Near Collapse)**

Representation of point D in plane $F_b - d_c$ through the transformations $F_{b.D} = F_{b.NC} = \alpha_0 \sum_k F_k$ and $d_{c.D} = d_{c.NC} = \delta_D$. It is important to underline

that the shear force $F_{b,NC}$ is calculated referring to the collapse multiplier α_0 , to evaluate, subsequently, the q factor as a function of the slope of the collapse mechanism equilibrium curve. Representation of the equivalent SDOF system in plane $F^* - d^*$ through the transformations $F_D^* = F_{NC}^* = F_{b,D}/\Gamma$ e $d_D^* = d_{NC}^* = d_{c,D}/\Gamma$.

The capacity in terms of spectral acceleration can be evaluated as follows:

$$F_{NC}^* = \frac{m^* S_{aNC}(T^*)}{q_{NC}} \quad (5.6.20)$$

$$S_{aNC}(T^*) = \frac{F_{NC}^*}{m^*} q_{NC} \quad (5.6.21)$$

$$q_{NC} = \frac{q_0}{\varphi} \quad (5.6.22)$$

The structure factor q_0 , expressed by the formulation of Nassar and Krawinkler, is obtained for $\gamma=0$ (stability coefficient) and consequently does not account for the second-order effects. To take these into account, the coefficient φ , defined as a function of the ductility μ and the slope of the equilibrium curve γ (expressing the sensitivity of the structure to second-order effects), has been introduced. Therefore:

$$q_0(\mu, T, \gamma=0) = [c(\mu_{NC} - 1) + 1]^{1/c} \quad (5.6.23)$$

$$\text{where } c = \frac{T^*}{1+T^*} + \frac{0.42}{T^*} \text{ and } \mu_{NC} = \frac{d_{NC}^*}{d_0^*}$$

$$\varphi = \frac{1 + 0.62(\mu_{NC} - 1)^{1.45}\gamma}{(1 - \gamma)} \quad (5.6.24)$$

$$q_{NC} = \frac{q_0}{\varphi} = \frac{[c(\mu_{NC} - 1) + 1]^{1/c}}{\frac{1 + 0.62(\mu_{NC} - 1)^{1.45}\gamma}{(1 - \gamma)}} \quad (5.6.25)$$

To verify all the limit state considered, the following inequality must be satisfied:

$$S_{aLS}(T^*)_{capacity} \geq S_{aLS}(T^*)_{demand}$$

CHAPTER 6

6 EXAMPLES OF APPLICATION OF THE PERFORMANCE-BASED ASSESSMENT APPROACH

6.1 Introduction

The definition of a new simplified assessment methodology requires the validation through the application, point by point, to case studies characterized by different design approaches.

This chapter contains three application examples for both MRFs [7] and CBFs [10]. It starts from the definition of the geometric scheme, the sections, and the acting forces, up to the comparison with the pushover curves obtained through the Sap 2000 structural analysis program [30].

In conclusion, the capacity-demand verification procedure for each analyzed structure is reported.

6.2 MRFs Numeric Examples

The simplified assessment procedure is applied to evaluate the capacity of a seven-storey and four-span steel moment resisting frame [7].

The permanent loads G_k are equal to 3.5 kN/m^2 while the live loads Q_k equal 3 kN/m^2 .

For the evaluation of gravitational loads on the beams, a frame tributary length of 6.00 m has been set. The steel used is S275.

A flowchart of the procedure is reported in Figure 6.2.1

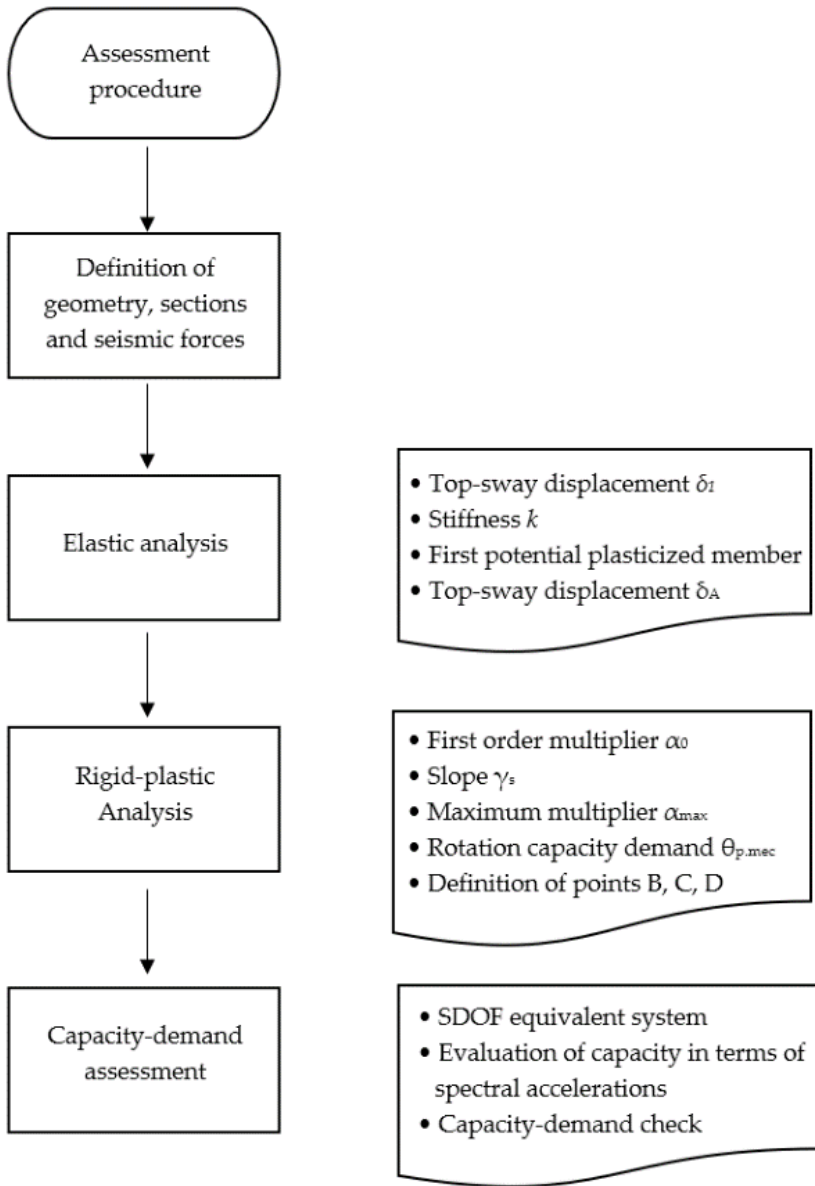


Figure 6.2.1 Flowchart of the procedure for MRFs

6.2.1 Global Moment Resisting Frames

Global moment resisting frames are designed according to the TPMC. The design results are reported in Figure 6.2.2.

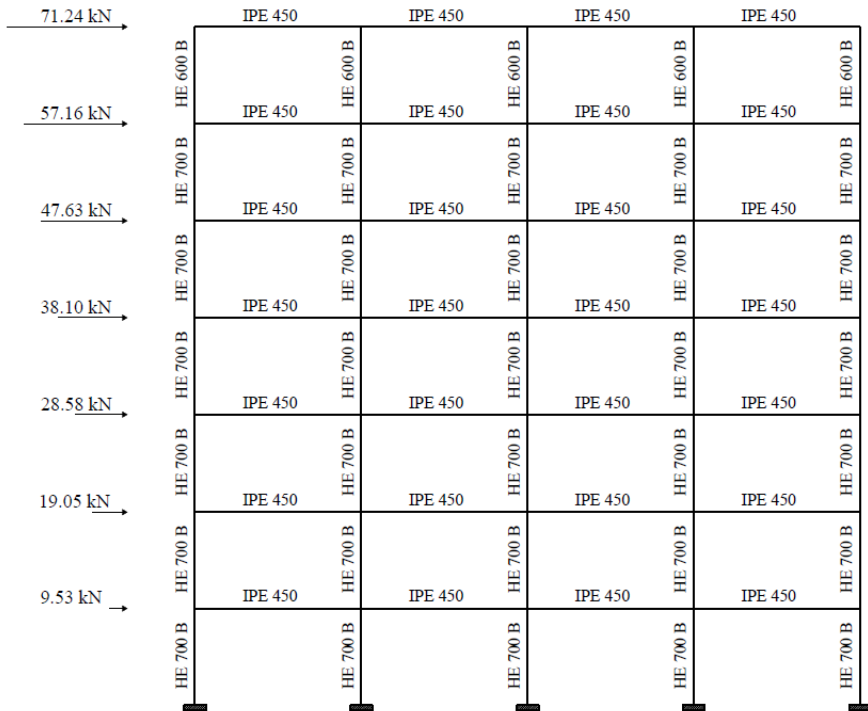


Figure 6.2.2 Representation of the frame with indication of beams, columns, and seismic forces (GMRF).

The trilinear capacity curve is shown in Figure 6.2.3, which also shows the characteristic performance points of the model.

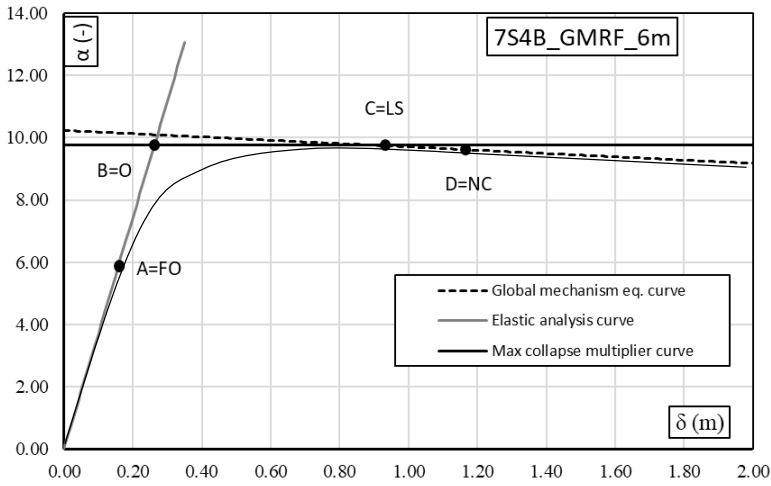


Figure 6.2.3 Trilinear model and characteristic points for the structure 7S4B_GMRF_6m

- Parameters obtained from the elastic analysis:

$$\delta_1(\alpha = 1) = 0.02684 \text{ m}$$

$$k = 37.2606 \text{ m}^{-1}$$

$$\delta_A = \delta_y = 0.1602 \text{ m}$$

$$\alpha_A = \alpha_y = k\delta_y = 5.999$$

- Parameters obtained from the rigid-plastic analysis:

$$\alpha_0 = 10.149$$

$$\gamma_s = 0.53 \text{ m}^{-1}$$

$$\alpha = \alpha_0 - \gamma_s(\delta - \delta_y) \rightarrow \alpha = 10.149 - 0.53(\delta - 0.1602)$$

$$\alpha(\delta = 0) = \alpha_0 + \gamma_s\delta_y = 10.234$$

$$H_0 = 24.5 \text{ m (Global collapse mechanism)}$$

- Evaluation of the maximum multiplier using the calibrated Merchant–Rankine formula:

$$\alpha_{max} = \frac{\alpha_0}{1 + \Psi\alpha_0\gamma_s\delta_1} = 9.7594$$

where:

$$\Psi = 0.28488 - 0.14042 \xi = 0.2763 \text{ with } \xi = \frac{\sum \frac{E I_b}{L_b}}{\sum \frac{E I_c}{L_c}} = 0.06129$$

and consequently $\delta_B = \frac{\alpha_{max}}{k} = 0.2619$ and $\delta_C = \delta_{mecc} = \frac{\alpha_0 - \alpha_{max}}{\gamma_s} + \delta_y = \frac{10.149 - 9.7594}{0.53} + 0.1602 = 0.8946 \text{ m}$

- Evaluation of the plastic rotation demand corresponding to the development of the collapse mechanism for the first plasticized element (first storey beams):

$$\theta_{p.mec} = \frac{n_s \delta_y}{H_0} \left[\frac{\Psi_1}{\Psi_2} \Psi_3 \left(\frac{\alpha_{max}}{\alpha_y} - 1 \right)^{\Psi_4} \frac{1 - \Psi_5 \gamma_s}{1 - \Psi_6 \gamma_s} \right] = 0.01886 \text{ rad}$$

The calculation of the corresponding capacity provides a final plastic rotation value of $8\theta_y = 8 \times 0.008257 = 0.06605 \text{ rad}$.

- Evaluation of the plastic rotation demand corresponding to the development of the collapse mechanism for the critical element (the mechanism is global, so the critical element is one of the first storey columns):

$$\theta_{p.mec} = \frac{n_s \delta_y}{H_0} \left[\frac{\Psi_1'}{\Psi_2'} \Psi_3' \left(\frac{\alpha_{max}}{\alpha_y} - 1 \right)^{\Psi_4'} \frac{1 - \Psi_5' \gamma_s}{1 - \Psi_6' \gamma_s} \right] = 0.01774 \text{ rad}$$

The calculation of the corresponding capacity, in the case of the first storey columns, provides a value of the ultimate plastic rotation equal to $8\theta_y = 8 \times 0.003714 = 0.02971 \text{ rad}$. Therefore, the ultimate conditions are governed by the columns of the first storey.

- Considering the plastic rotation capacity, the ultimate displacement is given by:

$$\delta_u = \delta_C + (\vartheta_{p,u} - \vartheta_{p,mecc}) H_0 = 0.8946 + (0.02971 - 0.01774) \times 24.5 = 1.188 \text{ m}$$

All the verification procedures considered use the transformation of the MDOF system into an equivalent SDOF system employing the participation coefficient of the main vibration mode Γ . For this reason, it is necessary to define:

- The eigenvector $\underline{\phi} = \{\phi_1, \phi_2, \phi_3, \phi_4, \phi_5, \phi_6\}$ that, assuming $\phi_k = \frac{F_k}{F_n}$, is:

$$\phi_1 = 0.134 \quad \phi_2 = 0.267 \quad \phi_3 = 0.401$$

$$\phi_4 = 0.535 \quad \phi_5 = 0.669 \quad \phi_6 = 0.802 \quad \phi_7 = 1.000$$

- The modal participation factor Γ :

$$\Gamma = \frac{\sum_{k=1}^n m_k \phi_k}{\sum_{k=1}^n m_k \phi_k^2} = 1.4381$$

being:

$$m_1 = 57.98 \times 10^3 \text{ kg} \quad m_2 = 57.98 \times 10^3 \text{ kg} \quad m_3 = 57.98 \times 10^3 \text{ kg}$$

$$m_4 = 57.98 \times 10^3 \text{ kg} \quad m_5 = 57.98 \times 10^3 \text{ kg} \quad m_6 = 57.98 \times 10^3 \text{ kg} \quad m_7 = 61.94 \times 10^3 \text{ kg}$$

- The dynamic parameters of the equivalent SDOF system are reported in Table 6.2.1.

Table 6.2.1 Dynamic parameters of the equivalent SDOF system (GMRFs)

m^*	k^*	ω^*	T^*
[kg 10 ³]	[kN/m]	[rad/s]	[s]
224.76	10108.5	6.7063	0.9369

Consequently, the performance points of the capacity curve are defined in the planes $\alpha - \delta$, $F_b - d_c$, $F^* - D^*$, $S_a - S_D$ assessing the capacity in terms of accelerations for both Nassar & Krawinkler and ADRS spectrum approaches. In Table 6.2.2 the results, based on the ADRS spectrum and the Nassar & Krawinkler formulation, are reported.

Table 6.2.2 Capacity in terms of Spectral acceleration and displacements (GMRFs)

		FO	O	LS	NC	NC ₀
F	[kN]	1627.71	2647.66	2647.66	2647.51	2776.3
F^*	[kN]	1131.83	1841.05	1841.05	1840.94	1930.53
d	[m]	0.1602	0.2619	0.8946	1.1879	
d^*	[m]	0.1114	0.1821	0.6220	0.8260	
μ	[m]	-	-	3.415	4.535	
$S_{a,ADRS}^*$	[g]	0.513	0.835	2.852	3.787	

$S_{a.N\&K}^*$	[g]	0.513	0.835	2.958	3.988	
$S_{a.push}^*$	[g]	0.513	0.835	2.9132	3.894	

6.2.2 Special Moment Resisting Frames

Special moment resisting frames are designed to fulfil the Eurocode 8 seismic provisions. The selected case study with the definition of the beam and column dimension is reported in Figure 6.2.4.

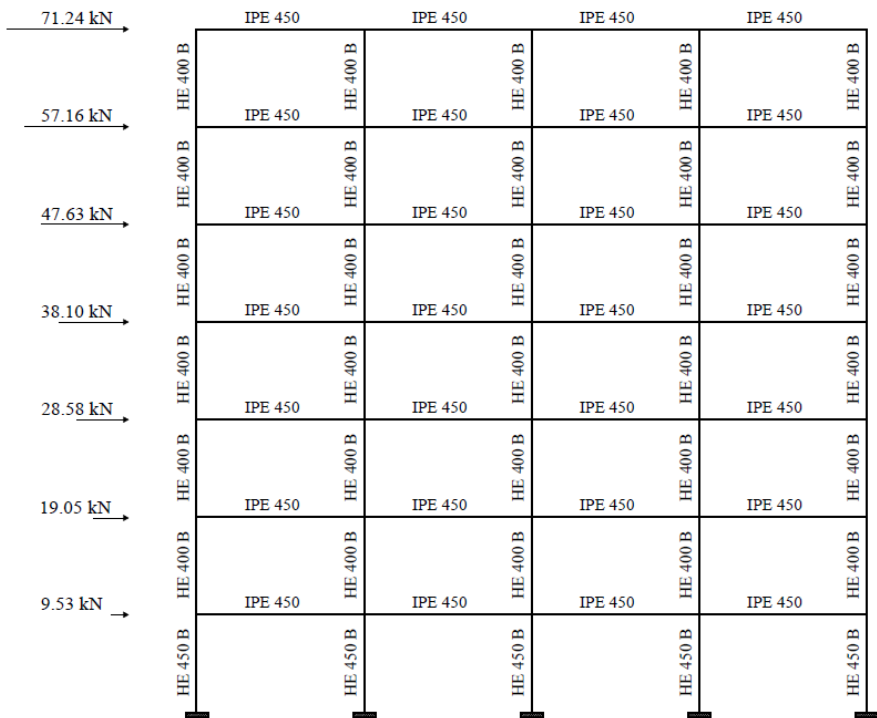


Figure 6.2.4 Representation of the frame with indication of beams, columns, and seismic forces (SMRF).

The trilinear capacity curve is shown in Figure 6.2.5, which also shows the characteristic performance points of the model.

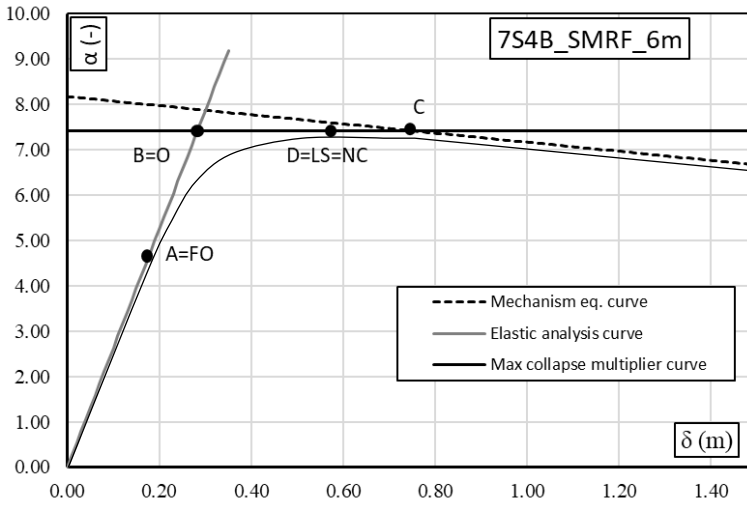


Figure 6.2.5 Trilinear model and characteristic points for the structure 7S4B_SMRF_6m

- Parameters obtained from the elastic analysis:

$$\delta_1(\alpha = 1) = 0.03814 \text{ m}$$

$$k = 15.8605 \text{ m}^{-1}$$

$$\delta_A = \delta_y = 0.1802 \text{ m}$$

$$\alpha_A = \alpha_y = k\delta_y = 4.736$$

- Parameters obtained from the rigid-plastic analysis:

$$\alpha_0 = 7.989$$

$$\gamma_s = 1.006 \text{ m}^{-1}$$

$$\alpha = \alpha_0 - \gamma_s(\delta - \delta_y) \rightarrow \alpha = 7.989 - 1.006(\delta - 0.1802)$$

$$\alpha(\delta = 0) = \alpha_0 + \gamma_s\delta_y = 8.1704$$

$$H_0 = 14.0 \text{ m (collapse mechanism Type 1, } i_m=4)$$

- Evaluation of the maximum multiplier using the calibrated Merchant–Rankine formula:

$$\alpha_{max} = \frac{\alpha_0}{1 + \Psi\alpha_0\gamma_s\delta_1} = 7.4056$$

where:

$$\Psi = 0.28488 - 0.14042 \xi = 0.2572 \text{ with } \xi = \frac{\sum \frac{EI_b}{L_b}}{\sum \frac{EI_c}{L_c}} = 0.1971$$

$$\text{and consequently } \delta_B = \frac{\alpha_{max}}{k} = 0.2824 \text{ and } \delta_C = \delta_{mecc} = \frac{\alpha_0 - \alpha_{max}}{\gamma_s} + \delta_y = \frac{7.989 - 7.4056}{1.006} + 0.1802 = 0.7605 \text{ m}$$

- Evaluation of the plastic rotation demand corresponding to the development of the collapse mechanism for the first plasticized element (first storey beams):

$$\theta_{p.mec} = \frac{n_s \delta_y}{H_0} \left[\frac{\Psi_1}{\Psi_2} \Psi_3 \left(\frac{\alpha_{max}}{\alpha_y} - 1 \right)^{\Psi_4} \frac{1 - \Psi_5 \gamma_s}{1 - \Psi_6 \gamma_s} \right] = 0.03043 \text{ rad}$$

The calculation of the corresponding capacity provides a final plastic rotation value of $8\theta_y = 8 \times 0.008257 = 0.06605 \text{ rad}$.

- Evaluation of the plastic rotation demand corresponding to the development of the collapse mechanism for the critical element (the mechanism is partial type 1 $i_m=4$, so the critical element is a first storey column):

$$\theta_{p.mec} = \frac{n_s \delta_y}{H_0} \left[\frac{\Psi_1'}{\Psi_2'} \Psi_3' \left(\frac{\alpha_{max}}{\alpha_y} - 1 \right)^{\Psi_4'} \frac{1 - \Psi_5' \gamma_s}{1 - \Psi_6' \gamma_s} \right] = 0.04587 \text{ rad}$$

The calculation of the corresponding capacity, in the case of first storey columns, provides a value of the ultimate plastic rotation equal to $8\theta_y = 8 \times 0.004212 = 0.033699 \text{ rad}$.

Therefore, the ultimate conditions are governed by the columns of the first storey.

- Considering the plastic rotation capacity, the ultimate displacement is given by:

$$\delta_u = \delta_C + (\vartheta_{p,u} - \vartheta_{p.mecc}) H_0 = 0.76 + (0.033699 - 0.04587) \times 14.0 = 0.5901 \text{ m}$$

Since the plastic rotation capacity of the third storey columns is lower than that necessary for the complete development of the kinematic mechanism, the points C and D corresponding to the limit states “Life Safety” and “Near

Collapse” are coincident and correspond to the aforementioned last displacement (δ_u).

All the verification procedures considered use the transformation of the MDOF system into an equivalent SDOF system by means of the participation coefficient of the main vibration mode Γ . For this reason, it is necessary to define:

- The eigenvector $\underline{\phi} = \{\phi_1, \phi_2, \phi_3, \phi_4, \phi_5, \phi_6\}$ that, assuming $\phi_k = \frac{F_k}{F_n}$, is:

$$\begin{aligned}\phi_1 &= 0.134 & \phi_2 &= 0.267 & \phi_3 &= 0.401 \\ \phi_4 &= 0.535 & \phi_5 &= 0.669 & \phi_6 &= 0.802 & \phi_7 &= 1.000\end{aligned}$$

- The modal participation factor Γ :

$$\Gamma = \frac{\sum_{k=1}^n m_k \phi_k}{\sum_{k=1}^n m_k \phi_k^2} = 1.4381$$

being:

$$\begin{aligned}m_1 &= 57.98 \times 10^3 \text{ kg} & m_2 &= 57.98 \times 10^3 \text{ kg} & m_3 &= 57.98 \times 10^3 \text{ kg} \\ m_4 &= 57.98 \times 10^3 \text{ kg} & m_5 &= 57.98 \times 10^3 \text{ kg} & m_5 &= 57.98 \times 10^3 \text{ kg} & m_7 \\ & & & & & = 61.94 \times 10^3 \text{ kg}\end{aligned}$$

- The dynamic parameters of the equivalent SDOF system are reported in Table 6.2.3.

Table 6.2.3 Dynamic parameters of the equivalent SDOF system (SMRFs)

m^*	k^*	ω^*	T^*
[kg 10^3]	[kN/m]	[rad/s]	[s]
224.76	7113.36	5.6257	1.117

Consequently, the performance points of the capacity curve are defined in the planes $\alpha - \delta$, $F_b - d_c$, $F^* - D^*$, $S_a - S_D$ assessing the capacity in terms of accelerations for both Nassar & Krawinkler and ADRS spectrum approaches. In Table 6.2.4. The results, based on the ADRS spectrum the Nassar & Krawinkler formulation, are reported.

Table 6.2.4 Capacity in terms of Spectral acceleration and displacements (SMRFs)

		FO	O	LS	NC	NC ₀
F	[kN]	1284.84	2009.08	2009.08	2009.08	-
F^*	[kN]	893.41	1397.01	1397.01	1397.01	-
d	[m]	0.1802	0.2824	0.5901	0.5901	
d^*	[m]	0.1253	0.1964	0.4103	0.4103	
μ	[m]	-	-	2.089	2.089	
$S_{a,ADRS}^*$	[g]	0.405	0.634	1.324	1.324	
$S_{a,N\&K}^*$	[g]	0.405	0.634	1.353	1.353	
$S_{a,push}^*$	[g]	0.405	0.634	1.353	1.391	

6.2.3 Ordinary Moment Resisting Frames

Ordinary moment resisting frames are designed without any seismic prescription aimed at mechanism control. The beams and column sections are reported in Figure 6.2.6.

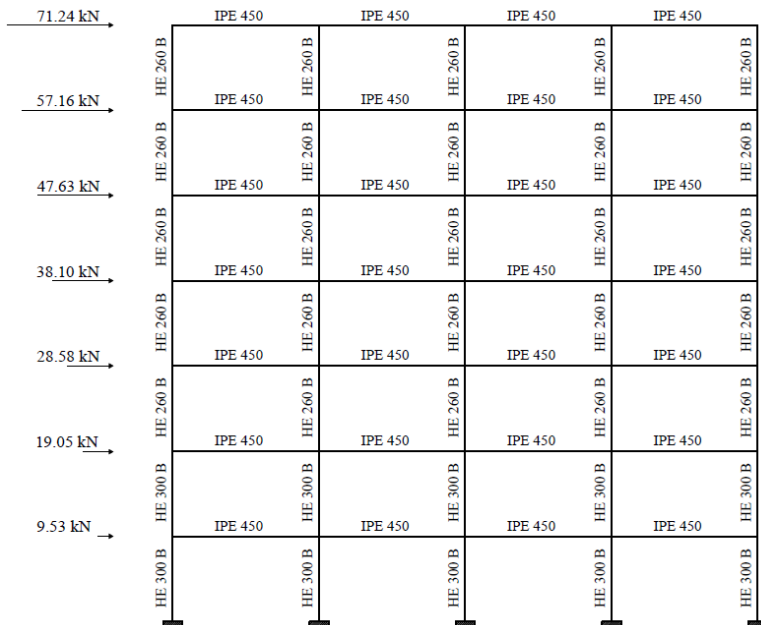


Figure 6.2.6 Representation of the frame with indication of beams, columns, and seismic forces (OMRF).

The trilinear capacity curve is shown in Figure 6.2.7, which also shows the characteristic performance points of the model.

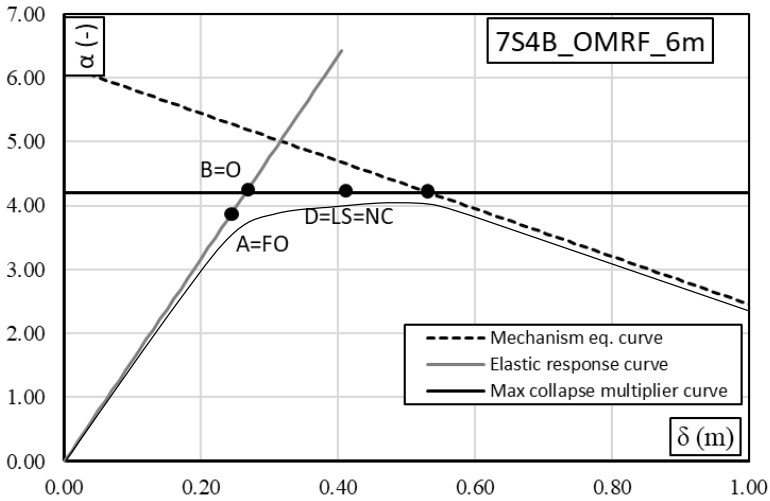


Figure 6.2.7 Trilinear model and characteristic points for the structure 7S4B_OMRF_6m

- Parameters obtained from the elastic analysis:

$$\delta_1(\alpha = 1) = 0.06305 \text{ m}$$

$$k = 15.8605 \text{ m}^{-1}$$

$$\delta_A = \delta_y = 0.2602 \text{ m}$$

$$\alpha_A = \alpha_y = k\delta_y = 4.128$$

- Parameters obtained from the rigid-plastic analysis:

$$\alpha_0 = 5.219$$

$$\gamma_s = 3.729 \text{ m}^{-1}$$

$$\alpha = \alpha_0 - \gamma_s(\delta - \delta_y) \rightarrow \alpha = 5.219 - 3.729(\delta - 0.2602)$$

$$\alpha(\delta = 0) = \alpha_0 + \gamma_s\delta_y = 6.1888$$

$$H_0 = 3.5 \text{ m (collapse mechanism Type 3, } i_m=3)$$

- Evaluation of the maximum multiplier using the calibrated Merchant–Rankine formula:

$$\alpha_{max} = \frac{\alpha_0}{1 + \Psi \alpha_0 \gamma_s \delta_1} = 4.2025$$

where:

$$\Psi = 0.28488 - 0.14042 \xi = 0.1970 \text{ with } \xi = \frac{\sum \frac{El_b}{L_b}}{\sum \frac{El_c}{L_c}} = 0.6255$$

and consequently $\delta_B = \frac{\alpha_{max}}{k} = 0.265$ and $\delta_C = \delta_{mecc} = \frac{\alpha_0 - \alpha_{max}}{\gamma_s} + \delta_y = \frac{5.219 - 4.2025}{3.729} + 0.2602 = 0.5326 \text{ m}$

- Evaluation of the plastic rotation demand corresponding to the development of the collapse mechanism for the first plasticized element (first storey beams):

$$\theta_{p.mec} = \frac{n_s \delta_y}{H_0} \left[\frac{\Psi_1}{\Psi_2} \Psi_3 \left(\frac{\alpha_{max}}{\alpha_y} - 1 \right)^{\Psi_4} \frac{1 - \Psi_5 \gamma_s}{1 - \Psi_6 \gamma_s} \right] = 0.06612 \text{ rad}$$

The calculation of the corresponding capacity provides a final plastic rotation value of $8\theta_y = 8 \times 0.008257 = 0.06605 \text{ rad}$.

- Evaluation of the plastic rotation demand corresponding to the development of the collapse mechanism for the critical element (the mechanism is partial type 3 $i_m = 3$, so the critical element is a third storey column):

$$\theta_{p.mec} = \frac{n_s \delta_y}{H_0} \left[\frac{\Psi_1'}{\Psi_2'} \Psi_3' \left(\frac{\alpha_{max}}{\alpha_y} - 1 \right)^{\Psi_4'} \frac{1 - \Psi_5' \gamma_s}{1 - \Psi_6' \gamma_s} \right] = 0.07693 \text{ rad}$$

The calculation of the corresponding capacity, in the case of the third storey columns, provides a value of the ultimate plastic rotation equal to $8\theta_y = 8 \times 0.005568 = 0.04454 \text{ rad}$.

Therefore, the ultimate conditions are governed by the columns of the third storey.

- Considering the plastic rotation capacity, the ultimate displacement is given by:

$$\delta_u = \delta_c + (\vartheta_{p.u} - \vartheta_{p.mecc})H_0 = 0.5326 + (0.04454 - 0.07693) \times 3.5 = 0.4192 \text{ m}$$

Since the plastic rotation capacity of the third storey columns is lower than that necessary for the complete development of the kinematic mechanism, the points C and D corresponding to the limit states “Life Safety” and “Near Collapse” are coincident and correspond to the aforementioned last displacement (δ_u).

All the verification procedures considered the use of the transformation of the MDOF system into an equivalent SDOF system using the participation coefficient of the main vibration mode Γ . For this reason, it is necessary to define:

- The eigenvector $\underline{\phi} = \{\phi_1, \phi_2, \phi_3, \phi_4, \phi_5, \phi_6\}$ that, assuming $\phi_k = \frac{F_k}{F_n}$, is:

$$\phi_1 = 0.134 \quad \phi_2 = 0.267 \quad \phi_3 = 0.401$$

$$\phi_4 = 0.535 \quad \phi_5 = 0.669 \quad \phi_6 = 0.802 \quad \phi_7 = 1.000$$

- The modal participation factor Γ :

$$\Gamma = \frac{\sum_{k=1}^n m_k \phi_k}{\sum_{k=1}^n m_k \phi_k^2} = 1.4381$$

being:

$$m_1 = 57.98 \times 10^3 \text{ kg} \quad m_2 = 57.98 \times 10^3 \text{ kg} \quad m_3 = 57.98 \times 10^3 \text{ kg}$$

$$m_4 = 57.98 \times 10^3 \text{ kg} \quad m_5 = 57.98 \times 10^3 \text{ kg} \quad m_6 = 57.98 \times 10^3 \text{ kg} \quad m_7 = 61.94 \times 10^3 \text{ kg}$$

- The dynamic parameters of the equivalent SDOF system are reported in Table 6.2.5.

Table 6.2.5 Dynamic parameters of the equivalent SDOF system (OMRFs)

m^*	k^*	ω^*	T^*
[kg 10^3]	[kN/m]	[rad/s]	[s]
224.76	4302.8	4.3753	1.436

Consequently, the performance points of the capacity curve are defined in the planes $\alpha - \delta$, $F_b - d_c$, $F^* - D^*$, $S_a - S_D$ assessing the capacity in terms of accelerations for both Nassar & Krawinkler and ADRS spectrum approaches. In Table 6.2.6. The results, based on the ADRS spectrum the Nassar & Krawinkler formulation, are reported.

Table 6.2.6 Capacity in terms of Spectral acceleration and displacements (OMRFs)

		FO	O	LS	NC	NC ₀
F	[kN]	1119.90	1140.12	1140.12	1140.12	-
F^*	[kN]	778.72	792.78	792.78	792.78	-
d	[m]	0.2602	0.265	0.4192	0.4192	
d^*	[m]	0.181	0.184	0.291	0.291	
μ	[m]	–	–	1.582	1.582	
$S_{a,ADRS}^*$	[g]	0.353	0.359	0.569	0.569	
$S_{a,N\&K}^*$	[g]	0.353	0.359	0.575	0.575	
$S_{a,push}^*$	[g]	0.353	0.359	0.583	0.583	

6.3 CBFs Numeric Examples

The simplified assessment procedure is applied to evaluate the capacity of three steel Concentrically Braced Frames designed according to three different approaches [10].

Permanent loads G_k are equal to 3.5 kN/m² while live loads Q_k equal to 3 kN/m².

A frame tributary length of 6.00 m has been considered for the evaluation of gravitational loads acting on the beams. The steel used is S275.

A flowchart of the procedure is reported in Figure 6.3.1

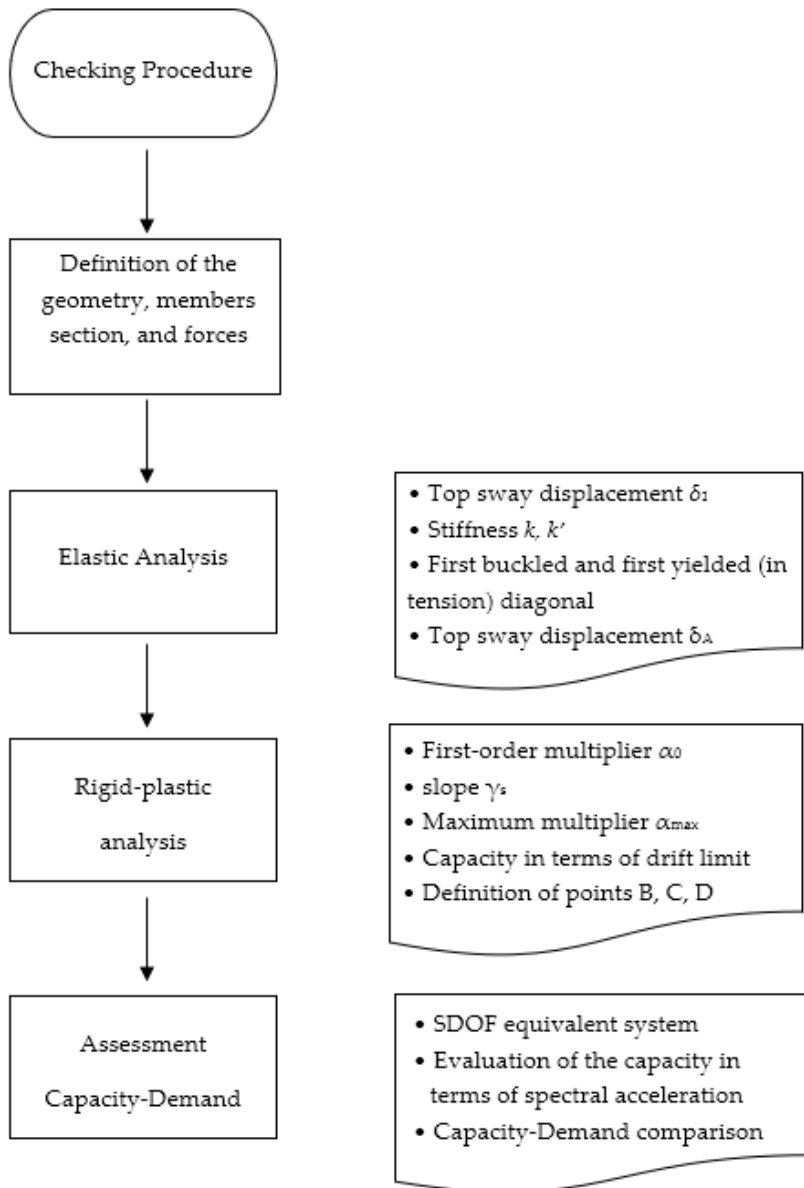


Figure 6.3.1 Flowchart of the procedure for CBFs

6.3.1 Global Concentrically Braced Frames

Global concentrically braced frames are designed according to the TPMC. The beams, diagonals, and column sections are reported in (Figure 6.3.2)

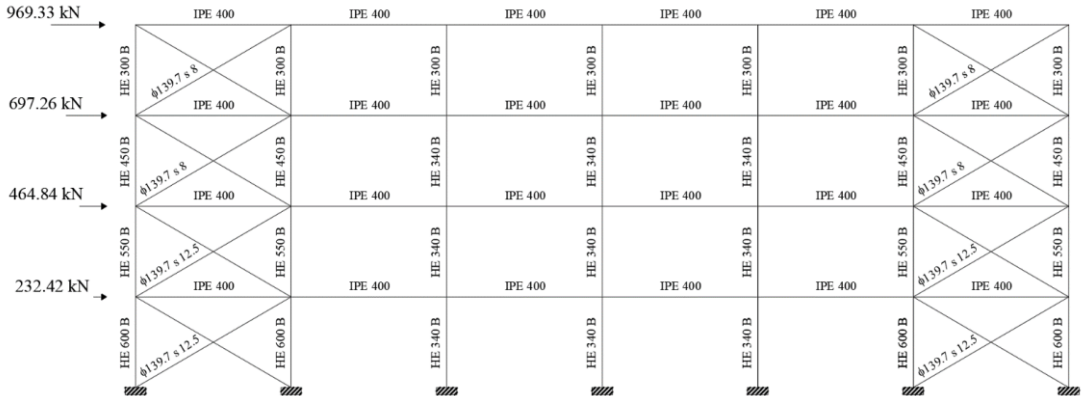


Figure 6.3.2 Representation of the frame with indication of beams, diagonals, columns, and seismic forces (GCBF).

The trilinear capacity curve, showing the characteristic points of the model, is reported in Figure 6.3.3)

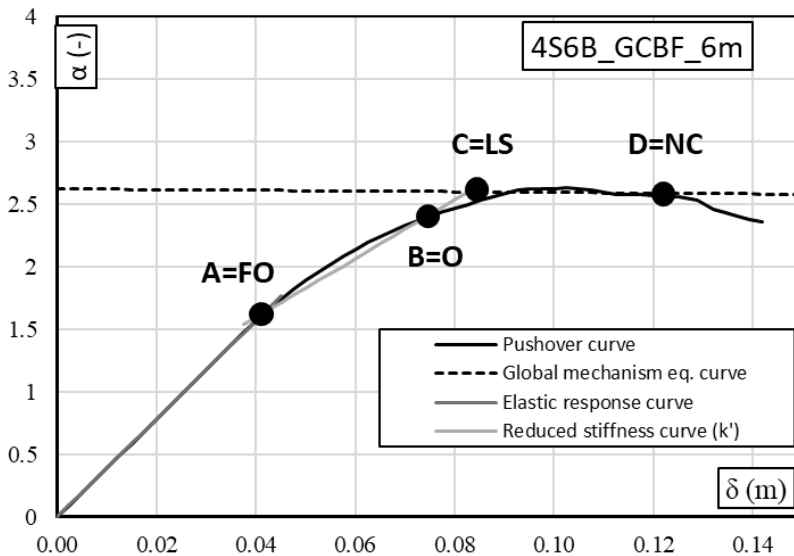


Figure 6.3.3 Trilinear model and characteristic points for the structure 4S6B_GCBF_6m

- Parameters obtained from the elastic analysis:

$$\delta_1(\alpha = 1) = 0.0255 \text{ m};$$

$$K = 39.161 \text{ m}^{-1};$$

$$K' = 23.4964 \text{ m}^{-1};$$

$$\delta_A(1^{\text{st}} \text{ buckling}) = 0.0426 \text{ m};$$

$$\alpha_A = k\delta_A = 1.6577.$$

- Parameters obtained from the rigid plastic analysis:

$$\alpha_0 = 2.598;$$

$$\gamma_s = 0.285 \text{ m}^{-1};$$

$$\alpha = \alpha_0 - \gamma_s(\delta - \delta_y) \rightarrow \alpha = 2.598 - 0.285(\delta - 0.07438);$$

$$\alpha(\delta = 0) = \alpha_0 + \gamma_s\delta_y = 2.620;$$

$$H_0 = 14 \text{ m (global collapse mechanism)}.$$

- Evaluation of the maximum multiplier through the calibrated Merchant–Rankine formula:

$$\alpha_{max} = \frac{\alpha_0}{1 + \Psi_{CBF}\alpha_0\gamma_s\delta_1} = 2.5058$$

where

$$\Psi_{CBF} = a + b\xi_{CBF} = 1.41068 + 0.29443 \xi_{CBF} = 1.698909;$$

$$\text{with } \xi_{CBF} = \frac{\sum_{n_{bc}} \frac{E A_{diag}}{L_{diag}} \frac{1}{1 + (L_b/h)^2}}{\sum_{n_c} \frac{E I_c}{h^3}} = 1.945191;$$

$$\text{consequently } \delta_B = \frac{\alpha_y - \alpha_A}{K'} + \delta_A = 0.07438;$$

$$\text{and } \delta_C = \frac{\alpha_0 - \alpha_A + K'\delta_A}{K' + \gamma_s} = 0.08163.$$

- According to the limitations given by Eurocode 8 for compressed diagonals at Near Collapse limit state ($\Delta_c \cdot 6$), the ultimate displacement is evaluated as:

$$\delta_D = \left(\frac{\delta_{d,cp}}{h_i \cos \theta} \right) \cdot H_0 = \left(\frac{0.026874}{3.5 \times 0.86378} \right) \times 14 = 0.12445 \text{ m}$$

The checking procedures exploit the transformation of the MDOF system into an equivalent SDOF system through the participation factor of the main vibration mode Γ . For this reason, it is necessary to define:

- The eigenvector $\underline{\phi} = \{\phi_1, \phi_2, \phi_3, \phi_4\}$ that, assuming $\phi_k = \frac{F_k}{F_n}$, is:

$$\begin{aligned}\phi_1 &= 0.2398 & \phi_2 &= 0.4795 & \phi_3 &= 0.7193 \\ \phi_4 &= 1.00\end{aligned}$$

- The modal participation factor Γ :

$$\Gamma = \frac{\sum_{k=1}^n m_k \phi_k}{\sum_{k=1}^n m_k \phi_k^2} = 1.343$$

being

$$\begin{aligned}m_1 &= 278.75 \times 10^3 \text{ kg} & m_2 &= 278.75 \times 10^3 \text{ kg} & m_3 &= 278.75 \times 10^3 \text{ kg} \\ m_4 &= 290.64 \times 10^3 \text{ k}\end{aligned}$$

- The dynamic parameters of the equivalent SDOF system (Table 6.3.1)

Table 6.3.1 Dynamic parameters of the equivalent SDOF system (GCBFs)

m^*	k^*	ω^*	T^*
[kg 10 ³]	[kN/m]	[rad/s]	[s]
691.67	92569.9	11.5688	0.5431

Consequently, the performance points of the capacity curve are defined in the planes $\alpha - \delta$, $F_b - d_c$, $F^* - D^*$, $S_a - S_D$ assessing the capacity in terms of accelerations for both Nassar & Krawinkler and ADRS spectrum approaches. In Table 6.3.2 the results, based on the ADRS spectrum and the Nassar & Krawinkler formulation, are reported.

Table 6.3.2 Capacity in terms of Spectral acceleration and displacements (GCBFs)

		FO	O	LS	NC	NC ₀
F	[kN]	3918.52	5683.83	6086.44	6057.55	6141.53
F^*	[kN]	2917.66	4232.08	4531.86	4510.35	4572.88
d	[m]	0.0426	0.0751	0.08163	0.12445	
d^*	[m]	0.0317	0.0559	0.0608	0.0927	

μ	[m]	-	-	-	1.524
$S_{a,ADRS}^*$	[g]	0.433	0.624	0.6679	0.9803
$S_{a,N\&K}^*$	[g]	0.433	0.624	0.6679	1.0177
$S_{a,push}^*$	[g]	0.433	0.624	0.6753	0.9986

6.3.2 Special Concentrically Braced Frames

Special concentrically braced frames are designed to fulfil the Eurocode 8 seismic provisions. The selected case study with the definition of the beam, diagonals, and column sections is reported in Figure 6.3.4.

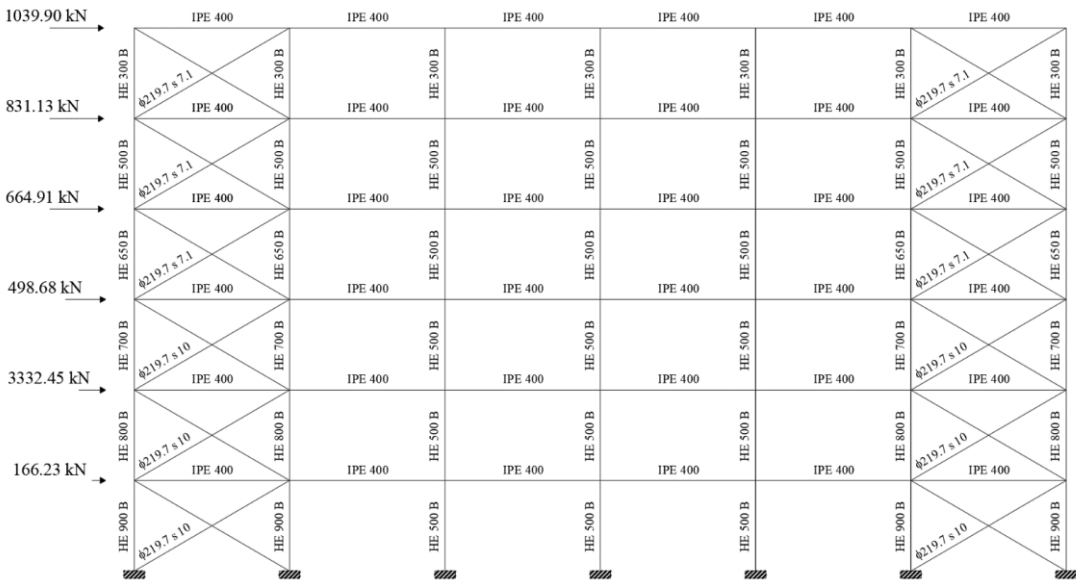


Figure 6.3.4 Representation of the frame with indication of beams, diagonals, columns, and seismic forces (SCBF).

The trilinear capacity curve, showing the characteristic points of the model, is reported in Figure 6.3.5

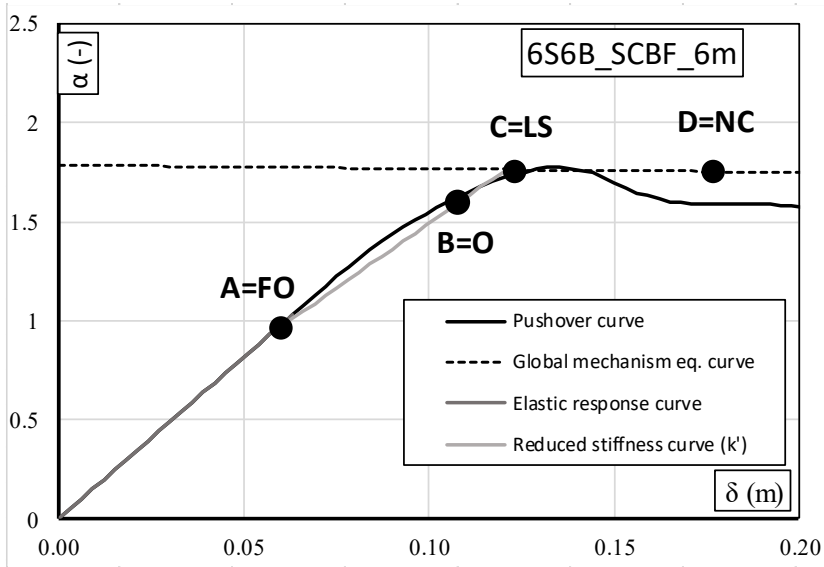


Figure 6.3.5 Trilinear model and characteristic points for the structure 6S6B_SCBF_6 m.

- Parameters obtained from the elastic analysis:

$$\delta_1(\alpha = 1) = 0.06133 \text{ m};$$

$$K = 16.305 \text{ m}^{-1};$$

$$K' = 13.044 \text{ m}^{-1};$$

$$\delta_A(1^{\text{st}} \text{ buckling}) = 0.0571 \text{ m};$$

$$\alpha_A = k\delta_A = 0.9311.$$

- Parameters obtained from the rigid plastic analysis:

$$\alpha_0 = 1.763;$$

$$\gamma_s = 0.185 \text{ m}^{-1};$$

$$\alpha = \alpha_0 - \gamma_s(\delta - \delta_y) \rightarrow \alpha = 1.763 - 0.185(\delta - 0.1171);$$

$$\alpha(\delta = 0) = \alpha_0 + \gamma_s\delta_y = 1.785;$$

$$H_0 = 21 \text{ m (global collapse mechanism).}$$

- Evaluation of the maximum multiplier through the calibrated Merchant–Rankine formula:

$$\alpha_{max} = \frac{\alpha_0}{1 + \Psi_{CBF} \alpha_0 \gamma_s \delta_1} = 1.7267$$

where

$$\Psi_{CBF} = a + b \xi_{CBF} = 1.00421 + 0.10265 \xi_{CBF} = 1.05338;$$

$$\text{With } \xi_{CBF} = \frac{\sum_{n_{bc}} \frac{EA_{diag}}{L_{diag}} \frac{1}{1 + (L_b/h)^2}}{\sum_{n_c} \frac{EI_c}{h^3}} = 0.47899;$$

$$\text{consequently } \delta_B = \frac{\alpha_y - \alpha_A}{K'} + \delta_A = 0.1171;$$

$$\text{and } \delta_C = \frac{\alpha_0 - \alpha_A + K' \delta_A}{K' + \gamma_s} = 0.11922.$$

- According to the limitations given by Eurocode 8 for compressed diagonals at Near Collapse limit state ($\Delta_c \cdot 6$), the ultimate displacement is evaluated as:

$$\delta_D = \left(\frac{\delta_{d,cp}}{h_i \cos \theta} \right) \cdot H_0 = \left(\frac{0.026874}{3.5 \times 0.86378} \right) \times 21 = 0.18667 \text{ m}$$

The checking procedures exploit the transformation of the MDOF system into an equivalent SDOF system through the participation factor of the main vibration mode Γ . For this reason, it is necessary to define:

- The eigenvector $\underline{\phi} = \{\phi_1, \phi_2, \phi_3, \phi_4, \phi_5, \phi_6\}$ that, assuming $\phi_k = \frac{F_k}{F_n}$, is:

$$\phi_1 = 0.1598 \quad \phi_2 = 0.3197 \quad \phi_3 = 0.4795$$

$$\phi_4 = 0.6394 \quad \phi_5 = 0.7992 \quad \phi_6 = 1.00$$

- The modal participation factor Γ :

$$\Gamma = \frac{\sum_{k=1}^n m_k \phi_k}{\sum_{k=1}^n m_k \phi_k^2} = 1.405$$

being

$$m_1 = 278.75 \times 10^3 \text{ kg} \quad m_2 = 278.75 \times 10^3 \text{ kg} \quad m_3 = 278.75 \times 10^3 \text{ kg}$$

$$m_4 = 278.75 \times 10^3 \text{ kg} \quad m_5 = 278.75 \times 10^3 \text{ kg} \quad m_6 = 290.64 \times 10^3 \text{ kg}$$

- The dynamic parameters of the equivalent SDOF system (Table 6.3.3).

Table 6.3.3 Dynamic parameters of the equivalent SDOF system (SCBFs)

m^*	k^*	ω^*	T^*
[kg 10 ³]	[kN/m]	[rad/s]	[s]
959.01	57610	7.75062	0.81067

Consequently, the performance points of the capacity curve are defined in the planes $\alpha - \delta$, $F_b - d_c$, $F^* - D^*$, $S_a - S_D$ assessing the capacity in terms of accelerations for both Nassar & Krawinkler and ADRS spectrum approaches. In Table 6.3.4 the results, based on the ADRS spectrum and the Nassar & Krawinkler formulation, are reported.

Table 6.3.4 Capacity in terms of Spectral acceleration and displacements (SCBFs)

		FO	O	LS	NC	NC ₀
F	[kN]	3290.01	6009.54	6151.51	6107.34	6229.56
F^*	[kN]	2340.99	4276.06	4377.08	4345.65	4432.62
d	[m]	0.0571	0.1171	0.1192	0.1867	
d^*	[m]	0.0406	0.0833	0.0848	0.1328	
μ	[m]	-	-	-	1.566	
$S_{a,ADRS}^*$	[g]	0.2488	0.4545	0.6525	0.0848	
$S_{a,N\&K}^*$	[g]	0.2488	0.4545	0.6525	0.7399	
$S_{a,push}^*$	[g]	0.433	0.624	0.6753	0.7548	

6.3.3 Ordinary Concentrically Braced Frames

Ordinary Concentrically Braced Frames are designed only to withstand horizontal design actions. The selected case study with the definition of the beam, diagonals, and column sections is reported in Figure 6.3.6

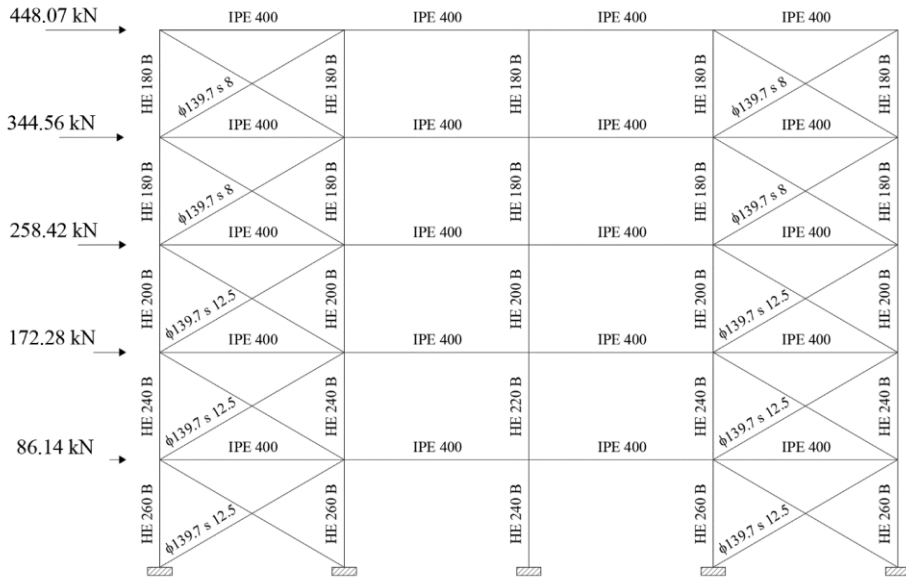


Figure 6.3.6 Diagram of the frame with indication of beams, diagonals, columns, and seismic forces (OCBF).

The trilinear capacity curve, showing the characteristic points of the model, is reported in Figure 6.3.7

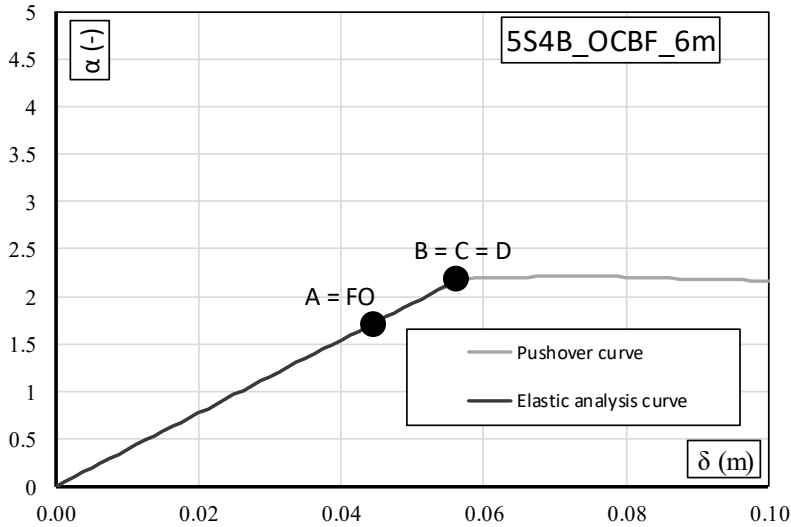


Figure 6.3.7 Trilinear model and characteristic points for the structure 5S4B_OCBF_6 m.

- Parameters obtained from the elastic analysis:

$$\delta_1(\alpha = 1) = 0.02597 \text{ m};$$

$$K = 38.501 \text{ m}^{-1};$$

$$K' = 25.02;$$

$$\delta_A = 0.1602 \text{ m};$$

$$\alpha_A = k\delta_A = 2.0680.$$

It is not necessary to perform rigid plastic analysis because the buckling of columns occurs for a multiplier of horizontal forces very close to α_A . Consequently,

$$\delta_u = \delta_B = \delta_C = \delta_D = 0.0575 \text{ m};$$

$$\alpha_u = \alpha_B = \alpha_C = \alpha_D = 2.18596.$$

The checking procedures exploit the transformation of the MDOF system into an equivalent SDOF system through the participation factor of the main vibration mode Γ . For this reason, it is necessary to define:

- The eigenvector $\underline{\phi} = \{\phi_1, \phi_2, \phi_3, \phi_4, \phi_5\}$ that, assuming $\phi_k = \frac{F_k}{F_n}$, is:

$$\phi_1 = 0.192 \quad \phi_2 = 0.384 \quad \phi_3 = 0.575$$

$$\phi_4 = 0.767 \quad \phi_5 = 1.00$$

- The modal participation factor Γ :

$$\Gamma = \frac{\sum_{k=1}^n m_k \phi_k}{\sum_{k=1}^n m_k \phi_k^2} = 1.379$$

being

$$m_1 = 123.89 \times 10^3 \text{ kg} \quad m_2 = 123.89 \times 10^3 \text{ kg} \quad m_3 = 123.89 \times 10^3 \text{ kg}$$

$$m_4 = 123.89 \times 10^3 \text{ kg} \quad m_5 = 129.17 \times 10^3 \text{ kg}$$

- The dynamic parameters of the equivalent SDOF system (Table 6.3.5).

Table 6.3.5 Dynamic parameters of the equivalent SDOF system (OCBFs)

m^*	k^*	ω^*	T^*
[kg 10^3]	[kN/m]	[rad/s]	[s]
366.82	37127.6	10.061	0.6245

Consequently, the performance points of the capacity curve are defined in the planes $\alpha - \delta$, $F_b - d_c$, $F^* - D^*$, $S_a - S_D$ assessing the capacity in terms of accelerations for both Nassar & Krawinkler and ADRS spectrum approaches. In Table 6.3.6 the results, based on the ADRS spectrum and the Nassar & Krawinkler formulation, are reported.

Table 6.3.6 Capacity in terms of Spectral acceleration and displacements (OCBFs)

		FO	O	LS	NC	NC ₀
F	[kN]	2235.76	2363.33	2363.33	2363.33	-
F^*	[kN]	1620.83	1713.31	1713.31	1713.31	-
d	[m]	0.0538	0.0575	0.0575	0.0575	
d^*	[m]	0.0390	0.0417	0.0417	0.0417	
μ	[m]	-	-	-	-	
$S_{a.ADRS}^*$	[g]	0.450	0.476	0.476	0.476	
$S_{a.N\&K}^*$	[g]	0.450	0.476	0.476	0.476	
$S_{a.push}^*$	[g]	0.450	0.487	0.487	0.487	

CHAPTER 7

7 VALIDATION OF THE METHODOLOGY THROUGH INCREMENTAL DYNAMIC ANALYSIS (IDA)

7.1 Introduction

The simplified method allows to define the capacity curve of a MRF or CBF steel structure through a trilinear approximation by using the elastic and rigid plastic analyses and has been calibrated by regression analysis on 420 structures designed for each structural type.

To assess the accuracy of the method, compared to other tools provided by the codes, in addition to pushover analysis, incremental dynamic analyses (IDA) were performed. These analyses were developed on real structures and simulated designs according to recent and old codes and whose data are available in the literature.

The IDAs have been developed with the OpenSees software [31], creating very accurate fiber models capable of catching the real behavior of the analyzed structures. In this way, it was possible to evaluate the actual percentage error between the seismic capacity defined by the simplified methodology and that obtained by the IDA, for each limit state considered.

To this end, an in-depth analysis of the cyclic behavior of the members is reported, in particular for CBFs. In fact, their behaviour is strongly affected by the dissipative capacity of the diagonal members, which, differently from the beams and the link members exhibit an asymmetric hysteresis behaviour that deserves to be accurately modelled.

7.2 Incremental Dynamic Analyses (IDA)

Incremental dynamic analysis (IDA) is an innovative method in the field of earthquake engineering.

It consists in subjecting the considered structure to one or more accelerograms (In the case study the structure was subjected to 7 accelerograms) of intensity scaled by means of an amplification factor (λ) to obtain one or more characteristic curves, in which the variation of the maximum value of a predetermined response parameter to the variation of a predetermined seismic intensity parameter is represented.

The curves obtained facilitate the understanding of the dynamic behavior of structures from the elastic field to collapse, but require a computational effort higher than all the other methods.

7.2.1 Evaluation of the reference earthquakes

For the purpose of evaluating the set of earthquakes for the development of incremental dynamic analysis, the design spectrum of our case study structure has been derived from the Italian technical standards [20] considering the following values expressed in Table 7.2.1.

Table 7.2.1 Seismic parameters of the design spectrum

a_g/g	a_g	g	S	T_B	T_C	T_D	η
[-]	[m/s ²]	[m/s ²]	[-]	[s]	[s]	[s]	[-]
0.261	2.56	9.81	1.15	0.157	0.47	2.64	1

For the type B soil category, 34 earthquakes occurred mainly in the Mediterranean including the Italian peninsula, Greece and Turkey, for which accelerograms, response spectra, and characteristics of seismic events are available, have been considered.

Through the simulation of a spreadsheet, it was possible to select 7 earthquakes scaling them appropriately (Table 7.2.2) so that the average spectrum obtained for these 7 seismic events does not exceed or subceed at any point in the $S_a(T)$ - T graph of a value of the 10% with respect to the design spectrum (Figure 7.2.1).

Table 7.2.2 Spectrum-compatible seismic events

	Event ID	MAX PGA [cm/s ²]	Length [s]	Npt	Scale factor
S1	GR-1995-0047	510.615	6.18	7958	1.50
S7	IT-2009-0009	355.460	11.75	20000	1.28
S9	IT-1976-0030	341.508	4.795	4919	0.50
S13	IT-2009-0009	644.247	7.695	20001	0.75
S21	EMSC-20161030_0000029 (CENTRAL ITALY)	476.428	10.395	10000	0.63
S25	IT-1980-0012	314.302	39.005	14152	0.80
S26	IT-1980-0012	58.702	35.200	10602	1.50

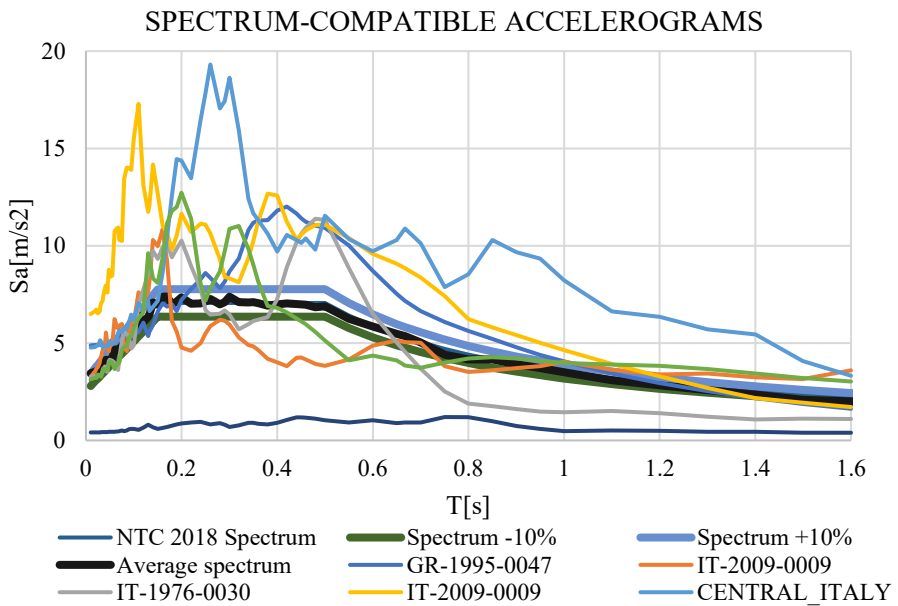


Figure 7.2.1 Spectrum-compatible accelerograms

7.3 Modelling in OpenSees

OpenSees (Open System for Earthquake Engineering) is an open-source finite element program used in engineering to simulate the nonlinear response of structural and geotechnical systems, and it is developed at the University of California, Berkeley. Its characteristic of being "open" allows a continuous evolution of libraries thanks to the interchangeability between users and developers. The solutions implemented mainly concern: the construction of the model, the analytical formulation of a given element, material models, analysis methods, numerical solvers, and useful procedures for data implementation. OpenSees uses the C++ language and has no graphical input or output interface: data input (geometries, mechanical parameters, external actions, and resolution strategy) takes place through a file written in the TCL language or, as recently developed, in the Python language, better in the field of post processing.

7.3.1 *Model construction syntax*

Each tcl or python file is characterized by a precise syntax and the structural system model must follow the following order [31]:

- Geometric data: the "basic model builder" is defined, as well as the size of the problem to be analyzed and the number of degrees of freedom of each node. For the study under consideration, it has been defined: `model basic -ndm 2 -ndf 3;`
- Nodal coordinates: definition of all the coordinates of the nodes in the reference system x, y, z where the x-y plane is the working plane;
- Constraints: definition of the boundary conditions with `fix` followed by 0 for free degrees of freedom and 1 for constrained degrees of freedom; In addition, for the structure under study, internal constraints such as the real hinges of the beams and diagonals have been inserted through the `EqualDof` command, binding the slave node to the master node which is the structural node of the ends of the columns in the degree of freedom 1 and 2.
- Materials: the materials of the system are defined using the constitutive laws present in the `uniaxialMaterial` library;
- Sections: the sections of the model are defined according to a fiber modeling; they are made with the `patch rect` and `wideFlange` command

according to a rectangular model with discretized fibers with the presence of 16 fibers.

- Transformation: the transformation of the reference system is defined with regard to the stiffness and stresses of the elements, in the specific case, it has been considered a P-delta transformation to take into account the second order effects, relevant for the aforementioned structural typology;
- Elements: the individual elements of the system are defined by associating the end nodes, the section and the geometric transformation of the reference system; Each element was modeled with the command `dispBeamColumn`, `nonLinearBeamColumn` and `elasticBeam` with 5 integration points for each element (corotational transformation).

Loads: loads are defined at nodes or on previously defined elements; To have a better resolution of the problem in the nonlinear field, the gravitational load was applied in 10 steps proportionally, fixing the load constant after the tenth step.

Recorders: the outputs of the analysis to be saved in appropriate .out files are defined; The stresses of the elements as well as the displacements of the structural nodes were derived for the purpose of data interpretations.

Analysis: the solver of the system of equations under analysis, the type of boundary conditions, the numbering of the equations and the degrees of freedom are defined. The convergence test on the equation matrix, and the algorithm used to solve a nonlinear system of equations, are also defined.

7.3.2 Fiber Elements and Uniaxial Material

The structural software Opensees (Open System for Earthquake Engineering) allows to perform a fiber modeling of the sections of the structural elements. Consequently, non-linear analysis on structures is performed attributing to each fiber constitutive links of materials that do not have purely elastic behavior. It turns out that each fiber constituting the element has a uniaxial behavior.

The structural element is divided into a series of control sections. For fiber elements, the concept of distributed plasticity is used, which differs from concentrated plasticity, involving the entire element rather than considering

plasticity concentrated in plastic hinges. Considering the concentrated plasticity, it is necessary to provide precise points of formation of the plastic hinges, in which all the non-linearity of the system is concentrated. This is not entirely in line with the real behavior of the structures, especially due to the difficulty of a precise identification of the position of the plastic hinge. On the other hand, this method allows to have a computational advantage since it makes the structural elements easily manageable. As far as fiber modeling is concerned, plasticity is widespread throughout the element. In this way, the determination of the point of formation of the plastic hinge and the calculation of the plasticization moment are not necessary. However, this way requires a greater computational burden, but in the face of a more realistic behavior of the element.

Therefore, in the context of a finite element program it is essential to use a numerical model that can guarantee a good level of accuracy without requiring too high a computational burden to handle the nonlinear analysis of individual structural elements. A fundamental aspect becomes the choice of the methodology for modelling non-linearities. Distributed plasticity models can be modeled according to the following formulations:

- Force Based Elements (FBE) /NonLinearBeamColumn
- Displacement Based Elements (DBE)

DBE is the most used methodology, in which the field of deformations of the element is obtained from the displacements of the end nodes through appropriate interpolating functions. Next, the virtual work principle is used to derive the nodal forces. To interpolate the deformation field, for the displacement is adopted $u(x)$ form functions with linear pattern and for the curvature $v(x)$ a function with quadratic trend. This results in a constant axial deformation, and a linear curvature. Due to the approximation chosen, it is therefore necessary to adopt a sufficiently refined discretization to be able to adequately grasp the deformation field. The fundamental limitation of such an approach is, therefore, related to the lack of precision in describing highly non-linear behaviors, without having to excessively refine the mesh.

For Forced Based elements, on the other hand, a dense discretization is not required, as the approximation will be adequate thanks to the use of control sections defined by the integration points. The response of the elements changes significantly depending on whether one type of element is used rather than the other, but a good approximation of the structural behavior is still obtained if the mesh is handled properly.

In this specific case, both models have been developed which, properly calibrated, have provided comparable results.

The fiber section was modeled using both the patch and the wideflange command, where the main dimensions of the section are assigned directly.

As regards the selection of the constitutive model of the materials, the fibers have been equipped with a uniaxial material of the type “Steel 01” and “Steel 02” Giuffrè-Menegotto-Pinto.

7.3.3 “Steel 02” Giuffrè-Menegotto-Pinto uniaxial material

For MRFs and CBFs the uniaxial material "Steel02" has been selected and calibrated for the specific case study [31].

This material is based on the Giuffrè-Menegotto-Pinto behavioural link (Figure 7.3.1) modified later by Filippou et al.[36] to include the isotropic hardening effect.

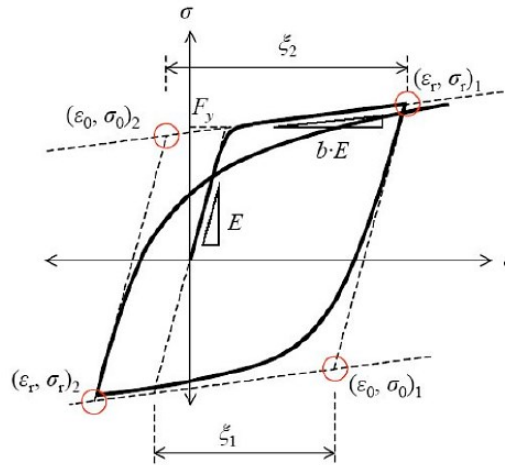


Figure 7.3.1 Giuffrè-Menegotto-Pinto constitutive link (Steel02).

According to this model, the constitutive link of the steel material is expressed by the relation:

$$\sigma^* = b \cdot \varepsilon^* + \frac{(1 - b) \cdot \varepsilon^*}{(1 + |\varepsilon^*|^{R(\xi)})^{1/R(\xi)}} \quad (7.3.1)$$

where ε^* and σ^* are, respectively, dimensionless deformation and stress, expressed by the relations:

$$\sigma^* = \frac{\sigma - \sigma_0}{\sigma_0 - \sigma_r} \quad (7.3.2)$$

$$\varepsilon^* = \frac{\varepsilon - \varepsilon_0}{\varepsilon_0 - \varepsilon_r} \quad (7.3.3)$$

where ε_0 and σ_0 are the coordinates of the intersection point of the two asymptotes of the current load phase, while ε_r and σ_r are the coordinates of the previous load reversal point.

b is the ratio between the elastic modulus of the hardening phase and that of the elastic phase;

$R(\xi)$ is a decreasing function of the parameter ξ expressing the overall deformation of the previous cycle and is expressed by the relation:

$$R(\xi) = R_0 - \frac{a_1 \cdot \xi}{a_2 + \xi} \quad (7.3.4)$$

where R_0 , a_1 and a_2 are parameters to be calibrated experimentally.

Figure 7.3.1 shows the first two load paths (compression and subsequent tension); Also highlighted are the coordinate points $(\varepsilon_0, \sigma_0)$ and $(\varepsilon_r, \sigma_r)$ for the same phases.

According to the model shown, the OpenSEES analysis program in the tcl language requires the specification of a series of input parameters for the definition of the material "Steel02".

The expected syntax is the following:

```
uniaxialMaterial Steel02 $matTag $Fy $E $b $R0 $cR1 $cR2 $a1 $a2 $a3
$a4
```

where:

- \$matTag is the numerical code that identifies the defined material (necessary for the assignment of the material to the fibers in the modeling of the sections);
- \$Fy is the yield stress of the material; - \$E is the initial tangent modulus of elasticity;
- \$b is the work hardening ratio (ratio between the tangent modulus of elasticity in the post-plasticization phase and the initial one);

- R_0 R_1 R_2 are parameters that control the transition from the elastic branch to the plastic branch. The following values are suggested for these parameters: 10-20 for R_0 , 0.925 for R_1 and 0.15 for R_2 ;
- α_1 α_2 α_3 α_4 are the parameters for the definition of isotropic hardening.

Especially:

- α_1 represents the factor of increase of the plastic threshold in compression after a plastic deformation of α_2 times the deformation at yield strength (F_y/E);
- α_3 represents the factor of increase of the plastic threshold in tension after a plastic deformation of α_4 times the deformation at yield strength (F_y/E).

The following is the syntax that is used for the Python language:

```
uniaxialMaterial('Steel02', matTag, Fy, E0, b, *params, a1=a2*Fy/E0,
a2=1.0, a3=a4*Fy/E0, a4=1.0, sigInit=0.0)
```

where the parameters are the same as those previously reported with regard to the TCL language.

7.4 Fiber Elements, Sections and Uniaxial Material in OpenSees for MRFs

In the case of MRFS, a fiber modeling of the sections of the structural elements has been selected. Consequently, non-linear analyses on structures are performed attributing to each fiber of the element a uniaxial behavior [31].

Non-linearities have been modelled through a distributed plasticity model can be modeled considering both Force Based Elements (FBE) and Displacement Based Elements (DBE)

The models, properly calibrated, have provided comparable results.

The fiber sections have been modeled using the wideflange command, where the main dimensions of the section are assigned directly.

The fiber section was modeled using the “wideflange” command in which the main dimensions of the section are assigned directly; the syntax used is as follows:

`section('WFSection2d', secTag, matTag, d, tw, bf, tf, Nfw, Nff)`

where:

secTag is the unique identifier tag for the section

matTag is the tag of the material assigned to the section

d is the height of the section

t_w is the thickness of the web

b_f is the base of the section, flange size

t_f is the thickness of the flange

N_{fw} is the number of fibers to be assigned in the direction of the web

N_{ff} is the number of fibers to be assigned in the direction of the flange

The following is an example for a section HEM300 (Figure 7.4.1) according to Python language:

```
ops.section('WFSection2d', HEM300, Steel02, 0.34, 0.0210, 0.310, 0.0390,
6, 8 )
```

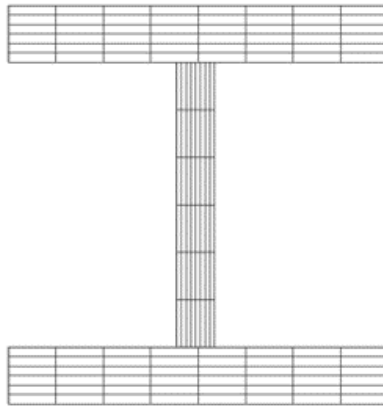


Figure 7.4.1 HEM 300 fiber section

As regards the selection of the constitutive model of the materials, the fibres have been equipped with a uniaxial material of the type “Steel 02” Giuffrè-Menegotto-Pinto, considering an S355 steel grade material.

The comparison between the static pushover curve obtained by SAP2000 and Opensees is reported in Figure 7.4.2. It is worth observing that the SAP2000 model considers a concentrated plasticity model through the use of the so-called P-Hinge properties. The Opensees material has been calibrated considering the absence of hardening. From the analysis of Figure 7.4.2 it seems to achieve the same behaviour of the structure modelled with concentrated plasticity.

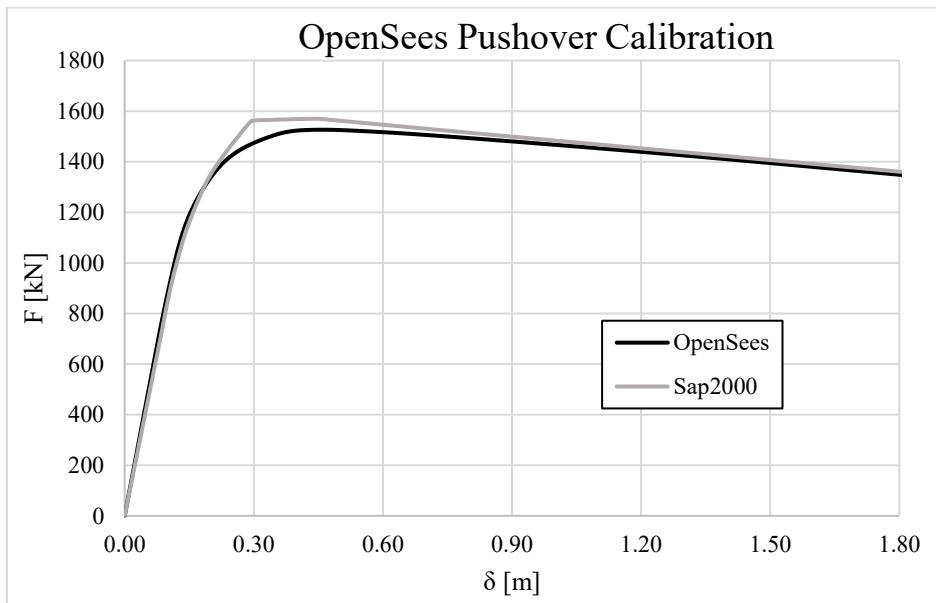


Figure 7.4.2 Comparison between concentrated and distributed plasticity models

The parameters have been set as reported in Table 7.4.1.

Table 7.4.1 Parameters used for steel02 uniaxial material (MRFs)

f_y [N/mm ²]	E_0 [N/mm ²]	b	R_0	cR_1	cR_2	a_1	a_2	a_3	a_4
355	210000	$\frac{1}{10^8}$	18	0.925	0.15	$a_2 * F_y / E_0$	$\frac{1}{10^8}$	$a_4 * F_y / E_0$	$\frac{1}{10^8}$

7.5 Non-linear Cyclic behaviour of Bracing Members

The seismic behavior of the CBFs is governed by the cyclic behavior of the bracing members, which constitute the dissipative elements.

The cyclic behavior of the bracing diagonals is characterized by a strongly non-linear trend, due to the drawing of buckling conditions, and rapidly degrading for cycles subsequent to the first, due to both the presence of the accumulated residual deformations and the Bauschinger effect, which occurs due to the translation of the plasticization surface (kinematic hardening), towards a point representative of the tensile stress state.

The typical trend of hysteresis cycles for symmetric load history is reported in Figure 7.5.1, where P_y and δ_y are, respectively, the plastic resistance of the beam in tension and the corresponding plastic axial deformation [31].

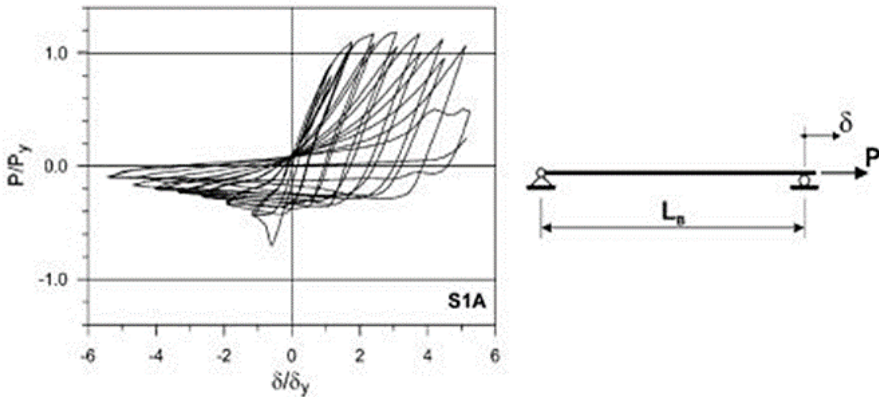


Figure 7.5.1 Hysteretic behavior of an axially loaded beam with symmetrical load history.

7.5.1 Studies on the fundamental parameters affecting the cyclic behaviour of axially loaded members.

The numerous studies [24],[25],[31]-[35] developed on the cyclic behavior of the axially loaded beams have highlighted the dependence of the dissipative capacities of the diagonals on three fundamental parameters:

- slenderness ratio
- constraint conditions
- cross section shape

The cyclic response of axially loaded members depends essentially on the slenderness λ , expressed by the ratio $\beta \cdot L/\rho$ between the effective length and the gyration radius (referred to the deflection plan).

Depending on the slenderness, the members can be divided into slender, intermediate and stocky. A member can be defined slender if the buckling load is less than or at most equal to half the yield strength 213[25]:

$$\sigma_{cr} \leq 0.5 \cdot \sigma_y \quad (7.5.1)$$

Considering the elastic critical stress defined through the Euler relationship:

$$\sigma_{cr} = \frac{\pi^2 E}{\lambda^2} \quad (7.5.2)$$

And combining Eq.(7.5.1) and Eq.(7.5.2), the following limitation is obtained for slender members:

$$\sigma_{slender} \geq \frac{\pi \cdot \sqrt{E/0.5}}{\sqrt{f_y}} \quad (7.5.3)$$

Where f_y is the yield strength of the steel and E is the elastic modulus.

Assuming E equal to 210000 N/mm², it is possible to write:

$$\sigma_{slender} \geq 2036/\sqrt{f_y} \quad (7.5.4)$$

Eq. (7.5.4) provides a slenderness limit value of 133 for S235 steel and 108 for S355 steel.

Too high slenderness ratio, produce a worsening of the overall behaviour of the structure. Slender members, in fact, are characterized by reduced stiffness in the unstable configuration, that rapidly increases when the straightening, due to the load reversal, occurs.

However, such straightening, if rapid, can also lead to the collapse of the connections at the ends of the diagonals themselves.

A member is instead defined as stocky when the response is governed by the local instability of the section, which determines the decrease in the flexural capacity of the plastic hinges.

Finally, intermediate members are characterized by the interaction between local and global instability.

A summary table for the classification in terms of slenderness, derived from the studies conducted by (Bruneau et al., 1998 [25]) and (Jain et al., 1978 [35]), is given below:

Steel	$\sigma_{slender}^{(1)}$	$\sigma_{int}^{(1)}$	$\sigma_{stocky}^{(2)}$
S235	$\sigma_{cr} \geq 133$	$60 < \sigma_{cr} < 133$	$\sigma_{cr} \leq 60$
S355	$\sigma_{cr} \geq 108$	$50 < \sigma_{cr} < 108$	$\sigma_{cr} \leq 50$

¹ Bruneau et al., 1998; ² Jain et al., 1978;

As regards the constraint conditions, the effects on the hysteretic behavior of axially loaded members have been analyzed by Black et al. [33],[34]. With the same slenderness and for constraining conditions of support-support and support-fixed end type, the results show, in the transition from the first constraint condition to the second, only a slight improvement in hysteretic behavior (increasing the area underlying the diagram).

The study of the effect of the cross-section type on the hysteretic response of axially loaded limbs was conducted by Black et al. [33],[34]. The work is based on the analysis of the hysteretic behaviour of six simply supported beams, one with a double T section, a T-section, two tubular, a boxed section, and finally one with coupled angles. The six members analyzed all have the same slenderness ratio $\lambda=80$. The results led to the identification of two modes of collapse of the members:

1. collapse due to local buckling;
2. collapse due to lateral-torsional buckling.

The improvement of the dissipative capacities of the members can be achieved by reducing the width-to-thickness ratio b/t for boxed sections, or d/t (diameter/thickness) for tubular sections and $b_f/2t_f$ (flange width/thickness) for double T sections.

On the basis of the results obtained, Black et al. [33],[34] classify the analysed sections in descending order according to dissipative capacity for a given overall slenderness value:

1. tubular members;

2. boxed members;
3. double T members;
4. T-shaped members;
5. members with coupled angles.

7.5.2 An analytical model for the characterization of the cyclic behavior of the axially loaded members

Georgescu's model [24],[25] provides an analytical formulation of the schematization of the hysteretic behavior of diagonals. The model investigates the effect of the initial deformations on the behavior of the axially loaded member. It is considered a beam with initial geometric imperfection f_0 , equivalent to the overall geometric and mechanical imperfections, also called "industrial beam"(Figure 7.5.2).

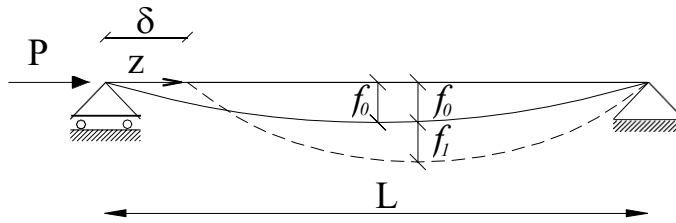


Figure 7.5.2 "Industrial beam" with initial imperfection.

The behavior of the axially loaded beam is described through three parameters: the axial stress P , the axial deformation δ , and the deflection f (transverse deformation).

Georgescu's model refers to a cycle that is divided into zones corresponding to several characteristic behaviours, defined as a function of the physical interpretation of the inelastic cyclic behaviour.

In Figure 7.5.3 the schematization of the first hysteretic cycle is reported [].

The schematization of the hysteretic cycle identifies several branches associated with the following meaning:

Branch O-A of elastic shortening in compression: the member is subjected, because of the axial compression, to a progressive shortening that ends at point A with the achievement of the buckling condition, corresponding to the critical load in compression P_{cr} .

Branch A-B: when the buckling condition is attained the member begins to skid sideways. As a result, a second-order bending moment arises along the beam equal to $P \cdot f(z)$, where $f(z)$ represents the deformation of the axis line. The lateral displacement, therefore, grows under constant load up to point B, where there is the formation of the plastic hinge in the centerline section. Consequently, in this branch, the shortening of the beam is substantially linked to the deflection.

Branch B-C: represents the mechanism equilibrium curve of the member. After the formation of the plastic hinge, the bending moment in the centerline section remains constant. For equilibrium, an increase in axial and therefore transverse deformation must be accompanied by a reduction in terms of axial load. The plastic hinge, therefore, continues to rotate until it reaches point C, where the reversal of the load occurs. The branch is characterized by a non-linear trend due to the normal stress-bending moment interaction.

Branch C-D of elastic elongation in compression: due to the reversal of the load, the reduction of the axial load is accompanied by a progressive elongation of the member. This branch is similar to the OA one, but it is obviously characterized by stiffness, and therefore by a slope, lower than the previous branch, due to the level of deformation reached at point C. In addition, point D is associated with a zero axial load but non-zero axial deformation and lateral displacement (residual deformations).

Branch D-E of elastic elongation in tension or straightening phase: due to the increase in the tensile load, there is a progressive elongation and therefore the simultaneous straightening of the member. As a result of the existing(residual) lateral deformation, a variable bending moment is generated along the member; when this equals the resisting moment in the centerline section, at point E, the formation of a plastic hinge is obtained.

Branch E-F: similarly to the B-C branch, it represents the equilibrium curve of the kinematic mechanism in which the member has been transformed; an increase in axial elongation is accompanied by a reduction in transverse deformation. Consequently, the tensile axial load must increase, resulting in a $P-\delta$ link that is still non-linear. At point F, the yield strength P_y is reached, which is associated with a residual transverse displacement.

Branch F-F' or yielding branch: the load remains constant, equal to the plastic stress (in the hypothesis of absence of hardening), while there is a progressive elongation of the member.

Branch F'-G of elastic shortening in tension: starting from point F' the beam is gradually released until it reaches point G, characterized by a zero axial load and non-zero residual axial deformation.

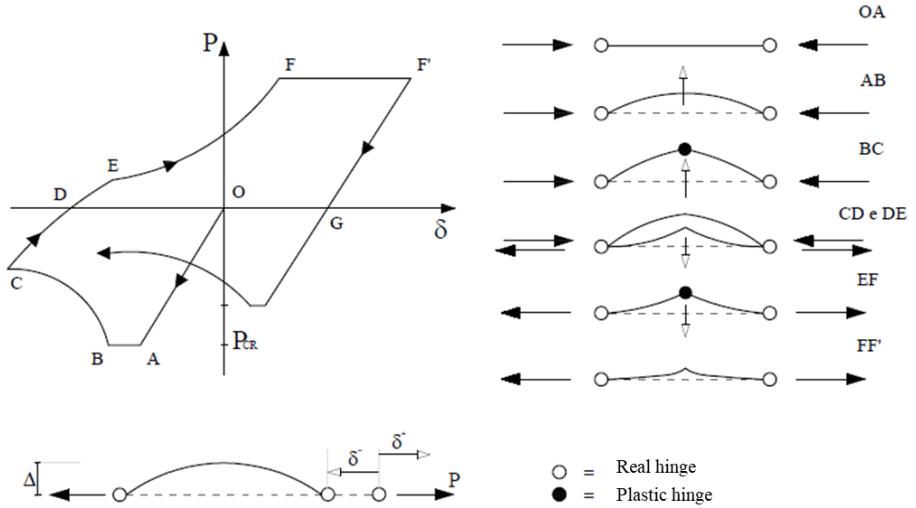


Figure 7.5.3 Cyclic behavior of an axially loaded beam.

The cycles following the first can be schematized in a similar way to what has been described so far, considering a translation of the reference system since the initial point of the *i*-th cycle corresponds to the final one of the *i*-1 cycle. For example, the second cycle will start from point G instead of O. However, for cycles subsequent to the first, it is necessary to take into account the reduction of the compression strength threshold, due to the accumulated residual deformations.

From the analytical point of view, a beam with initial imperfection f_0 is considered, equivalent to the overall geometric and mechanical imperfections, also called "industrial beam".

The initial deformed configuration can be expressed through the equation of a sine wave:

$$f_0(z) = f_0 \cdot \sin \frac{\pi \cdot z}{L} \tag{7.5.5}$$

where L is the length of the rod and z is the generic abscissa computed according to the reference system indicated in Figure 7.5.3. The generic abscissa z , for the equilibrium between the internal and external moment, must result:

$$M(z) = P \cdot (f_0(z) + f_1(z)) \quad (7.5.6)$$

where f_0 is the initial imperfection and f_1 is the differential deflection from the initial configuration. Taking into account the relationship between the elastic deflection of the beam $f_1(z)$ and bending moment, Eq.(7.5.6) gives the relation:

$$\frac{d^2 f_1(z)}{dz^2} + \frac{P}{EI} \cdot f_1(z) = -\frac{P}{EI} \cdot f_0(z) \quad (7.5.7)$$

from which, placed $K^2 = P/EI$, we obtain the equation of the elastic curve of the industrial beam subject to axial load P :

$$\frac{d^2 f_1(z)}{dz^2} + K^2 \cdot f_1(z) = -K^2 \cdot f_0(z) \quad (7.5.8)$$

From the resolution of the non-homogeneous differential equation (7.5.8) the variation of the deformed configuration of the beam is expressed starting from an initial configuration already deformed:

$$f_1(z) = \left(\frac{P/P_{Eul}}{1 - P/P_{Eul}} \right) \cdot f_0 \sin\left(\frac{\pi \cdot z}{L}\right) \quad (7.5.9)$$

where P_{Eul} represents the Eulerian buckling load, equal to $\pi^2 EI/L^2$ for a simply supported beam. Normal stress has to be expressed in absolute value.

By placing

$$f = \left(\frac{P/P_{Eul}}{1 - P/P_{Eul}} \right) \cdot f_0 \quad (7.5.10)$$

can be rewritten as:

$$f_1(z) = f \cdot \sin\left(\frac{\pi \cdot z}{L}\right) \quad (7.5.11)$$

In order to determine the axial deformation corresponding to the transversal deflection, reference is made to the infinitesimal element of the beam placed near the support, reported in Figure 7.5.4. For small displacements, it is possible to approximate the curvilinear deformation of the beam with a straight line. Consequently, the axial shortening of the infinitesimal element, related to the transverse deformation, can be expressed as:

$$dw = dz - dz \cos\alpha = dz \cdot (1 - \cos\alpha) \quad (7.5.12)$$

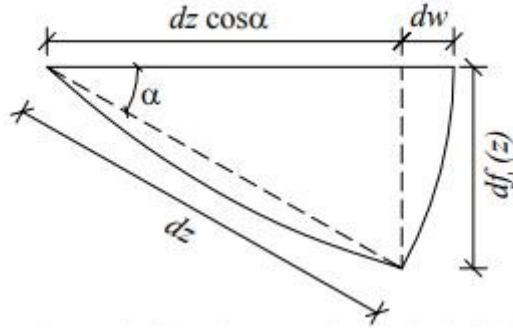


Figure 7.5.4 Infinitesimal element at the support.

The total shortening of the beam is obtained by integrating the (7.5.12) along the length of the beam:

$$dw = \int_0^L (1 - \cos\alpha) dz \quad (7.5.13)$$

Developing the Taylor series $\cos\alpha$ with zero starting point stopped at the second term ($\cos\alpha = 1 - \alpha^2/2$) and substituting this expression into the (7.5.13), it is obtained:

$$w = \int_0^L \left(1 - 1 + \frac{\alpha^2}{2} \right) dz = \frac{1}{2} \int_0^L (\alpha^2 dz) \quad (7.5.14)$$

On the other hand, the angle α can be expressed through the derivative of the transverse deformation:

$$\alpha = \frac{dy}{dz} \rightarrow \frac{dy}{dz} = \frac{\pi}{L} \cdot f \cdot \cos \cdot \left(\frac{\pi \cdot z}{L} \right) \quad (7.5.15)$$

where f is the total deflection of the midspan. Substituting the (7.5.15) in the (7.5.14), it is possible to write:

$$w = \frac{1}{2} \int_0^L \left[\frac{\pi}{L} \cdot f \cdot \cos \cdot \left(\frac{\pi \cdot z}{L} \right) \right]^2 dz \quad (7.5.16)$$

whose solution provides the shortening of the beam corresponding to the transverse deformation with deflection f :

$$w = \frac{\pi^2 f^2}{4} \frac{f^2}{L} \cong 2 \cdot \frac{f^2}{L} \quad (7.5.17)$$

With reference to the industrial beam, the total transverse deformation is provided by the sum of the initial deformation f_0 (imperfection of the beam) and the variation of the transverse deformation from the initial configuration f .

Consequently, it is possible to define the overall transverse deformation f_t as:

$$f_t = \left(\frac{P/P_{Eul}}{1 - P/P_{Eul}} \right) \cdot f_0 + f_0 = \frac{1}{\left(1 - \frac{P}{P_{Eul}} \right)} f_0 \quad (7.5.18)$$

where P , consistent with the convention assumed in (7.5.9), must be assumed in absolute value.

Ultimately, the overall shortening of the beam can be expressed as the sum of the elastic contribution, due to the acting axial load, and the contribution of the total deformation, i.e.:

$$\delta = \delta_i - \frac{\pi^2}{4} \cdot \frac{f_t^2}{L} + \frac{PL}{EA} \quad (7.5.19)$$

where δ_i represents the initial axial deformation, while it represents the overall flexural deformation. It should be noted that in f_t (7.5.19) axial load P must be taken in sign, where, by convention, the compressive stresses are defined as negative. In this way, the normal stress in compression and the transverse deformation provides concordant contributions, i.e., negative axial deformations that identify the shortening of the beam.

Finally, expressing the initial axial deformation δ_i as a function of the initial imperfection f_0 through ((7.5.17), the report (7.4. (7.5.19):

$$\delta = \frac{PL}{EA} - \frac{\pi^2}{4L} \cdot (f_t^2 - f_0^2) \quad (7.5.20)$$

With $f_t = \frac{1}{\left(1 - \frac{P}{P_{Eul}} \right)} f_0$ as reported in Eq.(7.5.18)

Given the relationship between transverse deformation and axial deformation (Eq.(7.5.20), and exploiting Eq.(7.5.18), it is possible to formulate the equations that define the different branches in Georgescu's model. The

Eulerian buckling load has been replaced with the critical buckling load P_{crit} , defined according to Eurocode 3.

The equations describing the model depend on the initial imperfection f_0 , defined according to Georgescu's model, considering the first yielding condition and Eurocode 3 buckling formulation (see chapter.....):

$$f_0 = \frac{W}{A} \alpha (\bar{\lambda}^2 - 0.04) \quad \text{with } \alpha = 0.21, \bar{\lambda} = \frac{\lambda}{\lambda_y} \quad (7.5.21)$$

where W is the plastic section modulus, A is the section area, α is a coefficient depending on the buckling curve, defined by Eurocode 3, λ is the geometric slenderness defined as the ratio between the effective buckling length L_0 and the radius of gyration ρ . $\lambda_y = \pi(E/f_y)^{1/2}$ is the slenderness corresponding to the yielding condition, E is the elastic modulus and f_y is the resistance of the steel in tension.

OA branch:

Given the axial displacement δ_{OA} , the axial load P can be defined as:

$$P = \frac{EA}{L} \delta_{OA} = K_d \delta_{OA} \quad \text{with } P \text{ limited to } P_{crit} \quad (7.5.22)$$

and consequently, **point A** (δ_A, P_{cr}) can be defined evaluating the displacement δ_A corresponding to the achievement of the critical buckling load P_{crit} :

$$\delta_A = \frac{P_{cr} L}{EA} \quad (7.5.23)$$

AB branch:

At point A, buckling occurs. The second-order bending moment increases until the formation of the plastic hinge in the centerline section occurs (point B). Taking into account the axial force-bending moment interaction, it is possible to define the total transversal deflection corresponding to point B as:

$$f_{tB} = \frac{M_{pl}}{P_{crit}} \left(1 - \frac{P_{crit}}{P_y} \right) \quad (7.5.24)$$

Where M_{pl} is the plastic resisting moment of the section and P_y is the axial resistance in tension.

Consequently, **point B** (δ_B, P_{cr}) can be defined evaluating the displacement δ_B exploiting Eq.(7.5.20) (valid if buckling occurs) for $P = P_{crit}$ and $f_t = f_{tB}$:

$$\delta_B = \frac{P_{crit}L}{EA} - \frac{\pi^2}{4L}(f_{tB}^2 - f_0^2) \quad (7.5.25)$$

BC branch:

At point B, a mechanism occurs, whose equilibrium curve is still expressed through Eq.(7.5.24) and (7.5.25), but considering a generic axial stress P :

$$f_t = \frac{M_{pl}}{P} \left(1 - \frac{P}{P_y} \right) \text{ with } P < P_{crit} \quad (7.5.26)$$

$$\delta_{BC} = \frac{PL}{EA} - \frac{\pi^2}{4L}(f_t^2 - f_0^2) \quad (7.5.27)$$

Point C is defined according to EC8 shortening limits or to the cyclic test performed.

The OA and AB branches, thus represented, are a simplification of the real model. Substituting Eq.(7.5.18) in Eq.(7.5.20), A hyperbolic function with horizontal asymptote $P=P_{crit}$ is obtained. Point B, strictly speaking, should be determined as the intersection between the curve previously defined and the mechanism equilibrium curve BC, shown below.

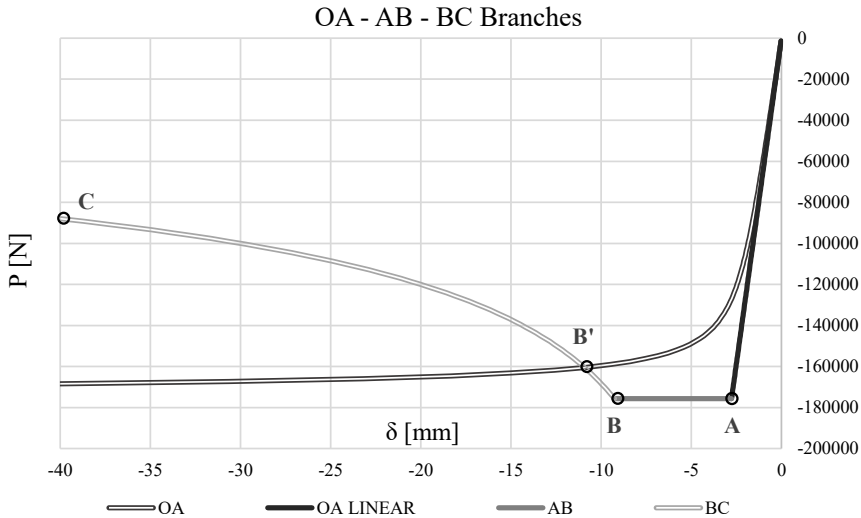


Figure 7.5.5 Shape of the first three branches (OA-AB-BC) - Ø 139,7 s 5

CD branch:

The C-D branch is linear and is similar to the OA branch. It is therefore possible to use the same formulations by making a proper translation of the axes at point D. Point d is on the x-axis so the transversal deflection at point D is seen as the initial imperfection f_0 of the (7.5.18), in the new reference system. Placing $f_{tD} = f_0$, the (7.5.18) represents the variation of the total transverse deflection:

$$f_t = \frac{1}{1 - P/P_{cr}} f_{tD} \quad (7.5.28)$$

As a result, it is possible to obtain the total deflection f_{tD} exploiting the (7.5.28) for point C:

$$f_{tC} = \frac{1}{1 - P_C/P_{cr}} f_{tD} \quad (7.5.29)$$

Consequently:

$$f_{tD} = f_{tC}(1 - P_C/P_{cr}) \quad (7.5.30)$$

With the values of P_C and f_{tC} defined using the equations of the BC branch.

Equation (7.5.20) gives for $P = P_C$, $f_t = f_{tC}$ and $f_0 = f_{tD}$ axial deformation at point C, according to the new reference system:

$$\delta_{C'} = \frac{P_C L}{EA} - \frac{\pi^2}{4L} (f_{tC}^2 - f_{tD}^2) \quad (7.5.31)$$

From which it is possible to derive the axial deformation at the point D through the relation:

$$\delta_D = \delta_C - \delta_{C'} \quad (7.5.32)$$

DE branch:

The D-E branch is still characterized by a linear trend. It is still possible to adopt the same formulations of the O-A branch. In particular, assuming a local reference system with origin in D, the transverse deformation can be expressed through (7.5.18) by substituting the initial imperfection with the transverse deformation f_{tD} . In addition, a reversal of the sign to the denominator is carried out in such a way that for increasing values of the axial load in tension, there is a reduction of the transverse deformation compared to that corresponding to the D point, obtaining:

$$f_t = \frac{1}{1 + P/P_{cr}} f_{tD} \quad (7.5.33)$$

By analogy, the axial deformation of the D-E branch, relative to the local reference system, will be expressed by the relation (Eq.(7.5.20) translated by δ_D , considering f_{tD} as initial imperfection):

$$\delta = \delta_D + \frac{PL}{EA} - \frac{\pi^2}{4L} (f_t^2 - f_{tD}^2) \quad (7.5.34)$$

However, the D-E branch is only fully defined once the axial load at the end point E has been determined. This value is estimated by considering the EF branch equation.

EF branch:

In analogy to the BC branch, it is represented by the mechanism equilibrium curve (Eq.(7.5.26))

The transverse deformation of point E can be expressed through Eq.(7.5.33) for $P = P_C$ and $f_0 = f_{tD}$:

$$f_{tE} = \frac{1}{1 + P_E/P_{cr}} f_{tD} \quad (7.5.35)$$

The equilibrium curve, calculated at point E, gives:

$$f_{tE} = \frac{M_{pl}}{P_E} \left(1 - \frac{P_E}{P_y} \right) \quad (7.5.36)$$

Substituting the (7.5.35) into (7.5.36), it is possible to derive P_E (and consequently f_{tE}) through the following second order equation:

$$P_E^2 + B \cdot P_E \cdot -(P_y \cdot P_{Eul}) = 0 \quad (7.5.37)$$

where it is placed $B = (\Delta_D \cdot P_{Eul} \cdot P_y / \gamma M_{pl}) + P_{Eul} - P_y$.

Known the value of the axial load P_E , are fully defined both the DE and EF branches, considering that the load in F is known and is equal to P_y in the case in which it reaches the yield strength.

In this case, the point F corresponds to a total transverse deformation $f_t = 0$.

FG branch:

The FG branch is defined by the final load P_G , corresponding to the reverse point of the load, and the yield ratio of the material. This branch should be represented only if the yield strength is reached.

A simplification has also been implemented for the CD and DE branches. Strictly speaking, this branch is represented by the hyperbolic function (7.5.34). This function was defined by two straight lines through points D, C and E (Figure 7.5.6).

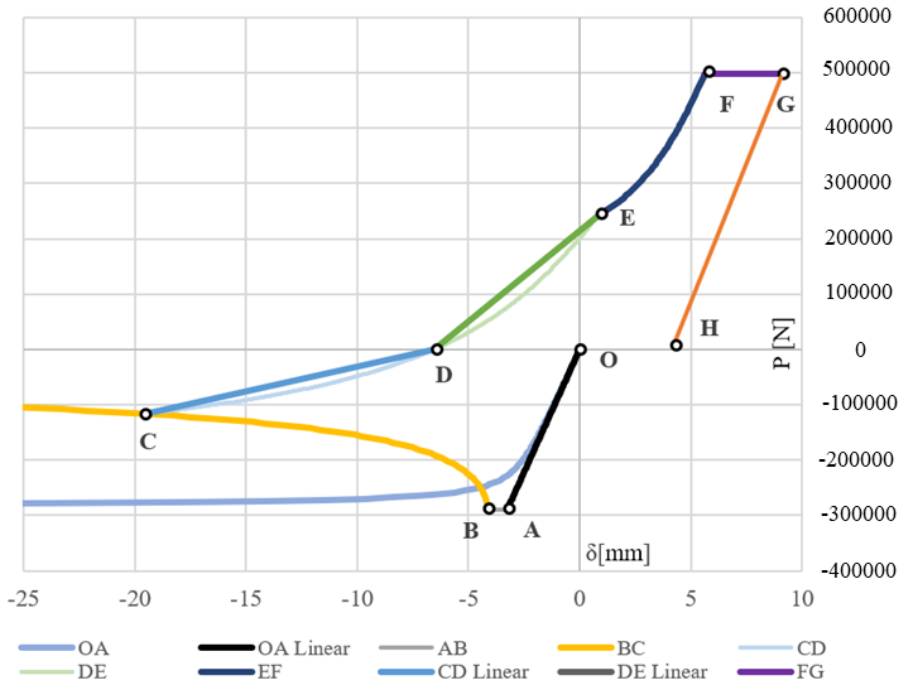


Figure 7.5.6 Shape of the Georgescu's model - Ø 139,7 s 5

GH branch:

The GH branch still has a linear trend, so that, as in the previous cases, fixing at point H the local reference system, the transverse deformation is described by Eq.(5.6.18), assuming $f_0 = f_{tH}$. In particular, inverting the relation for $P=P_G$ and then $f_t = f_{tG}$, The unknown value of the transverse deformation is deduced f_{tH} :

$$f_{tH} = f_{tG} \cdot \left(1 + \frac{P_G}{P_{cr}}\right) \quad (7.5.38)$$

The axial deformation at point G in the new reference system can be expressed by the Equation (7.5.20) for $P = P_G$ and $f_0 = f_{tH}$:

$$\delta_{G'} = \frac{P_G L}{EA} - \frac{\pi^2}{4L} (f_{tG}^2 - f_{tH}^2) \quad (7.5.39)$$

Consequently:

$$\delta_H = \delta_G - \delta_{G'} \quad (7.5.40)$$

The reported expressions of the Georgescu's model allow to fully characterize the first cycle of hysteresis of an axially loaded member. However, they can be used for the characterization of subsequent cycles provided, of course, replacing the initial deformation f_0 with the residual one of the previous cycles, i.e. corresponding to the point G, and estimating the degradation of the compressive resistant load.

7.6 Characterization of the Cyclic Behaviour of Diagonal Members in OpenSees

The modeling of the nonlinear behavior of the members was carried out using elements with distributed plasticity "nonlinear Beam Column", exploiting a discretization of the sections of fiber type [31].

OpenSEES does not have a specific library element that can accurately reproduce the cyclic behavior of axially loaded members. It was therefore necessary to develop a model to represent nonlinear behavior in compression (due to buckling) and degrading for cycles subsequent to the first.

The calibration of the initial imperfection was carried out using the Perry-Robertson formula which expresses the compressive strength as a function of the dimensionless slenderness $\bar{\lambda}$ and the imperfection coefficient η . With reference to the industrial beam with initial imperfection f_0 subject to axial load P , Considering the first yielding condition, it is possible to write the Perry-Robertson formula [13],[21] as:

$$\bar{P} = \frac{(1 + \bar{\lambda}^2 + \eta) \mp \sqrt{(1 + \bar{\lambda}^2 + \eta)^2 - 4 \cdot \bar{\lambda}^2}}{2\bar{\lambda}^2} \quad (7.6.1)$$

where

$$\eta = \frac{A}{W} \cdot f_0 \quad (7.6.2)$$

According to EC3, the expression of the imperfection coefficient that gives the best approximation of the instability curves is as follows:

$$\eta = \alpha \cdot \sqrt{\bar{\lambda}^2 - 0.04} \quad (7.6.3)$$

With α expressed as a function of the instability curve considered Table 7.6.1

Table 7.6.1 Values for α coefficient according to EC3

Buckling curve	a	b	c	d
α	0.21	0.34	0.49	0.76

Combining equations and it is possible to express the initial imperfection as:

$$f_0 = \frac{W}{A} \alpha (\bar{\lambda}^2 - 0.04) \quad \text{with } \alpha = 0.21 \div 0.76, \bar{\lambda} = \frac{\lambda}{\lambda_y} \quad (7.6.4)$$

The proposed scheme for modelling the axially loaded member in OpenSEES is shown in Figure 7.6.1. In addition to the end nodes, five intermediate nodes are defined. Obviously, the greater is the number of intermediate nodes used, the better is the approximation.; In this regard, the choice was made in order to achieve a good compromise between the accuracy of results and the containment of processing times.

To take account of the initial imperfection, a fictitious force was applied in the centerline, orthogonal to the axis of the diagonal, modeled as a rectilinear element. The value of the fictitious force is such as to determine an initial deflection equal to the imperfection calibrated based on the Eq. (7.6.4). Thus, give the scheme of simply supported beam, the fictitious force F can be determined as:

$$F = \frac{48 \cdot E \cdot I}{l^3} \cdot f_0 \quad (7.6.5)$$

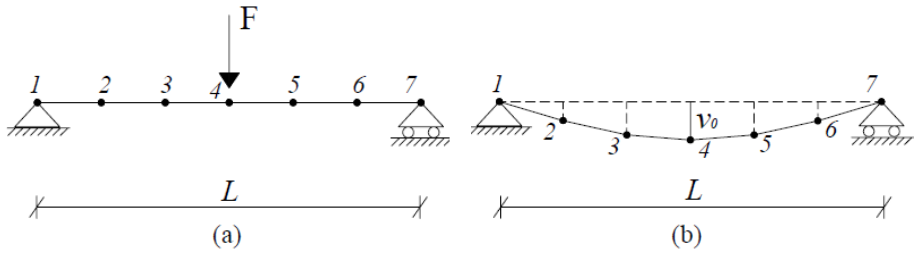


Figure 7.6.1 Initial imperfection model in OpenSees.

Tests carried out on a sufficient number of elements have shown that the proposed model provides a well-approximated estimation of the maximum compressive load and the non-linear cyclic behaviour. Some comparisons between the Georgescu model and the curves derived from the application of the model proposed in the OpenSEES are shown in Figure 7.6.2a. The curves are relative to three beams with cross sections of type HEA 180, HEA 220, and HEA 260, respectively, having the same length $L=721$ cm and therefore slenderness of 160, 130, and 110 respectively. The dashed curves reproduce the Georgescu model for the first cycle, while the continuous curves are those derived from the application of the model proposed in the OpenSEES for the same displacement story.

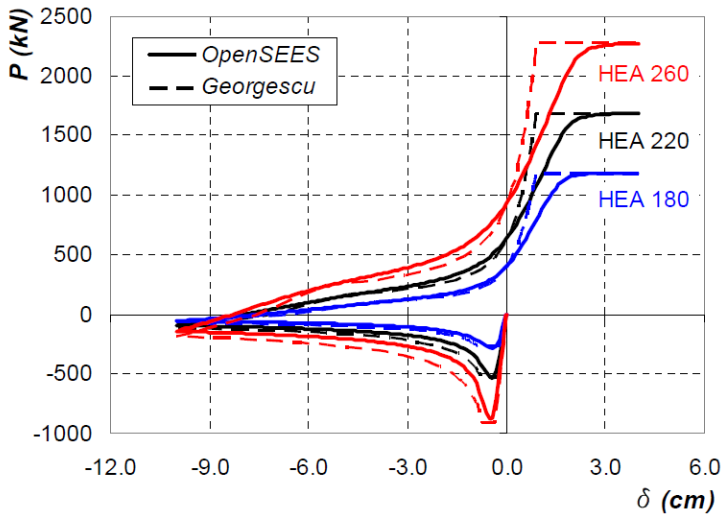


Figure 7.6.2 Comparison between Georgescu's model and OpenSees model for the first cycle – Diagonals HEA 180, HEA 220, HEA 260 ($L=721$ cm, $f_y=275$ N/mm²)

In addition, the simulations conducted in the cyclic field have shown that the proposed imperfection model is effective for modeling the behavior of bracing members for the purpose of simulating dynamic analysis. The analyses conducted had a different outcome by introducing a model characterized by an initial configuration that reproduces a sine wave with a transversal deflection equal to the initial imperfection f_0 (Figure 7.6.2b). In this case, during cyclic analysis, the diagonal, recovering a rectilinear configuration, loses memory of the initial imperfection, and consequently the compression resistance threshold is equal to the plastic stress, i.e. equal to the tensile one.

The application of the fictitious force determines an additional rate of bending moment in the centerline section which would tend to anticipate the plasticization of the section thus providing an underestimation of the normal compressive resistant stress. Appropriate corrections should therefore be made. However, for slender diagonals, such as those commonly used in bracing, the values of the fictitious force are so low that it has been considered appropriate to neglect this effect. The additional normal stress contributions transmitted to the columns due to the presence of fictitious forces are also negligible).

In Figure 7.6.3 is reported the diagonal inserted in the structural mesh of the bracing, where $i, j, k,$ and l represent the nodes for the definition of structural geometry. The member is then modeled by defining:

- two end nodes, 1 and 7, having the same coordinates as the nodes of the structural mesh i and k , respectively, and bound, through the element "equalDOF", to have the same horizontal and vertical displacements of those nodes in order to simulate the presence of the hinge constraint;
- five intermediate nodes, 2-6, which, as described above, constitute a good compromise between the accuracy of results and containment of processing times (in particular with reference to nonlinear dynamic analysis);
- a fictitious force applied in the centerline section, orthogonal to the axis of the diagonal, the value of which is determined through the (7.6.5) in order to determine an initial deflection equal to the imperfection calibrated on the Perry-Robertson formula (Eq. (7.6.4)).

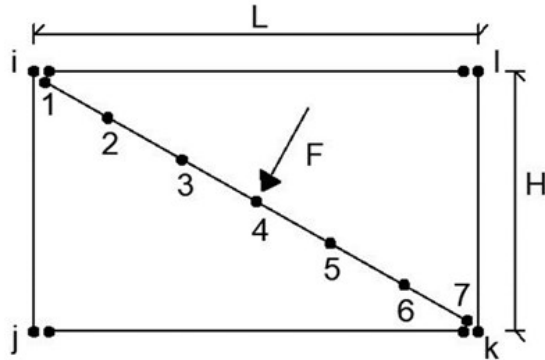


Figure 7.6.3 Model of the diagonal inserted in the structural mesh of the bracing.

7.7 Fiber Elements, Sections and Uniaxial Material in OpenSees for CBFs

In the case of CBFS, a fiber modeling of the sections of the structural elements has been selected. Consequently, non-linear analyses on structures are performed attributing to each fiber of the element a uniaxial behavior [31].

Non-linearities have been modelled through a distributed plasticity model can be modeled considering both Force Based Elements (FBE) and Displacement Based Elements (DBE). The models, properly calibrated, have provided comparable results.

The fiber sections have been modeled using the “wideflange” command for beams and columns, while the “patch rect” command for diagonal members.

In this case, the two opposite vertices that build the rectangular patch are inserted. The syntax used is the following:

```
patch('quad', matTag, numSubdivY, numSubdivZ, *crdsI, *crdsJ, )
```

dove:

- matTag- identificative tag of the material
- numSubdivY- number of fibers in Y direction
- numSubdivZ- number of fibers in Z direction
- *crdsI- coordinates in plane y-z of first vertex I

- *crdsJ- coordinates in the y-z plane of the second vertex J

The following is an example for a UPE220 section:

```
ops.section('Fiber',UPE220)
```

```
ops.patch('rect',Steel02,8,2,-0.027, 0.098, 0.058, 0.11)
```

```
ops.patch('rect',Steel02,2,8,-0.027, -0.098, -0.0205, 0.098)
```

```
ops.patch('rect',Steel02,8,2,-0.027, -0.11, 0.058, -0.098)
```

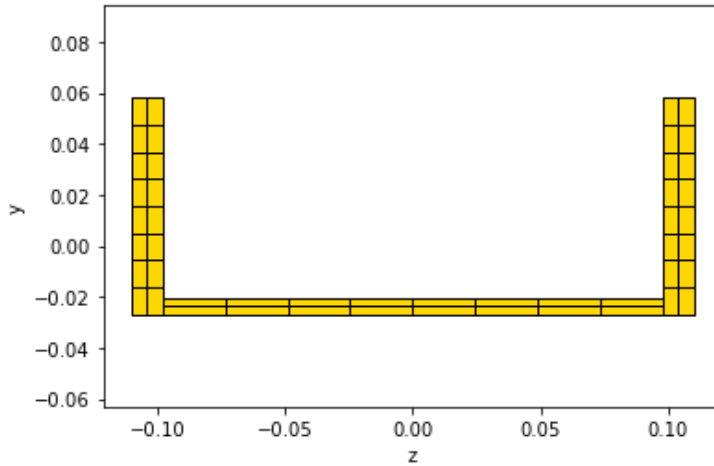


Figure 7.7.1 UPE220 fiber section

7.7.1 Calibration of the cyclic behaviour

The proposed model for the characterization of the cyclic behavior of axially loaded members has been calibrated and validated through the comparison with experimental tests available in the literature.

The effect of the degradation of the compressive strength for cycles subsequent to the first, it has been modeled using the "Steel02" library material for the bracing members, through an appropriate calibration of the parameters required at the input.

Reference was made to experimental data obtained from the NEES website (Network for Earthquake Engineering Simulation) related to the project "Large Scale Tests and Micromechanics-based simulation of Ultra-Low Cycle Fatigue (ULCF) and Fracture in Steel Structures" developed at the University of

Berkeley in collaboration with Stanford University (<http://cee.engr.ucdavis.edu/faculty/kanvindel/NEESPage/default.htm>) [37],[38].

The first simulated experimental test is a cyclic test with symmetrical load history conducted on a beam with a section HSS 4x4x1/4 (boxed of 10.16cm side and thickness of 0.635cm) with slenderness $\lambda=79$.

The model used for the simulation of the experimental test is shown in Figure 7.6.1a with $L=305\text{cm}$. The value of the initial imperfection calibrated on the Perry-Robertson formula (assumed $\alpha=0.21$ at the curve a) is:

$$f_0 = \frac{W}{A} \alpha \cdot \sqrt{\lambda^2 - 0.04} = 0.73 \text{ cm} \quad (7.7.1)$$

from which it is derived the value of the fictitious force applied at the centerline section:

$$F = \frac{48 \cdot E \cdot I}{l^3} \cdot f_0 = 8.706 \text{ kN} \quad (7.7.2)$$

The member was subjected to a cyclic push-over analysis in displacement control, where the displacement history assumed is the one applied in the test phase (Table 7.7.1). In Figure 7.7.2 is reported the theoretical curve derived from the simulation carried out by OpenSEES, where P_y and P_c represent, respectively, the yielding load and the normal compressive strength determined in accordance with the provisions of Eurocode 3.

Table 7.7.1 Displacement history for cyclic test

Load Step	Peak Displacement [cm]	Number of Cycles
1	0.1016	6
2	0.1524	6
3	0.2286	6
4	0.3048	4
5	1.5494	2
6	2.794	2
7	4.0386	2
8	6.0452	2
9	7.5946	2

The parameters for the characterization of the Steel02 material obtained from the calibration are shown below(N,mm):

uniaxialMaterial Steel02 2 475 210000 0.0001 20 0.925 0.15 0.00001 0.1
0.00001 0.1

where the yield stress value is assumed to be the actual value derived from the results of the experimental test. The values used for the parameters a_1 , a_2 , a_3 e a_4 clearly indicate the absence of the effect of isotropic hardening. (Kinematic hardening effect according to the Bauschinger effect - an increase in tensile yield stress corresponds to a decrease in compression yield stresses)

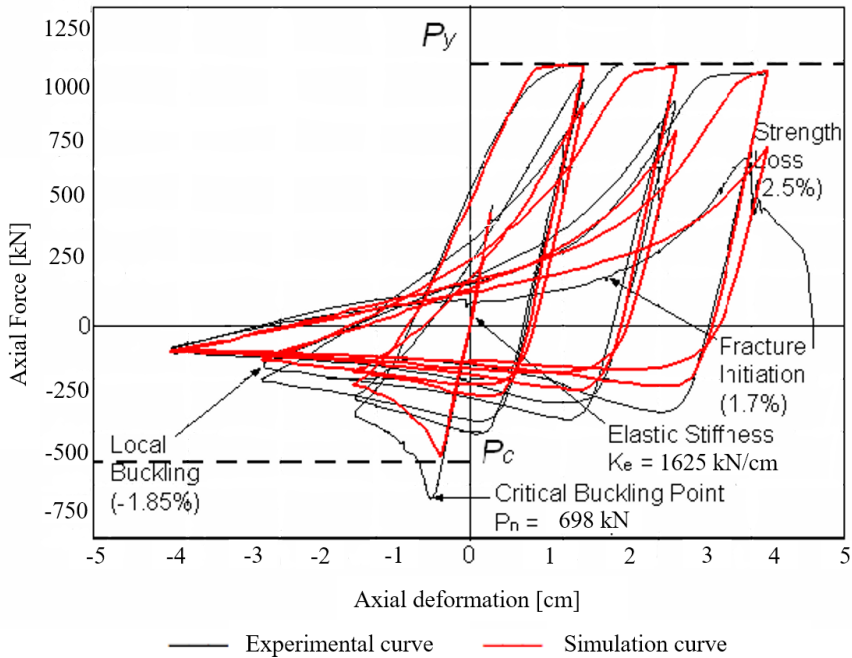


Figure 7.7.2 Comparison between the experimental curve and the theoretical curve derived from the OpenSees model (Test 1: HSS 4x4x1/4, $\lambda=79$)

Figure 7.7.2 shows a good agreement between the experimental curve and the theoretical model. A substantial difference is related to the compression phase and, in particular, to the underestimation of the resistant normal stress justified by the fact that the theoretical model is calibrated on the value of the normal resistant stress in compression provided by the code, of which it provides only a good approximation.

Figure 7.7.3 shows the comparison between the experimental and the theoretical curve related to a member with tubular profile 3STD (diameter 8.89

cm and thickness 0.5486 cm) having the same length as the previous one and subjected to the same loading procedure described in Table 7.7.1. The member is characterized by a slenderness $\lambda=103$.

The geometric model used is still the one reported in the previous case. The value of the initial imperfection calibrated on the Perry-Robertson formula (assumed $\alpha = 0.21$) at curve (a) is:

$$f_0 = \frac{W}{A} a \cdot \sqrt{\lambda^2 - 0.04} = 0.5977 \text{ cm} \quad (7.7.3)$$

$$F = \frac{48 \cdot E \cdot I}{l^3} \cdot f_0 = 2.6159 \text{ kN} \quad (7.7.4)$$

The parameters used for the characterization of the Steel02 material are the same as in the previous case, while the yield stress, derived from the results of the experimental test, is equal to 408 N/mm^2 .

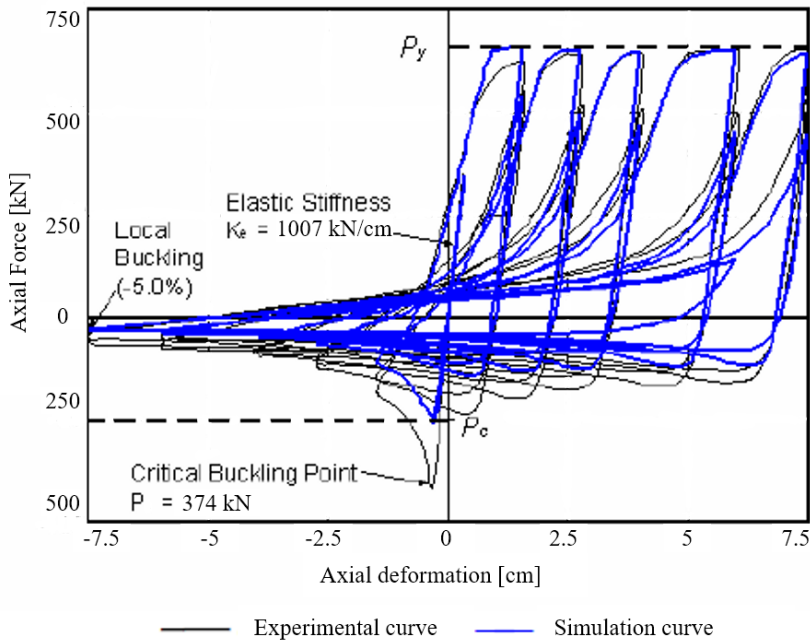


Figure 7.7.3 Comparison between the experimental curve and the theoretical curve derived from the OpenSees model (Test 7: PIPE 3STD, $\lambda=103$)

Figure 7.7.3 shows a good agreement between the results derived from the theoretical simulation, conducted using OpenSees, and the experimental data.

Once again it is observed that the most significant differences are related to the compression phase.

It should also be noted that the approximation provided by the theoretical model for the second experimental test is better than in the previous case. This is justified by the fact that, due to the greater slenderness and type of section, the second diagonal is less sensitive to local instability phenomena that cannot be taken into account through a modeling of the elements of the fiber type and which, therefore, inevitably compromise the accuracy of the results provided by the theoretical modeling.

The excellent results obtained, regardless of the type of steel considered and the type of section, allow to exploit the coefficients obtained through calibration also in the case study addressed in this work characterized by S355 steel grade for bracing members.

7.8 Case Study 1 for MRFs

The dynamic analyses were carried out with reference to the compatible spectrum earthquakes and to the models developed in the previous paragraphs.

The case study is a MRF belonging to a five-storey building consisting of five symmetrical bays of 4 m in each direction.

The building was designed according to a pre-1970 design code (ACI 1968) [15]. The reference site has been hypothesized in L'Aquila (high seismic risk area in Italy) and is characterized by a type B soil and a topographic category T1.

The floors have been designed to withstand a variable load of 2.00 kN/m² and a permanent non-structural load of 2.00 kN/m². The interstorey height is 3.00 m, the thickness of the floors is 140 mm, and the total height of the building is 15.00 m. The weight per unit volume of concrete is assumed to be 24.00 kN/m³. The beams have IPE300 section while the columns have HEA400 section, the characteristic yield strength of the steel is 355 MPa.

In Figure 7.8.1 the planimetric configuration of the building and the tributary area of the analyzed frame, are represented. In Figure 7.8.2 the frontal view, the designed cross sections, and the seismic design forces are reported [15].

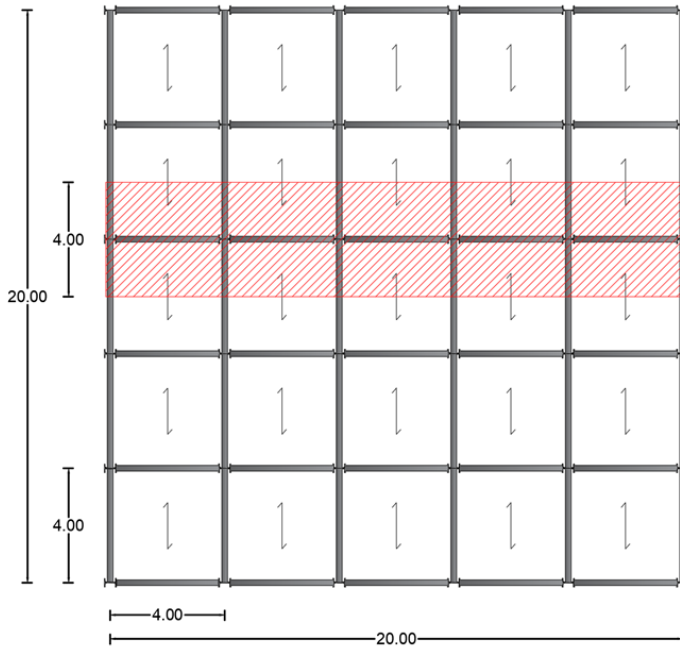


Figure 7.8.1 Plan configuration and tributary area of the case study



Figure 7.8.2 Frontal view and seismic design forces

7.8.1 Application of the Trilinear Simplified Model

The collapse mechanism equilibrium curve, as described above, can be obtained by a rigid-plastic analysis extended to second-order effects.

First, it is necessary to evaluate, for each possible collapse mechanism, the first-order collapse multiplier α_0 and the corresponding slope of the mechanism equilibrium curve γ_s .

The mechanism that will be activated, in a field of displacements compatible with the local ductility supplies, will be the one characterized by the equilibrium curve located below the others.

Table 7.8.1 First order collapse multiplier and slopes of the mechanism equilibrium curves.

i_m	$\alpha_{0im}^{(1)}$	$\alpha_{0im}^{(2)}$	$\alpha_{0im}^{(3)}$	$\gamma_{im}^{(1)}$	$\gamma_{im}^{(2)}$	$\gamma_{im}^{(3)}$
	[-]	[-]	[-]	[m ⁻¹]	[m ⁻¹]	[m ⁻¹]
1	10.96	5.04	10.96	3.02	0.49	3.02
2	6.81	7.41	11.74	1.41	0.59	2.59
3	5.62	10.13	13.70	0.88	0.72	2.26
4	5.27	16.46	18.26	0.63	0.99	2.01
5	5.39	32.87	32.87	0.49	1.81	1.81

From the analysis of Table 7.8.1 the collapse mechanism that can potentially be activated is the global one, being characterized by the lowest first-order multiplier.

- Parameters obtained through the elastic analysis:

$$\delta_1(\alpha = 1) = 0.04 \text{ m}$$

$$k = 25.00 \text{ m}^{-1}$$

$$\delta_A = \delta_y = 0.086 \text{ m}$$

$$\alpha_A = \alpha_y = k\delta_y = 2.27$$

- Parameters obtained through rigid-plastic analysis:

$$\alpha_0 = 5.04$$

$$\gamma_s = 0.49$$

$$\alpha = \alpha_0 - \gamma_s(\delta - \delta_y) \rightarrow \alpha = 5.04 - 0.49(\delta - 0.086)$$

$$\alpha(\delta = 0) = \alpha_0 + \gamma_s \delta_y = 5.09$$

$$H_0 = 15 \text{ m (Collapse mechanism of Type 2 - } i_m = 1)$$

- Evaluation of the maximum multiplier exploiting the calibrated Merchant-Rankine formula:

$$\alpha_{max} = \frac{\alpha_0}{1 + \Psi \alpha_0 \gamma_s \delta_1} = 4.81$$

$$\Psi = 0.358 - 0.1331 \xi \text{ e } \xi = \frac{\sum \frac{EI_b}{L_b}}{\sum \frac{EI_c}{L_c}} = 0.116$$

Starting from the trilinear approximation of the push-over curve, the four characteristic points of the structural behavior curve have been identified, each of these points is associated with a specific limit state.

- Point A (Fully Operational)

$$\delta_A = \delta_y = 0.086 \text{ m}$$

$$\alpha_A = \alpha_y = 2.27$$

- Point B (Operational)

$$\alpha_B = \alpha_{max} = 4.81$$

$$\delta_B = \alpha_{max} \delta_1 = 0.181 \text{ m}$$

- Point C (Life Safety)

$$\alpha_C = \alpha_{max} = 4.81$$

$$\delta_C = \delta_{mecc} = \frac{\alpha_0 - \alpha_{max}}{\gamma_s} + \delta_y = 0.554 \text{ m}$$

- Point D (Near Collapse)

Evaluation of the plastic rotation demand corresponding to the development of the collapse mechanism for the first plasticized element (first storey beam):

$$\theta_{p.mec} = \frac{n_s \delta_y}{H_0} \left[\frac{\Psi_1}{\Psi_2} \Psi_3 \left(\frac{\alpha_{max}}{\alpha_y} - 1 \right)^{\Psi_4} \frac{1 - \Psi_5 \gamma_s}{1 - \Psi_6 \gamma_s} \right] = 0.018 \text{ rad}$$

The computation of the corresponding capacity gives a value of the ultimate plastic rotation equal to $8\vartheta_y = 8 \frac{\gamma_{ov} M_p m l_m}{6EI_m} = 0.074 \text{ rad}$

Evaluation of the plastic rotation demand corresponding to the development of the collapse mechanism for the critical element (first storey column):

$$\theta_{p.mec} = \frac{n_s \delta_y}{H_0} \left[\frac{\Psi_1'}{\Psi_2'} \Psi_3' \left(\frac{\alpha_{max}}{\alpha_y} - 1 \right)^{\Psi_4'} \frac{1 - \Psi_5' \gamma_s}{1 - \Psi_6' \gamma_s} \right] = 0.057 \text{ rad}$$

The computation of the corresponding capacity gives a value of the ultimate plastic rotation equal to $8\vartheta_y = 8 \frac{\gamma_{ov} M_p m l_m}{4EI_m} = 0.063 \text{ rad}$

Evaluation of the plastic rotation demand corresponding to the achievement of the maximum load-bearing capacity for the first plasticized element:

$$\theta_{p.\alpha_{max}} = \frac{n_s \delta_y}{H_0} \left[\frac{\Psi_7}{\Psi_8} \Psi_9 \left(\frac{\alpha_{max}}{\alpha_y} - 1 \right)^{\Psi_{10}} \frac{1 - \Psi_{11} \gamma_s}{1 - \Psi_{12} \gamma_s} \right] = 0.004 \text{ rad}$$

The most unfavorable condition is $\theta_{p.mec} = 0.057 \text{ rad}$.

$$\delta_D = \delta_C + (\vartheta_{p.u} - \vartheta_{p.mecc}) H_0 = 0.858 \text{ m}$$

$$\alpha_D = \alpha_0 - \gamma_s (\delta_D - \delta_y) = 4.66$$

To evaluate the accuracy of the trilinear model obtained, a static nonlinear analysis, or push-over, was carried out using the SAP2000 computer program [30].

Beams and columns were modeled using beam-column elements, whose non-linearities were concentrated in hinges ("p-hinge" elements) placed at their ends. In particular, plastic hinges have been defined for the columns, which take into account the interaction between axial force and bending moment.

The push-over analysis was conducted under displacement control taking into account geometric and mechanical nonlinearities.

In Figure 7.8.3 the non-dimensional pushover curve obtained by SAP2000 and the trilinear model obtained by applying the procedure described above are reported.

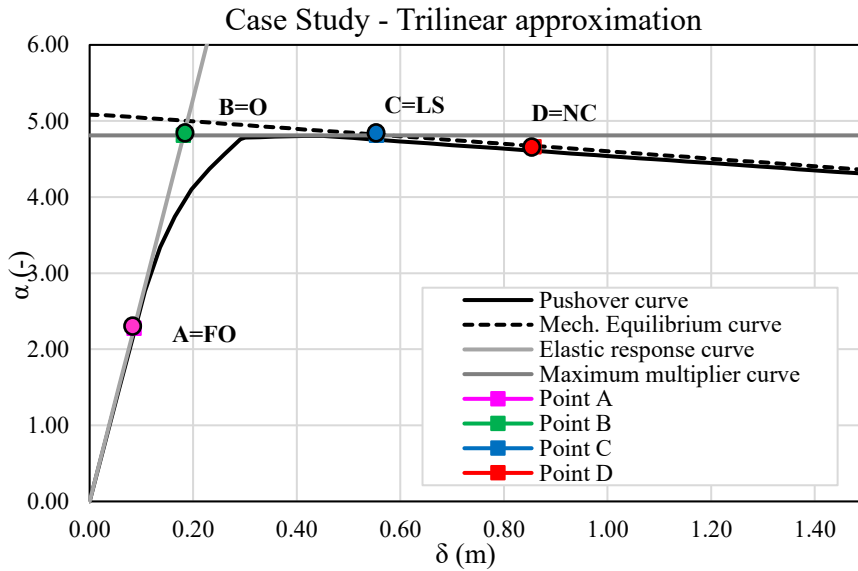


Figure 7.8.3 Trilinear approximation and performance points (MRF case study)

After defining the trilinear model and the performance points, the transformation procedure of the multiple degrees of freedom (MDOF) system into an equivalent single degree of freedom (SDOF) system was applied through the modal participation coefficient Γ . Subsequently, known the dynamic properties of the SDOF system, the simplified curve and the performance points were represented in the ADRS plan. In this way, the capacity in terms of spectral displacements and accelerations was defined according to the "ADRS spectrum" and "Nassar & Krawinkler" models.

It was, therefore, necessary to define:

- The eigenvector $\underline{\phi} = \{\phi_1, \phi_2, \phi_3, \phi_4, \phi_5\}$ that, assuming $\phi_k = \frac{F_k}{F_n}$, is:

$$\begin{aligned} \phi_1 &= 0.206 & \phi_2 &= 0.402 & \phi_3 &= 0.608 \\ \phi_4 &= 0.788 & \phi_5 &= 1.00 \end{aligned}$$

- The modal participation factor Γ :

$$\Gamma = \frac{\sum_{k=1}^n m_k \phi_k}{\sum_{k=1}^n m_k \phi_k^2} = 1.364$$

being:

$$m_1 = 60.346 \times 10^3 \text{ kg} \quad m_2 = 60.346 \times 10^3 \text{ kg} \quad m_3 = 60.346 \times 10^3 \text{ kg}$$

$$m_4 = 60.346 \times 10^3 \text{ kg} \quad m_5 = 60.346 \times 10^3 \text{ kg}$$

- the dynamic parameters of the equivalent SDOF system (Table 7.8.2).

Table 7.8.2 Dynamic parameters of the equivalent SDOF system (MRF Case Study).

\mathbf{m}^*	\mathbf{k}^*	$\boldsymbol{\omega}^*$	\mathbf{T}^*
[kg 10 ³]	[kN/m]	[rad/s]	[s]
181.04	8668.21	6.9195	0.90803

Therefore, the characteristic points of the capacity curve are defined in the planes $\alpha - \delta$, $F_b - d_c$, $F^* - D^*$, $S_a - S_D$ assessing the capacity in terms of accelerations for Nassar & Krawinkler approach and ADRS spectrum approach. In particular, in Table 7.8.3 the results based on the use of the ADRS spectrum and the Nassar & Krawinkler formulation, are reported [28],[29].

Table 7.8.3 Capacity in terms of spectral acceleration and displacements according to ADRS Spectrum and Nassar & Krawinkler approach (MRF case study).

$\mathbf{T}^* > \mathbf{TC}$		FO	O	LS	NC
$\boldsymbol{\alpha}$	[-]	2.27	4.81	4.81	4.66
$\boldsymbol{\delta}$	[m]	0.086	0.181	0.554	0.858
$\boldsymbol{\delta}^*$	[m]	0.063	0.133	0.406	0.629
F	[kN]	742.99	1572.21	1572.21	1523.57
F*	[kN]	544.86	1152.96	1152.96	1117.28
Sa(T*) ADRS Spectrum	[g]	0.307	0.649	1.983	3.071
Sa(T*) Nassar & Krawinkler	[g]	0.307	0.649	2.040	3.151

7.8.2 IDA Results and Comparison with the Simplified Method (MRF)

The accelerograms previously obtained were applied, individually, to the structure, scaled with multiple levels of intensity. In this way has been possible to get response curves parameterized with the intensity level.

The maximum interstorey drift, i.e. the ratio between the maximum relative interstorey displacement and the interstorey height, have been evaluated as a function of the peak ground acceleration (PGA) for each earthquake and for each intensity level.

The MIDR provide an estimate of the maximum rotation exhibited by the members (columns) of the structure and can be compared with the plastic rotation capacity of the same for each different limit state considered. The rotation capacity has been defined according to Eurocode 8 – Part 3 provisions (Table 7.8.4).

Table 7.8.4 Rotation Capacity defined according to Eurocode 8 – Part 3 [19]

Limit State	DL	SD	NC
Rotation capacity θ	0.0078	0.047	0.063

The corresponding PGA/g value was evaluated for each rotation as reported in Figure 7.8.4

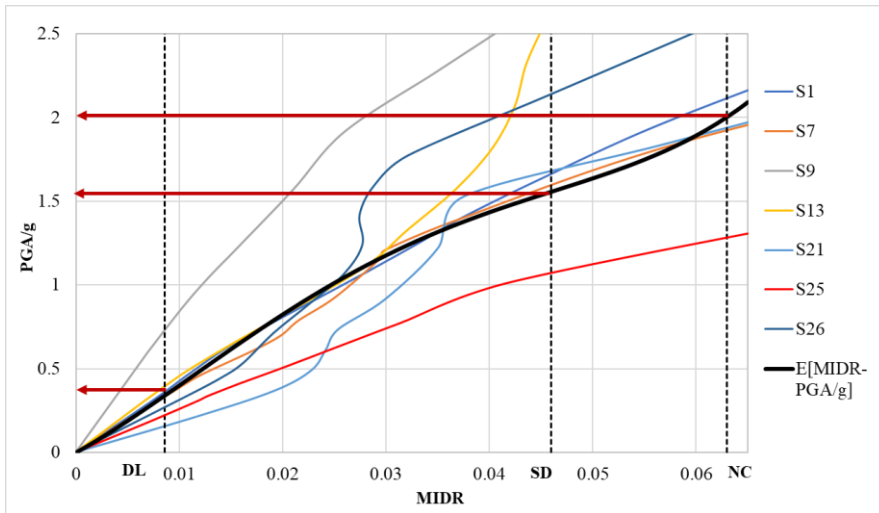


Figure 7.8.4 PGA/g value evaluated for each MIDR limit provided by codes (rotation limit).

For each earthquake, the PGA/g corresponding to the achievement of the two limit states considered was derived and the average value was determined.

Given the PGA/g mean, the corresponding spectral acceleration was derived by constructing a specific response spectrum in terms of accelerations (Figure 7.8.5).

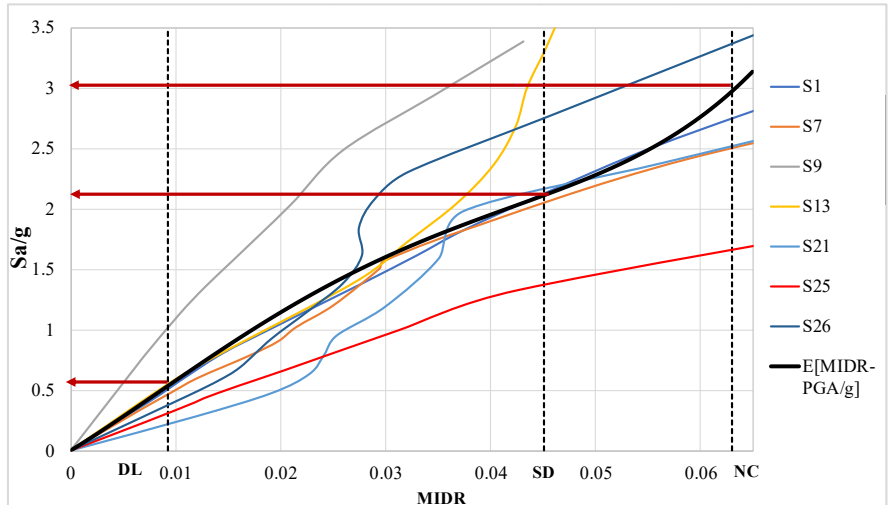


Figure 7.8.5 Sa/g value evaluated for each MIDR limit provided by codes (rotation limit).

The accelerations thus obtained were compared with those obtained through the application of the verification procedures described in the proposed simplified method.

Table 7.8.5 Comparison between IDA results and Simplified Method in terms of spectral accelerations (MRF)

Limit State	ϑ_C	PGA/g	Sa(T*)/g IDA	Sa(T*)/g ADRS	Sa(T*)/g N. & K.
A - FO	-	0.206	0.293	0.307	0.307
B - O	0.0078	0.429	0.618	0.649	0.649
C - LS	0.047	1.522	2.180	1.983	2.040
D - NC	0.063	2.063	3.010	3.071	3.151

From the analysis of Table 7.8.5 there is a percentage error in the evaluation of capacity in terms of spectral acceleration, between Simplified Method and IDA, equal to 4.5% for the "Fully Operational" limit state, 4.7% for the "Operational" limit state, 6.4% for the "Life Safety" limit state and 2% for the

"Near Collapse" limit state. The error exceeds the results of the IDAs for the limit states FO and NC, while subceeds for limit states O and LS.

7.9 Case Study 2 for MRFs

The dynamic analyses were carried out with reference to the compatible spectrum earthquakes and to the models developed in the previous paragraphs.

The case study is a MRF belonging to a three-storey building (Figure 7.9.1) whose plan configuration is depicted in Figure 7.9.2 [16].

The building, located in Amatrice, Italy, was built decades ago, before the introduction of modern seismic design standards. The building was damaged following the 2016-2017 Amatrice earthquakes. Amatrice is a high seismic risk area in Italy and as reported in the building area is characterized by a type B soil and a topographic category T1.

The building is trapezoidal, measuring 6.6 and 8.5 m wide and 22.5 m long. The interstorey height is variable (about 3.6 m), as reported in Figure 7.9.3.

The floors have been designed to withstand a variable load of 2.00 kN/m² and a permanent non-structural load of 1.76 kN/m².

The flooring systems consist of concrete slabs on a corrugated sheet of steel with a thickness of 10 mm. The cross sections of the outer and inner beams are HEA160 and HEA300 respectively, and all columns are HEA200.





Figure 7.9.1 Frontal and lateral view - real

All cross-sections can be classified as Class 1 cross-sections, and the steel grade used in the design is S235. The beam-column connections are completely welded. The infills consist of a double layer of perforated brick measuring $120 \times 250 \times 80$ mm, for a total thickness of 160 mm.

The proper weight of the slab is assumed to be 4.88 kN/m^2 .

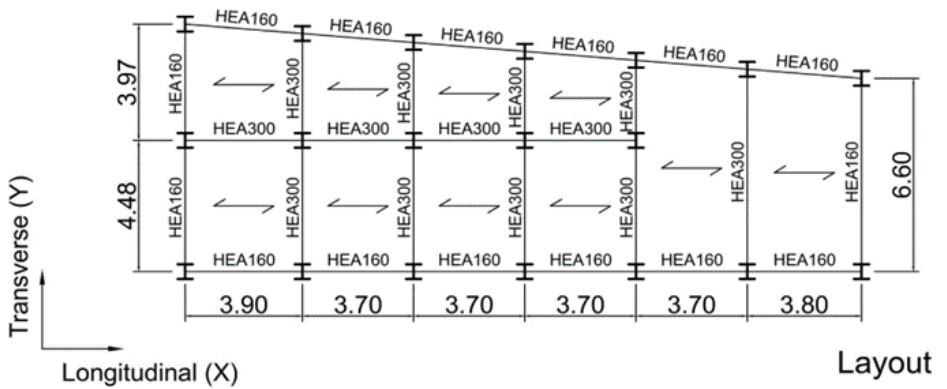


Figure 7.9.2 Plan configuration of the case study

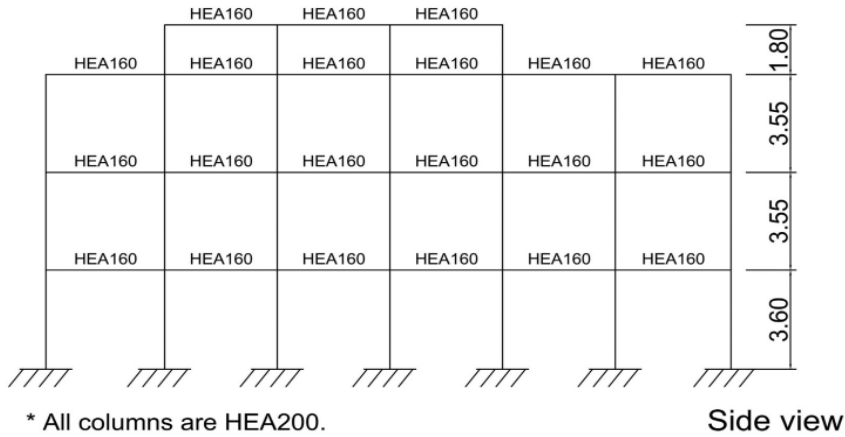


Figure 7.9.3 side view of the case study

7.9.1 Application of the Trilinear Simplified Model

The collapse mechanism equilibrium curve, as described above, can be obtained by a rigid-plastic analysis extended to second-order effects.

First, it is necessary to evaluate, for each possible collapse mechanism, the first-order collapse multiplier α_0 and the corresponding slope of the mechanism equilibrium curve γ_s .

The mechanism that will be activated, in a field of displacements compatible with the local ductility supplies, will be the one characterized by the equilibrium curve located below the others.

Table 7.9.1 First order collapse multiplier and slopes of the mechanism equilibrium curves.

i_m	$\alpha_{0im}^{(1)}$	$\alpha_{0im}^{(2)}$	$\alpha_{0im}^{(3)}$	$\gamma_{im}^{(1)}$	$\gamma_{im}^{(2)}$	$\gamma_{im}^{(3)}$
	[-]	[-]	[-]	[m ⁻¹]	[m ⁻¹]	[m ⁻¹]
1	0.66	1.17	0.66	1.64	0.48	1.64
2	1.27	1.80	0.96	0.77	0.61	1.43
3	1.33	3.00	1.48	0.48	1.07	1.07

From the analysis of Table 7.9.1 the collapse mechanism that can potentially be activated is the “Soft storey” ($i_m=1$), being characterized by the lowest first-order multiplier.

- Parameters obtained through the elastic analysis:

$$k = 4.25 \text{ m}^{-1}$$

$$\delta_A = \delta_y = 0.096 \text{ m}$$

$$\alpha_A = \alpha_y = k\delta_y = 0.42$$

- Parameters obtained through rigid-plastic analysis:

$$\alpha_0 = 0.66$$

$$\gamma_s = 1.64$$

$$\alpha = \alpha_0 - \gamma_s(\delta - \delta_y) \rightarrow \alpha = 0.66 - 1.64(\delta - 0.096)$$

$$\alpha(\delta = 0) = \alpha_0 + \gamma_s\delta_y = 0.835$$

$$H_0 = 10.7 \text{ m} \quad (\text{Type 3-}i_m = 1)$$

- Evaluation of the maximum multiplier exploiting the calibrated Merchant-Rankine formula:

$$\alpha_{max} = \frac{\alpha_0}{1 + \alpha_0\gamma_s\delta_1} = 0.53$$

Starting from the trilinear approximation of the push-over curve, the four characteristic points of the structural behavior curve have been identified, each of these points is associated with a specific limit state.

- Point A (Fully Operational)

$$\delta_A = \delta_y = 0.096 \text{ m}$$

$$\alpha_A = \alpha_y = 0.42$$

- Point B (Operational)

$$\alpha_B = \alpha_{max} = 0.53$$

$$\delta_B = \alpha_{max} \delta_1 = 0.124 \text{ m}$$

- Point C (Life Safety)

$$\alpha_C = \alpha_{max} = 0.53$$

$$\delta_C = \delta_{mecc} = \frac{\alpha_0 - \alpha_{max}}{\gamma_s} + \delta_y = 0.188 \text{ m}$$

- Point D (Near Collapse)

Evaluation of the plastic rotation demand corresponding to the development of the collapse mechanism for the first plasticized element (first storey column):

$$\theta_{p.mec} = \frac{n_s \delta_y}{H_0} \left[\frac{\Psi_1}{\Psi_2} \Psi_3 \left(\frac{\alpha_{max}}{\alpha_y} - 1 \right)^{\Psi_4} \frac{1 - \Psi_5 \gamma_s}{1 - \Psi_6 \gamma_s} \right] = 0.054 \text{ rad}$$

The computation of the corresponding capacity gives a value of the ultimate plastic rotation equal to $8\vartheta_y = 8 \frac{\gamma_{ov} M_{p.m} l_m}{6EI_m} = 0.070 \text{ rad}$

Evaluation of the plastic rotation demand corresponding to the development of the collapse mechanism for the critical element (first storey column):

$$\theta_{p.mec} = \frac{n_s \delta_y}{H_0} \left[\frac{\Psi_1'}{\Psi_2'} \Psi_3' \left(\frac{\alpha_{max}}{\alpha_y} - 1 \right)^{\Psi_4'} \frac{1 - \Psi_5' \gamma_s}{1 - \Psi_6' \gamma_s} \right] = 0.054 \text{ rad}$$

The computation of the corresponding capacity gives a value of the ultimate plastic rotation equal to $8\vartheta_y = 8 \frac{\gamma_{ov} M_{p.m} l_m}{4EI_m} = 0.070 \text{ rad}$

Evaluation of the plastic rotation demand corresponding to the achievement of the maximum load-bearing capacity for the first plasticized element:

$$\theta_{p.\alpha_{max}} = \frac{n_s \delta_y}{H_0} \left[\frac{\Psi_7}{\Psi_8} \Psi_9 \left(\frac{\alpha_{max}}{\alpha_y} - 1 \right)^{\Psi_{10}} \frac{1 - \Psi_{11} \gamma_s}{1 - \Psi_{12} \gamma_s} \right] = 0.0011 \text{ rad}$$

The most unfavorable condition is $\theta_{p.mec} = 0.054 \text{ rad}$.

$$\delta_D = \delta_C + (\vartheta_{p.u} - \vartheta_{p.mec}) H_0 = 0.254 \text{ m}$$

$$\alpha_D = \alpha_0 - \gamma_s (\delta_D - \delta_y) = 0.40$$

To evaluate the accuracy of the trilinear model obtained, a static nonlinear analysis, or push-over, was carried out using the SAP2000 computer program [30].

Beams and columns were modeled using beam-column elements, whose non-linearities were concentrated in hinges ("p-hinge" elements) placed at their ends. In particular, plastic hinges have been defined for the columns, which take into account the interaction between axial force and bending moment.

The push-over analysis was conducted under displacement control taking into account geometric and mechanical nonlinearities.

In Figure 7.9.4 the non-dimensional pushover curve obtained by SAP2000 and the trilinear model obtained by applying the procedure described above are reported.

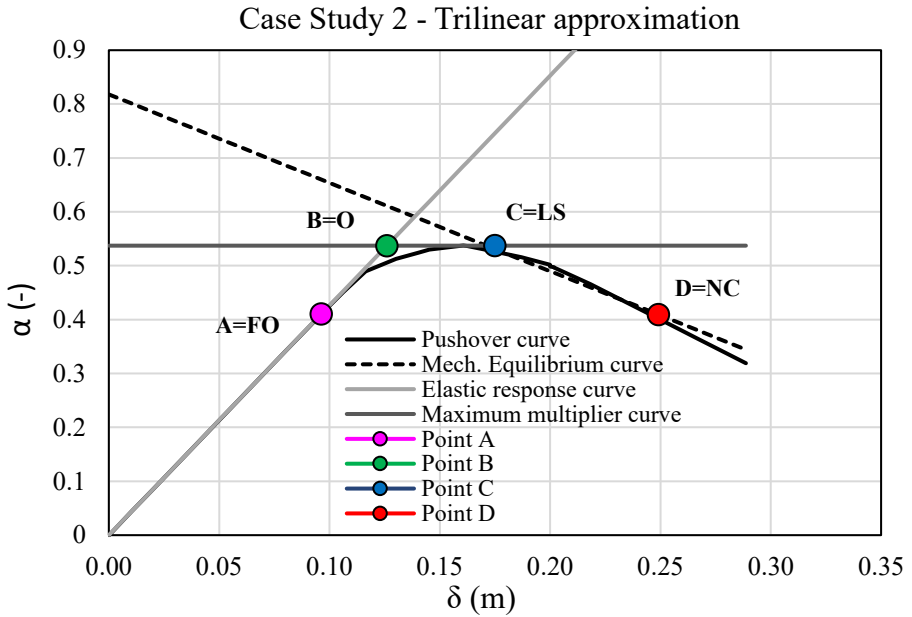


Figure 7.9.4 Trilinear approximation and performance points (MRF case study 2)

After defining the trilinear model and the performance points, the transformation procedure of the multiple degrees of freedom (MDOF) system into an equivalent single degree of freedom (SDOF) system was applied through the modal participation coefficient Γ . Subsequently, known the dynamic properties of the SDOF system, the simplified curve, and the performance points were represented in the ADRS plan. In this way, the capacity in terms of spectral displacements and accelerations was defined according to the "ADRS spectrum" and "Nassar & Krawinkler" models.

It was, therefore, necessary to define:

- The eigenvector $\underline{\phi} = \{\phi_1, \phi_2, \phi_3, \phi_4, \phi_5\}$ that, assuming $\phi_k = \frac{F_k}{F_n}$, is:

$$\phi_1 = 0.262 \quad \phi_2 = 0.519 \quad \phi_3 = 1.00$$

- The modal participation factor Γ :

$$\Gamma = \frac{\sum_{k=1}^n m_k \Phi_k}{\sum_{k=1}^n m_k \Phi_k^2} = 1.331$$

being:

$$m_1 = 54.234 \times 10^3 \text{ kg} \quad m_2 = 54.234 \times 10^3 \text{ kg} \quad m_3 = 54.234 \times 10^3 \text{ kg}$$

- the dynamic parameters of the equivalent SDOF system (Table 7.9.2).

Table 7.9.2 Dynamic parameters of the equivalent SDOF system (MRF Case Study 2).

\mathbf{m}^*	\mathbf{k}^*	$\boldsymbol{\omega}^*$	\mathbf{T}^*
[kg 10 ³]	[kN/m]	[rad/s]	[s]
96.63	1152.32	3.443	1.82

Therefore, the characteristic points of the capacity curve are defined in the planes $\alpha - \delta$, $F_b - d_c$, $F^* - D^*$, $S_a - S_D$ assessing the capacity in terms of accelerations for Nassar & Krawinkler approach and ADRS spectrum approach. In particular, in Table 7.9.3 the results based on the use of the ADRS spectrum and the Nassar & Krawinkler formulation, are reported [28],[29].

Table 7.9.3 Capacity in terms of spectral acceleration and displacements according to ADRS Spectrum and Nassar & Krawinkler approach (MRF case study).

$\mathbf{T}^* > \mathbf{TC}$		FO	O	LS	NC
$\boldsymbol{\alpha}$	[-]	0.42	0.53	0.53	0.40
$\boldsymbol{\delta}$	[m]	0.096	0.124	0.188	0.245
$\boldsymbol{\delta}^*$	[m]	0.072	0.093	0.141	0.184
F	[kN]	115.48	145.73	145.73	109.98
F*	[kN]	86.77	109.49	109.49	82.63
Sa(T*) ADRS Spectrum	[g]	0.087	0.112	0.171	0.224
Sa(T*) Nassar & Krawinkler	[g]	0.087	0.112	0.182	0.236

7.9.2 IDA Results and Comparison with the Simplified Method (MRF 2)

The accelerograms previously obtained were applied, individually, to the structure, scaled with multiple levels of intensity. In this way has been possible to get response curves parameterized with the intensity level.

The maximum interstorey drift, i.e. the ratio between the maximum relative interstorey displacement and the interstorey height, has been evaluated as a function of the peak ground acceleration (PGA) for each earthquake and for each intensity level.

The MIDR provides an estimate of the maximum rotation exhibited by the members (columns) of the structure and can be compared with the plastic rotation capacity of the same for each different limit state considered. The rotation capacity has been defined according to Eurocode 8 – Part 3 provisions (Table 7.9.4).

Table 7.9.4 Rotation Capacity defined according to Eurocode 8 – Part 3 [19]

Limit State	DL	SD	NC
Rotation capacity θ	0.0088	0.053	0.070

The corresponding S_a/g value was evaluated for each rotation as reported in Figure 7.9.5

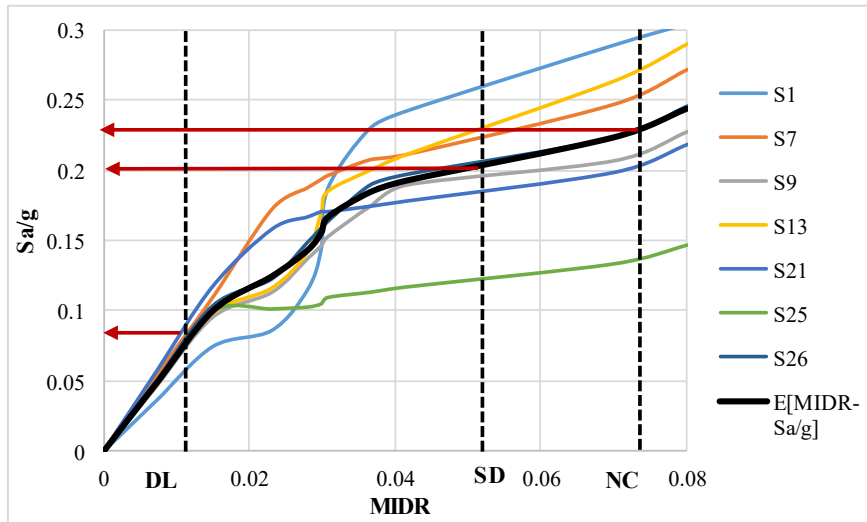


Figure 7.9.5 Sa/g value evaluated for each MIDR limit provided by codes (rotation limit).

For each earthquake, the PGA/g corresponding to the achievement of the two limit states considered was derived and the average value was determined.

Given the PGA/g mean, the corresponding spectral acceleration was derived by considering a specific response spectrum in terms of accelerations.

The accelerations thus obtained were compared with those obtained through the application of the verification procedures described in the proposed simplified method.

Table 7.9.5 Comparison between IDA results and Simplified Method in terms of spectral accelerations (MRF)

Limit State	ϑ_c	Sa(T*)/g IDA	Sa(T*)/g ADRS	Sa(T*)/g N. & K.
A - FO	-	0.078	0.087	0.087
B - O	0.009	0.0892	0.112	0.112
C - LS	0.053	0.201	0.171	0.182
D - NC	0.070	0.230	0.224	0.236

From the analysis of Table 7.9.5 there is a percentage error in the evaluation of capacity in terms of spectral acceleration, between Simplified Method and IDA, equal to 10.3% for the "Fully Operational" limit state, 19.7% for the "Operational" limit state, 9.4% for the "Life Safety" limit state and 2.5% for the "Near Collapse" limit state. The error exceeds the results of the IDAs for the limit states O and FO.

7.10 Case Study for CBFs

The analyzed structure is a simulated design of a concentrically "X" braced structure located in L'Aquila (IT), with type B soil [17]. The design spectrum considered refers to a return period of 475 years.

The structure has 5 floors and extends for 5 bays of 6 m in the X direction and for 3 bays of 7 m in the Y direction. The interstorey height is 3.5 m and the braced bays are those at the ends. The permanent loads were calculated considering the prefabricated slab of type "Predalles" ($G_1 = 3.70 \text{ kN/m}^2$). The destination is for offices, so accidental loads are equal to $Q_k = 3.0 \text{ kN/m}^2$. The steel used is grade S355 for the diagonals and S235 for the other members.

The plan arrangement of seismoresistant macroelements is shown in Figure 7.10.1. The profiles used for beams, columns, and diagonals, are shown in Table 7.10.1.

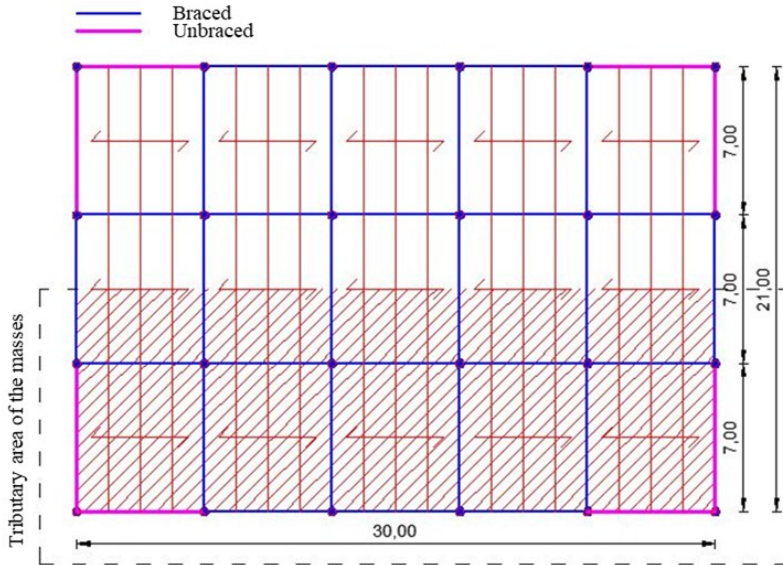


Figure 7.10.1 Plan and bracing configuration of the case study

Table 7.10.1 Beams, columns, and braces sections for the case study.

Storey (k th)	Beams				Columns		Braces
	X		Y		X, Y		X, Y
	external	internal	braced	unbraced	external	internal	Seismic design
1	HEA 300	HEA 400	HEA 340	HEA 220	HEM 300	HEM 240	UPE 220
2	HEA 300	HEA 400	HEA 320	HEA 220	HEM 240	HEM 220	UPE 200
3	HEA 300	HEA 400	HEA 300	HEA 220	HEM 200	HEM 200	UPE 200
4	HEA 300	HEA 400	HEA 260	HEA 220	HEM 200	HEM 200	UPE 180
5	HEA 260	HEA 320	HEA 220	HEA 220	HEM 200	HEM 200	UPE 140

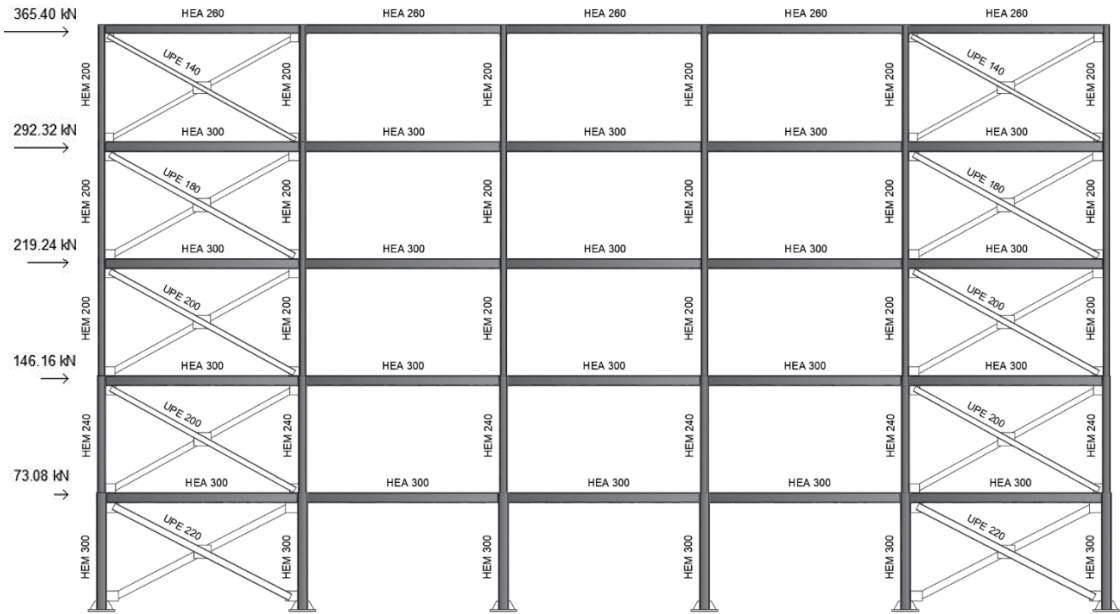


Figure 7.10.2 Frontal view and seismic design forces – X direction.

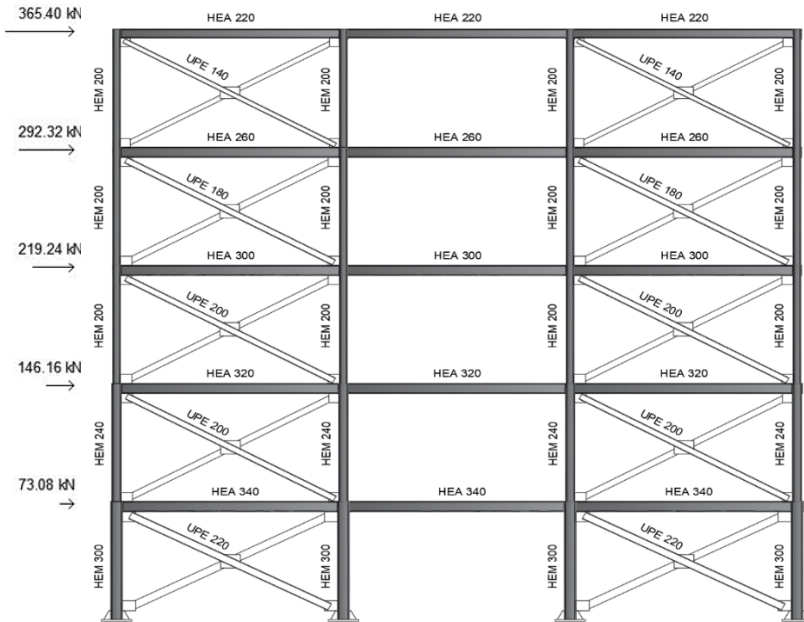


Figure 7.10.3 Frontal view and seismic design forces – Y direction.

The elevations of the seismoresistant frames and the design seismic forces evaluated according to the Italian NTC 2018 standard, are shown in Figure 7.10.2, Figure 7.10.3.

7.10.1 Application of the simplified method – X direction

After describing in detail the geometric and mechanical characteristics of the building under study, the next step is the application of the simplified method for the evaluation of seismic performances. In the second phase, the validation process through incremental dynamic analysis (IDA) will be performed.

This method, through the use of linear elastic analysis and rigid-plastic analysis extended to second-order effects, allows to represent the pushover curve of the considered structure.

It is also possible to define the performance points (A, B, C, D) to which specific limit states provided by current codes are associated (Fully Operational, Operational, Life Safety, Near Collapse).

The trilinear capacity curve is shown in Figure 7.10.4.

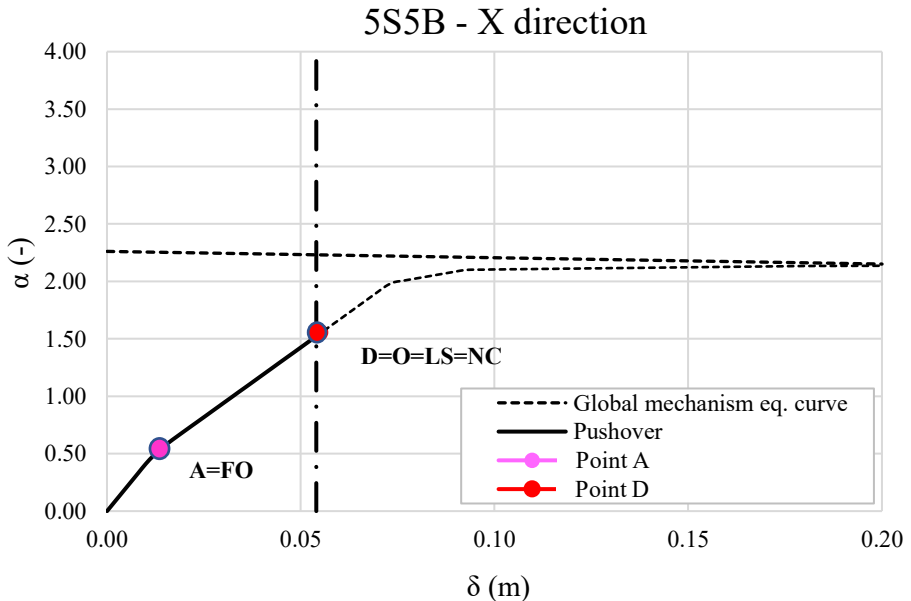


Figure 7.10.4 Simplified non-dimensional pushover curve and performance points – X direction.

Table 7.10.2 First order collapse multiplier and slopes of the mechanism equilibrium curves – X direction.

i_m	$\alpha_{0im}^{(1)}$	$\alpha_{0im}^{(2)}$	$\alpha_{0im}^{(3)}$	$\gamma_{im}^{(1)}$	$\gamma_{im}^{(2)}$	$\gamma_{im}^{(3)}$
	[-]	[-]	[-]	[m ⁻¹]	[m ⁻¹]	[m ⁻¹]
1	2.64	2.29	2.64	1.89	0.31	1.89
2	2.18	2.47	2.57	0.88	0.35	1.62
3	2.16	2.68	2.68	0.55	0.44	1.42
4	2.24	3.07	3.20	0.40	0.61	1.26
5	2.29	3.97	3.97	0.31	1.13	1.13

- Parameters obtained by elastic analysis:

$$\delta_1(\alpha = 0.48) = 0.0117 \text{ m}$$

$$K = 41.10 \text{ m}^{-1}$$

$$K' = 30.72 \text{ m}^{-1}$$

$$\delta_A(\text{1st buckling}) = 0.012016 \text{ m}$$

$$\alpha_A = k\delta_A = 0.4939$$

- Parameters obtained by rigid-plastic analysis:

$$\alpha_0 = 2.220$$

$$\gamma_s = 0.55 \text{ m}^{-1}$$

$$\alpha = \alpha_0 - \gamma_s(\delta - \delta_y) \rightarrow \alpha = 2.220 - 0.55(\delta - 0.074)$$

$$\alpha(\delta = 0) = \alpha_0 + \gamma_s\delta_y = 2.260$$

$$H_0 = 7 \text{ m} \text{ (partial type 1 collapse mechanism, storey 2)}$$

- Evaluation of the maximum multiplier through the Merchant-Rankine formula:

$$\alpha_{max M-R} = \frac{\alpha_0}{1 + \Psi_{CBF}\alpha_0\gamma_s\delta_1} = 2.1888$$

Where:

$$\Psi_{CBF} = a + b\xi_{CBF} = 1.41068 - 0.29443 \xi = 1.4103$$

$$\text{with } \xi_{CBF} = \frac{\sum_{nbc} \frac{EA_{diag}}{L_{diag}} \frac{1}{1+(L_b/h)^2}}{\sum_{nc} \frac{EI_c}{h^3}} = 0.0102$$

In accordance with the limitation of Eurocode 8 regarding the shortening of the diagonal members for the "Near Collapse" limit state ($\Delta_c \cdot 6$), the ultimate displacement of the structure is evaluated as follows:

$$\Delta_c = 0.00118 \text{ m}$$

$$\delta_{D,cp} = 6 \cdot \Delta_c = 0.0708 \text{ m}$$

$$\cos \theta = 0.86378$$

$$\begin{aligned} \delta_D &= \delta_A + \left(\frac{\delta_{d,cp}}{h_i \cdot \cos \theta} \right) \cdot H_0 = 0.012016 + \left(\frac{0.0708}{3.5 \times 0.86378} \right) \cdot 17.5 \\ &= 0.0529 \text{ m} \end{aligned}$$

After defining the trilinear model and the performance points, the transformation procedure of the multiple degrees of freedom (MDOF) system into an equivalent single degree of freedom (SDOF) system was applied through the modal participation coefficient Γ . Subsequently, known the dynamic properties of the SDOF system, the simplified curve, and the performance points were represented in the ADRS plan. In this way, the capacity in terms of spectral displacements and accelerations was defined according to the "ADRS spectrum" and "Nassar & Krawinkler" models.

It was, therefore, necessary to define:

- The eigenvector $\underline{\phi} = \{\phi_1, \phi_2, \phi_3, \phi_4, \phi_5\}$ assuming $\phi_k = \frac{F_k}{F_n}$,

$$\begin{aligned} \phi_1 &= 0.20 & \phi_2 &= 0.40 & \phi_3 &= 0.60 \\ \phi_4 &= 0.80 & \phi_5 &= 1.00 \end{aligned}$$

- The modal participation factor Γ :

$$\Gamma = \frac{\sum_{k=1}^n m_k \phi_k}{\sum_{k=1}^n m_k \phi_k^2} = 1.364$$

Where:

$$m_1 = 147.7 \times 10^3 \text{ kg} \quad m_2 = 147.7 \times 10^3 \text{ kg} \quad m_3 = 147.7 \times 10^3 \text{ kg}$$

$$m_4 = 147.7 \times 10^3 \text{ kg} \quad m_5 = 147.7 \times 10^3 \text{ kg}$$

$$m^* = \sum_{k=1}^n m_k \phi_k$$

The dynamic parameters of the equivalent SDOF system in the x-direction are given in Table 7.10.3

Table 7.10.3 Dynamic parameters of the equivalent SDOF system – X direction.

Γ	m^*	k^*	k^*	ω^*	T^*
-	kg	kN/m	N/m	[rad/s]	s
1.364	443100	45059.3356	45059336	10.0842	0.623072

All the characteristic points of the capacity curve are reported in the plans $\alpha - \delta$, $F_b - d_c$, $F^* - D^*$, $S_a - S_D$ and represent the capacity in terms of spectral accelerations and displacements according to Nassar & Krawinkler and ADRS spectrum approaches (Table 7.10.4).

Table 7.10.4 Capacity in terms of spectral displacement and acceleration – X direction

T*>TC		FO	O	LS	NC
α	[-]	0.4939	1.5047	1.5047	1.5047
δ	[m]	0.0120	0.0530	0.0530	0.0530
δ^*	[m]	0.0088	0.0389	0.0389	0.0389
F	[kN]	541.4	1649.4	1649.4	1649.4
F^*	[kN]	397.1	1209.6	1209.6	1209.6
Sa(T*) ADRS Spectrum	[g]	0.0896	0.3952	0.3952	0.3952
Sa(T*) Nassar & Krawinkler	[g]	0.0896	0.3952	0.3952	0.3952

7.10.1 Application of the simplified method – X direction

The paragraph defines the performance points for the Y direction. (A, B, C, D) to which are associated specific limit states provided for by current codes (Fully Operational, Operational, Life Safety, Near Collapse).

The trilinear capacity curve is shown in Figure 7.10.5 where the performance points are also represented according to the simplified method.

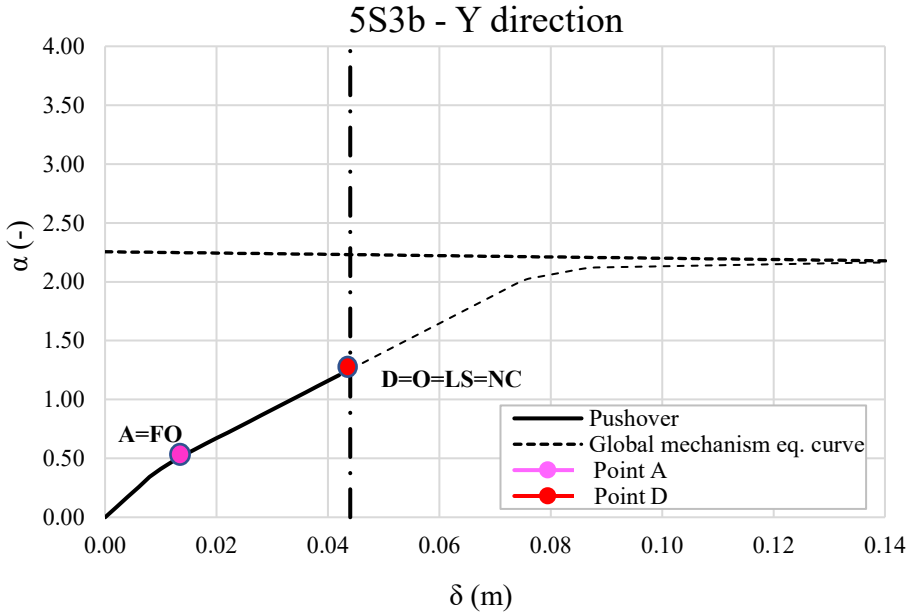


Figure 7.10.5 Simplified non-dimensional pushover curve and performance points – Y direction.

Table 7.10.5 First order collapse multiplier and slopes of the mechanism equilibrium curves – Y direction.

i_m	$\alpha_{0im}^{(1)}$	$\alpha_{0im}^{(2)}$	$\alpha_{0im}^{(3)}$	$\gamma_{im}^{(1)}$	$\gamma_{im}^{(2)}$	$\gamma_{im}^{(3)}$
	[-]	[-]	[-]	[m ⁻¹]	[m ⁻¹]	[m ⁻¹]
1	2.82	2.35	2.82	1.89	0.31	1.89
2	2.29	2.56	2.85	0.88	0.35	1.62
3	2.23	2.78	2.90	0.55	0.44	1.42
4	2.31	3.20	3.49	0.40	0.61	1.26
5	2.35	4.27	4.27	0.31	1.13	1.13

- Parameters obtained by elastic analysis:

$$\delta_1(\alpha = 0.34) = 0.0080 \text{ m}$$

$$K = 42.75 \text{ m}^{-1}$$

$$K' = 25.65 \text{ m}^{-1}$$

$$\delta_A(1\text{st buckling}) = 0.0080 \text{ m}$$

$$\alpha_A = k\delta_A = 0.3426$$

- Parameters obtained by rigid-plastic analysis (Table 7.10.5):

$$\alpha_0 = 2.232$$

$$\gamma_s = 0.55 \text{ m}^{-1}$$

$$\alpha = \alpha_0 - \gamma_s(\delta - \delta_y) \rightarrow \alpha = 2.232 - 0.55(\delta - 0.076)$$

$$\alpha(\delta = 0) = \alpha_0 + \gamma_s\delta_y = 2.263$$

$$H_0 = 7 \text{ m} \text{ (partial type 1 collapse mechanism, storey 2)}$$

- Evaluation of the maximum multiplier through the Merchant-Rankine formula:

$$\alpha_{max M-R} = \frac{\alpha_0}{1 + \Psi_{CBF}\alpha_0\gamma_s\delta_1} = 2.21$$

Where:

$$\Psi_{CBF} = a + b\xi_{CBF} = 1.41068 - 0.29443 \xi = 1.4103$$

$$\text{with } \xi_{CBF} = \frac{\sum_{n_{bc}} \frac{EA_{diag}}{L_{diag}} \frac{1}{1+(L_b/h)^2}}{\sum_{n_c} \frac{EI_c}{h^3}} = 0.0102$$

In accordance with the limitation of Eurocode 8 regarding the shortening of the diagonal members for the "Near Collapse" limit state ($\Delta_c \cdot 6$), the ultimate displacement of the structure is evaluated as follows:

$$\Delta_c = 0.00118 \text{ m}$$

$$\delta_{D,cp} = 6 \cdot \Delta_c = 0.0708 \text{ m}$$

$$\cos \theta = 0.86378$$

$$\delta_D = \delta_A + \left(\frac{\delta_{a,cp}}{h_i \cdot \cos \theta} \right) \cdot H_0 = 0.012016 + \left(\frac{0.0708}{3.5 \times 0.86378} \right) \cdot 17.5$$

$$= 0.0431 \text{ m}$$

$$\alpha_D = \alpha_A + K' \cdot (\delta_D - \delta_A) = 0.343 + 25.65 \cdot (0.0431 - 0.0080) = 1.24$$

After defining the trilinear model and the performance points, the transformation procedure of the multiple degrees of freedom (MDOF) system into an equivalent single degree of freedom (SDOF) system was applied through the modal participation coefficient Γ . Subsequently, known the dynamic properties of the SDOF system, the simplified curve, and the performance points were represented in the ADRS plan. In this way, the capacity in terms of spectral displacements and accelerations was defined according to the "ADRS spectrum" and "Nassar & Krawinkler" models.

It was, therefore, necessary to define:

- The eigenvector $\underline{\phi} = \{\phi_1, \phi_2, \phi_3, \phi_4, \phi_5\}$ assuming $\phi_k = \frac{F_k}{F_n}$:

$$\phi_1 = 0.20 \quad \phi_2 = 0.400 \quad \phi_3 = 0.60$$

$$\phi_4 = 0.80 \quad \phi_5 = 1.00$$

- The modal participation factor Γ :

$$\Gamma = \frac{\sum_{k=1}^n m_k \phi_k}{\sum_{k=1}^n m_k \phi_k^2} = 1.364$$

where:

$$m_1 = 147.7 \times 10^3 \text{ kg} \quad m_2 = 147.7 \times 10^3 \text{ kg} \quad m_3 = 147.7 \times 10^3 \text{ kg}$$

$$m_4 = 147.7 \times 10^3 \text{ kg} \quad m_5 = 147.7 \times 10^3 \text{ kg}$$

$$m^* = \sum_{k=1}^n m_k \phi_k$$

The dynamic parameters of the equivalent SDOF system in the x-direction are given in Table 7.10.6.

Table 7.10.6 Dynamic parameters of the equivalent SDOF system – Y direction.

Γ	m^*	k^*	k^*	ω^*	T^*
-	kg	kN/m	N/m	[rad/s]	s
1.364	443100	46867.67	46867668	10.28456	0.610934

All the characteristic points of the capacity curve are reported in the plans $\alpha - \delta$, $F_b - d_c$, $F^* - D^*$, $S_a - S_D$ and represent the capacity in terms of spectral accelerations and displacements according to Nassar & Krawinkler and ADRS spectrum approaches (Table 7.10.7).

Table 7.10.7 Capacity in terms of spectral displacement and acceleration – Y direction.

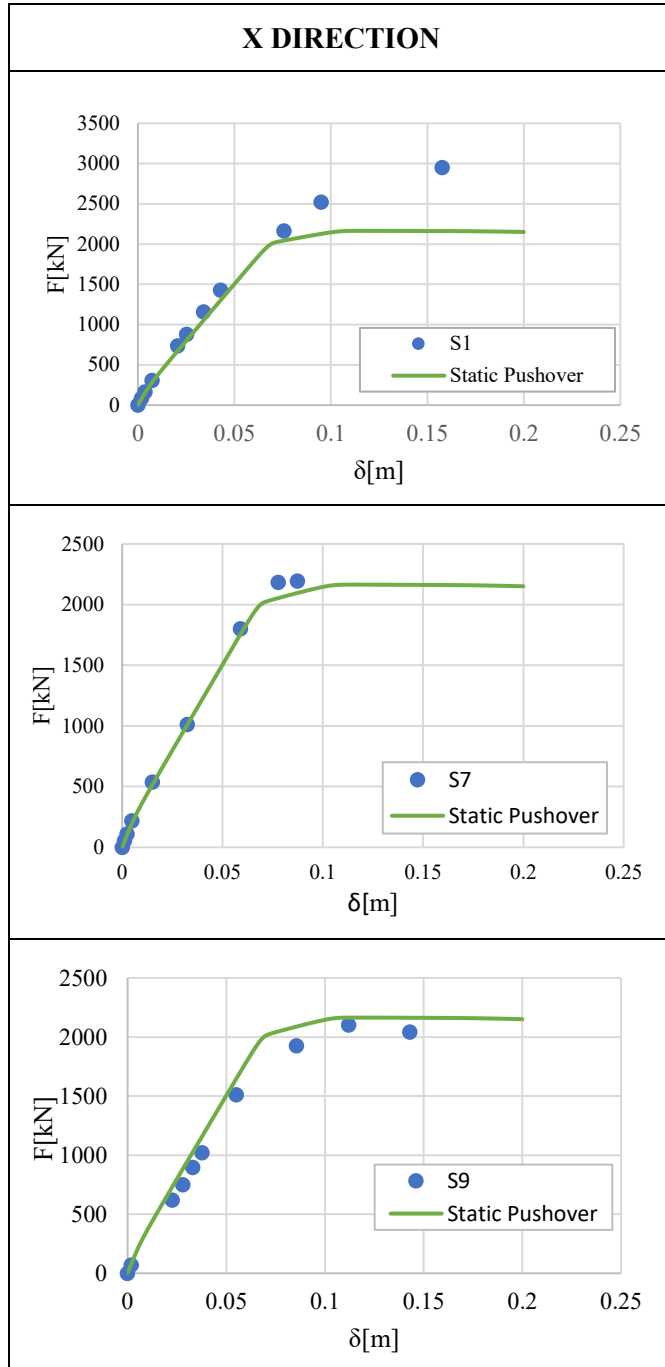
$T^* > T_C$		FO	O	LS	NC
α	[-]	0.3426	1.2438	1.2438	1.2438
δ	[m]	0.0080	0.0431	0.0431	0.0431
δ^*	[m]	0.0059	0.0316	0.0316	0.0316
F	[kN]	375.6	1363.4	1363.4	1363.4
F^*	[kN]	275.4	999.8	999.8	999.8
Sa(T^*) ADRS Spectrum	[g]	0.0622	0.3346	0.3346	0.3346
Sa(T^*) Nassar & Krawinkler	[g]	0.0622	0.3346	0.3346	0.3346

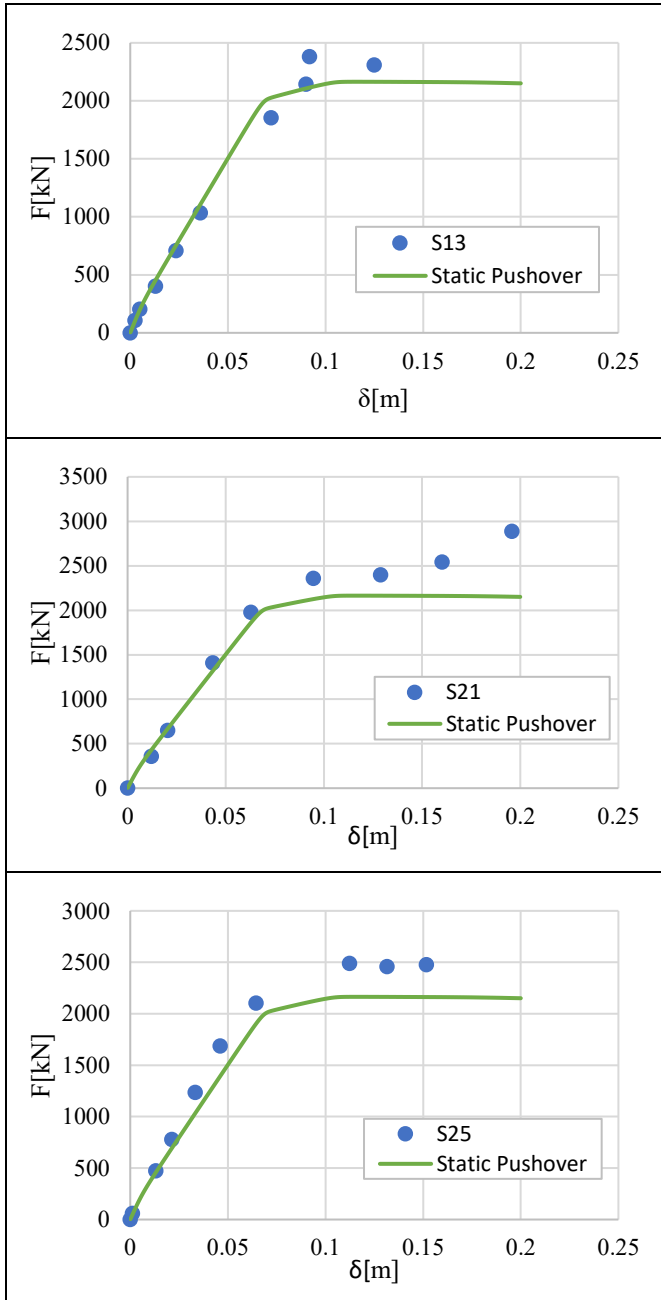
7.10.2 IDA Results and Comparison with the Simplified Method (CBF)

To evaluate the overall seismic performance of the structure, nonlinear dynamic analyses were performed. Preliminary, a non-linear static analysis was also carried out in OpenSees, after which incremental dynamic analyses were carried out with reference to the earthquakes taken into consideration.

The primary objective of this analysis is the dynamic pushover evaluation, to be compared with the static one. The dynamic pushover, for each earthquake, was built considering the maximum top sway displacement and the maximum base shear for each step of increment.

In Figure 7.10.6 the comparisons for each considered earthquake, in X direction, are reported; in Figure 7.10.7 the comparisons for each considered earthquake, in Y direction, are reported.





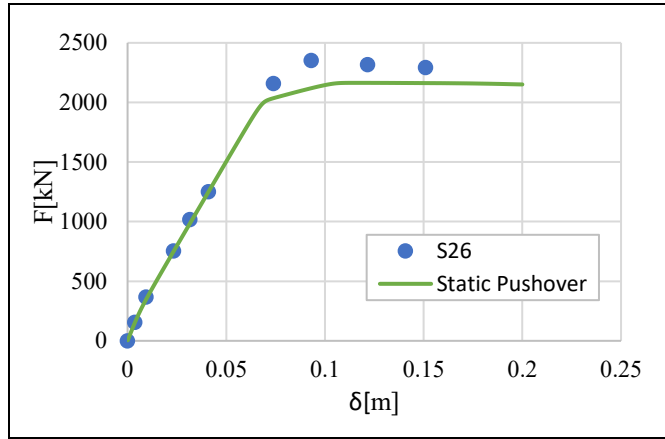
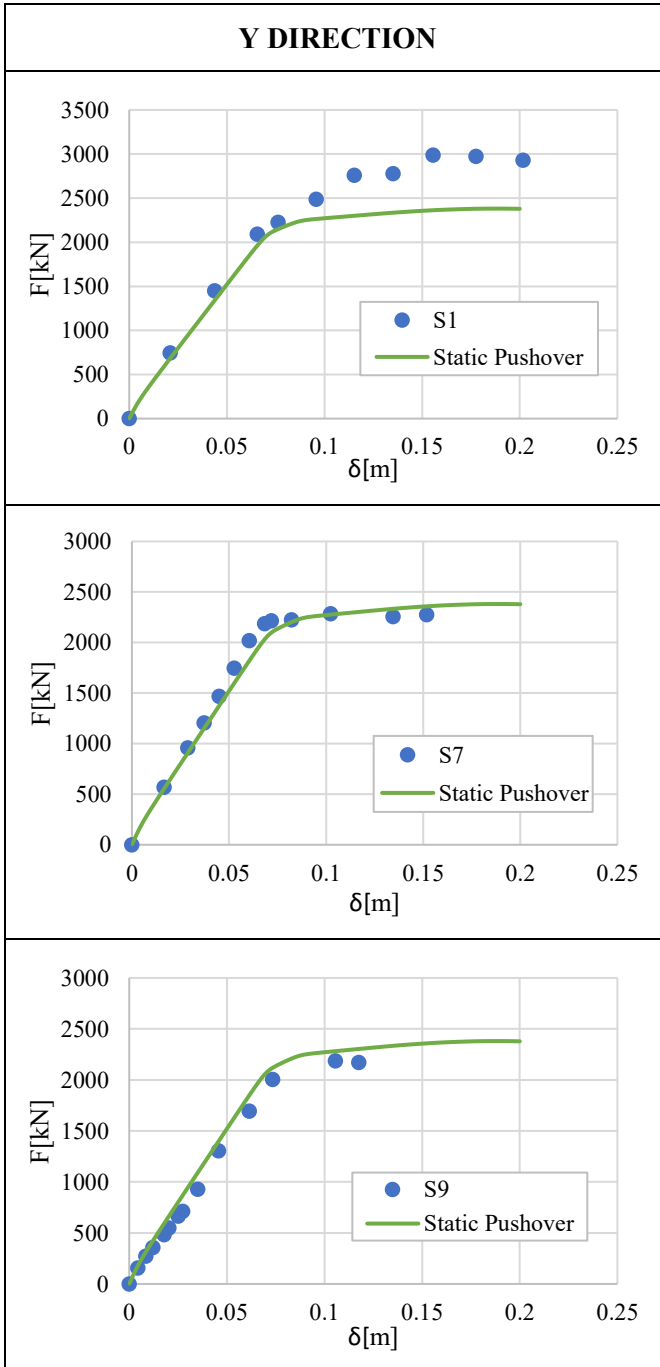
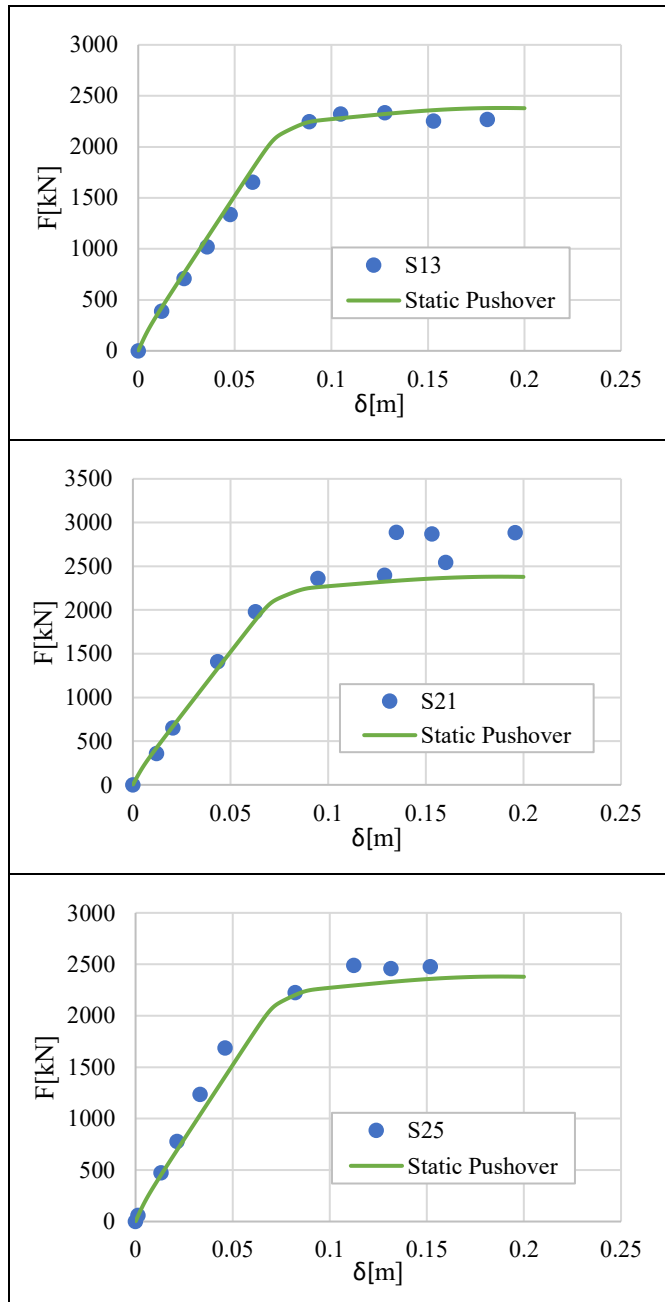


Figure 7.10.6 Comparison between static and dynamic pushover – X direction





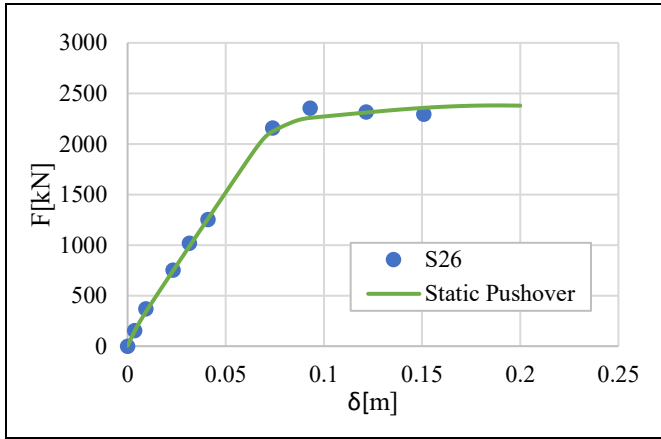


Figure 7.10.7 Comparison between static and dynamic pushover – Y direction

Subsequently, depending on the limits imposed by the EC8 in terms of shortening of the diagonal members, for each limit state (Table 7.10.8), the corresponding values of peak ground acceleration (PGA) and consequently of spectral acceleration S_a have been identified for each earthquake considered. The average values obtained were compared with the capacity in terms of spectral acceleration defined by the proposed simplified methodology (Table 7.10.9-Table 7.10.10).

Table 7.10.8 EC8 Shortening limits expressed as a function of the shortening corresponding to the critical load Δ_c .

Class of cross-section	Limit State		
	DL	SD	NC
1	$0.25 \Delta_c$	$4.0 \Delta_c$	$6.0 \Delta_c$
2	$0.25 \Delta_c$	$1.0 \Delta_c$	$2.0 \Delta_c$

Table 7.10.9. Comparison between IDA results and Simplified Method in terms of displacements and spectral acceleration – X direction

X direction		FO	O	LS	NC
δ (IDA)	[m]	0.0098	0.0495	0.0495	0.0495
δ (S.M.)	[m]	0.0120	0.0530	0.0530	0.0530
S_a (T*) IDA	[kN]	0.0797	0.3695	0.3695	0.3695
S_a (T*) ADRS Spectrum	[g]	0.0896	0.3952	0.3952	0.3952
S_a (T*) Nassar & Krawinkler	[g]	0.0896	0.3952	0.3952	0.3952

Table 7.10.10 Comparison between IDA results and Simplified Method in terms of displacements and spectral acceleration – Y direction

Y direction		FO	O	LS	NC
δ (IDA)	[m]	0.0071	0.0397	0.0397	0.0397
δ (S.M.)	[m]	0.0080	0.0430	0.0430	0.0430
Sa(T*) IDA	[kN]	0.052	0.289	0.289	0.289
Sa(T*) ADRS Spectrum	[g]	0.062	0.335	0.335	0.335
Sa(T*) Nassar & Krawinkler	[g]	0.062	0.335	0.335	0.335

Finally, a summary graph is shown (Figure 7.10.8-Figure 7.10.9) in which are reported, by points, all the dynamic pushovers obtained and the static pushover. On the graph the displacement limits have been identified by means of a vertical line and consequently the corresponding base shear, for the limit states DL and NC (green IDA, red Simplified Method).

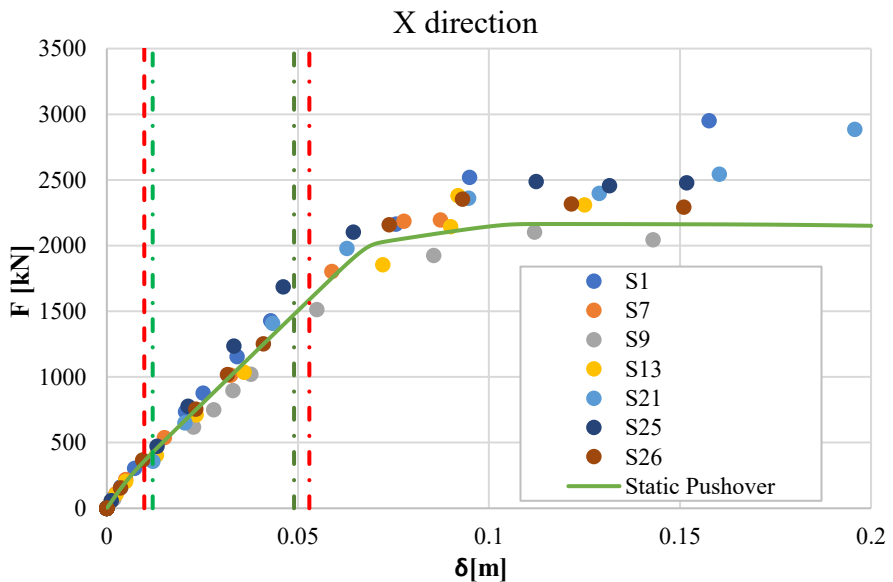


Figure 7.10.8 Comparison between static and dynamic pushover for each earthquake – X direction.

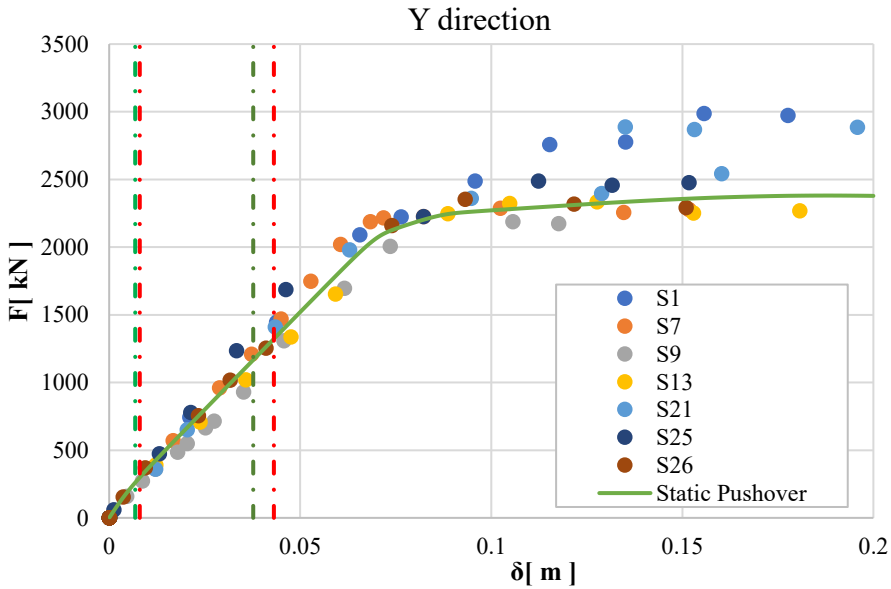


Figure 7.10.9 Comparison between static and dynamic pushover for each earthquake – Y direction

From the analysis of Table 7.10.9 (X direction), there is a percentage error in the evaluation of capacity in terms of spectral acceleration, between Simplified Method and IDA, equal to 11% for the "Fully Operational" limit state and 6% for the "Near Collapse" limit state.

From the analysis of Table 7.10.10 (Y direction), there is a percentage error in the evaluation of capacity in terms of spectral acceleration, between Simplified Method and IDA, equal to 16% for the "Fully Operational" limit state and 12% for the "Near Collapse" limit state.

CHAPTER 8

8 CONCLUSIONS

The simplified performance-based approach herein presented has the aim of assessing the seismic vulnerability of existing steel Moment Resisting Frames (MRFs) and Centrically Braced Frames (CBFs) subjected to seismic actions, without using any static non-linear or dynamic non-linear analysis.

To check the validity and the field of application of the method, an extensive parametric analysis was carried out on 420 frames for each structural type, designed according to 3 different approaches.

The capacity can be estimated through the pushover curves whose trend can be approximated by a trilinear capacity curve.

In the case of MRFs, among its three branches, the first one is representative of the elastic behaviour, the second of the maximum load multiplier, and the third of the collapse mechanism equilibrium curve.

In the case of CBFs, the proposed methodology consists of a trilinear approximation of the structure behavioural curve whose first two branches are obtained through elastic analysis, while, rigid-plastic analysis, taking into account second-order effects helps to define the third "softening" branch.

In addition, four characteristic points of the curve are identified and connected to four limit states corresponding to achieved target performances of the structures. Their evaluation has been obtained by means of mathematical relations opportunely calibrated on the basis of a wide parametric analysis including 420 structures on which pushover analyses have been carried out.

In Chapter 4 the validation and the calibration results have been reported. In particular, for MRFs the maximum loading multiplier (Merchant-Rankine) and the plastic rotation demand relations have been defined through linear

regression, showing a high accuracy due to the determination coefficients close to the unit value, the trendline close to the bisector and the regression points leaning against the trendline.

Also for CBFs the Merchant-Rankine formula has been calibrated but considering different regression parameters, based on the specificity of the structural typology. In addition, a regression analysis has been performed also to define the reduction factor β of the stiffness, characterizing the second branch of the trilinear model. The parameter has been set between 0.7 and 0.75.

The same accuracy of MRFs has been detected for CBFs, testifying to the great flexibility and adaptability of the method and the proposed relationships.

The simplified method has been applied to all 840 structures designed. From the analysis of Figure 4.3.6-Figure 4.3.7 for MRFs and Figure 4.4.6-Figure 4.4.7 for CBFs, we report the synthetic results in terms of medium percentage error in the definition of the maximum multiplier and the points C and D, in terms of top sway displacement, referring to the results obtained by pushover analyses (Table 8.1).

Table 8.1 Comparison between simplified method and pushover results

	α_{max} [%]	δ_{mec} [%]	δ_u [%]
GMRFs	0.9	1.9	5.3
SMRFs	5.2	9.5	4.8
OMRFs	1.8	5.1	7.2
GCBFs	0.8	1.2	5.6
SCBFs	4.7	3.5	6.3
OCBFs	-	-	-

In Chapter 6, some numeric examples explaining the application of the simplified method are reported. As can be seen from the given numerical examples, the methodology is of easy and rapid application. The methodology is also completely analytical since the equations of the branches constituting the trilinear model can be obtained uniquely, given the horizontal seismic actions and the sections of beams and columns of the analyzed frame.

The speed of application and the uniqueness show that this methodology is strongly indicated for the evaluation of seismic performances in the immediate post-earthquake or the large-scale assessment of the seismic vulnerability of the

built heritage. Furthermore, it constitutes a suitable tool to check the capacity of the buildings designed with the new seismic code prescriptions. The feasibility of the procedure is very high and makes it suitable to be applied indiscriminately to frames belonging to different historical periods.

Finally, in Chapter 7, is reported the validation of the method through Incremental Dynamic Analysis (IDA) applied to simulated design structures whose data are available in the literature. The IDAs have been developed with the Abaqus software, creating a very accurate fiber model capable of catching the real behavior of the analyzed structures. In this way, it was possible to evaluate the actual percentage error between the seismic capacity defined by the simplified methodology and that one obtained through the IDAs, for each limit state considered.

In the case of MRFs the objective was the definition of the MIDR – PGA/g (Sa/g) curves for each of the 7 earthquakes considered. The comparison in terms of spectral acceleration capacities between the simplified method and IDAs provided consistent results. The analysis of Table 7.8.5 (Table 7.9.5) results in an error equal to 4.5% (10.3%) for the "Fully Operational" limit state, 4.7% (19.7%) for the "Operational" limit state, 6.4% (9.4%) for the "Life Safety" limit state and 2% (2.5%) for the "Near Collapse" limit state.

In the case of CBFs, the objective was the definition of dynamic pushover curves for the two braced frames considered and for each of the 7 earthquakes considered. The curves obtained showed good adherence compared to the static ones. Finally, a comparison in terms of spectral acceleration capacities between the simplified method and IDAs was made. The analysis of Table 7.10.9 (Table 7.10.10) results in an error of 11% (16%) for the "Fully Operational" limit state and an error of 6% (12%) for the Near Collapse limit state.

I would like to underline that the proposed methodology aims to achieve a high level of precision for the ultimate limit states, being devoted to the assessment of seismic vulnerability over long time periods. In this sense, the results obtained are satisfactory, presenting a very low percentage error (2% - 12%).

In conclusion, the main advantage of the proposed methodology is that the equations of the branches constituting the trilinear model can be obtained uniquely and analytically, given the seismic action distribution and the sections of beams and columns of the analysed frame.

Consequently, it is recommended in the large-scale mapping of the seismic vulnerability of the built heritage, according to given performance criteria because of the uniqueness of the method and the statistical reliability in operating on a large-scale number of structures.

REFERENCES

- [1] Montuori, R., Nastri, E., Piluso, V. "Problems of modeling for the analysis of the seismic vulnerability of existing buildings" (2019) *Ingegneria Sismica*, 36 (2), pp. 53-85.
- [2] Hu, S., Wang, W., Alam, M.S. Performance-based seismic design method for retrofitting steel moment-resisting frames with self-centering energy-absorbing dual rocking core system (2022) *Journal of Constructional Steel Research*, 188, art. no. 106986. DOI: 10.1016/j.jcsr.2021.106986
- [3] Silva, A., Macedo, L., Monteiro, R., Castro, J.M. "Earthquake-induced loss assessment of steel buildings designed to Eurocode 8" (2020) *Engineering Structures*, 208, art. no. 110244.
- [4] Hickey, J., Broderick, B. "Loss impact factors for lifetime seismic loss assessment of steel concentrically braced frames designed to EC8" (2019) *Journal of Structural Integrity and Maintenance*, 4 (3), pp. 110-122.
- [5] Mohammadi, A., Azizinamini, A., Griffis, L., Irwin, P. "Performance Assessment of an Existing 47-Story High-Rise Building under Extreme Wind Loads" (2019) *Journal of Structural Engineering (United States)*, 145 (1), art. no. 04018232.
- [6] Montuori, R., Nastri, E., Piluso, V., Todisco, P. "A simplified performance based approach for the evaluation of seismic performances of steel frames" (2020) *Engineering Structures*, 224, art. no. 111222, DOI: 10.1016/j.engstruct.2020.111222

- [7] Montuori, R., Nastri, E., Piluso, V., Todisco, P. “Evaluation of the seismic capacity of existing moment resisting frames by a simplified approach: Examples and numerical application” (2021) *Applied Sciences* (Switzerland), 11 (6), art. no. 2594, DOI: 10.3390/app11062594
- [8] Montuori, R., Nastri, E., Todisco, P. “Influence of the seismic shear proportioning factor on steel MRFs seismic performances” (2021) *Soil Dynamics and Earthquake Engineering*, 141, art. no. 106498, DOI: 10.1016/j.soildyn.2020.106498
- [9] Montuori, R., Nastri, E., Piluso, V., Todisco, P. “Performance-based rules for the simplified assessment of steel CBFs” (2022) *Journal of Constructional Steel Research*, 191, art. no. 107167, DOI: 10.1016/j.jcsr.2022.107167
- [10] Montuori, R., Nastri, E., Piluso, V., Todisco, P. “Simplified Approach for the Seismic Assessment of Existing X Shaped CBFs: Examples and Numerical Applications” (2022) *Journal of Composites Science*, 6 (2), art. no. 62, DOI: 10.3390/jcs6020062
- [11] Longo, A., Montuori, R., Piluso, V. Moment frames – concentrically braced frames dual systems: analysis of different design criteria *Structure and Infrastructure Engineering*, 2016, 12(1), pp. 122–141
- [12] Piluso, V., Montuori, R., Nastri, E., Paciello, A. “Seismic response of MRF-CBF dual systems equipped with low damage friction connections”, (2019) *Journal of Constructional Steel Research*, 154, pp. 263-277.
- [13] Mazzolani F.M., Piluso V. (1996). *Theory and Design of Seismic Resistant Steel Frames*. E&FN Spon, London.
- [14] Mazzolani F.M., Piluso V. (1997). *Plastic Design of Seismic Resistant Steel Frames*. *Earthquake Engineering and Structural Dynamics*, Vol. 26, 167-191.
- [15] Ismail, M., “Seismic Retrofit of Steel Frame Structures” *Pollack Periodica, An International Journal for Engineering and Information Sciences* Vol. 15, No. 2, pp. 106–117 (2020) DOI: 10.1556/606.2020.15.2.10

- [16] Di Sarno, L., Jing-Ren Wu, J.-R., "Seismic assessment of existing steel frames with masonry infills", *Journal of Constructional Steel Research*, Volume 169, 2020, 106040, ISSN 0143-974X, <https://doi.org/10.1016/j.jcsr.2020.106040>.
- [17] Di Cuia, A., Lombardi, L., De Luca, F., De Risi, R., Caprili, S., Salvatore, W., "Linear Time-History Analysis for EC8 design of CBF structures" (2017) *Procedia Engineering*, Volume 199, Pages 3522-3527, ISSN 1877-7058, <https://doi.org/10.1016/j.proeng.2017.09.502>.
- [18] Eurocode 8 (2004). EN 1998-1: Design of Structures for Earthquake Resistance – Part 1: general Rules, Seismic Actions and Rules for Buildings, CEN.
- [19] Eurocode 8 (2004). EN 1998-3: Design of Structures for Earthquake Resistance – Part 3: Assessment and retrofitting of buildings, CEN
- [20] NTC 2018 Italian Code: Chapter 7 "Design for seismic actions".
- [21] Eurocode 3 (2005). UNI EN 1993-1-1: Design of steel structures Part 1-1: General rules and rules for buildings, CEN.
- [22] Montuori, R., Nastri, E., Piluso, V., Advances in theory of plastic mechanism control: Closed form solution for MR-Frames, (2015) *Earthquake Engineering and Structural Dynamics*, 44 (7), pp. 1035-1054.
- [23] Piluso, V., Pisapia, A., Castaldo, P., Nastri, E. "Probabilistic Theory of Plastic Mechanism Control for Steel Moment Resisting Frames", (2019) *Structural Safety*, 76, pp. 95-107.
- [24] Georgescu, D., Toma, C., Gosa, O., "Post-critical behaviour of 'K' braced frames", *Journal of Constructional Steel Research*, (1992) Volume 21, Issues 1–3, Pages 115-133, ISSN 0143-974X, [https://doi.org/10.1016/0143-974X\(92\)90022-7](https://doi.org/10.1016/0143-974X(92)90022-7).
- [25] Bruneau, M., Chia-Ming Uang and Andrew S. Whittaker. "Ductile design of steel structures." (1997) McGraw-Hill, Network.
- [26] Gupta A., Krawinkler H., Feasibility of push-over analyses for estimation of strength demand, Stessa 2003, - Behaviour of Steel Structures in Seismic Areas: Proceedings of the 4th International Specialty Conference, Naples, Italy, 9-12 June 2003.

- [27] A.Gupta and H. Krawinkler, "Seismic Demands for Performance Evaluation of Steel Moment Resisting Frame Structures," 1999.
- [28] Nassar, AA and Krawinkler, H. (1991). Seismic Demands for SDOF and MDOF Systems. John A Blume Earthquake Engineering Center Technical Report 95. Stanford Digital Repository
- [29] Newmark, N., & Hall, W. (1982). Earthquake Spectra and Design. In EERI Monographs.
- [30] CSI 2007. SAP2000: Integrated Finite Element Analysis and Design of Structures. Analysis Reference. Computer and Structure Inc. University of California, Berkeley.
- [31] OpenSEES – Open System for Earthquake Engineering Simulation (1999): Pacific Earthquake Engineering Research Centre, University of Berkeley, California.
- [32] Tremblay, R. "Inelastic seismic response of steel bracing members" (2002) Journal of Constructional Steel Research, Vol.58, pp 665-701, Elsevier Science.
- [33] Black, C.; Makris, N.; Aiken, I. "Component testing, stability analysis and characterization of Buckling-Restrained Unbonded Braces" (2008), PEER report 2002/08.
- [34] Black, R.G., Wenger, W.A., and Popov, E.P. "Inelastic Buckling of Steel Structures under Cyclic Load and Reversal" (1980), Report UBC/EERC-80/40, Earthquake Engineering Research Center, University of California, Berkeley.
- [35] Jain, A.K., Goel, S.C. and Hanson, R.D. "Hysteresis Behaviour of Bracing Members and Seismic Response of Braced Frames with Different Proportions" (1978), Report UMEE 78R3, Department of Civil Engineering, The University of Michigan.
- [36] Filippou, F.C.; Bertero, V.V.; Popov, E.P. "Effects of bond deterioration on hysteretic behaviour of reinforced concrete joints" (1983), Earthquake Engineering Research Centre, Report 83/19, University of California, Berkeley.
- [37] Andrew T. Myers, Amit M. Kanvinde, Gregory G. Deierlein, Benjamin V. Fell, Xiangyang Fu, "Large Scale Tests and Micromechanics-Based Models to Characterize Ultra Low Cycle

- Fatigue in Welded Structural Details", Structural Engineering Research Frontiers (2007) P.1-16, doi:10.1061/40944(249)35
- [38] Fell, B. & Myers, Andrew & Deierlein, Gregory & Kanvinde, A. (2006). Testing and simulation of Ultra-Low Cycle Fatigue and fracture in steel braces. 8th US National Conference on Earthquake Engineering 2006. 10.

